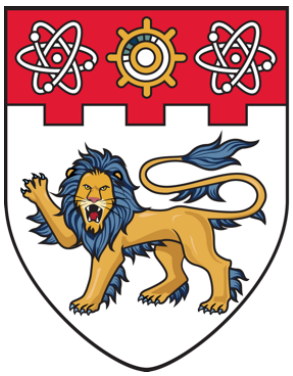

NANYANG TECHNOLOGICAL UNIVERSITY
SINGAPORE

IRE-1 REGULATES CELLULAR HOMEOSTASIS DURING DISRUPTED LIPID METABOLISM

JHEE HONG KOH

SCHOOL OF BIOLOGICAL SCIENCES

2021

IRE-1 REGULATES CELLULAR HOMEOSTASIS DURING DISRUPTED LIPID METABOLISM

JHEE HONG KOH

SCHOOL OF BIOLOGICAL SCIENCES

A thesis submitted to the Nanyang Technological University in partial fulfilment of the requirement for the degree of Doctor of Philosophy

2021

Statement of Originality

I hereby certify that the work embodied in this thesis is the result of original research done by me except where otherwise stated in this thesis. The thesis work has not been submitted for a degree or professional qualification to any other university or institution. I declare that this thesis is written by myself and is free of plagiarism and of sufficient grammatical clarity to be examined. I confirm that the investigations were conducted in accord with the ethics policies and integrity standards of Nanyang Technological University and that the research data are presented honestly and without prejudice.

22 Jan 2021

. . . . . .

Date

. . . . . .

Jhee Hong Koh

Supervisor Declaration Statement

I have reviewed the content and presentation style of this thesis and declare it of sufficient grammatical clarity to be examined. To the best of my knowledge, the thesis is free of plagiarism and the research and writing are those of the candidate's except as acknowledged in the Author Attribution Statement. I confirm that the investigations were conducted in accord with the ethics policies and integrity standards of Nanyang Technological University and that the research data are presented honestly and without prejudice.

23 Jan 2021

. . . . . .

Date

. . . . . .

Guillaume Thibault

Authorship Attribution Statement

Please select one of the following; *delete as appropriate:

*(B) This thesis contains material from ONE paper(s) published in the following peer-reviewed journal(s) in which I am listed as an author.

Parts of Chapter 1 and Chapter 2 is published as Jhee Hong Koh*, Lei Wang*, Caroline Beaudoin-Chabot, Guillaume Thibault, Journal of Cell Science 2018 131: jcs217992 doi: 10.1242/jcs.217992 Published 21 November 2018

The contributions of the co-authors are as follows:

- Lei Wang and I are co-authors. I prepared the manuscript drafts. The manuscript was revised together with Asst Prof Guillaume Thibault.

22 Jan 2021

. . . . . .

Date

. . . . . .

Jhee Hong Koh

The following publications were a result of work conducted during doctoral study:

1. **Jhee Hong Koh***, Lei Wang*, Caroline Beaudoin-Chabot, Guillaume Thibault
   Lipid bilayer stress-activated IRE-1 modulates autophagy during endoplasmic reticulum stress
   J Cell Sci 2018 Nov 21. doi. 10.1242/jcs.217992
   *Co-first authors

2. Nurulain Ho, Wei Sheng Yap, Jiaming Xu, Haoxi Wu, **Jhee Hong Koh**, Wilson W.B. Goh, Bhawana George, Shu Chen Chong, Stefan Taubert, Guillaume Thibault
   Stress sensor Ire1 deploys a divergent transcriptional program in response to lipid bilayer stress
   J Cell Biol 2020 Apr 29. doi. 10.1083/jcb.201909165

3. Caroline Beaudoin-Chabot, Lei Wang, Cenk Celid, Aishah Abdul Khalid, Subhash Thalappilly, **Jhee Hong Koh**, Shiyi Xu, Cherie Ching Li Teow, Guillaume Thibault
   ER stress transducer IRE-1 differentially modulates the lifespan of young and aged *C. elegans* fed glucose
   Nat Comm (Under revision)

Acknowledgements

The following researchers contributed to the experimental data shown in the Figures throughout the thesis:

1. Asst. Professor Guillaume Thibault for illustrating Figures 1.1.
2. Lei Wang for contributing to the experiments shown in Figure 3.11, 3.16a, 3.18 and 3.19.
3. Reut Dudkevich from Prof. Sivan Henis-Korenblit laboratory (Bar Ilan University, Israel) who performed the experiment and contributed to Figures 3.8 and 3.9.
4. Caroline Beaudoin-Chabot for contributing to the experiments shown in Figures 3.12 and 3.18.

My sincerest thanks and gratitude,

To Asst. Professor Guillaume Thibault for affording me the opportunity work in his laboratory and mentoring me since I was an undergraduate student and being patient with me throughout this journey.

To my committee members, Asst. Professor Woo Wei Meng and Assoc. Professor Koh Cheng Gee.

To my fellow lab members both past and present for their support.

To Caroline, for caring and aiding me throughout the past six years.

To Wei Sheng, for influencing me with his passion for science and research.

To my seniors who have left this lab, Peter, Xiu Hui, and Nurulain for still being present for me and keeping me sane.

To William, my constant in this hectic world.

And to my mother, York Ying, and brothers Jhee Son, Jhee Herng and Jhee Qing for their unwavering faith, love, support and encouragement.

Table of Contents

List of Figures

List of Tables

Appendix

Summary

Metabolic disorders, such as non-alcoholic fatty liver disease (NAFLD), are emerging as epidemics that affect the global population. One facet of these disorders is attributed to the disturbance of membrane lipid composition. Typically activated by misfolded protein accumulation within the ER, perturbation of endoplasmic reticulum (ER) homeostasis through alteration in membrane phospholipids or change in membrane lipid saturation to unsaturation ratio also activate the unfolded protein response (UPR) and cause dramatic transcriptional and translational changes in the cell. To restore cellular homeostasis, the three highly conserved UPR transducers ATF6, IRE1, and PERK mediate adaptive responses upon ER stress. Understanding the differences of how lipid dysregulation causes ER perturbation is critical, as it will provide insights into the pathophysiological mechanism of metabolic diseases. Furthermore, new insights into how proteotoxic stress differs from lipid bilayer stress (LBS) may also aid in specific targeting of the UPR for a better therapeutic outcome. Our goal in this project is to establish a model system in the nematode *Caenorhabditis elegans* to differentiate proteotoxic stress-induced UPR and LBS-induced UPR. We evaluated sources of stress that activate UPR^{LBS} and identified three factors that warrant further studies. These factors are (1) increased lipid unsaturation through cold stress, (2) increased lipid saturation through glucotoxicity, and (3) phosphatidylcholine (PC) deficiency through silencing of the PC biosynthesis gene phosphatidylethanolamine N-methyltransferase 2 (*pmt-2*). They share the common theme where perturbed cellular homeostasis caused by these factors activate IRE-1 through LBS. We show that the worms are highly responsive to PC depletion and strongly activates the UPR^{LBS}. Hence, we focused our understanding of the UPR^{LBS} by utilizing the PC deficiency model. Transcriptional profiling of PC-deficient worms revealed a unique subset of genes regulated in a UPR-dependent manner that is independent from proteotoxic stress. Among these, we show that autophagy is modulated through the conserved IRE-1–XBP-1 axis, strongly suggesting of the importance of autophagy in maintaining cellular homeostasis during the LBS-induced UPR.

Abbreviations

Abbreviation	Description
ATF6/ATF-6	Activating transcription factor 6
BiP	Immunoglobulin heavy chain binding protein
bZIP	Basic leucine zipper domain
C. elegans	*Caenorhabditis elegans*
CDP DAG	Cytidine diphosphate diacylglycerol
CHOP	CCAAT-enhancer-binding protein homologous protein
DHC	Dihydroceramide
DHS	Dihydrosphingosine
eIF2α	Eukaryotic translation initiation factor 2 alpha
ER	Endoplasmic reticulum
FA	Fatty acid
GADD34	Growth arrest and DNA damage-inducible protein
GFP	Green fluorescent protein
HGD	High glucose diet
IRE1/IRE-1	Inositol requiring enzyme 1
LBS	Lipid bilayer stress
LGG-1-PE	Phosphatidylethanolamine -conjugated LGG-1
LD	Luminal domain
MDT-15	Mediator subunit 15
MUFA	Monounsaturated fatty acid
NAFLD	Non-alcoholic fatty liver disease
NASH	Non-alcoholic steatohepatitis
ND	Normal diet
PA	Phosphatidic acid
PC	Phosphatidylcholine
PE	Phosphatidylethanolamine
PEMT/PMT	Phosphatidylethanolamine N-methyltransferase
PERK/PEK-1	Protein kinase RNA-like ER kinase
PT	Proteotoxic stress

PUFA	Polyunsaturated fatty acid
RIDD	IRE-1-dependent decay of mRNA
SFA	Saturated fatty acid
T2D	Type 2 diabetes
TMD	Transmembrane domain
Tm	Tunicamycin
UPR	Unfolded protein response
XBP-1	Transcription factor X-box binding protein 1

Chapter 1: Introduction

1.1. Non-alcoholic fatty liver disease (NAFLD) and lipotoxicity

Excess caloric consumption due to increased food availability and global change to a more sedentary lifestyle in developed countries has led to an increase in the prevalence of poor metabolic health. Consequently, cases of liver pathologies termed non-alcoholic fatty liver disease (NAFLD) has been rising steadily for the past decades. NAFLD is the most common cause of chronic liver disease worldwide. It is primarily associated with obesity and diabetes and its prevalence has increased significantly in Singapore, thus becoming an important public health issue. Using hepatic imaging through ultrasound as the NAFLD diagnostic method, NAFLD prevalence is estimated at around 40% among a cohort of 167 overweight participants (Wong et al., 2018). Increasingly, the burden of fatty liver among non-obese individuals is elevating with 40% of the NAFLD population appear to be non-obese or lean. This statistic is even more apparent in Asian countries where a sampling study involving 63,017 participants showed 40.8% of the NAFLD cases are attributed to non-obese individuals (Ye et al., 2020). NAFLD is a non-heterogeneous disease ranging from simple hepatic steatosis with no apparent symptoms to non-alcoholic steatohepatitis (NASH), which is characterized by the presence of hepatic steatosis and inflammation with hepatocyte injury. NASH can develop into hepatic fibrosis, cirrhosis, and ultimately hepatocellular carcinoma (HCC) (Yoon and Cha, 2014).

Lipid content within cells is tightly regulated to maintain cellular homeostasis and is crucial in many physiological processes including energy storage, signaling, and membrane formation. The disruption in lipid homeostasis has been strongly associated with obesity and NAFLD and is often characterized by excessive accumulation of harmful fatty acids in liver, pancreatic and adipose tissues, leading to lipotoxicity (Doycheva et al., 2017; Puri et al., 2007; Tiniakos et al., 2010). Cells faced with lipotoxicity then enter deleterious pathways such as inflammation and apoptosis, resulting in cellular dysfunction (Donnelly et al., 2005). From a metabolic point of view, dysfunctional lipid homeostasis is often caused by an imbalance in fatty acid flux where the capacity of the liver clearing the fatty acid is lower than the amount of peripheral fatty acid entering the liver (Donnelly et al., 2005). Excessive accumulation of lipids in the liver can interfere with intracellular insulin signaling, thus causing insulin resistance, an established risk factor for the progression of metabolic disease. While triglycerides storage in the liver

as lipid droplets are inert, diacylglycerol and ceramides have been found to accumulate in the livers of NAFLD patients and have been implicated in causing insulin resistance, thus complicating the progression of NAFLD. The liver is the metabolic organ playing an essential part in lipid metabolism. Most enzymes and proteins responsible for lipid metabolism are found within the endoplasmic reticulum (ER). Perturbation to the liver due to lipotoxicity in the context of NAFLD disturbs the homeostatic balance of the ER and triggers ER stress.

1.2. The endoplasmic reticulum (ER) and ER stress

The ER is a eukaryotic organelle made up of a membranous network of membrane-enclosed cisternae in the rough ER (RER) and tubular structures found in the smooth ER (SER). The RER is decorated with ribosomes on its cytosolic surface and has proximity to the nucleus. Both the ER and outer nucleus share a continuous membrane. Cell types with various functions may own different ratios of RER to SER with hepatocytes having an abundance of RER and the largest volume of ER as their organelle. The ER is crucial in the synthesis of proteins, carbohydrates, and lipids. It also folds protein molecules, guides their maturation through post-translational modifications, and maintains calcium balance in a cell (Braakman and Bulleid, 2011; Schroder and Kaufman, 2005a). The ER is the site of lipid synthesis that provides the majority of lipids (neutral lipids, sterols, sphingolipids, and phospholipids) and lipoproteins to the cell (Lagace and Ridgway, 2013; Wu et al., 2014).

The ER has evolved to have the ability to adapt to a wide range of metabolic changes such as an increased capacity for proteins and lipids synthesis. A widely known view of ER homeostasis can be defined as a balance between the protein folding capacity of the ER (chaperone function and protein degradation machinery) and the protein load, where disruption of this homeostatic state leads to misfolded protein accumulation and inducing ER stress (Ron and Walter, 2007). Additionally, multiple studies have shown that prolonged disruption of the ER such as imbalance fatty acid flux and lipid accumulation may permanently tilt the balance of ER homeostatic state, triggering unresolved ER stress, which is associated with metabolic diseases (Fu et al., 2011; Han and Kaufman, 2016).

1.3. The unfolded protein response (UPR)

In response to ER stress, organisms from yeast to mammals possess a highly conserved ER-to-nucleus signaling pathway termed the unfolded protein response (UPR) to ease the molecular insults present within the ER. A successful UPR involves induction of quality control mechanisms such as ER-associated degradation (ERAD), increased chaperone production, lipid production, and signaling and reduction of protein load which ultimately lead to ER homeostasis. The first evidence on ER homeostasis could be attributed to Kozutsumi and colleagues in 1988 where they observed glucose-regulated proteins (GRPs) acting like ER chaperones to aid in proper protein folding (Kozutsumi et al., 1988). To counter ER stress and maintain ER functionality, eukaryotes have evolved transcriptional and translational regulatory pathways collectively termed as the UPR (Cox and Walter, 1996; Schroder and Kaufman, 2005a; Shen et al., 2004). As part of the transcriptional program, a subset of genes is upregulated to remodel various cellular pathways to ease stress and maintain viability, and the failure to reach ER homeostasis may result in cell death through apoptosis (Mota et al., 2016; Oyadomari et al., 2002; Wu et al., 2014).

In metazoan, the UPR comprises three conserved ER transmembrane proteins that detect ER stress and coordinate downstream cellular signaling to alleviate the source of stress. These proteins are inositol-requiring enzyme 1α (IRE1α), PKR-like ER kinase (PERK), and activating transcription factor 6 (ATF6) (Fig. 1.1) (Cox and Walter, 1996; Schroder and Kaufman, 2005b; Shen et al., 2005). Of note, IRE1 is the most highly conserved UPR activator and is the sole ER stress sensor in yeast. Similar to metazoan, *C. elegans* possesses three UPR sensor orthologs called IRE-1, PEK-1, and ATF-6. Upon ER stress, each sensor activates their cognate downstream effectors resulting in general translational shutdown and the upregulation of target genes to restore cellular homeostasis (Walter and Ron, 2011; Wu et al., 2014). In the event of an acute response to excessive ER stress, the UPR transcriptional program leads to cell death through the IRE1 and PERK branches (Harding et al., 2003; Novoa et al., 2001). On the other hand, chronic ER stress triggers an adaptive response of the UPR program that leads to differential expression of pro-survival signals, thereby bypassing apoptosis induction (Kim et al., 2017; Rubio et al., 2011; Rutkowski et al., 2006). The UPR is complex because of the interwoven relationship between the sensors themselves and crosstalk to a myriad of cellular signaling pathways. Therefore, a comprehensive understanding of the mechanism of the UPR activation and regulation is

essential and provides clinical relevance for the development of therapeutics targeting metabolic diseases.

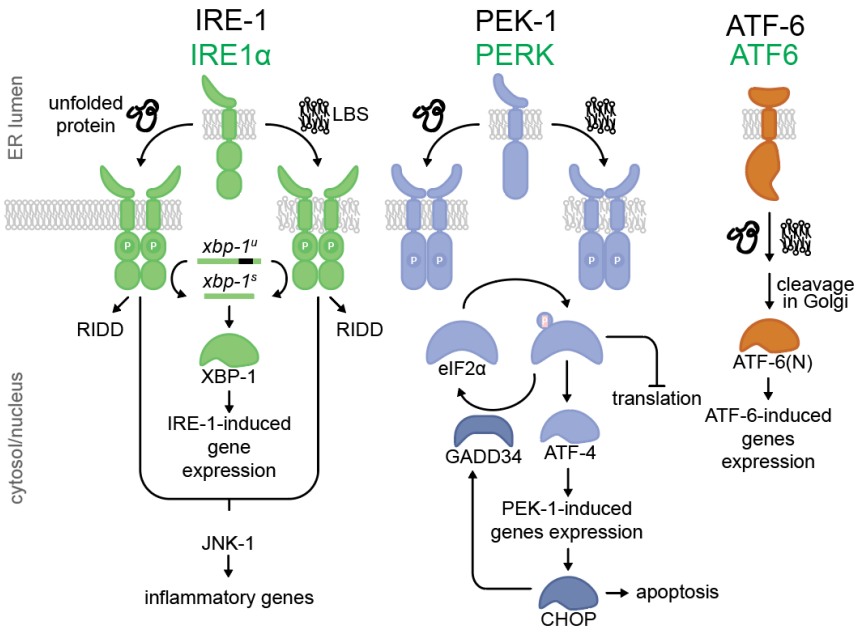

Figure 1:1: Unfolded protein response (UPR) signaling cascade in *C. elegans*.

Accumulation of misfolded proteins within the ER lumen or perturbation of the ER membrane causes ER stress and triggers UPR activation. The UPR is mediated by the three UPR transducers IRE-1, PEK-1, and ATF-6 (orthologs of mammalian IRE1α, PERK, and ATF6, shown in green text). During ER stress, IRE-1 oligomerizes and phosphorylates itself, thereby activating its ribonuclease domain and splices *xbp-1* mRNA, resulting in translation of the transcription factor XBP-1. XBP-1 then mediates downstream UPR signaling cascade. Additionally, IRE-1 also mediates regulated IRE-1-dependent decay of mRNA (RIDD) where cleavage of the RIDD substrates aids in restoring ER homeostasis. IRE-1 is also capable of activating the JNK-1 signaling pathway. Similarly, during ER stress PEK-1 oligomerizes and transautophosphorylates; this activates the cytosolic domain and GCN-2, the primary eIF2α kinase is then phosphorylated and causes translational attenuation. Upon ER stress, ATF-6 translocates to the Golgi, where it is cleaved by proteases to form an active transcription factor, ATF-6(N-terminal) which then translocates to the nucleus and regulates the UPR. Adapted from (Fun and Thibault, 2020).

1.4. Activating transcription factor 6 (ATF6) signaling pathway

ATF6 (ATF-6 in *C. elegans*) is a single-pass type II transmembrane protein (i.e., N-terminal domain is cytosolic) that is constitutively expressed in the ER (Fig. 1.2) (Haze et al., 1999). ATF6 activation upon ER stress through misfolded protein sensing or LBS entails the transportation of the integral membrane ATF6 from the ER to the Golgi apparatus for proteolytic cleavage by Site-1 protease (S1P) and Site-2 protease (S2P) (Okada et al., 2003; Shen et al., 2002; Ye et al., 2010). S1P and S2P recognize the conserved RxxL and asparagine/proline motifs of ATF6 for successive processing, respectively (Ye et al., 2000). These proteolytic events release the N-terminal domain, termed ATF6(N) which relocates to the nucleus and functions as a basic region leucine zipper (b-ZIP) transcription factor that recognizes substrates with ER stress response elements (ERSE) present in their promoter region. The ERSE generally contains the consensus sequence CCAAT-N9-CCACG (Fig. 1.2) (Roy and Lee, 1999; Yoshida et al., 1998). In addition, a later study reported that the highly responsive ER-resident membrane protein Herp contains a new ERSE with the motif ATTGG-N-CCACG, now termed ERSE-II is also regulated by ATF6(N) (Kokame et al., 2001).

Of the three UPR transducers, the precise mechanism of ATF6 activation is the least known. A study proposed that similar to IRE1 and PERK, dissociation of GRP78/BiP from the misfolded protein sensing luminal domain activates ATF6 but the underlying mechanism is still unclear. In a recent study, Tam and colleagues shed light on a possible mechanism in which ATF6 is activated through lipotoxic stress (Tam et al., 2018). Two early sphingolipid intermediates dihydrosphingosine (DHS) and dihydroceramide (DHC) directly activate the mammalian ATF6 via a unique motif found within the ATF6 transmembrane domain to mediate transcriptional activation of ATF6 target genes such as lipid synthetic and metabolic genes. Importantly, the activation of ATF6 through the transmembrane domain is independent of proteotoxic stress that would initiate the UPR through its luminal domain.

Activation of ATF6 is linked to cytoprotective and pro-survival pathways through transcriptional regulation of ER resident molecular chaperones such as GRP78 or BiP, GRP94, and calnexin (Ye et al., 2010). ATF6 also induces XBP1 expression, establishing crosstalk between the UPR pathways and signal integration (Yoshida et al., 2001). In the context of human health, ATF6 mutation was found to cause achromatopsia (total color blindness). Furthermore, similar to IRE1 and PERK, ATF6 is critical in normal development and tissue homeostasis.

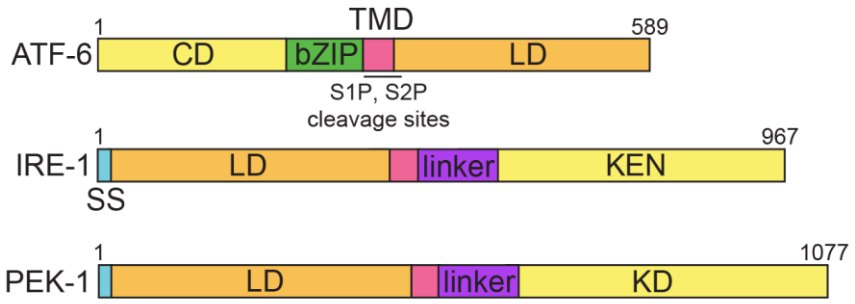

Figure 1:2: *C. elegans* ER stress sensors domains.

The cytosolic domain (CD, yellow box) of ATF-6 contains a bZIP motif (green box) that matures into a functional transcription factor when Site-1 protease (S1P) or Site-2 protease (S2P) in the Golgi apparatus cleaves ATF-6. IRE-1 and PEK-1 belong to the class of type I transmembrane protein (N-terminal within the ER lumen) whereas ATF-6 is a type II protein that is anchored with a signal-anchor sequence, which become the transmembrane domain. Unlike IRE-1 and PEK-1, C-terminus of ATF-6 is targeted to the ER lumen. In the cytoplasm, both IRE-1 and PEK-1 have a linker connecting the cytosolic domains to the transmembrane domains (TMD, pink box). In IRE-1, the kinase endonuclease domain (KEN, yellow box) serves two functions. The kinase domain allows for autophosphorylation of IRE-1 upon dimerization, which activates the endoribonuclease domain for RNase activity. The number of amino acid residues for each protein is labeled in the figure accordingly (UniProt, 2019).

1.5. Protein kinase R-like ER kinase (PERK) signaling pathway

PERK (PEK-1 in *C. elegans*) is a single-pass type 1 ER transmembrane protein that resembles IRE1. Under basal condition, the luminal domain of PERK is occupied with GRP78/BiP. Upon proteotoxic stress, BiP dissociates from the luminal domain and PERK then oligomerizes and undergoes autophosphorylation, subsequently phosphorylate the α-subunit of eukaryotic translation initiation factor-2 (eIF2α) at Ser51. This phosphorylation results in translation inhibition and induces translation of ATF4, which activates transcription of genes involved in amino acid metabolism and cell death (Harding et al., 2003; Novoa et al., 2001). eIF2α phosphorylation is considered a hallmark for PERK activation and is frequently used to detect PERK activation through immunoblotting. It attenuates global translational activity and decreases protein load entering the ER to alleviate stress.

While most protein synthesis is halted when PERK is activated, a group of transcripts with an upstream open reading frame (uORF) in the 5'-untranslated region (5'-UTR) such as activating transcription factor-4 (*ATF4*) has enhanced transcription. ATF4 induces expression of transcription factor C/EBP homologous protein (CHOP) that stimulates apoptosis and growth arrest. Additionally, CHOP also

regulates the expression of DNA damage-inducible 34 (GADD34), a negative regulator of eIF2α that serves as a phosphatase that attenuates PERK signaling by dephosphorylating eIF2α (Novoa et al., 2001; Ron and Habener, 1992; Szegezdi et al., 2006). In mammalian cells exposed to the saturated fatty acid palmitic acid, PERK was observed to activate the UPR. The evidence is strengthened by the fact that despite PERK lacks its proteotoxic stress-sensing luminal domain, the truncated PERK autophosphorylated and activate the downstream UPR pathway (Volmer et al., 2013).

1.6. Inositol-requiring enzyme 1 (IRE1) signaling pathway

IRE1 (IRE-1 in *C. elegans*) is the most evolutionarily conserved UPR pathway with the budding yeast *Saccharomyces cerevisiae* owning Ire1 as its sole UPR sensor while metazoans have two isoforms of IRE1, IRE1α that is constitutively expressed and IRE1β that is expressed in epithelial cells lining mucosal surfaces such as the epithelial cells found lining the intestine (Kaufman, 2002). It is a type 1 transmembrane protein that contains an ER luminal and a single-pass transmembrane domain with cytosolic domains containing a kinase domain and an endoribonuclease domain with RNase activity (Fig. 1.2). There are currently two models of IRE1 activation during ER stress. The first model (competition model) suggests that in a basal state the luminal domain of the monomeric IRE1 is constitutively bound to the ER chaperone BiP/GRP78. The presence of a high number of misfolded proteins in the ER lumen results in the binding of ER chaperones to those misfolded proteins and therefore titrate BiP away from IRE1, thus allowing the monomeric IRE1 to dimerize and undergo activation (Bertolotti et al., 2000; Kimata et al., 2007). The second model (direct association model) proposes that the major histocompatibility complex (MHC)-like IRE1 luminal domain senses misfolded protein directly, hence promoting its dimerization for downstream UPR activation (Credle et al., 2005). In a biological system, the two models may take place together where BiP would first recognize misfolded proteins and dissociate from IRE1, followed by direct binding of the misfolded protein to IRE1 (Kimata et al., 2007). A study in yeast has shown that dimerized Ire1 can trans-autophosphorylate nearby IRE1 monomers, acting as a seed for IRE1 to cluster into foci and form a higher-order oligomer structure (Korennykh et al., 2009). In a separate study using mammalian cells, foci formation that supports IRE1 oligomerization was also observed (Li et al., 2010). However, levels of UPR enzymatic activity resulted from IRE1 dimerization or oligomerization are still debatable. Our recent study has

shown that during lipid bilayer stress (LBS), yeast Ire1 activated the UPR despite not showing accumulation of foci as seen in DTT-treated cells, suggesting that Ire1 dimerization is sufficient for UPR activation (Ho et al., 2020).

Upon sensing of ER stress, the IRE1 monomers dimerize or oligomerize, triggering trans-autophosphorylation, activates the RNase domain, and allowing it to cleave 26 nucleotides intron from the *XBP1* mRNA (*XBP1u*, unspliced) to the mature form of *XBP1* (*XBP1s*, spliced). During this splicing event, 5' and 3' ends of the *XBP1* mRNA are ligated together by tRNA ligase. This unique phenomenon is independent of the spliceosome and typical machinery for mRNA splicing. Splicing of *XBP1* mRNA creates a frameshift that removes the premature stop codon, increases its translational efficiency, and yield a highly potent transcriptional activator that translocates to the nucleus, binds and activates the UPR elements (UPRE), and induces expression of UPR-related genes (Mori et al., 2000). Similar to ATF4 which can recognize and bind to ERSE-I and ERSE-II, XBP1 was found to bind to the CAGCAC/G consensus motif present in its substrate mRNA that encodes for ER chaperones, ERAD components, and lipid metabolism genes.

In addition to XBP1, IRE1 can also participate in regulated IRE1-dependent decay (RIDD) through the RNase domain to maintain ER homeostasis. It is worth noting that IRE-1-mediated XBP-1 activation and RIDD may occur concomitantly to achieve a desired cellular homeostasis outcome. RNase domain of active IRE1 primarily targets mRNAs encoding for secretory and transmembrane proteins that contain a dual stem-loop structure for degradation, thus reducing protein load during ER stress (Han et al., 2009; Hollien et al., 2009; Moore and Hollien, 2015). Interestingly, RIDD activity is reduced as a response to general translational inhibition by PERK, possibly due to a decrease of available mRNA substrate because of PERK activity. Paradoxically, RIDD can also induce a cell death response in the event of irreversible ER stress where it degrades pre-mRNA encoding for pro-survival proteins, ultimately induces apoptosis (Upton et al., 2012). Recently, a study has shown that RIDD controls germline differentiation in *C. elegans* independent of ER stress, demonstrating the complex role of IRE-1 in regulating various cellular processes (Levi-Ferber et al., 2020).

The primary role of IRE1 is to restore ER homeostasis and ensure cell survival. However, during chronic ER stress that cannot be unmitigated, IRE1 can switch its signaling pathway to favor apoptosis. When IRE1 oligomerizes, its kinase domain interacts with the tumor necrosis factor receptor-associated factor

2 (TRAF2), resulting in the activation of apoptosis signal-regulating kinase (ASK1) and its downstream target c-jun NH2-terminal kinase (JNK) and p38-MAP kinase (MAPK). ASK1 phosphorylation of JNK1 inhibits anti-apoptotic factors such as BCL2 and MLC1 while stimulates pro-apoptotic factors BID, BIM, and PUMA (p53 upregulated modulator of apoptosis) (Deng et al., 2001; Kim et al., 2009). Furthermore, BIM and PUMA have also been proposed to directly interact with IRE1 through their BH3 domains and promote sustained activation of IRE1 (Rodriguez et al., 2012). Interestingly, JNK1 signaling can also have a pro-survival role where JNK1 phosphorylation of BCL2 dissociates BCL2 from Beclin1, thereby promote autophagy and thus cell survival (Wei et al., 2008a).

From an evolutionary perspective, the presence of three UPR sensors may seem redundant. However, studies have uncovered that they serve more purposes other than sensing ER stress such as tissue differentiation and organism development. In addition, each of the sensors may be temporally regulated differently and they may regulate each other as in the case where ATF6 controls transcription of *XBP1* mRNA or PERK regulates RIDD activity.

1.7. UPR and lipid metabolism

One of the earliest pieces of evidence that connects lipid metabolism to Ire1 was done in the budding yeast where inositol was found to be required for the growth of the yeast *IRE1* deletion mutant (Nikawa and Yamashita, 1992). In the absence of inositol, which is required for membrane phospholipid synthesis, IRE1 is strongly activated (Cox et al., 1997). Downstream of IRE1, XBP1 has been implicated in lipid metabolism. By using hepatocyte specific conditional *XBP1* knockout mice, hepatocytes lacking XBP1 have reduced *de novo* lipid biosynthesis (Lee et al., 2008). The transcriptional targets of XBP1 include lipogenic factors such as diacylglycerol acetyltransferase 2 (DGAT2), stearoyl-CoA reductase 1 (SCD1), and acetyl-CoA carboxylase (ACC2). In a large-scale screening in yeast, deletion of lipid processes genes caused heightened UPR signaling in yeast (Jonikas et al., 2009). Previously, we have demonstrated that changes in membrane lipid composition through the ablation of the *de novo* phosphatidylcholine (PC) biosynthesis gene OPI3 (mammalian PEMT ortholog) activate the essential intervention of the UPR to remodel the protein homeostasis network in budding yeast (Thibault et al., 2012). The UPR is directly activated from ER membrane LBS independent from the accumulation of misfolded proteins (Adams et al., 2019; Volmer et al., 2013). A study demonstrated a piece of more

convincing evidence that lipotoxic stress may directly activate the UPR independent of the effect from proteotoxic stress in yeast where deletion of subregion III of the misfolded protein sensing luminal domain (henceforth named ΔIII) mutant rendered Ire1 insensitive to proteotoxic stress while activating the UPR through inositol depletion (Promlek et al., 2011). As mentioned in the earlier section, near-total deletion of IRE1 and PERK luminal domains in mammalian cells retained their ability to sense an increase in lipid saturation through palmitic acid supplementation (Volmer et al., 2013). Recently, it was proposed that the amphipathic helix located near the transmembrane domain of yeast Ire1 senses biophysical changes to the ER phospholipid bilayer during LBS, thus changing its configuration and allowing it to interact with proximal Ire1 to dimerize or oligomerize (Halbleib et al., 2017). Furthermore, we have also demonstrated that a mutation located at the interface of the amphipathic and transmembrane helices rendered Ire1 insensitive to detect LBS (Ho et al., 2020). In addition, we showed that deletion of the Ire1 luminal domain retained the ability of Ire1 to stimulate the UPR program during LBS that is vastly divergent from proteotoxic stress (Ho et al., 2020). In mammalian cells however, mutation in the amphipathic helix did not inactivate the ability of IRE1 in sensing LBS (Cho et al., 2019). Instead, a serine and tryptophan residues found within the transmembrane helix were reported to be necessary for the for IRE1 dimer formation during palmitic acid-induced LBS. The identification of various lipid-sensing residues within the transmembrane domain in different organisms highlights the conserved function of IRE1 as a lipid sensor.

Purified hepatic ER from obese mice showed altered phosphatidylcholine to phosphatidylethanolamine (PC/PE) ratio and inhibition of sarco/endoplasmic reticulum calcium ATPase (SERCA) activity, thus activating chronic ER stress (Fu et al., 2011). PC is the most abundant phospholipid in eukaryotic biological membranes, followed by PE (Casares et al., 2019). Perturbed PC/PE molar ratios are linked to metabolic disease progression, highlighting the role of these abundant phospholipids in regulating energy metabolism (van der Veen et al., 2017). PC is synthesized at the ER and its biosynthesis is important for proper ER function. There are two evolutionary conserved PC biosynthetic pathways in eukaryotes, including *C. elegans* (Brendza et al., 2007; Lochnit and Geyer, 2003). The CDP-DAG pathway involves synthesis of PC from PE while the Kennedy pathway utilizes choline acquired from diet to synthesize PC that is responsible for the majority of PC synthesis in most tissues (Fagone and Jackowski, 2013; Li et al., 2006). In the CDP-DAG pathway, also known as the Bremer-Greenberg pathway, methylation of phosphatidylethanolamine by PE N-methyltransferase (PEMT) to

phosphatidylmonomethylethanolamine (pMME) is followed by two-step methylation by PEMT to phosphatidyldimethylethanolamine (pDME) and subsequently to PC. This process is mostly found to occur in the mitochondria and ER of hepatocytes and adipocytes in mammals (Horl et al., 2011; Jon Bremer, 1961; Shields et al., 2003). In *C. elegans*, methylation-dependent PC synthesis occurs through the S-adenosylmethionine-dependent phosphoethanolamine N-methyltransferase pathway that is different from the CDP-DAG pathway in mammals (Brendza et al., 2007; Palavalli et al., 2006; Walker et al., 2011). Simultaneously blocking the two PC biosynthesis pathways from the ablation of the gene encoding for PEMT and the deprivation of dietary choline in mice leads to hepatic ER stress that correlates with steatosis progression (Li et al., 2006). These observations link lipid perturbation, ER stress, and metabolic diseases.

The cause of chronic ER stress may not be singular and can be attributed to perturbation in several cellular processes. Altered hepatic lipid content overtime triggers *de novo* lipogenesis that is composed of a higher level of saturated fatty acids (SFAs), possibly leading to ER stress activation (Volmer et al., 2013). Furthermore, consistent with the finding that PC/PE ratio is altered in obese mice, genes regulating PE and PC synthesis, choline-phosphate cytidyltransferase A (*PCYT1A*) and phosphatidylethanolamine N-methyltransferase (*PEMT*) had increased levels as well (Fu et al., 2011). Similar to the NAFLD mouse model lacking the *PEMT* gene (Li et al., 2006; Li et al., 2005), we utilized a yeast model lacking the *OPI3* (*PEMT* homolog) gene and showed LBS altered the biochemical landscape of the yeast cells by activating the UPR and remodeled the protein homeostasis network through cellular process such as ERAD. In another study, LBS caused by *OPI3* deletion selectively degrades a subset or ER-resident protein presumably as a consequence of altered membrane properties that lead to destabilization of these ER proteins (Shyu et al., 2019). In addition, accumulation of lipid droplets (LDs) was also observed, presumably a mechanism to circumvent lipotoxicity by shuttering excess lipids into the relatively inert LD (Lee et al., 2012; Li et al., 2011; Thibault et al., 2012).

C. elegans models have been developed to block PC synthesis by the loss-of-function (lof) mutants of *PEMT* orthologs *pmt-1* and *pmt-2* or the upstream precursor S-adenosylmethionine synthetase 1 (*sams-1*) (Ding et al., 2015). In *sams-1* RNA interference (RNAi) worms, PC synthesis is drastically reduced due to the lack of precursor S-adenosylmethionine (SAMe) as the methyl donor. As a result, LD accumulation, which is characteristic of NAFLD, was observed (Walker et al., 2011). In another

study, depletion of *mdt-15*, a subunit of the transcriptional regulator complex Mediator, was shown to increase membrane saturation and activate IRE-1 and PEK-1 without significant alteration in the proteostasis state of the organism (Hou et al., 2014). This suggests that UPR activation during LBS can occur independently of misfolded protein triggered UPR.

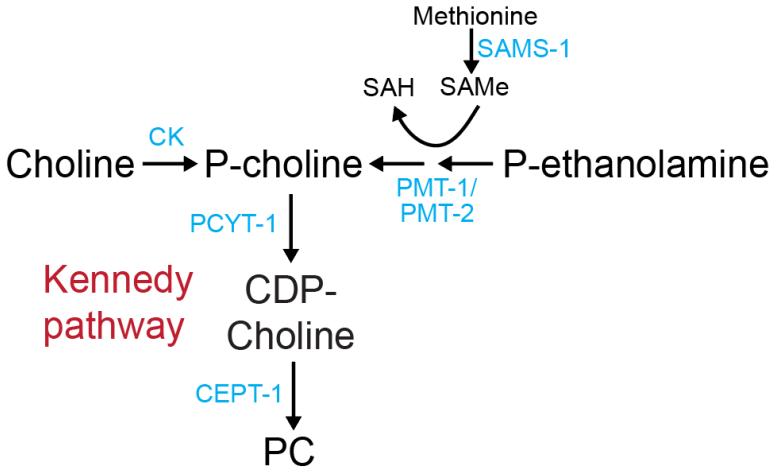

Figure 1:3: Phosphatidylcholine (PC) synthesis pathways in *C. elegans*.

There are two known PC biosynthesis pathways in *C. elegans*. The methylation-dependent biosynthesis of PC starts with a three-step methylation of P-ethanolamine by phosphoethanolamine N-methyltransferase-1 and 2 (PMT-1 and PMT-2) with *S*-adenosylmethionine (SAMe) as methyl donor in each successive step to P-choline, while liberating *S*-adenosylhomocysteine (SAH) in the process, then undergoes the rate-limiting catalysis by PCYT-1 and CEPT-1 to PC. S-adenosylmethionine synthetase (SAMS-1) catalyzes SAMe formation from methionine. Alternatively, PC can be synthesized through the Kennedy pathway via choline acquired from the diet by choline kinase (CK), choline-phosphate cytidylyltransferase (PCYT-1), and choline/ethanolaminephosphotransferase 1 (CEPT-1). Human orthologs are shown in brackets. Modified from (Walker et al., 2011).

1.8. Autophagy

As described above, the UPR is essential for alleviating burdens to the ER caused by proteotoxicity and lipid perturbation. In addition to translational attenuation, ER chaperone induction of apoptosis, autophagy activation was identified as a protective signaling pathway during ER stress. The link between the UPR and autophagy is demonstrated by showing the requirement of IRE1 in activating autophagy through the IRE1-JNK (c-Jun N-terminal kinase) axis, where ablation of IRE1 results in reduced autophagic activity and persistent ER stress (Ogata et al., 2006). Autophagy is a catabolic process that degrades and recycles cytoplasmic components through the lysosomes. The now well-

characterized program comprises more than 30 autophagy-related (ATG) genes that can be broadly characterized into three processes: macroautophagy, microautophagy, and chaperone-mediated autophagy (Fig. 1.4). In macroautophagy, the pre-autophagosomal structure (PAS) formation kickstarts the autophagy process. As the phagophore forms, more autophagy-related proteins are recruited to the cargo, forming autophagosomes. One such autophagy-related protein is LGG-1 conjugated to PE. Lipidated LGG-1 contributes to autophagosome maturation and the autophagosome then fuses with the lysosome to form autolysosome (Nakatogawa et al., 2007). Contents within the autolysosome are degraded in an acidic environment by the hydrolases and their building blocks released. Microautophagy is a non-selective process and is mediated by the direct fusion of cytosolic components to the lysosome through membrane invagination. Chaperone-mediated autophagy (CMA) substrates require the presence of the amino acid motif KFERQ that is recognized by cytosolic chaperones such as heat shock protein-1 (HSP-1). The substrate-chaperone complex then translocates through the receptor lysosome-associated membrane protein type 2 (LMP-2) and subject for degradation.

In addition to regulating protein homeostasis, autophagy has also been shown in regulating lipid metabolism where autophagy is required for LD breakdown during a high-fat diet (Singh et al., 2009). A subtype of macroautophagy, hereby termed lipophagy, is involved in the facilitation of LD components for degradation to the lysosomes by lysosomal enzymes (Singh et al., 2009). In *C. elegans*, lipophagy is initiated by BEC-1 (ortholog of mammalian Beclin 1), along with other autophagy-related proteins such as VPS-34 and VPS-15 (Liang et al., 2001). LGG-1-PE positive autophagosome then engulfs LDs to form lipoautophagosome. Lipoautophagosome delivers LDs to lysosomes where lipase such as LIPL-4 degrades the lipid cargo and liberate FFAs (Lapierre et al., 2011). In short, different cellular stressors have been shown to stimulate autophagy activation through distinct UPR transducer. However, to our knowledge, the mechanism on how ER lipid perturbation stimulates autophagy through the UPR is still an important question that has not been addressed.

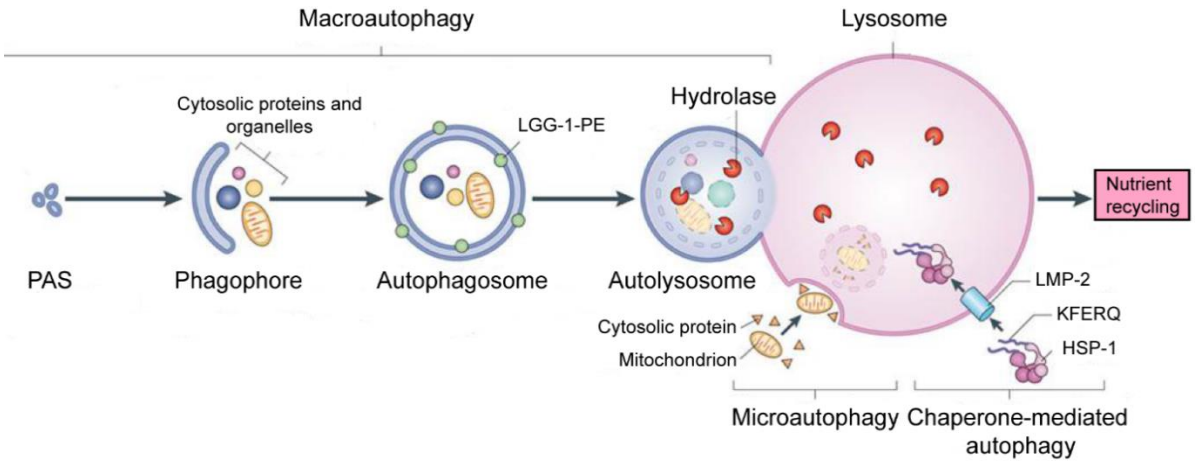

Figure 1:4: Autophagy pathway in *C. elegans*.

Three modes of autophagy: macroautophagy, microautophagy, chaperone-mediated autophagy are involved in different aspects of cellular material recycling and stress response. In autophagy, a portion of the cellular material is wrapped inside an autophagosome mediated by ATG genes, the now double membrane bound vesicle then fuses with the lysosome to form autophagolysosome. The acidic environment within the autophagolysosome is mainly composed of lysosomal hydrolases breakdown of the cellular materials. During microautophagy, lysosome invaginations trap cytosolic materials such as proteins and mitochondria for degradation and the subsequent cellular building block recycling. In chaperone-mediated autophagy (CMA), soluble CMA substrates containing KFERQ amino acid motif are recognized by cytosolic heat shock protein-1 (HSP-1), and the substrates are subjected to degradation in the lysosome by translocating through the multimeric LMP-2. Adapted and modified from (Kaur and Debnath, 2015).

1.9. Research gap

Most studies have focused on dissecting the mechanism of the UPR through proteotoxic ER stress stimulation by pharmacological agents such as N-linked glycosylation inhibitor tunicamycin or the reducing agent dithiothreitol (DTT). Disruption of protein modification within the ER lumen by tunicamycin or DTT causes the accumulation of misfolded proteins. The luminal domain of IRE-1 then directly binds to the misfolded proteins through the peptide-binding groove, which dimerizes with other proximate IRE-1 monomers to form higher-order IRE-1 oligomers that can trans-autophosphorylate and, thus activating the downstream UPR program. While the UPR function in resolving proteotoxic stress is well-established, the mechanism on how the UPR contributes to the pathology of lipotoxicity-related in NAFLD and T2D is less elucidated. One of the main functions of the UPR involves lipid synthesis. Unsurprisingly, disruption of lipid homeostasis in metabolic diseases compromise ER

function, leading to disease development. Lipid dependent activation of the UPR has been shown through saturated fatty acids loading to yeast and mammalian cells, disruption of sphingolipids synthesis, and disruption of ER membrane precursor synthesis through inositol depletion and blockage of PC synthesis (Cox et al., 1997; Hou et al., 2014; Tam et al., 2018; Thibault et al., 2012; Volmer et al., 2013). Additionally, the lipid sensing capability of the UPR sensors during LBS has been shown through characterization of mammalian ATF6, yeast Ire1 and mammalian PERK transmembrane domain capable of detecting LBS through their transmembrane domains (Ho et al., 2020; Tam et al., 2018). However, most studies mentioned were performed in an *in vitro* environment or done in yeast with Ire1 as its sole UPR sensor. To dissect the UPR regulation more comprehensively during LBS, we propose the use of the animal model *C. elegans*.

1.10. Research aims and thesis organization

In this study, we characterized the UPR function during LBS-induced chronic ER stress. We hypothesized that LBS may elicit chronic ER stress that is distinctly different from acute ER stress. Of the three UPR pathways, the IRE1-XBP1 axis is the most evolutionary conserved. Because of the large cellular pathways IRE1 regulates, it presents itself as a lucrative target for therapeutics and warrants our attention for further studies. Despite a vast number of studies done on IRE1, a thorough mechanistic insight on how IRE1-XBP1 axis signaling is controlled under various stress conditions as well as its function in different tissues remains incomplete. By utilizing the *C. elegans*, together with the robust genetic, biochemical, and cellular tools available, we focused on dissecting the role of IRE1 and understand its physiological relevance in mediating homeostasis response during LBS.

To dissect the UPR function during LBS independent from proteotoxic stress, we constructed UPR mutants lacking the misfolded protein-sensing luminal domains. We first focused our effort on characterizing the IRE-1 function devoid of its luminal domain. Next, to establish *C. elegans* as a model for LBS, we sought out to explore experimental conditions that can stimulate UPR^{LBS}. Firstly, we attempted to alter the membrane lipid saturation in worms through cold stress and high glucose diet (HGD) exposure. We confirmed the change in lipid composition in worms through fatty acid analysis. Cold stress-induced lipid unsaturation and HGD-induced lipid saturation activated the UPR,

corroborating earlier finding where the UPR sensors could directly detect a change of lipid composition (Volmer et al., 2013).

Subsequently, we aimed to recapitulate the process of LBS through the induction of PC deficiency. In *C. elegans*, synthesis of PC through the CDP-DAG pathway is largely similar to mammals except for the participation of PMT-1 and PMT-2 enzymes instead of PEMT. By raising the UPR mutants, *atf-6(lof)*, *ire-1(lof),* and *pek-1(lof)*, in a choline-deficient environment and simultaneously knocking down *pmt-2* with RNAi, we were able to dissect the UPR activation upon LBS. As expected, genetic attenuation of *pmt-2* resulted in the perturbation of lipid homeostasis with a large decrease of PC level, which correlates with the UPR activation. Although conventionally seen as a linear response from ER stress, our findings demonstrate a strikingly different outcome of the UPR program when activated from LBS-induced (UPR^{LBS}) as opposed to proteotoxic-induced (UPR^{PT}) ER stress. Interestingly, the data indicate that the ER stress sensor IRE-1 is necessary to restore lipid homeostasis by regulating the autophagy pathway suggesting a reciprocal relationship between lipid homeostasis and autophagy as mediated by the UPR to prevent excessive lipid droplet accumulation. Hence, answering these questions will further our understanding of the nature of metabolic diseases and uncover strategies to overcome the diseases.

In our further studies, we aim to identify other lipid processes-related factors that may play a role in IRE-1 activation. Hence, an enhancer RNAi screen consisted of lipid metabolism-related genes was carried out using *ire-1(lof)* worms. We hypothesized the lack of IRE-1 may eliminate the main compensatory function of the UPR in restoring lipid homeostasis during lipid dysregulation caused by gene silencing. From our screen, we identified the lack of phosphatidic acid phosphatase protein LPIN-1 (mammalian Lipin1 homolog) may activate IRE-1 in a yet unknown mechanism, prompting further investigation.

Chapter 2: Materials and Methods

2.1. Statistics

Error bars indicate standard error of the mean (s.e.m.), calculated from at least three biological replicates unless otherwise indicated. P values were calculated using one-way ANOVA with Tukey's post hoc test unless otherwise indicated and reported as P values with 4 significant digits in the figures. All statistical tests were performed using GraphPad Prism 7 software.

2.2. *C. elegans* strains, growth conditions, and RNAi constructs

All strains were grown at 20°C using standard *C. elegans* methods as previously described (Brenner, 1974; Stiernagle, 2006). Nematode growth media (NGM) agar plates were seeded with *Escherichia coli* strain OP50 for normal growth and with HT115 bacteria for RNAi feeding. The OP50 strain used is a uracil auxotroph to prevent excessive bacterial growth in the NGM media that may obstruct observation of the worms. RNAi feeding was performed as previously described (Timmons and Fire, 1998), and the RNAi library was obtained from the Fire lab (Timmons and Fire, 1998). The plasmids were sequenced with pL4440-RNAi primer (Table 2.2) to confirm their identity. The strains used in this study are listed in Table 2.1. For autophagy induction, worms at larval stage 4 (L4) were collected in M9 buffer and treated with 1 mM spermidine (Sigma-Aldrich, St. Louis, MO) for 16 h at 20°C with shaking.

Table 2.1: Strains used for this study.

Strain	Genotype	Strain origin
CGT0001	N2	CGC
KP3948	*eri-1(mg366) IV; lin-15B(n744) X*	CGC
RB545	*pek-1(ok275) X.*	CGC
RB772	*atf-6(ok551) X.*	CGC
RB925	*ire-1(ok799) II*	CGC
VC1952	*pmt-2(ok2419) V*	CGC
VC8	*jnk-1(gk7) IV*	CGC
AGD927	*rab-3p::xbp-1s, myo-2p::tdTomato*	(Taylor and Dillin, 2013)
AGD1379	*gly-19p::xbp-1s;myo-2p::tdTomato*	(Taylor and Dillin, 2013)
DA2123	*lgg-1p::GFP::lgg-1 + rol-6(su1006)*	(Kang et al., 2007)
SJ17	*zcIs4[hsp-4::GFP]; xbp-1(zc12)*	(Calfon et al., 2002)

SJ4005	*zcIs4 [hsp-4::GFP] V*	(Calfon et al., 2002)
VS25	*vha-6p::GFP::C34B2.10(SP12)*	(Xu et al., 2012)
CGT0147	*pek-1(ok275) backcross six times*	This study
CGT0151	*atf-6(ok551) backcross six times*	This study
CGT0207	*eri-1;;plgg-1p::gfp::lgg-1*	This study
CGT0237	*ire-1(ok799) backcrossed three times*	This study
CGT0252	*ire-1p::3xHA::ire-1ΔLD(sybSi11); ire-1(ok799) II*	This study
CGT0252	*ire-1p::3xHA::ire-1ΔLD(sybSi11); ire-1(ok799) II*	This study
CGT0265	*hsp-4p::gfp;ire-1p::3xHA::ire-1ΔLD(sybSi11)*	This study
CGT0269	*ire-1(ok799) II, H435F amino acid substitution*	This study
CGT0270	*ire-1(ok799) II, T442A amino acid substitution*	This study
CGT0271	*ire-1(ok799) II, W455A amino acid substitution*	This study
PHX1204	*ire-1p::3xHA::ire-1ΔLD(sybSi11)*	This study
PHX933	*atf-6 (syb933)*	This study
PHX951	*pek-1(syb951)*	This study

2.3. RNAi by feeding

RNAi was carried out as previously described (Timmons and Fire, 1998). Briefly, HT115 bacteria harboring pL4440 plasmids were grown in LB medium containing 100 µg/ml ampicillin at 37°C until log phase (OD_{600} 0.6) and seeded onto NGM agar plates containing 50 µg/ml carbenicillin and 1 mM isopropyl β-D-1-thiogalactopyranoside (IPTG). Gravid adult worms were treated with hypochlorite and eggs were hatched overnight in M9 buffer (0.02 M KH_2PO_4, 0.04 M Na_2HPO_4, 0.09 M NaCl, and 0.12 M $MgSO_4$) at 20°C to obtain larval stage 1 (L1) synchronized worms. Hatched L1 larvae were transferred to RNAi agar plates and grown until L4 larval to young adult stages. L4/young adult worms were harvested and incubated with 25 µg/ml tunicamycin in M9 medium for 4 hours at 20°C followed by M9 washes when indicated. To measure body length, worms were transferred to 6 cm NGM plates without bacteria. Bright field images were acquired with a dissecting microscope (Nikon SMZ1500) fitted with a JVC digital camera at 100X magnification. Length measurements were performed in Fiji with the WormSizer plugin (Moore et al., 2013). For double RNAi feeding, worms were fed with an equal amount of HT115 bacteria harboring pL4440 plasmids and the efficacy of gene silencing was assessed by quantitative real-time PCR.

2.4. Quantitative real-time PCR

Ten thousand L4/young adult worms were collected, resuspended in M9 buffer, and lysed by bead beating. Total RNA was isolated using TRIzol reagent (Thermo Fisher, Waltham, MA) and subsequently purified using RNeasy Mini (Qiagen, Venlo, Netherlands) columns following the manufacturer's protocols. DNase treatment in columns was carried out with RNase-Free DNase (Qiagen, Venlo, Netherlands) following manufacturer's protocol. cDNA was synthesized from 2 µg of total RNA using RevertAid Reverse Transcriptase (Thermo Fisher, Waltham, MA) following manufacturer's protocol. SYBR Green quantitative real-time PCR (qPCR) experiments were performed following the manufacturer's protocol using a QuantStudio 6 Flex Real-time PCR system (Applied Biosystems, Waltham, MA). Thirty nanograms of cDNA and 50 nM of paired-primer mix were used for each reaction. Relative mRNA was determined with the comparative Ct method (ΔΔCt) normalized to housekeeping gene *act-1*. Oligonucleotides used in this study are listed in Table 2.2.

Table 2.2: List of primers used in this study.

Gene	Sequence (5' to 3')	Assay
act-1	Forward (F): AGGACTGGGTGCTCTTCTGG Reverse (R): GAGCACGGTATCGTCACCAA	qPCR
atg-16.2	F: ATGTGCTGGCTGGATCTTCG R: GAGCCGAATCTGATCTCGCAG	qPCR
atg-18	F: CCGAAGTCAGACACTAGTCGAG R: TCGGAACCGATTGGTTGCTTG	qPCR
atg-4.1	F: AGGAAGATGGAATCGAGGCAA R: TGCAACCCCATCCTTGATCC	qPCR
atg-9	F: ATGGAATCGTTCTTCTCACTG R: GCAGGAGGTATTGTATCTTCTC	qPCR
bec-1	F: AAGCTCTGACTGGACATTCTCG R: GCGTCAGAGCAATCATTACAAAC	qPCR
C02F5.5	F: CATCTTTTGAGCTTATGATGGTGCT R: AAGCACCAAGGAACACGAGAT	qPCR
cht-1	F: TTGGGCTGGAGAAGGAATGT R: ACTCCATCCTCCGAACGAGA	qPCR
creb (F40F12.7)	F: CATTGCCCGATGTGATCAGT R: CTGACATTGCCGAAGATCCA	qPCR
epg-4	F: CCAATTCCTCTTATCACACCA R: GTCGAAGAAGTAATCGAAACAG	qPCR
F26D2.10	F: CTCTTGTGGCAGCTCATGGT R: CGTGGATCAAAAACAGCGGC	qPCR
fat-5	F: GTTCCAGAGGAAGAACTACCTCCCC R: GGGTGAAGCAGTAACGGAAGAGGGC	qPCR
hsp-3	F: AGAAGGAGACCAAGTATGGAACC R: TGATACGGTTTCCTTGGTCGTT	qPCR
hsp-3	F: AGAAGGAGACCAAGTATGGAACC R: TGATACGGTTTCCTTGGTCGTT	qPCR
hsp-4	F: CATCTCGTGGAATCAACCCT R: TGACGTCAAGAAGGACAACA	qPCR
hsp-4	F: CATCTCGTGGAATCAACCCT	qPCR

	R: TGACGTCAAGAAGGACAACA	
ire-1	F: ACAATGGCTAGTCAGCGAGG R: CAATCCAGCCATCGGTTCCT	qPCR
lgg-1	F: TCGTGATGGTCCTGGTAGAGT R: ACGCATCCAACTTCGTCCA	qPCR
pL4440-RNAi	GTTTTCCCAGTCACGACGTT	Sequencing primer
pmt-2	F: AGAACGTGGTCATTTGGAGCAG R: TTCGCGTTGGGTAAACTTCGAC	qPCR
xbp-1	F: TCCGCTTGGGCTCTTGAGATGTTC R: TGTCGTCGTCGGAGGAGAGGATCG	RT-PCR

2.5. Lipid extraction and phospholipid analysis

Approximately 10,000 L4 to young adult worms were harvested and washed thoroughly with M9 buffer, lysed with 1 mm silica beads by bead beating, and subsequently lyophilized overnight (Virtis). All subsequent steps were carried out at 4°C. Total lipids were extracted from dried samples with chloroform:methanol (2:1) and concentrated. Total lipid extracts and POPE (1-palmitoyl-2-oleoyl-sn-glycero-3-phosphoethanolamine; 16:0-18:1n9 PE; Avanti Polar Lipids, Alabaster, AL) / DOPC (1,2-dioleoyl-sn-glycero-3-phosphocholine; 18:1n9 PC; Avanti Polar Lipids, Alabaster, AL) standard mix were spotted on high-performance thin-layer chromatography (HPTLC) Silica gel 60 plates (Merck) using Linomat 5 (CAMAG, Switzerland) and separated with chloroform:methanol:acetic acid:acetone:water (35:25:4:14:2). Phospholipids were visualized under long-wave ultraviolet (λ = 340 nm) by spraying 0.05 mg/ml of primuline dye in acetone:water (80:20) onto the dried plates. Spots corresponding to PE and PC were scraped off the silica plates and transferred into 2 ml glass tubes. One hundred microliters of 1 mM C15:0 (pentadecanoic acid) was added to the tubes containing silica-bound phospholipids as an internal standard. The phospholipids were hydrolyzed and esterified to fatty acid methyl esters (FAME) with 300 µl of 1.25 M HCl-methanol for 1 h at 80°C. FAMEs were extracted three times with 1 ml of hexane. Combined extracts were dried under nitrogen, resuspended in 100 µl hexane. FAMEs were separated by gas chromatography with flame ionization detector (GC-FID) (GC-2014; Shimadzu, Kyoto, Japan) using a ULBON HR-SS-10 50 m x 0.25 mm column (Shinwa, Tokyo, Japan). Supelco 37 component FAME mix was used to identify corresponding fatty acids (Sigma-Aldrich, St. Louis, MO). Data were normalized using the internal standard C15:0 and worm dry weight.

2.6. Lipid droplets analysis by Oil-Red-O

Following RNAi feeding, lipid droplets of L4 to young adult stage worms were stained with Oil-Red-O (ORO) (Sigma-Aldrich, St. Louis, MO). The worms were collected and washed thrice with PBS (137 mM NaCl, 2.7 mM KCl, 10 mM Na_2HPO_4, and 1.8 mM KH_2PO_4 in distilled water), allowed to settle by

gravity, then permeabilized for 1 h at room temperature with equal volume of PBS and 2X MWRB buffer (160 mM KCl, 40 mM NaCl, 20 mM EDTA, 10 mM spermidine, 30 mM HEPES and 50% methanol) containing 2% paraformaldehyde. Permeabilized animals were washed once with PBS. Three-hundred microliters of 60% isopropanol were then added, and the worms were incubated for 15 minutes. Thereafter, pelleted worms were incubated for 2 h at room temperature in 1 ml ORO working solution. The working solution is prepared by diluting 5 g/L ORO stock solution in isopropanol with water to a final concentration of 60% ORO per volume. Thereafter, the worms were allowed to settle with gravity, followed by two washes of PBS containing 0.01% Tween and a small number of worms were pipetted onto 2% agarose pads for imaging. The samples were imaged with a Zeiss Live Cell Observer fluorescence microscope at 10X magnification (Zeiss) taken with AxioCam IC color camera (Zeiss) with the same exposure settings used across all the conditions. Using ImageJ, the RGB images were split into their respective color channel while images from the green channel were retained for further analysis as the maximum molar extinction coefficient of ORO falls between 510-517 nm that is closest to the wavelength of the green channel (Ramirez-Zacarias et al., 1992). The images were inverted and the intensity of the ORO staining immediately behind the pharynx of each worm was measured with the oval selection tool with a fixed area of 70 pixels radius across all the samples. The intensity of ORO staining is derived from the mean intensity of ORO stain minus the average mean intensity of the background multiplied by the area of selection (Yen et al., 2010).

2.7. Lipid droplets analysis by Sudan Black

Following RNAi feeding, lipid droplets of L4 worms were stained with Sudan Black B (Sigma-Aldrich, St. Louis, MO) as described previously with few modifications (Ogg and Ruvkun, 1998). Briefly, worms were fixed in 1% paraformaldehyde in M9 buffer for 30 minutes at room temperature, followed by three freeze-thaw cycles using liquid nitrogen. Worms were washed once with M9 and gradually dehydrated with 25%, 50%, and 70% ethanol. Subsequently, fixed worms were stained with 50% saturated Sudan Black B in 70% ethanol (filtered with 0.22 µm membrane) for 30 minutes at room temperature with rocking. Stained worms were washed once with 25% ethanol for 30 minutes with rocking. Worms were mounted on 2% agarose pads for imaging. Bright-field images of worms were taken with DMi8 inverted epifluorescence microscope (Leica, Wetzlar, Germany) with 20x and 63x objective lenses. To quantify lipid droplets, TIFF images taken at 63x magnification were converted to 8-bit grayscale, followed by background subtraction and thresholding with Fiji imaging software. Lipid droplets were divided into

three size groups based on the diameter of LDs: small (0.8 - 3 µM), medium (3.1 - 6 µM), and large (> 6 µM). The percentage of LDs per size group against the sum of measured LDs per condition was presented.

2.8. Cold stress treatment

Age-synchronized day 1 adult worms grown on OP50 bacteria were divided into two cohorts. One cohort was grown at their physiological temperature of 20°C, while another cohort was grown in a 2.1°C incubator for 24 h. After 24 h, the cold stress cohort worms were harvested with M9 buffer stored in the same incubator, thus minimizing temperature fluctuation during the washing process. For each condition, roughly 20,000 worms were washed three times with M9 buffer and prepped for total fatty acid analysis described above. For fluorescence imaging, the worms were picked at 0 h, 10 h, 24 h, 48 h during the cold stress treatment, mounted on an agarose pad, and imaged immediately.

2.9. Epifluorescence imaging of *hsp-4p::gfp* worms

hsp-4p::gfp worms challenged with cold stress (described in Section 2.8) were mounted on a 2% agarose pad and anesthetized by using 500 mM sodium azide prepared in M9 buffer (Sigma). Images of the worms were captured by using an AxioCam (Zeiss) camera attached to Zeiss Axio Observer microscope. ImageJ (Schneider et al., 2012) was used to quantify the fluorescence intensity of the whole worm body and the background signals were subtracted to obtain final fluorescence intensity.

2.10. High glucose diet feeding

Gravid adult worms were treated with hypochlorite and the eggs were hatched overnight in M9 medium at 20°C with rocking to obtain L1 synchronized worms. On the next day, hatched L1 worms were seeded onto NGM agar plates with UV-killed OP50 bacteria and allowed to grow to L3/L4 stage. UV-killing of OP50 was carried out in a biosafety cabinet with the UV light turned on overnight. The agar plate lid was removed to ensure adequate exposure of the UV to the bacteria lawn. The L3/L4 stage worms were then transferred to fresh NGM plates with UV-killed bacteria containing 50 mM 5-fluorodeoxyuridine (FUDR) and allowed to grow until adulthood (ChemGood, catalog number C-1484). The worms raised in this condition are denoted as normal diet (ND). At day 1 of adulthood, a subset of the worms was transferred to NGM plates with UV-killed bacteria containing 50 mM FUDR and 2% glucose (v/v) for 24 hours. This batch of worms was denoted as high glucose day 1 (HGD1) worms. Separately, at day 5 of adulthood, another subset of worms that were grown under ND condition was

transferred to NGM plates with UV-killed bacteria containing 50 mM FUDR and 2% glucose (v/v) for 24 hours. This batch of worms was denoted as high glucose day 5 (HGD5) worms. The HGD1 and HGD5 worms were collected for fatty acid analysis at different time-points and are accompanied by their respective ND controls.

2.11. Lipid extraction and total fatty acid analysis of HGD-fed worms by GC-FID

Approximately 10,000 adult worms were harvested, washed thoroughly with M9 buffer, and homogenized by bead beating three times for 30 s at 6,500 rpm. A portion of the lysates was cleared, and protein concentration was measured by using a BCA assay kit (Thermo Scientific). Protein concentration was used to adjust the lysate used to the same amount for fatty acids extraction. Thereafter, the lysates were transferred to glass tubes and lyophilized overnight. One hundred microliters of 1 mM C15:0 (pentadecanoic acid) and 1 mM C23:0 (lignoceric acid) were added to the tubes as internal standards. The worms were hydrolyzed and esterified to FAME with 500 µl of 1.25 M HCl-methanol for 1 h at 80°C. FAMEs were extracted three times with 1 ml of hexane. Combined extracts were dried under nitrogen gas, resuspended in 20 µl hexane. FAMEs were separated by gas chromatography with flame ionization detector (GC-FID) (GC-2014; Shimadzu, Kyoto, Japan) using a ULBON HR-SS-10 50 m x 0.25 mm column (Shinwa, Tokyo, Japan). Supelco 37 component FAME mix was used to identify corresponding fatty acids (Sigma-Aldrich, St. Louis, MO). At the end of the run, retention times of fatty acids in the chromatograms are compared to the standard and manually aligned and then peaks were partitioned into bins according to retention time values. Data were normalized using the internal standard C15:0, C23:0. Heatmap was prepared with GraphPad Prism 8.

2.12. Immunoblotting

Five thousand worms treated with RNAi were collected, washed in M9 buffer, and subsequently lysed in RIPA buffer (50 mM Tris, 150 mM NaCl, 1% NP-40, 0.1% SDS, 2 mM EDTA, pH 8.0, and 0.5% sodium deoxycholate) with protease inhibitor cocktail (Roche, Basel, Switzerland) by bead beating three times for 30 seconds at 6,500 rpm with the samples chilled on ice between the homogenization steps. Samples were then centrifuged at 10,000 x g for 5 minutes at 4°C to remove debris. Cleared supernatant containing extracted proteins were transferred to a new tube and the protein concentration was measured using the BCA Assay Kit (Thermo Fisher, Waltham, MA). Sixty micrograms and 80 µg of total proteins were loaded into 10% SDS-PAGE to detect free GFP and GFP::LGG-1, respectively,

transferred to nitrocellulose membranes and stained with REVERT Total Protein Stain (Li-COR Biosciences, Lincoln, NE) for normalization. For detection of phosphorylated-IRE-1, 80 µg of total proteins were loaded into 10% SDS-PAGE gel and α-phosphorylated-IRE-1 (Novus Biologicals, catalog number NB100-2323, 1:200 dilution) was used as the primary antibody. Alpha-tubulin antibody (DSHB, 1:5,000 dilution) was used as a normalization control. For detection of HA, 80 µg of total proteins were loaded into 10% SDS-PAGE and α-HA (Covance, 1:2,000 dilution) was used as the primary antibody. Membranes were blocked for 1 h with Odyssey Blocking Buffer TBS (Li-COR Biosciences, Lincoln, NE) at room temperature, incubated with 1:1,000 of monoclonal anti-GFP overnight at 4°C (Roche, catalog number 11814460001), washed, and incubated with 1:10,000 of IRDye 800CW anti-mouse IgG (Li-COR Biosciences, Lincoln, NE, catalog number 925-32210). Membranes were washed and scanned with an Odyssey CLx Imaging System (Li-COR Biosciences, Lincoln, NE).

2.13. Quantification of autophagic vesicles

To quantify autophagic vesicles, *eri-1;lgg-1p::gfp::lgg-1* worms were immobilized in M9 containing 0.5 M NaN3 and mounted on a 2% agarose pad and imaged using LSM Zeiss 710 scanning confocal microscope (Zeiss, Oberkochen, Germany). GFP excitation and emission wavelengths were adjusted to 493 and 517 nm, respectively, to reduce autofluorescence. Z-stacks were acquired with a 63x objective of 0.6 µM thickness. Line average scanning was set to eight times to increase the signal-to-noise ratio. Maximum intensity projection was acquired from the z-stack images with ZEN software (Zeiss, Oberkochen, Germany). GFP positive puncta were quantified in one 1000 μm^2 area around the anterior intestines with ZEN software.

2.14. DNA microarray

Three independent populations of WT, *atf-6(lof)*, *ire-1(lof)*, *pek-1(lof),* and *pmt-2(lof)* worms were synchronized by hypochlorite treatment. L1 stage animals were treated with *pmt-2* RNAi or pL4440 empty vector for 48 h. Next, total RNA from the treated worms was isolated as described above. RNA quality control for microarray analysis was carried out using Agilent 2100 Bioanalyzer (Agilent Technologies, Santa Clara, CA). RNA samples with RIN score > 9.5 were deemed suitable for microarrays. The cDNAs were then synthesized from 100 ng of total RNA, purified, fragmented, and hybridized to GeneChip *C. elegans* Gene 1.0 ST Arrays. Differentially expressed genes were identified using Affymetrix Transcriptome Analysis Console (TAC) 3.0 software. Threshold for selecting

differentially expressed genes was set at a difference of more than 1.5-fold and one-way between-subjects ANOVA P value < 0.05. GOrilla (http://cbl-gorilla.cs.technion.ac.il/) (Eden et al., 2009), REViGO (http://revigo.irb.hr/) (Supek et al., 2011), and DAVID (https://david.ncifcrf.gov/) (Huang et al., 2007b) were used for GO terms analysis. Heat maps in the figures were generated using R Studio. Venn diagrams were generated using the following generator (http://bioinfo.genotoul.fr/jvenn/example.html) (Bardou et al., 2014). For gene expression analysis, normalized and log-transformed array data were imported to Cluster 3.0 for fold cut-off and hierarchical clustering. Genes were filtered to obtain those with a significant change in gene expression (fold change > 1.5 between RNAi treated and untreated samples and P < 0.05). The filtered data set was hierarchically clustered based on average linkage and Pearson correlation method, and the output was displayed in TreeView (Saldanha, 2004). Quantitative real-time PCR was performed to verify the mRNA expression of selected gene targets.

2.15. RNAi screening of lipid and metabolism-related genes

RNAi screen was carried out as previously described with minor modifications (Lehner et al., 2006). Briefly, WT or *ire-1(lof)* L1 larval stage animals were synchronized by hypochlorite treatment. Thereafter, worms were washed thrice with M9 buffer, and five to ten worms were seeded into a 96-well plate containing RNAi clones of lipid and metabolism-related functions. Phenotypes of the worms were monitored over five days. Phenotypes were compared to control RNAi plates where the worms were scored with sterility and reduced body size semi-quantitatively on a scale from 0 (wild type) to 2 (100% sterility or stunted growth). Images of the worms in 96-well plates were taken with a stereomicroscope (Nikon SMS745) fitted with an analog eyepiece camera (Dino-Lite AM422X).

2.16. RNAi screening of autophagy-related genes

RNAi screen was carried out as previously described with minor modifications (Lehner et al., 2006). Briefly, WT L1 larval stage animals were synchronized by hypochlorite treatment and exposed to *pmt-2* RNAi on NGM agar plates for 36 h. Thereafter, worms were washed thrice with M9 and five to ten worms were seeded into a 96-well plate containing RNAi clones of autophagy-related functions. Control RNAi plates comprised worms exposed to pL4440 empty vector for 48 h and subsequently seeded into 96-well plates containing the same RNAi clones as above. Phenotypes of the worms were monitored over five days. Phenotypes were compared to control RNAi plates where the worms were scored with

sterility and reduced body size semi-quantitatively on a scale from 0 (wild type) to 2 (100% sterility or stunted growth) (Lehner et al., 2006).

2.17. *xbp-1* splicing analysis

RNA extraction and cDNA synthesis were described in Section 2.4. RT-PCR was performed with 30 ng of cDNA with Taq polymerase (NEB) for 15 cycles using the *xbp-1* primer pair listed in Table 2.2. The primer pair was designed around the 23 bp intron region of unspliced *xbp-1* mRNA and allowed visualization of both spliced *xbp-1* (*xbp-1s*) and unspliced *xbp-1* (*xbp-1u*). The PCR product was run on a 10% TBE-polyacrylamide gel at 15 V/cm, stained with 1:3000 dilution of Gel Red (1st Base) for thirty minutes in water, and visualized with a UV transilluminator. *act-1* expression was used as a normalization control.

2.18. Live embryo imaging

GFP::SP12 expressing worms were treated with RNAi as described in section 2.3. Dissection and imaging of the embryos were carried out as described (Gorjanacz et al., 2007). Day 1 adulthood worms treated with RNAi were dissected in M9 buffer with a hypodermic needle to release the embryos. The dissection was carried out on a coverslip. After dissection, the coverslip was inverted and placed in contact with 2% agarose pad prepared on a glass slide. Nail polish was used to seal the gap between the coverslip and the glass slide. The embryos were analyzed by using a laser scanning microscope (LSM) 710 confocal microscopy with differential interference contrast (DIC) objectives. Images were acquired with a 100X objective with numerical aperture (NA) of 1.3. The GFP signal was captured at 8% laser power. Line average scanning was set to eight times to increase the signal-to-noise ratio. Images captured were then processed with ImageJ (Schneider et al., 2012).

Chapter 3: Results

3.1. *C. elegans* IRE-1 luminal domain deletion and transmembrane domain mutations did not augment the LBS sensing capability of IRE-1

In this study, we aimed to construct a *C. elegans* strain that lacks *ire-1* luminal domain to characterize LBS-specific activation of the UPR. To our knowledge, this is the first attempt at creating a UPR mutant lacking its entire luminal domain while retaining intact IRE-1 function for sensing LBS. It was reported that the murine IRE1 lacking its luminal domain was sufficient to detect LBS at the ER membrane (Volmer et al., 2013). Similarly, we designed a construct expressing 3XHA-tagged ER-targeted IRE-1 devoid of its luminal domain and performed insertional mutagenesis via transposon method to *ire-1(loss-of-function, lof)* worms. The *ire-1(lof)* worm strain expressing IRE-1ΔLD protein is henceforth referred to as *ire-1ΔLD* (Fig. 3.1).

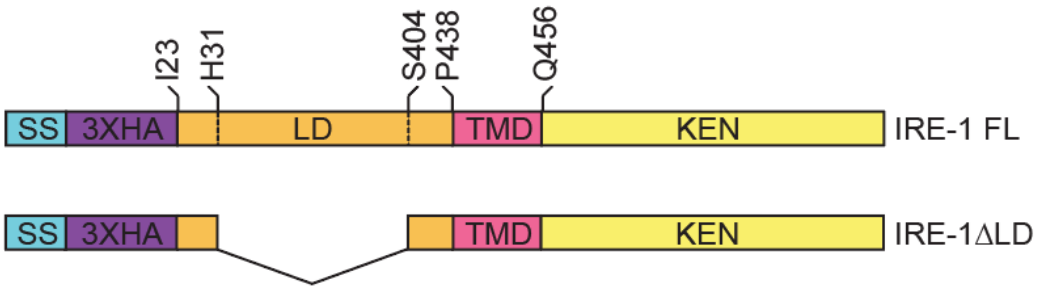

Figure 3:1: Scheme depicting the design of *ire-1ΔLD* mutant used in this study.

Full-length IRE-1 (IRE-1 FL) and IRE-1ΔLD contain the signal sequence (ss, cyan) followed by 3XHA tag (purple). This is continued by the luminal domain (orange) from position 23 to 438. The transmembrane domain (TMD, pink) is located from position 439 to 456 of the protein. The kinase endonuclease (KEN) domain is labeled in yellow. In the *ire1ΔLD* strain, the luminal domain is truncated from amino acids 31-404.

We hypothesized that the expression of IRE-1ΔLD will be sufficient to induce the UPR during LBS as observed in both the mammalian system and in yeast (Ho et al., 2020; Volmer et al., 2013). Furthermore, *ire-1ΔLD* mutant worms should be insensitive to proteotoxic stress, showing the specificity of IRE-1 transmembrane domain in sensing LBS. To verify if IRE-1ΔLD is capable of sensing LBS, we

challenged the worms with LBS through *pmt-2* RNAi or *mdt-15* RNAi in which silencing of these genes will induce UPR^{LBS} (Hou et al., 2014; Koh et al., 2018). The mediator subunit-15 (MDT-15) is a transcription factor required for maintaining membrane lipid desaturation, silencing of *mdt-15* was shown to disrupt lipid synthesis and increase membrane saturation, thus inducing UPR^{LBS} (Hou et al., 2014; Koh et al., 2018). Silencing of the *PEMT* ortholog *pmt-2* decreases PC synthesis, resulting in disrupted phospholipid balance and induces UPR^{LBS} (Ding et al., 2015; Thibault et al., 2012). Our results show that the ER resident proteins and canonical substrates for IRE-1, heat-shock protein 3 (*hsp-3,* ortholog of the mammalian *HSP70),* and heat-shock protein 4 (*hsp-4,* ortholog of the mammalian *HSP70)*, and the PEK-1-regulated *creb* (cAMP response element binding protein, ortholog of the mammalian *CREB*) were activated in wild type worms as a response to tunicamycin-induced proteotoxic stress (Fig. 3.2). In addition, LBS also induced expression of *hsp-3* and *hsp-4* in wild type worms but not in *ire-1ΔLD* worms during LBS, suggesting the inability of the transmembrane domain of IRE-1ΔLD in sensing LBS. In addition, *creb* expression, which is a downstream effector of PEK-1, was significantly increased in *ire-1(lof)* and *ire-1ΔLD* worms challenged with proteotoxic stress and LBS, suggesting intact signaling from other branches of the UPR in the *ire-1* mutants despite the inability of IRE-1ΔLD to sense LBS. Noticeably, *pmt-2* RNAi did not cause significant induction of *hsp-4* in WT worms. However, we observed significant increase in *hsp-3* mRNA levels in response to *pmt-2* RNAi-treated WT worms, suggesting a UPR^{LBS} response that remains intact (Fig. 3.2). One possible explanation for the lack of significant *hsp-4* mRNA induction can be attributed to phasic response of HSP-3 and HSP-4 to *pmt-2* RNAi treatment. HSP-3 is constitutively expressed and responsive to stress, and HSP-4 is more strongly induced by the UPR (Kapulkin et al., 2005; Shen et al., 2001). Additionally, *hsp-3* is inducible by the heat shock response (HSR) in addition to the UPR, thus explaining the differential gene expression (Guisbert et al., 2013). Seventy-two-hour *pmt-2(RNAi)* may have stimulated two-fold *hsp-3* mRNA expression while leaving *hsp-4* mRNA in basal expression level because (i) prolonged *pmt-2(RNAi)* emulated chronic LBS that dampened hsp-3 and hsp-4 activation as IRE-1 may switch to RIDD activity, or (ii) HSP-3 and HSP-4 operate in a phasic manner where in this condition *hsp-3* mRNA expression is sufficient to exert positive UPR to LBS (Hollien et al., 2009; Hollien and Weissman, 2006). When IRE-1 transautophosphorylates, the RNase domain splices 23 bp intron of *xbp-1* mRNA that are localized within the cytosolic vicinity of the ER membrane. The spliced *xbp-1* mRNA (*xbp-1s*) then translates into a mature transcription factor that activates downstream UPR genes, including *hsp-3* and

hsp-4. To corroborate the qPCR findings, we performed an *xbp-1* splicing assay. Both tunicamycin-induced proteotoxic stress and *mdt-15* or *pmt-2* RNAis-induced LBS showed increased accumulation of *xbp-1s* compared to empty vector control (Fig. 3.3). Of note, *pmt-2(RNAi)* induced a higher accumulation of unspliced *xbp-1* mRNA *(xbp-1u)* and a slight increase in *xbp-1s* compared to tunicamycin treatment and *mdt-15(RNAi),* adding to the complexity of UPR activation under different modes of LBS. Our *xbp-1* splicing assay did not show increased splicing *xbp-1*, suggesting a lack of IRE-1 activation in *ire-1ΔLD* during LBS.

Based on our results, we posit that the *ire-1ΔLD* worm strain we constructed behaved more like the *ire-1(lof)* strain. This prompted us to assess if the IRE-1ΔLD protein was being expressed properly. We added a 3XHA tag in the N-terminal of the IRE-1ΔLD construct after the signal sequence for ease of IRE-1 detection due to the lack of a specific IRE-1 antibody for use in worms. We performed immunoblotting using a HA antibody and found that the IRE-1ΔLD with 3XHA tag was expressed at a smaller size of 25 kDa than the expected 112 kDa, indicating probable truncation or degradation (Fig. 3.4). To test for the specificity of the HA antibody in worms, protein lysate prepared from yeast expressing carboxypeptidase tagged to HA (CPY*-HA) was included as a positive control. In addition, wild type and *ire-1(lof)* worms that do not express HA were used as negative controls. One possible explanation for this observation could be attributed to the proteins expressed were misfolded and not integrated to the ER membrane, resulting in its degradation through ER-associated degradation (ERAD). To substantiate this claim, genes encoding for the components of ERAD such as the ubiquitin conjugation enzymes *ubc-6*, *hrd-1,* or ER degradation-enhancing alpha-mannosidase-like protein 1 *edem-1* can be silenced via RNAi and the expression of IRE-1ΔLD can be assessed (Jones et al., 2002; Safra and Henis-Korenblit, 2014; Sasagawa et al., 2007). Additionally, truncation of IRE-1ΔLD protein because of premature termination of mRNA synthesis, unexpected termination of protein elongation during translation, or proteolysis are also possible, leading to the observed smaller IRE-1ΔLD product than expected.

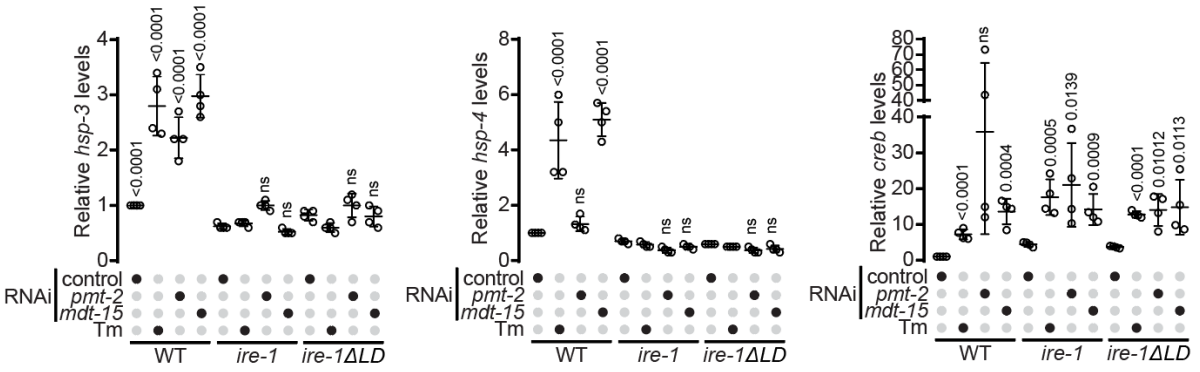

Figure 3:2: *pmt-2* and *mdt-15* silencing did not lead UPR^{LBS} induction.

qPCR comparing expression of *hsp-3, hsp-4, and creb* in WT, *ire-1(lof),* or *ire-1ΔLD* worms treated with empty vector, *pmt-2(RNAi)*, *mdt-15*(RNAi) for 72 h or treated with 2.5 µg/ml tunicamycin for 4 h. Data shown is the mean ± s.e.m. of four independent experiments. Statistical analysis was subjected to one-way ANOVA followed by Tukey's multiple comparisons adjustment. ns, non-significant.

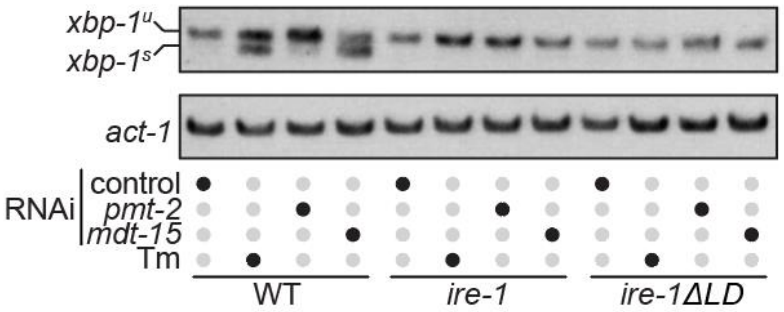

Figure 3:3: IRE-1ΔLD did not induce *xbp-1* splicing during UPR^{LBS}.

WT, *ire-1* or *ire-1ΔLD* worms were treated with empty vector, *pmt-2(RNAi)*, *mdt-15*(RNAi) for 72 h or treated with 2.5 µg/ml tunicamycin for 4 h. *xbp-1* mRNA was detected by RT-PCR. The two forms of *xbp-1* are indicated as *xbp-1u* (unspliced) and *xbp-1*s (spliced). The experiment was repeated three times.

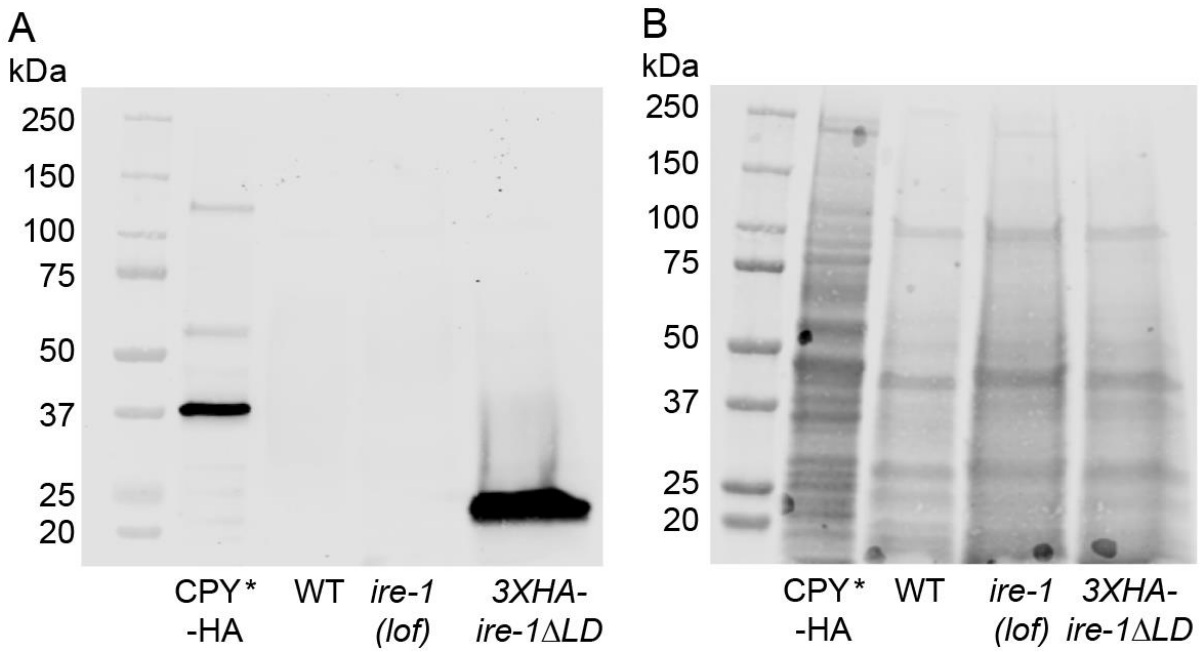

Figure 3:4: IRE-1ΔLD is expressed in *ire-1(lof)* worms but undergo degradation.

Immunoblot of HA proteins extracted from *ire-1ΔLD* mutant worms. (A) A wild type yeast expressing carboxypeptidase tagged with HA (CPY*-HA) was used as a control to test for the specificity of the HA antibody. Wild type and *ire-1(lof)* worms were included as negative controls. Eighty micrograms of lysates were loaded into each well. The dilution factor for HA-antibody used was 1:2000. (B) REVERT total protein stain was used to verify equal loading of the proteins. The experiment was performed once.

A study pointed that the LBS-sensing capability of the IRE-1 TMD is not sequence specific, where swapping of the mammalian IRE1 and PERK TMD to an unrelated TMD of ER protein still allowed for UPR activation (Volmer et al., 2013). In addition, a recent study concluded that generic membrane-spanning features of IRE1 are sufficient for IRE1 TMD to sense aberrant membrane saturation (Kono et al., 2017). These studies suggest that although responsiveness to LBS requires the presence of a transmembrane domain, it is not sequence specific. However, in another study, Ser450 and Trp457 amino acid residues that reside within the mammalian IRE1 TMD are essential in initiating dimerization of the TMD during membrane lipid saturation, adding to the complexity of IRE-1 regulation during LBS (Fig. 3.5) (Cho et al., 2019). In addition, studies in yeast have shown that Phe531, Val535, and Arg537 residues within the amphipathic helix are essential in sensing LBS (Fig. 3.5) (Halbleib et al., 2017; Ho et al., 2020). Building on their work, we aimed to identify key components governing UPR^{LBS} regulation by IRE-1 in worms. We predicted three residues His435 (H435), Thr442 (T442), and Trp455 (W455)

that are important for lipid sensing based on the hydrophobic properties of these amino acids (Figs. 3.5 & 3.6). We employed the use of CRISPR/Cas9 to generate the amino acid substitution mutants. The positively charged residue H435 was mutated to the hydrophobic phenylalanine (F), and the polar residue T442 and the amphipathic W455 residue were mutated to the hydrophobic alanine (A). To test if the constructed mutants sensed LBS, we treated the worms with *mdt-15*(RNAi). Among the three mutants, we have not observed dampening of *hsp-4* mRNA levels from *mdt-15*(RNAi)-mediated LBS while the *ire-1(lof)* mutant showed complete abolishment of the UPR induction (Fig. 3.7). In fact, in these mutants, *hsp-4* levels induced by LBS through *mdt-15(RNAi)* are comparable to that in wild type worms, suggesting intact lipid stress sensing capability of the IRE-1 transmembrane domain mutants (Fig. 3.7). As expected, tunicamycin-induced UPR activation led to *hsp-4* expression in wild type worms and the three mutants created. Although we were unsuccessful in generating the *ire-1ΔLD* mutants or the *ire-1* TMD amino acid substitution mutants, a probe into how full-length IRE-1 regulates the UPR will be valuable in advancing our knowledge on the pathophysiology of metabolic diseases. In the subsequent sections, we will discuss our work on identifying a suitable LBS model in worms to further our understanding of the UPR.

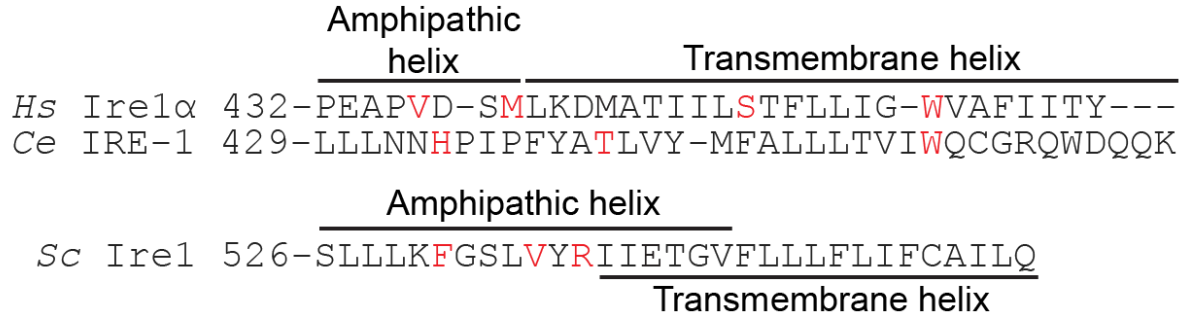

Figure 3:5: Alignment of IRE-1 shows relatively poor sequence similarity between species.

C. elegans mutation of IRE-1 amino acid residues found within the amphipathic helix (AH) or transmembrane helix (red text) is detailed in Figure 3.6. In human, V437R, and M440R within the AH did not inhibit Ire1α sensing of LBS while S450A and W457A within the transmembrane helix affected Ire1α activity during saturated fatty acid induced LBS (Cho et al., 2019). On the contrary, F531R, V535R and R537Q mutations in the yeast AH compromised the ability of Ire1 to sense LBS (Halbleib et al., 2017; Ho et al., 2020). *Hs, Homo sapiens; Ce, C. elegans; Sc, S. cerevisiae.*

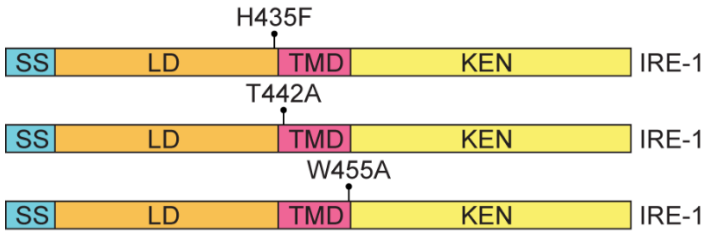

Figure 3:6: Three IRE-1 amino acid substitution mutants were created using CRISPR/Cas9.

Three amino acid residues were selected for substitution mutation based on the propensity of these amino acid residues in sensing LBS. SS, signal sequence; LD, luminal domain; TMD, transmembrane domain; KEN, kinase-endonuclease domain.

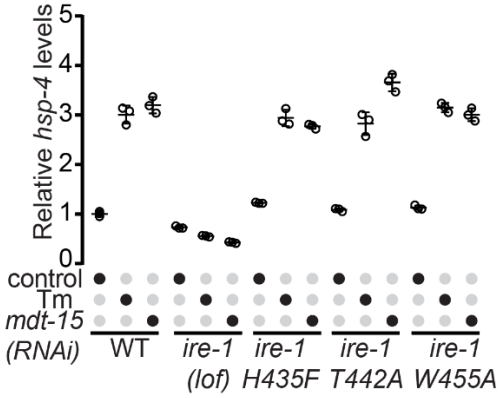

Figure 3:7: IRE-1 amino acid substitution mutants were responsive to UPR^{PT} and UPR^{LBS}.

Relative mRNA level of *hsp-4* in *mdt-15* RNAi-treated or tunicamycin (Tm)-treated worms. RNAi was carried out for 48 h and Tm treatment was carried out for 4 h at the concentration of 25 µg/ml. Data shown is the mean ± s.e.m. of technical replicates from one experiment.

3.2. Cold stress induces UPR^{LBS} in *C. elegans*.

Membrane fluidity is essential for an organism to maintain proper cellular functions. The ratio of acyl-chain saturation to unsaturation dictates membrane fluidity and alteration to this ratio causes ER stress (van Meer et al., 2008). Saturation of membrane lipids through palmitic acid supplementation is known to cause ER stress and subsequently UPR activation (Karaskov et al., 2006; Xu et al., 2015). The addition of unsaturated oleic acid was reported to reverse this effect. This evidence points to the importance of membrane homeostasis preservation in preventing lipotoxicity-induced ER stress. Conversely, we asked if increased unsaturation in membrane lipid in worms would perturb ER

homeostasis and lead to UPR activation. Indeed, mediator subunit-15 (MDT-15) was reported to play a crucial role in maintaining lipid composition when membrane unsaturation/saturation ratio is affected by low temperature exposure (Lee et al., 2019).

To alter the membrane saturation levels, we subjected the worms to cold stress Low temperature induces changes in the physical conformation of the biological membranes by increasing the level of lipid unsaturation, hence enhancing membrane fluidity and provide stabilization to the cells as an adaptive response (Chen and Thelen, 2013; Miquel et al., 1993). In addition, carbon isotope labeling has shown that ~4.5% of membrane lipids undergo turnover every hour, showing the dynamic of lipid metabolism in worms that is susceptible to environmental manipulation (Dancy et al., 2015). A study showed that moderate hypothermia (28°C - 32°C) for 24 h induces ER stress in human cortical neurons (HCNs) with activation of the UPR including mild XBP1 splicing and increased mRNA expression of XBP1 mRNA in the cooling phase and subsequently increase in CHOP transcript level during prolonged cold stress (Rzechorzek et al., 2015). This finding of sequential UPR activation explains coordinated effort of IRE1 and ATF6 to buffer the possible change of homeostatic landscape in the initial phase of cold stress and activation of PERK to confer tolerance to a hypothermic state without activation of apoptosis (Peretti et al., 2015; Rzechorzek et al., 2015; Saito et al., 2010).

To investigate the regulatory role of IRE-1 during lipid unsaturation-induced LBS, our collaborator, Sivan Henis-Korenblit laboratory (Bar-Ilan University), exposed wild type and *ire-1(lof)* worms to cold stress at 2.1°C. They first assessed the fitness of the worms after 48 h cold stress treatment and observed that while wild type worms were largely alive, more than 90% of the *ire-1(lof)* worms were dead. This finding signifies the importance of IRE-1-regulated UPR in ensuring survival under cold stress. Upon ER stress, IRE-1 trans-autophosphorylates, and this process can be detected through immunoblot by using phosphorylation specific antibody. Using the IRE-1 phosphorylation assay, our collaborator found an increased level of phosphorylated IRE-1 in wild type and *jnk-1(lof)* worms, but not in *ire-1(lof)* worms, indicating cold stress treatment activates the UPR through *ire-1* (Fig. 3.8). As mentioned in the Introduction, JNK-1 encodes for the human ortholog of MAPK10 that was reported to be regulated through IRE-1 in addition to its canonical cellular signaling through the plasma membrane (Glover-Cutter et al., 2013). Under the basal condition, *jnk-1(lof)* worms exhibited increased IRE-1 activation, suggesting a compensatory response by IRE-1 to increase the UPR output to maintain cellular

homeostasis such as autophagy, mRNA stability, and ER and Golgi biogenesis (Hetz et al., 2020). The phosphorylation of IRE-1 is slightly increased in *jnk-1(lof)* worms during cold stress exposure, further indicating the importance of compensatory IRE-1 function.

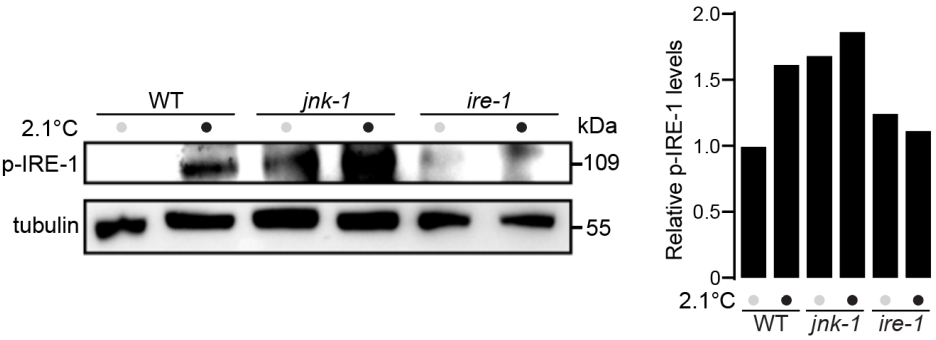

Figure 3:8: Cold stress activates the UPR in an *ire-1*-dependent manner.

WT*, jnk-1(lof),* or *ire-1(lof)* worms were either treated with 2.1°C cold stress for 24 h or raised in the physiological temperature of 20°C. The lysates were prepared and analyzed by immunoblotting with anti-phospho-IRE-1 antibody and normalized to tubulin. Right panel shows quantification of p-IRE-1 protein levels relative to the wild-type control. The experiment was conducted once.

Our collaborator next assessed if cold stress treatment might induce ER stress through the IRE-1/ XBP-1 axis. Hence, they monitored the mRNA expression of *hsp-4,* a known substrate of the mature XBP-1. Activation of the UPR from cold stress showed a time-dependent increase in *hsp-4* expression over a 48 h period through the use of *hsp-4p::gfp* reporter (Fig. 3.9). As *ire-1(lof)* worms were highly susceptible to cold stress, they could not measure the UPR activation with the *hsp-4p::gfp* reporter in an *ire-1* null background. Our data suggest that IRE-1 responds to physiological cold stress and is essential for survival, corroborating an earlier study where the UPR cascade was activated in HCNs under hypothermic conditions (Rzechorzek et al., 2015).

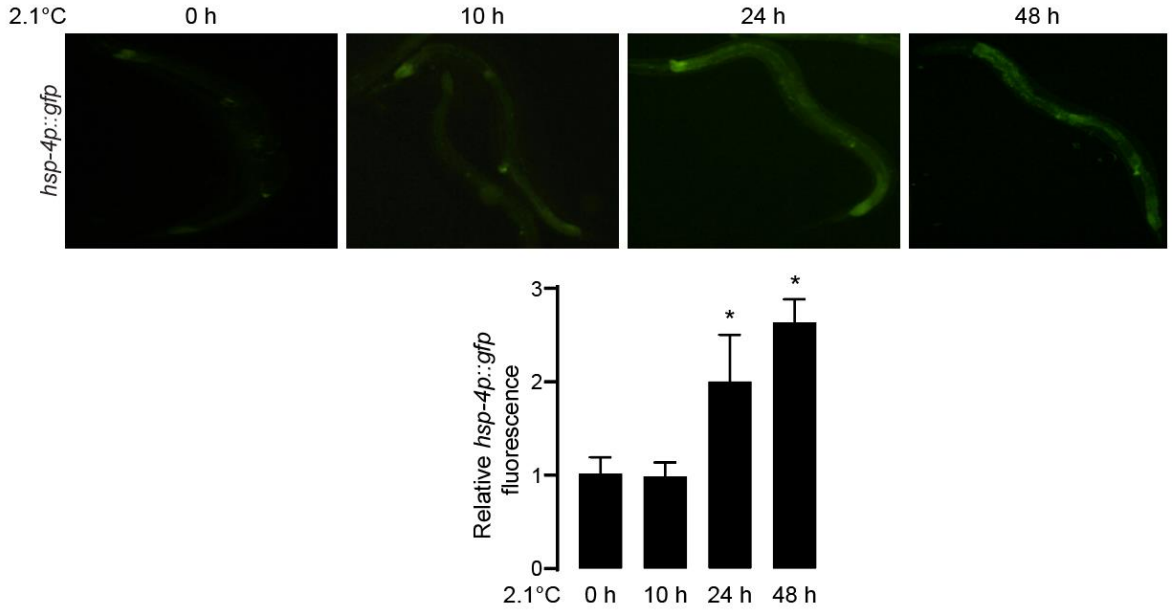

Figure 3:9: The IRE-1-inducible HSP-4 increased in expression during prolonged period of cold stress.

Representative fluorescence images show *hsp-4p::gfp* worms with cold stress exposure at 0 h, 10 h, 24 h or 48 h. Data shown is the mean ± s.e.m. of at least three independent experiments. Statistical analysis was subjected to Student's t-test. *, $p < 0.05$ when compared to 0 h; ns, non-significant. n= 13-25 worms used.

In general, the unsaturated fatty acids content in lipid membranes increases with decreasing temperature in most organisms. Such transition is mediated by lipases and desaturases such as the Δ9 desaturase FAT-6 whose expression is controlled by XBP-1 transcription factor (Imanikia et al., 2019). Based on our observation of IRE-1 activation in cold stress, we asked if the UPR induction remodels the lipid content of the worms. To quantify changes in lipid saturation during cold stress-induced LBS, we quantified the distribution of fatty acids by GC-FID after 24 h of cold stress exposure (Fig. 3.10). While we have not observed meaningful changes in fatty acid from wild type worms challenged with cold stress, we observed significant reduction of saturated fatty acids (SFA) in cold stress treated *ire-1(lof)* worms compared to wild type control, suggesting increased lipid unsaturation.

In addition to decreased SFA level, cold stress treated *ire-1(lof)* worms showed increased γ–linolenic acid (GLA, C18:3n6) and eicosapentaenoic acid (EPA, C20:5n3) levels compared to the control. PUFAs have a protective role in attenuating ER stress through modulation of the transcriptional activity of

lipogenic genes such as sterol regulatory element-binding protein-1 (SREBP-1) and C/EBP (Wang et al., 2015). However, although there was an increased PUFA levels in cold stress treated *ire-1(lof)* worms, it was not sufficient to exert a protective effect as most *ire-1(lof)* worms die from prolonged cold stress as our collaborator has demonstrated in their cold stress survival assay. The decrease in SFA levels, coupled with increased PUFAs presumably decreased the unsaturated/saturated lipids ratio that affected the survival of *ire-1(lof)* worms. Overall, our findings corroborate what was observed in other models where cold stress induces UPR activation for protective effects (Karabudak et al., 2014; Miquel et al., 1993). Taken together, our data suggests that cold stress treatment may induce lipid unsaturation in worms, as previously reported, and activates the UPR in an *ire-1*-dependent manner (Murray et al., 2007). Importantly, more experiments need to be done to validate the UPR activation and change in lipid profile during cold stress. Here, we show that cold stress induced IRE-1 to regulate downstream UPR activation. However, the involvement of ATF-6 and PEK-1 upon cold stress has yet to be clarified. In addition, how IRE-1 in exerts its protective effect during cold stress remains to be elucidated.

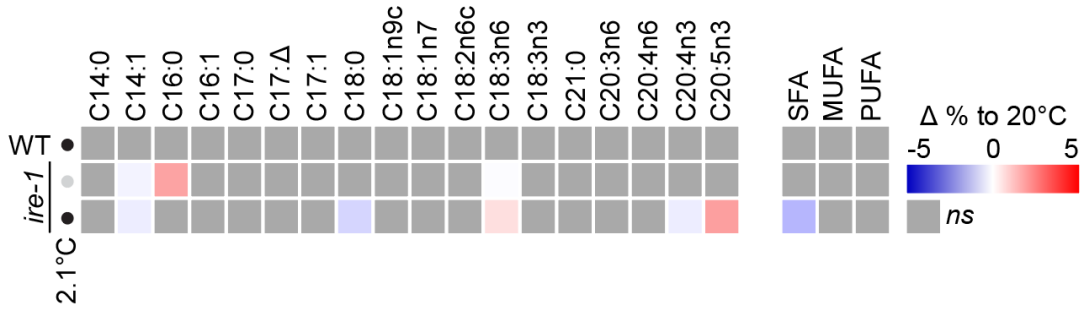

Figure 3:10: Total fatty acid analysis shows overall increase in fatty acid unsaturation upon cold stress.

Heat map of percentage change in fatty acids (FAs), distribution of FA length, and saturation of adult wild type and *ire-1(lof)* worms exposed to cold stress for 24 h at 2.1°C compared to control worms raised in 20°C. Extracted peak areas for all fatty acid species were log-transformed after normalization to pentadecanoic acid (C15:0) and worm dry weight. SFA, saturated fatty acid; MUFA, monounsaturated fatty acid; PUFA, polyunsaturated fatty acid. The experiments were independently performed four times. Statistical analysis was subjected to one-way ANOVA followed by Tukey's multiple comparisons adjustment. Briefly, the percentage change of each fatty acid species in various conditions was compared to the fatty acid value of the control wild type worms. P-values > 0.05 were deemed non-significant (*ns*).

3.3. High glucose diet induces activation of the UPR^{LBS}

Our second approach to induce LBS involved increasing the membrane lipid saturation in worms. Saturation of the membrane lipids is associated with membrane stiffening and decreased fluidity, thus affecting membrane-protein interaction dynamics and initiate the UPR activation (Quinn, 1981; Stubbs, 1983; Stubbs and Smith, 1984). Saturated fatty acid supplementation is conventionally used to induce LBS. Unlike yeast or mammalian culture where uptake of fatty acids supplemented in the media is rather efficient, we faced challenges in augmenting the fatty acids composition in worms through supplementation of fatty acids to induce LBS. Fatty acids supplementation requires conjugation of the fatty acids to bovine serum albumin. In addition, the *E. coli* present in the worm diet may also consume and metabolize fatty acids included in the worm growth media, thus affecting the consistency of fatty acids uptake in worms. To circumvent this problem, we performed supplementation of glucose rich diet to the worms. Glucotoxicity is known to decrease membrane fluidity in worms (Svensk et al., 2016). We hypothesized that excessive glucose intake may result in glucotoxicity that can cause accumulation of SFAs and subsequently alter membrane lipid composition. Most glucotoxicity studies involved the use of young worms (Lee et al., 2015; Lee et al., 2009). We postulated that aged worms might have a lower tolerance to glucose owing to the reduced carbohydrate metabolism, resulting in increased glucotoxicity and exacerbated LBS (Elahi and Muller, 2000). Under glucotoxicity, the IRE1-XBP1 axis is activated to handle increased protein folding load. The induction of the UPR is correlated with an increase in toxic protein modification of genes related to protein folding, protein synthesis, serine/threonine kinase signaling, glycolysis, and gluconeogenesis through mass spectrometry analysis (Irshad et al., 2019). A study assessed the role of the UPR in glucotoxicity through evaluation of misfolded protein accumulation caused by proinsulin overload in cultured pancreatic islet cells found increased *XBP1* splicing and eIF2α phosphorylation, indicating the involvement of IRE1 and PERK in resolving ER stress (Arunagiri et al., 2018). Here, we asked if glucotoxicity stimulated by high glucose diet (HGD) could induce LBS in *C. elegans*.

To dissect the UPR function under HGD-induced LBS, we subjected young (D1 adulthood) and old (D5 adulthood) worms to 2% HGD. The maintenance of cellular homeostasis including proteostasis, metabolism, and ER function become diminished with age as senescence takes place and toxic protein aggregates and reactive oxygen species accumulate. Thus, HGD treatment in old worms may exacerbate glucotoxicity and result in a pronounced change in lipid composition. Wild type worms day

1 (D1) and day 5 (D5) of adulthood were fed with UV-killed *E. coli* OP50 diet supplemented with 2% glucose (henceforth referred as HGD1 and HGD5, respectively). Additionally, 5-fluoro-2'-deoxyuridine (FUdR) was included in the media to prevent progenies formation. After 24 h exposure to either normal diet (ND) or HGD, the worms were harvested for qPCR analysis. The UPR was highly responsive to glucotoxicity as there was significant induction of *cht-1, hsp-4,* and *F40F12.7* mRNA levels that are regulated through ATF-6, IRE-1, and PEK-1, respectively (Fig. 3.11). HGD5 worms showed decreased *hsp-4* mRNA expression compared to HGD1 treatment, suggesting a dampened IRE-1 response to glucotoxicity. This is supported by a study that showed aged worms exhibited reduced UPR activation through IRE-1 in response to tunicamycin-induced proteotoxic stress (Taylor and Dillin, 2013). In contrast, *cht-1* and *F40F12.7* mRNA levels were increased in response to HGD5, showing higher ATF-6 and PEK-1 UPR activity in response to ER stress (Figure 3.11). Our data suggest that despite the diminished capacity of the UPR to respond to ER stress in aged worms, glucotoxicity highly induced the UPR in an attempt to restore cellular homeostasis (Paz Gavilan et al., 2006). In the hepatic steatosis mice model, inhibition of ATF6 activity exacerbated metabolic dysfunction and caused severe steatosis and insulin resistance when the mice were fed with a high fat and high sugar diet, corroborating our observation of high *cht-1* expression in HGD worms (Chen et al., 2016). ATF-6 and XBP-1 possess similar DNA-binding capacities, suggesting they may share the same downstream target such as lipid metabolism-related genes (Lee et al., 2003; Yamamoto et al., 2010; Yamamoto et al., 2004). Our mRNA expression data showed that *cht-1* is highly induced, suggesting increased UPR output from ATF-6 compared to IRE-1 and PEK-1 branches of the UPR. We then asked if increased UPR activity might correlate with a change in the lipid profile of HGD1 and HGD5 worms.

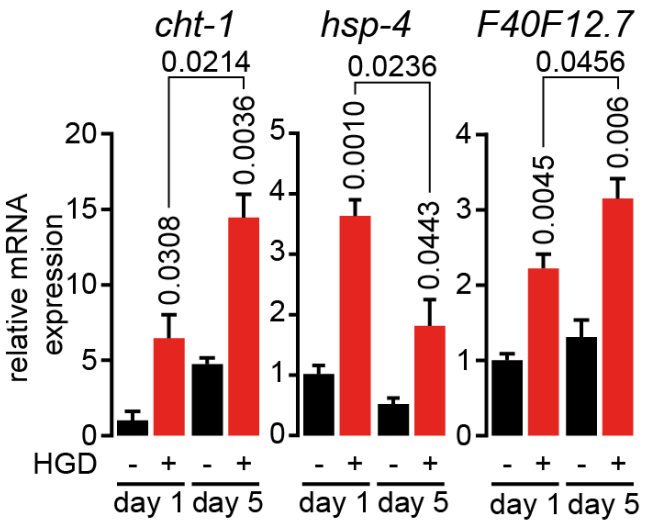

Figure 3:11: HGD induced the UPR activation in young and old worms.

qPCR comparing expression of *cht-1*, *hsp-4*, and *F40F12.7* induced from ATF-6, IRE-1, and PEK-1, respectively, in WT worms fed with normal dead OP50 *E. coli* diet or diet supplemented with 2% glucose (high glucose diet, HGD) at day 1 and day 5 adulthood (HGD1 & HGD5) for 24 h. The worm growth media also include 50 mM of FUDR to prevent progenies formation. Statistical analysis was subjected to Student's t-test. The experiments were independently performed three times.

To compare the effect of HGD on the possible change of fatty acid composition, HGD1 or HGD5 worms were harvested for total fatty acid analysis by GC-FID. Our total fatty acid analysis showed HGD-fed worms exhibited an increase in saturated fatty acids (SFAs) and polyunsaturated fatty acids (PUFAs) with a decrease in monounsaturated fatty acid (MUFAs) in both HGD1 and HGD5 (Fig. 3.12). Compared to ND worms, HGD5 worms showed diminished γ-linolenic acid (C18:3n6) level with the accumulation of its precursor palmitic acid (C16:0). Our finding corroborates previously reported data where 2% glucose feeding similarly increased palmitic acid accumulation and increased saturated fat content of the worms, thus reducing their lifespan (Lee et al., 2015). Palmitic acid supplementation is known to induce LBS through increasing membrane saturation and activate the UPR through IRE1 and PERK in mammalian cells (Volmer et al., 2013; Wei et al., 2006). Consistent with their findings, we observed UPR activation in our HGD1 and HGD5 treated worms (Fig. 3.11). In addition, there is a marked decrease in MUFA levels in both HGD1 and HGD5 worms. MUFAs provide a cytoprotective role from metabolic insults. A study found that adipose and hepatic tissues of mice with high MUFAs accumulation devoid of metabolic disease hallmarks that can be found in obese or dyslipidemic mice (Cao et al.,

2008). From our findings, we posit that HGD altered the lipid composition of the worms by causing accumulation of toxic lipid species, thus activating the UPR. It is important to note that we have not ruled out the possibility that glucotoxicity may induce proteotoxic stress in worms, therefore further studies are needed. Indeed, assessment of UPR activation reveals that HGD-fed worms activated ER stress through all three branches of the UPR, indicating the possibility that HGD altered lipid metabolism of the worms, which led to a concerted UPR activation to counteract this form of stress. However, the caveat in our data lies in the lack of assessment of misfolded protein in our experimental condition that could confound the data. Additionally, the mechanism governing the potential compensatory role of the UPR during glucotoxicity remains to be elucidated.

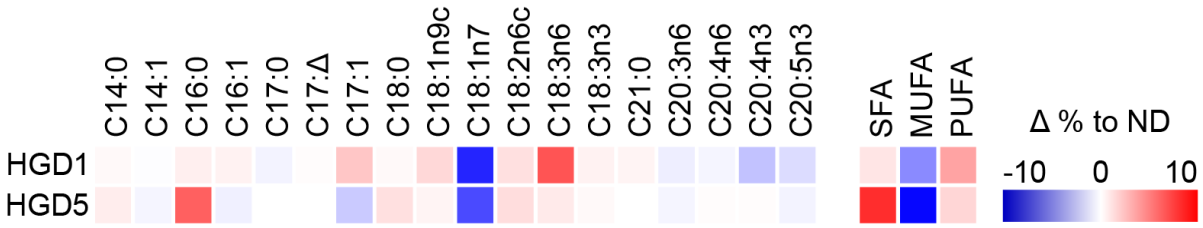

Figure 3:12: High glucose diet stimulates modest increase in saturated fatty acids.

Heat map of the percentage change in fatty acids (FAs), distribution of FA length, and saturation of HGD1 and HGD5 worms compared to normal diet (ND) control. Extracted peak areas for all fatty acid species were normalized to pentadecanoic acid (C15:0) and protein concentration. SFA, saturated fatty acid; MUFA, monounsaturated fatty acid; PUFA, polyunsaturated fatty acid. The experiments were independently performed twice.

3.4. The attenuation of *pmt-2* activates the UPR by reducing total phosphatidylcholine

Next, we induced LBS through disruption of membrane phospholipid metabolism by silencing phosphatidylcholine (PC) synthesis enzyme. PMT-1 and PMT-2 are both required for the synthesis of PC from phosphatidylethanolamine (PE) in *C. elegans* (Brendza et al., 2007; Li et al., 2011; Palavalli et al., 2006) (Fig. 1.3). In the absence of dietary choline, both genes are essential for the development of *C. elegans,* and silencing one of the genes from larvae stage-one (L1) leads to sterility (Brendza et al., 2007). PC cannot be obtained from standard laboratory worm diet as the conventionally used *E. coli* strains OP50 and HT115(DE3) lack PC (Morein et al., 1996; Oursel et al., 2007). Thus, PC levels in

worms can be altered by genetically silence *pmt-1* or *pmt-2* to induce LBS thereby activating the UPR (Fig. 3.13).

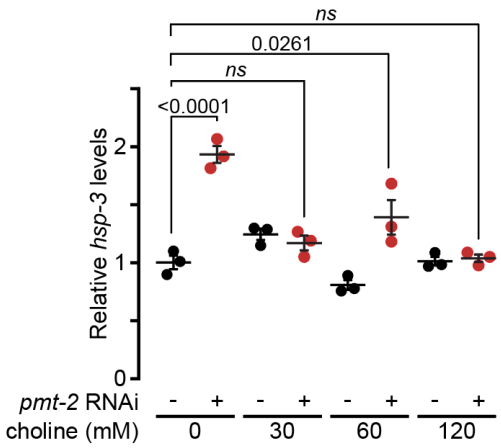

Figure 3:13: Choline supplementation restores ER homeostasis in PC depleted animals.

qPCR of *hsp-3* expression level in WT worms. L1 worms were grown on *pmt-2* RNAi or empty vector on plates supplemented with 0, 30, 60, or 120 mM choline for rescue. Data shown is the mean ± s.e.m. of at least three independent experiments. Statistical analysis was subjected to one-way ANOVA followed by Tukey's multiple comparisons adjustment. *ns*, non-significant.

To better understand the role of the UPR during LBS, we subjected synchronized L1 worms to *pmt-2* RNA interference (RNAi) for 48 h. Two-day RNAi feeding was sufficient to decrease *pmt-2* mRNA in wild type (WT) animals close to the background signal of *pmt-2(lof)* (Fig. 3.14). As previously reported, *pmt-2(RNAi)* animals showed a developmental defect characterized by reduced body size, which is rescued by choline supplementation (Fig. 3.15) (Palavalli et al., 2006). PC is synthesized from choline through the Kennedy pathway (Fig. 1.3). Supplementing *pmt-2(RNAi)* animals with 30 mM choline was sufficient to prevent UPR activation while the growth defect was alleviated with 60 mM choline (Fig. 2.3).

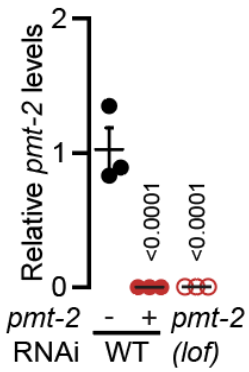

Figure 3:14: *pmt-2* mRNA levels after RNAi knockdown is comparable to *pmt-2(lof)* worms.

qPCR results comparing expression of *pmt-2* in *pmt-2(RNAi)* and *pmt-2(lof)* animals. Data shown is the mean ± s.e.m. of at least three independent experiments. Statistical analysis was subjected to Student's t-test.

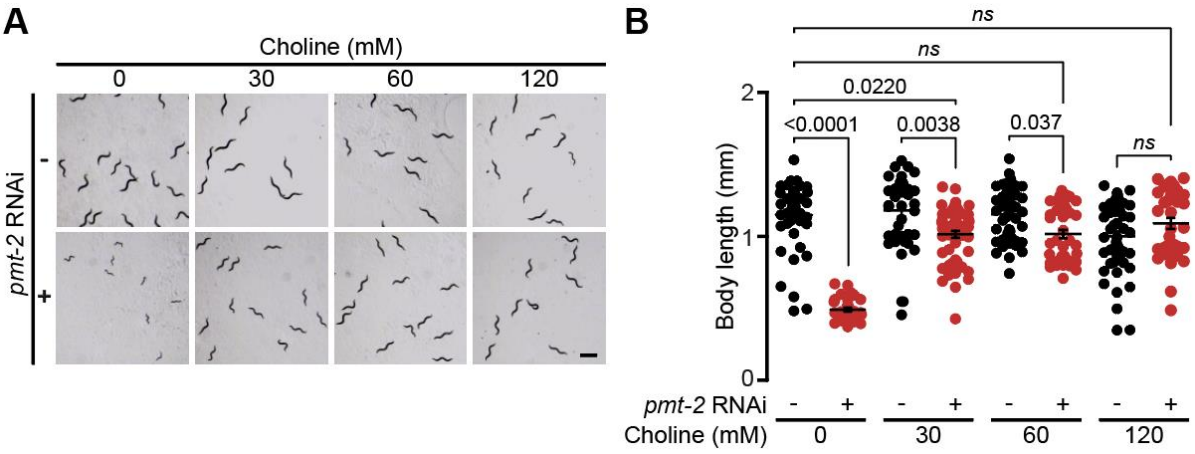

Figure 3:15: Choline supplementation rescues developmental defect caused by *pmt-2* RNAi.

Representative choline rescue assay of *pmt-2(RNAi)* developmental defect. (A) L1 worms were grown on *pmt-2* RNAi or empty vector on plates supplemented with 0, 30, 60, or 120 mM choline, and images were taken after 48 h. Scale bar, 100 µm. The RNAi feeding experiment was repeated at least three times. (B) Body length quantification of worms from A. WT, 0 mM choline, n=47(-), n=32(+); 30 mM choline, n=39(-), n=58(+); 60 mM choline, n=48(-), n=43(+); 120 mM choline, n=54(-), n=38(+). Data shown is the mean ± s.e.m. of at least three independent experiments. Statistical analysis was subjected to Student's t-test. *ns*, non-significant.

To further characterize *pmt-2(RNAi)* worms, PC was separated from the total lipid extract of worms by thin-layer chromatography (TLC). This was followed by a transesterification reaction to derive fatty acid methyl esters (FAMEs) specifically from PC, which were further quantified by gas chromatography with a flame ionization detector (GC-FID). We found that the PC level in *pmt-2(RNAi)* worms was markedly reduced to 36% of the vector control worms (Fig. 3.16A). Attenuating *pmt-2* expression was not

sufficient to fully eliminate PC in WT animals due to the large phospholipid reserve of stage L1 worms in addition to the long half-lives of phospholipids (Dowd et al., 2001). As LBS can lead to ER stress, we measured the transcriptional levels of the UPR-induced ER-resident molecular chaperone Hsp70 family (Urano et al., 2002). The mRNA levels for both human Hsp70 orthologs, *hsp-3* and *hsp-4*, were upregulated transcriptionally in *pmt-2(RNAi)* worms compared to WT (Fig. 3.16B). The mRNA level of *hsp-3* in *pmt-2(RNAi)* worms was similar to that of WT worms incubated with the strong UPR inducer tunicamycin (Tm) for 4 h. Tm inhibits protein N-glycosylation leading to a severe accumulation of unfolded proteins in the ER (Ericson et al., 1977). In contrast, *hsp-4* mRNA level was remarkably higher in Tm-treated animals compared to LBS. This result suggests that *hsp-4* expression might be modulated differently by the UPR program depending on the nature of stress. As the UPR is activated from low PC, *C. elegans* subjected to *pmt-2* RNAi mimics NAFLD where altered PC/PE ratios and UPR activation are interconnected (Fu et al., 2011; Ozcan et al., 2004; Shyu et al., 2019; Thibault et al., 2012).

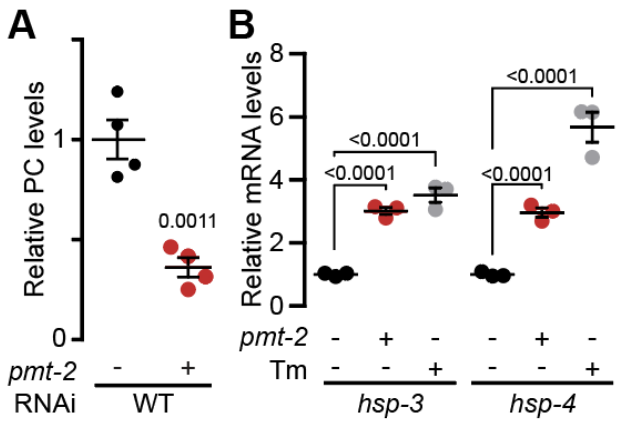

Figure 3:16: *pmt-2* silencing is sufficient to activate the UPR by lipid bilayer stress.

(A) Comparison of PC levels in WT and *pmt-2(RNAi)* animals by GC-FID. (B) qPCR results comparing the expression of UPR marker genes *hsp-3* and *hsp-4* in *pmt-2(RNAi)* and WT worms treated with 25 µg/ml tunicamycin for 4 h. Data shown is the mean ± s.e.m. of at least three independent experiments. Statistical analysis was subjected to Student's t-test.

3.5. Attenuated phosphatidylcholine synthesis leads to lipid droplet accumulation

To investigate the regulatory role of the three ER stress transducers during LBS (Shen et al., 2005), *atf-6(lof)*, *ire-1(lof),* and *pek-1(lof)* mutant worms were subjected to *pmt-2* RNAi as described above (Fig. 3.17). The simultaneous ablation of two or three UPR branches is not possible as any combination is lethal (Shen et al., 2005). Treatment with *pmt-2* RNAi resulted in the reduction of PC across the three UPR mutants that is comparable to WT worms (Fig. 3.18 & 3.19).

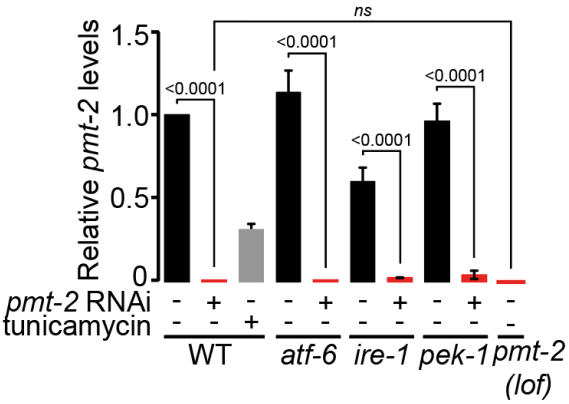

Figure 3:17: *pmt-2* mRNA levels after RNAi knockdown is comparable to *pmt-2(lof)* worms.

qPCR of *pmt-2* expression after *pmt-2* RNAi treatment in WT, *atf-6(lof)*, *ire-1(lof)*, and *pek-1(lof)* worms. WT worms were treated with 25 µg/ml tunicamycin for 4 h. *pmt-2(lof)* worms were used as a control. *pmt-2* RNAi treatment efficiently silenced expression of *pmt-2* across all the strains tested. Data shown is the mean ± s.e.m. of at least three independent experiments. Statistical analysis was subjected to one-way ANOVA followed by Tukey's multiple comparisons adjustment. *ns*, non-significant.

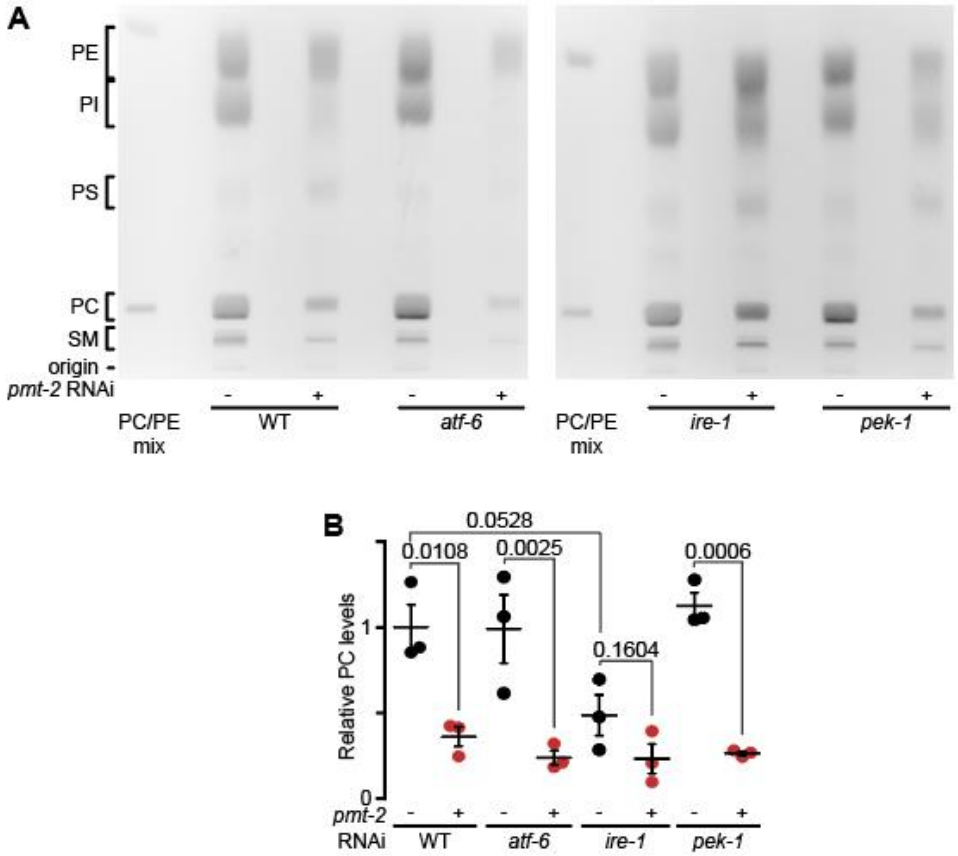

Figure 3:18: Inactivation of *pmt-2* decreased PC content in worms.

(A) Representative separation of phosphatidylethanolamine (PE), monomethyl-phosphatidylethanolamine (MMPE), dimethyl-phosphatidylethanolamine (DMPE), and phosphatidylcholine (PC) from total lipid extract using thin-layer chromatography (TLC). Comparison of phospholipid levels in WT, *atf-6(lof)*, *ire-1(lof),* and *pek-1(lof)* animals treated with *pmt-2* RNAi. POPE (1-palmitoyl-2-oleoyl-sn-glycero-3-phosphoethanolamine; 16:0-18:1n9 PE) and DOPC (1,2-dioleoyl-sn-glycero-3-phosphocholine; 18:1n9 PC) were used as markers. (B) Comparison of PC levels in WT, *atf-6(lof)*, *ire-1(lof),* and *pek-1(lof)* animals treated with *pmt-2* RNAi as quantified by GC-FID. Data shown is the mean ± s.e.m. of at least three independent experiments. Statistical analysis was subjected to one-way ANOVA followed by Tukey's multiple comparisons adjustment.

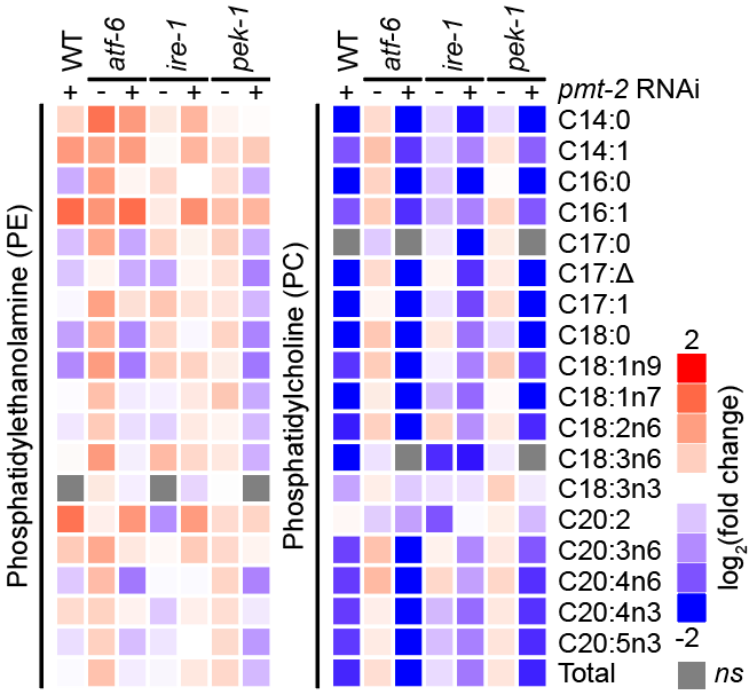

Figure 3:19: *pmt-2* RNAi effectively depletes PC levels in WT and UPR mutant worms.

Heat map representation of all significant PE- and PC-derived fatty acids changes to untreated WT as quantified by GC-FID. Extracted peak areas for all fatty acid species were log-transformed after normalization to pentadecanoic acid (C15:0) and worm dry weight. WT and UPR mutant worms were treated with *pmt-2* RNAi. Grey box indicates non-significant change (ns).

As a reduction in PC level leads to lipid droplet (LD) accumulation in eukaryotes (Horl et al., 2011; Li et al., 2011; Thibault et al., 2012; Walker et al., 2011), Sudan Black staining of fixed worms treated with *pmt-2* RNAi was carried out to visualize lipid droplets by Nomarski microscopy (Fig. 3.20). To compare LD expansion in *pmt-2* RNAi treated worms, the diameter of LDs was measured and classified into small (0.8 - 3 µM), medium (3.1 - 6 µM), and large (> 6 µM) groups. We observed accumulation of large LDs but fewer total LDs in WT, *atf-6(lof)*, *ire-1(lof)*, and *pek-1(lof)* worms treated with *pmt-2* RNAi, corresponding to previous studies in *sams-1(RNAi)* and *pmt-1(RNAi)* worms where reduced PC increased LD formation (Ding et al., 2015; Walker et al., 2011) .

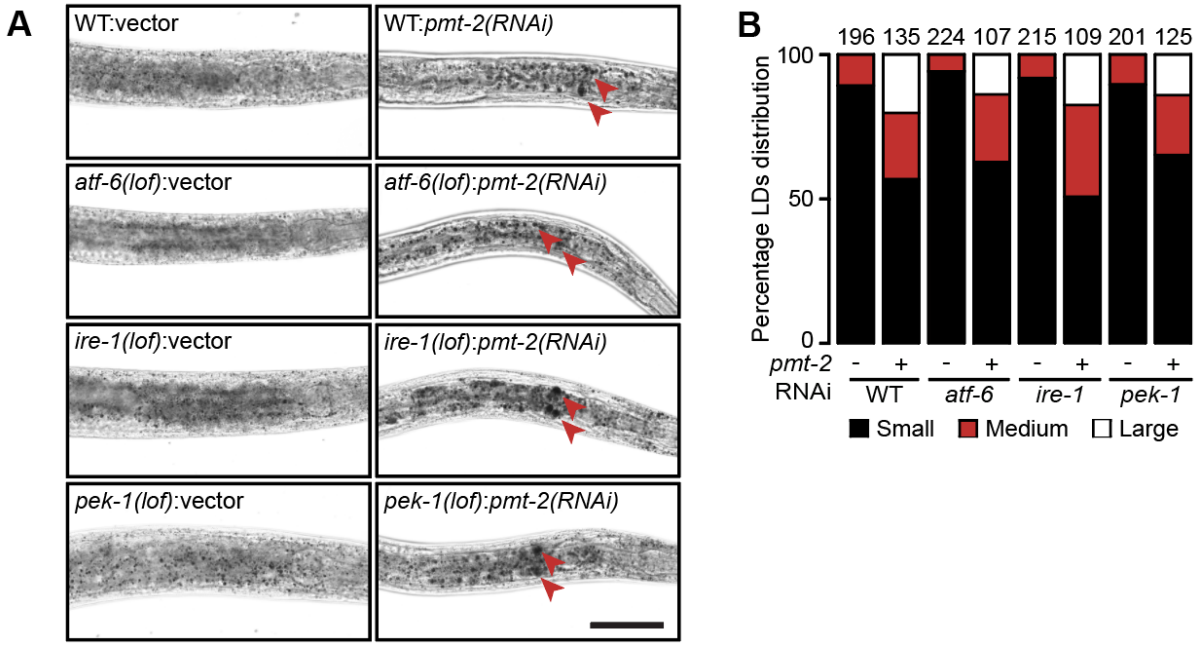

Figure 3:20: UPR^{LBS} leads to the accumulation of lipid droplets.

(A) Representative images of lipid droplet visualized using Sudan Black B staining of WT, *atf-6(lof)*, *ire-1(lof),* and *pek-1(lof)* animals treated with *pmt-2* RNAi. Bright field images of stained worms are shown using a 63X objective lens. Red arrowhead highlights large LDs. Scale bar, 100 µm. (B) Lipid droplet (LD) size distribution quantified from bright-field images of Sudan Black B staining of WT and mutant animals. LD sizes are classified into small (0.8 – 3 µM), medium (3.1 – 6 µM), and large (>6 µM) categories. Numbers above each bar refer to lipid droplets present per worm. WT, n=12 (-), n=15 (+); *atf-6(lof)*, n=13 (-), n=14 (+); *ire-1(lof)*, n=18 (-), n=14 (+); *pek-1(lof)*, n=12 (-), n=13 (+), respectively.

To ensure that *pmt-2* RNAi treatment is sufficient to induce ER stress in the UPR mutants, we monitored the mRNA expression of two downstream target genes of IRE-1, *hsp-3,* and *hsp-4*, by quantitative RT-PCR. As expected, both ER-resident chaperones *hsp-3* and *hsp-4* levels were significantly increased upon *pmt-2* RNAi and tunicamycin treatments in WT and mutant strains except for *ire-1(lof)* (Fig. 3.21). Activation of the UPR from LBS was further validated *in vivo* by immunoblotting using the *hsp-4p::gfp* reporter worms (Calfon et al., 2002). Consistent with *hsp-4* mRNA levels, *pmt-2* RNAi treatment resulted in almost two-fold increase in GFP in *hsp-4p::gfp* animals while tunicamycin induced stronger upregulation (Fig. 3.22). As expected, an increase in GFP was not detected in *xbp-1;hsp-4p::gfp* animals treated with *pmt-2* RNAi nor with tunicamycin as HSP-4 is specifically upregulated from the IRE-1/XBP-1 axis upon ER stress (Acosta-Alvear et al., 2007). Additionally, Walker *et al*. also showed that *sams-1(RNAi)* animals that have reduced PC exhibit HSP-4 activation in an IRE-1/XBP-1-

dependent manner, further supporting our claims that the UPR controls phospholipid metabolism (Walker et al., 2011).

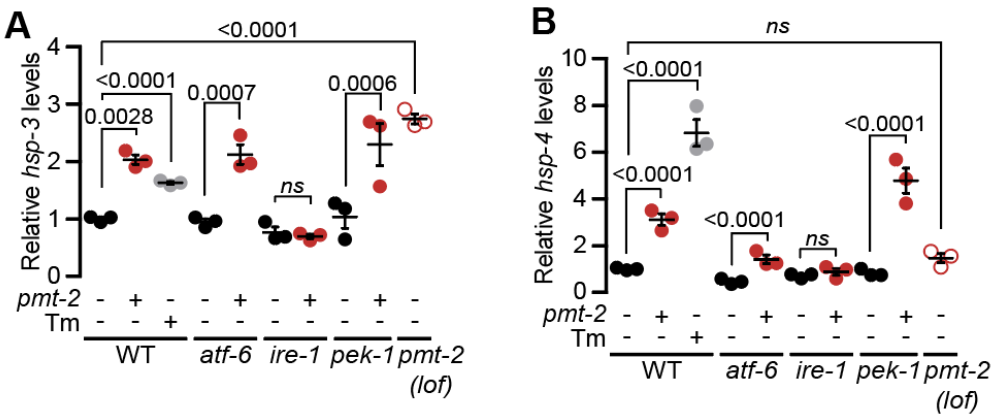

Figure 3:21: *hsp-3* and *hsp-4* expression are dependent on IRE-1 during UPR^{LBS}.

qPCR results comparing the expression of UPR marker genes *hsp-3* (A) and *hsp-4* (B) in WT and mutant animals treated with *pmt-2(RNAi)* for 48 h and WT worms treated 4 h with 25 µg/ml tunicamycin (Tm). Data shown is the mean ± s.e.m. of at least three independent experiments. Statistical analysis was subjected to one-way ANOVA followed by Tukey's multiple comparisons adjustment. *ns*, non-significant.

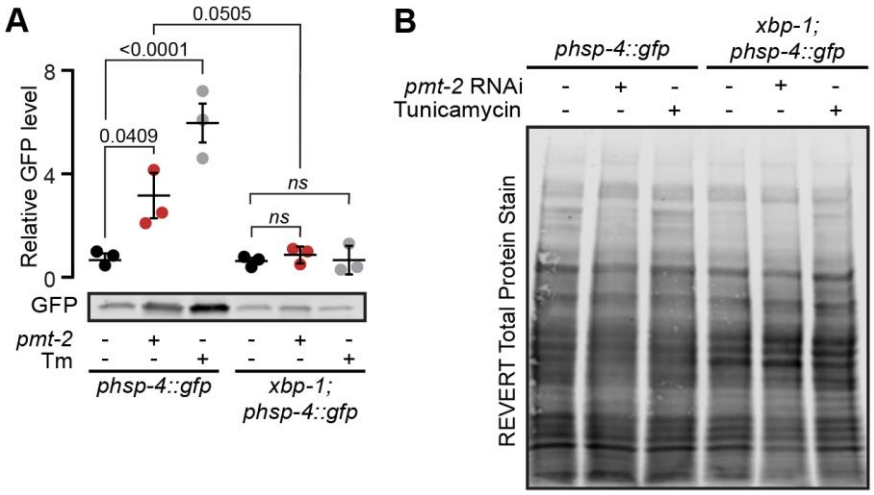

Figure 3:22: LBS activates the UPR in an *ire-1/xbp-1*-dependent manner.

(A) Quantification of immunoblot signaling of worms treated with *pmt-2(RNAi)* for 48 h or 4 h with 25 µg/ml tunicamycin (Tm) and probed with anti-GFP antibodies and normalized to REVERT Total Protein Stain. (B) Total protein stain verified equal loading and served as a normalization control for the immunoblot. *ns*, non-significant.

3.6. UPR^{LBS} upregulates a distinct subset of genes from UPR^{PT}

Several studies suggest that the essential role of the UPR in maintaining metabolic and lipid homeostasis is highly conserved across species. A novel ER stress sensing mechanism was proposed in which the UPR is activated by LBS independently of unfolded protein accumulation in the ER (Halbleib et al., 2017; Promlek et al., 2011; Volmer et al., 2013). Thus, ER stress triggered by proteotoxic stress or LBS might differentially modulate the UPR to reach cellular homeostasis. To answer this question, DNA microarray analysis was performed using RNA extracted from WT, *atf-6(lof)*, *ire-1(lof),* and *pek-1(lof)* animals treated with *pmt-2* RNAi. WT worms incubated with tunicamycin for 4 h were included in the analysis to identify genes modulated by proteotoxic-induced UPR (UPR^{PT}) and subsequently uncouple those specifically modulated by LBS-induced UPR (UPR^{LBS}) (Fig. 3.24). To validate the quality of microarray data, qPCR was performed on a subset of genes (Fig. 3.23).

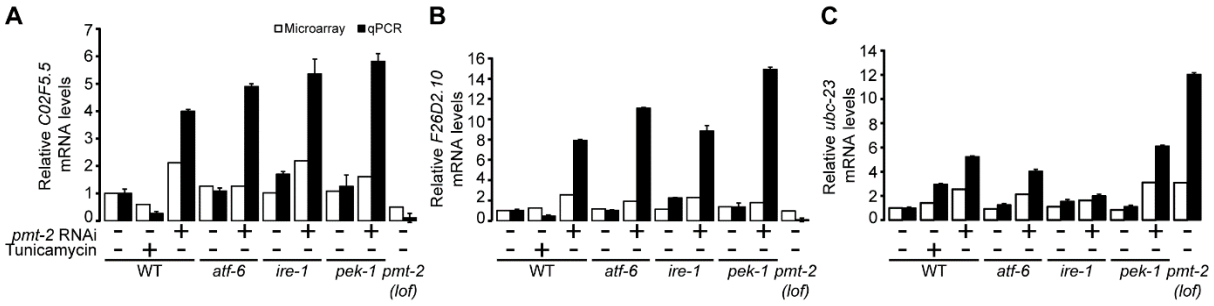

Figure 3:23: UPR^{LBS} induces expression of a group of known UPR-related targets.

Comparison of *C02F5.5* (A), *F26D2.10* (B), and *ubc-23* (C) gene expression in WT, *atf-6(lof)*, *ire-1(lof),* and *pek-1(lof)* animals treated with *pmt-2* RNAi by DNA microarray (white bars) and qPCR (black bars). *C02F5.5* and *F26D2.10*, are both uncharacterized genes; *ubc-23*, a member of the BCL-2 family. The figure represents technical triplicates.

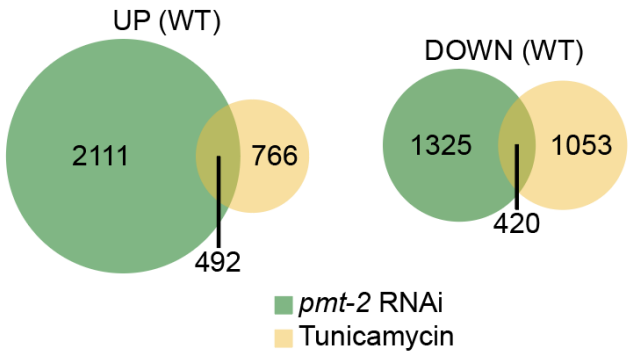

Figure 3:24: UPR^{LBS} and UPR^{PT} lead to distinct transcriptomic outcomes.

Venn diagram representation of upregulated (UP) and downregulated (DOWN) genes at a minimum of 1.5-fold in *pmt-2(RNAi)* and WT worms treated with 25 µg/ml tunicamycin for 4 h compared to untreated WT worms.

To explore how the UPR elicits a differential stress response during LBS and proteotoxic stress, we filtered the 2111 gene candidates that were upregulated only in *pmt-2(RNAi)* animals and excluding genes upregulated in tunicamycin-treated animals, respectively (Fig. 3.24). Genes with unaltered expression in at least one of the UPR mutants subjected to *pmt-2* RNAi are modulated by UPR^{LBS}. From these criteria, 1069 genes were upregulated in a UPR^{LBS}-dependent manner (Fig. 3.24, Table A2). We identified 181, 417, and 25 genes that are specifically upregulated from ATF-6, IRE-1, and PEK-1 branches, respectively, while 446 genes are modulated from at least two of the three UPR branches, suggesting compensatory roles of one or more UPR transducers in the absence of the other branches. In addition, we grouped genes with at least 1.5-fold change by hierarchical clustering (Fig. 3.26). This allowed us to visualize genes that were similarly regulated throughout the array from UPR^{LBS}. Manual inspection of our array data demonstrates that the upregulation of known UPR target genes agrees with previous reports (Fig. 3.27) (Shen et al., 2005; Thibault et al., 2011; Travers et al., 2000).

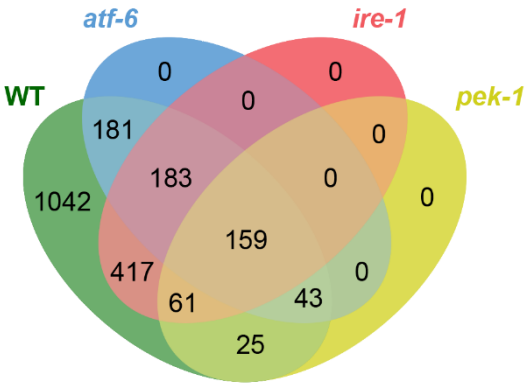

Figure 3:25: ATF-6, IRE-1 and PEK-1 regulate distinct groups transcriptomic targets during UPR^{LBS}.

Four-way Venn diagram depicts transcriptional targets of WT, *atf-6(lof)*, *ire-1(lof)* and *pek-1(lof)* worms upregulated during lipid bilayer stress and excluding genes commonly upregulated from *pmt-2* RNAi and tunicamycin treatments. Fold-change > 1.5, ANOVA P values < 0.05.

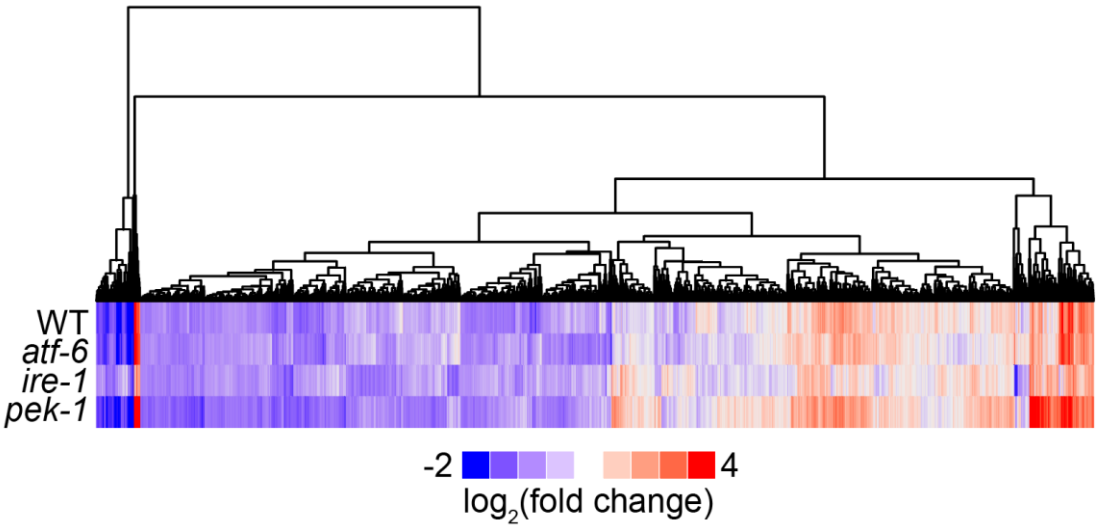

Figure 3:26: Hierarchical clustering shows genome-wide differences in gene regulation by ATF-6, IRE-1 and PEK-1 during LBS.

Hierarchical clustering of 8045 genes with significant changes based on Pearson correlation coefficients. Gene expression of WT, *atf-6(lof)*, *ire-1(lof)*, *pek-1(lof)* worms treated with *pmt-2* RNAi were compared against their respective untreated worms (empty vector).

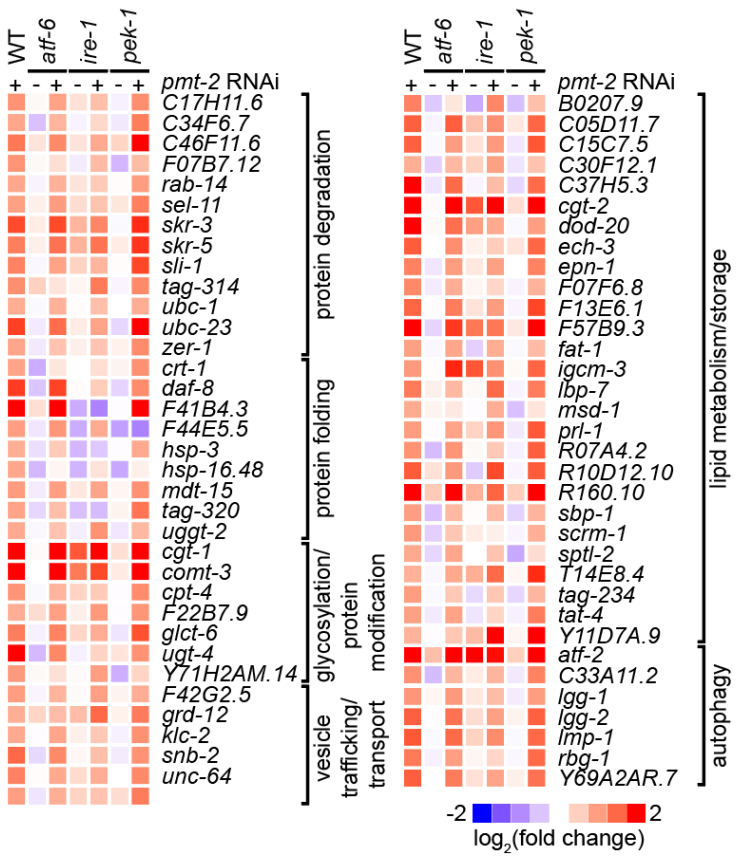

Figure 3:27: Lipid bilayer stress induces well-known transcriptional targets of the UPR.

Heat map representation of previously reported UPR-regulated genes of worms. Gene expression $\log_2$ fold changes were normalized to untreated WT worms.

To further understand the role of the UPR^{LBS} program, we performed functional annotation for 1069, 181, 417, and 25 upregulated genes identified from *pmt-2(RNAi)*, *atf-6(lof)*; *pmt-2(RNAi)*, *ire-1(lof)*; *pmt-2(RNAi)*, and *pek-1(lof)*; *pmt-2(RNAi)* animals, respectively, using the gene ontology tool DAVID (Table A3) (Huang et al., 2007a). Immune regulatory genes were found to be enriched in the upregulated categories of WT and *ire-1(lof)* animals (Fig. 3.28A, C). This agrees with a previous report where innate immunity was found to be modulated by *sams-1*, the methyl donor to *pmt-1* and *pmt-2* (Ding et al., 2015). Our data suggest that innate immune response is positively and negatively regulated by IRE-1 and PEK-1, respectively (Fig. 3.28). As expected, GO terms related to ER stress were found to be enriched in the upregulated categories of WT and mutant animals when PC is depleted (Fig. 3.28) (Ding et al., 2015). We also identified enrichment of downregulated genes in WT related to translational

initiation factors including *eif-1.A, eif-3.C* and *eif-3.E*, a characteristic effect of UPR activation (Ling et al., 2009; Long et al., 2002).

Protein tyrosine phosphatase activity is significantly regulated by ATF-6 upon LBS (GO ID: 0035335, n = 6, Benjamini P-value 0.047) (Fig. 3.28B). This class of genes is activated in response to ER stress (Agouni et al., 2011). Transcriptional regulation (GO ID: 0006355, n = 49, Benjamini P-value 3.3E-09) is enriched among IRE-1 dependent genes and supports the evidence that it alleviates ER stress by widespread transcriptional modification process (Fig. 3.28C) (Ng et al., 2000). In addition, genes involved in lipid and fatty acid processes were also enriched by IRE-1 and PEK-1 (Fig. 3.28C, D). Lastly, protein tyrosine phosphatase activity (GO ID: 0004725, n = 4, Benjamini P-value = 0.039) is enriched by PEK-1, suggesting its involvement in protein modifications and cell signaling cascade during LBS (Fig. 2.16D) (Bettaieb et al., 2012). Interestingly, we observed upregulation of autophagy-related processes that are IRE-1 dependent shown in the volcano plot, where autophagy-related genes with at least 1.5-fold change and FDR P values less than 0.05 were displayed on the plot (Fig. 3.29). Crosstalk between the UPR and autophagy in the context of protein clearance has been well documented.

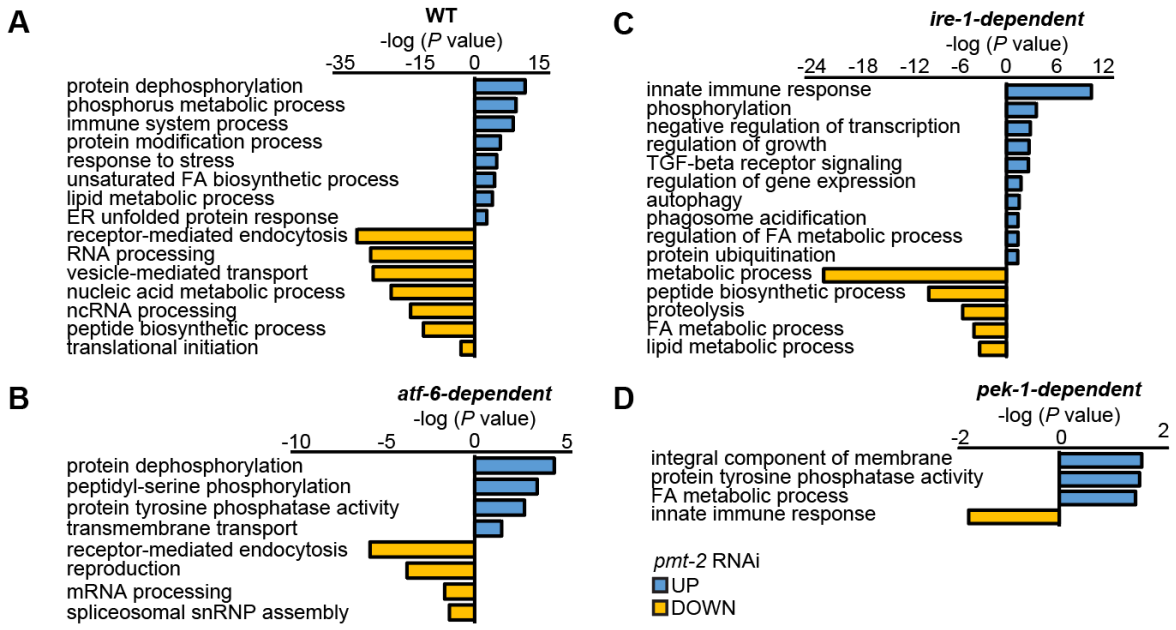

Figure 3:28: Depletion of PC increases autophagy and lipid metabolism activity in an IRE-1-dependent manner.

(A-D) Bar plot of the GO analysis of genes upregulated (blue) and downregulated (yellow) in WT (A), *atf-6(lof)* (B), *ire-1(lof)* (C) and *pek-1(lof)* (D) subjected to *pmt-2* RNAi and compared to their respective untreated strains (empty vector). Refer to Table A3 for genes corresponding to the GO terms.

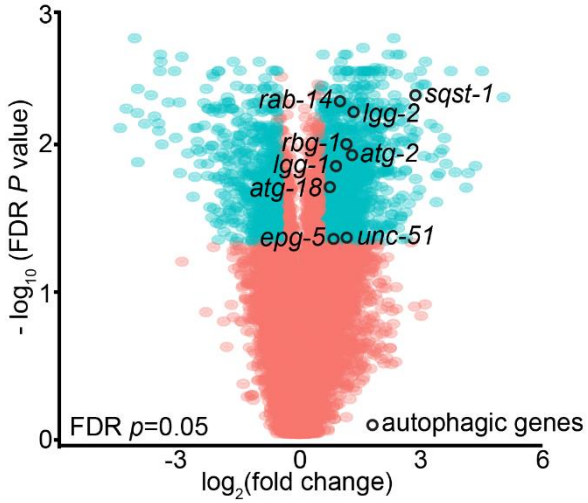

Figure 3:29: UPR^{LBS} drives expression of autophagic genes.

Volcano plot depicts changes in gene expression during UPR^{LBS}. Log_2 gene fold changes are plotted against negative log_{10} FDR p values. Genes that are upregulated or downregulated by more than 1.5-fold and with false-discovery rate (FDR) < 0.05 are labeled in black circles. Autophagic (opened circle) genes regulated in an IRE-1-dependent manner are shown in black.

3.7. IRE-1/XBP-1 axis regulates autophagy during UPR^{LBS}

To investigate if the autophagic process is activated during the UPR^{LBS}, we carried out an RNAi screen of autophagy-related genes. To decrease PC levels, WT worms were first subjected to 36 h of *pmt-2* RNAi followed by 5 days of autophagy-related gene RNAi treatment (Fig. 3.30). Phenotypes following RNAi treatment were classified as 0 (little difference in growth and brood size), 1 (smaller brood size, sick), and 2 (sterile, very sick) compared to empty vector negative control. The screen was carried out twice and scores were designated for both WT animals pre-treated with vector and *pmt-2* RNAi. A clone was classified as positive if the difference of the sum of *pmt-2* RNAi treatment to vector treatment is ≥ 3 (Table A4, page 112-114).

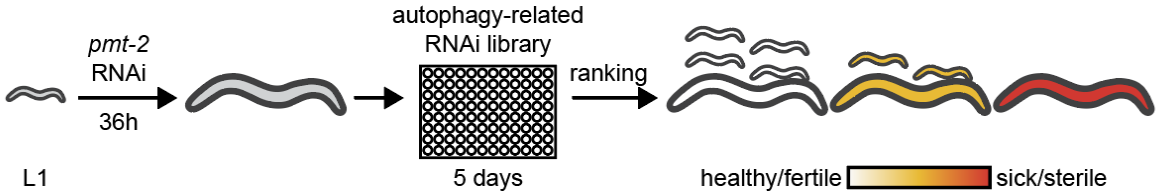

Figure 3:30: Schematic representation of the RNAi screening to identify potential autophagy genes that participate in lipid bilayer stress.

WT worms were treated with *pmt-2* RNAi for 36 h and subsequently transferred to 96-well plates containing RNAi of autophagy-related target genes. Worms were scored for growth defects, sterility, mobility, and embryonic lethality.

From the 40 RNAi clones, seven were found to induce development defects upon RNAi treatment compared to vector control (Fig. 3.31). As positive controls, we incorporated *ero-1* and *pmt-2* RNAis as lead to either developmental defects or sterility. The screen revealed that some autophagy-related genes are required during UPR^{LBS} and their absence contributes to the observed detrimental phenotypes. Identified genes include *atg-7* (ortholog of human *ATG7*, autophagosome conjugation), *atg-13* (ortholog of human *ATG13*, autophagosome formation), *bec-1* (ortholog of human Beclin1, vesicle nucleation), and *wdfy-3* (ortholog of human *WDFY3*, autophagy adaptor) (Jia et al., 2007; Melendez et al., 2003; Takacs-Vellai et al., 2005; Wang et al., 2018). Additionally, the screen has identified potential autophagy-related genes that are less characterized and prompt further investigation. These include *rsks-1* (ortholog of human RPS6KB1, negative regulator of autophagy),

sepa-1 (no human ortholog identified, P-granules-associated autophagy), and *trpp-8* (ortholog of human *GSG1*, autophagic processes).

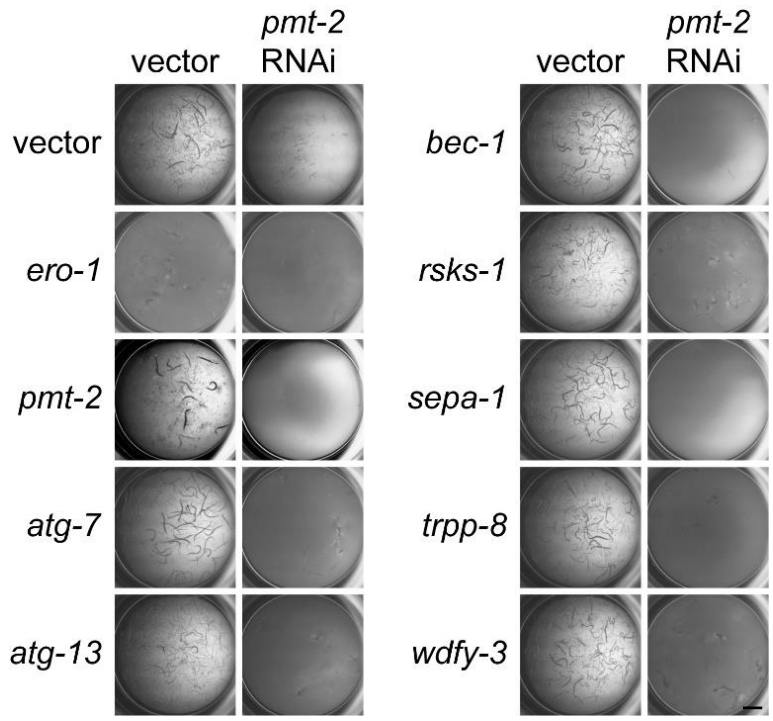

Figure 3:31: Autophagy is essential during lipid perturbation.

WT worms were treated with vector or *pmt-2* RNAi for 36 h and subsequently subjected to RNAi in liquid media in a 96-well plate for 5 days. The worms were scored based on their developmental defects as described in Fig. 2.18. *ero-1* RNAi was included as a positive control. The experiment was conducted twice with technical duplicates in each experiment. Scale bar, 1 mm. Refer to Table A4 (pages 112-114) for phenotype scoring.

To better understand the crosstalk between UPR^{LBS} and autophagy, we monitored the transcription levels of key autophagy-regulatory genes. Both *bec-1* and *lgg-1* (ortholog of human MAP1LC3, autophagosome formation) genes were found to be significantly upregulated in WT, *atf-6(lof),* and *pek-1(lof)* but not in *ire-1(lof)* compared to control upon *pmt-2* RNAi treatment (Fig. 3.32). These results suggest that IRE-1 modulates *bec-1* and *lgg-1* expression during LBS. We validated that *bec-1* and *lgg-1* are both upregulated by tunicamycin as previously reported (Ogata et al., 2006). Once IRE-1 is activated, the endoribonuclease within the IRE-1 cytoplasmic domain cleaves *xbp-1* mRNA through an

unconventional splicing. This is followed by the translation of the XBP-1 transcription factor that regulates a downstream signaling cascade (Ho et al., 2018; Walter and Ron, 2011) that modulates the expression of target genes including *hsp-3* during UPR^{LBS} (Fig. 3.33). Thus, we monitored *bec-1* and *lgg-1* mRNA levels in *xbp-1(lof)* treated with *pmt-2* RNAi. The upregulation of *bec-1* and *lgg-1* was abolished in *xbp-1(lof)* suggesting that XBP-1 modulates autophagy during UPR^{LBS} (Fig. 3.34A, B). A similar increase in mRNAs of *atg-18* (ortholog of human WIPI) and *epg-4* (ortholog of human EI24) was observed in *pmt-2(RNAi)* but not in *xbp-1(lof);pmt-2(RNAi)* animals (Fig. 3.34C, D) (Devkota et al., 2016; Tian et al., 2010). On the other hand, no significant transcriptional variations in *atg-4.1* (ortholog of human ATG4) and *atg-9* (ortholog of human ATG9) were observed, while *atg-16.2* (ortholog of human ATG16L1) was upregulated upon LBS in an XBP-1-independent manner (Fig. 3.35). Altogether, these findings suggest that the UPR program transcriptionally regulates a subset of autophagy genes during LBS.

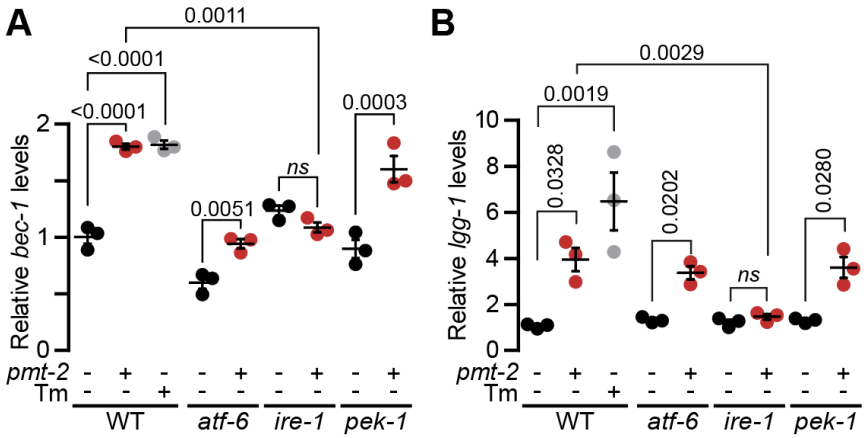

Figure 3:32: A subset of autophagy genes is regulated through IRE-1 upon lipid bilayer stress-induced UPR.

qPCR comparing expression of *bec-1* (A) and *lgg-1* (B) in WT, *atf-6(lof)*, *ire-1(lof)* and *pek-1(lof)* worms. Data shown is the mean ± s.e.m. of at least three independent experiments. Statistical analysis was subjected to one-way ANOVA followed by Tukey's multiple comparisons adjustment. *ns*, non-significant.

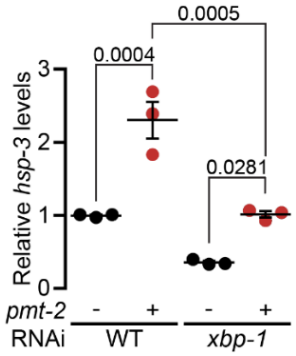

Figure 3:33: XBP-1 modulates expression of downstream IRE-1 target *hsp-3*.

qPCR comparing expression of *hsp-3* in WT and *xbp-1(lof)* worms. Data shown is the mean ± s.e.m. of at least three independent experiments. Statistical analysis was subjected to Student's t-test.

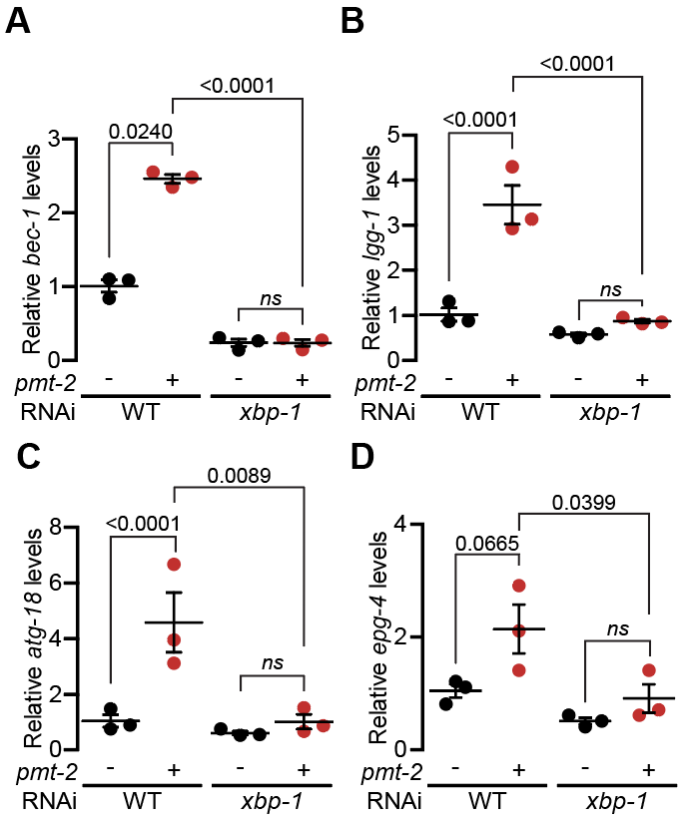

Figure 3:34: A subset of autophagy genes is regulated through the IRE-1/XBP-1 axis upon lipid bilayer stress-induced UPR.

qPCR comparing expression of *bec-1* (A), *lgg-1* (B), *atg-18* (C), and *epg-4* (D) in WT and *xbp-1(lof)* animals treated with *pmt-2* RNAi. Data shown is the mean ± s.e.m. of at least three independent experiments. Statistical analysis was subjected to Student's t-test. *ns*, non-significant.

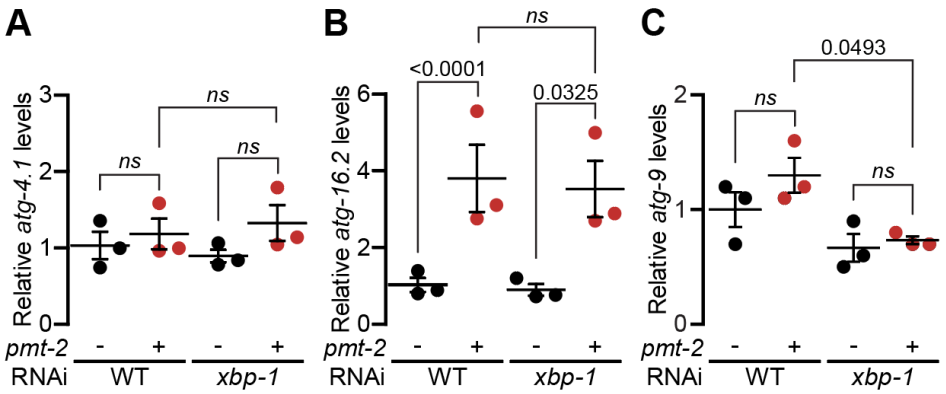

Figure 3:35: Autophagy is partially dependent on XBP-1.

qPCR comparing expression of *atg-4.1* (A), *atg-16.2* (B), *atg-9* (C) in WT and *xbp-1(lof)* mutants treated with *pmt-2* RNAi. Data shown is the mean ± s.e.m. of at least three independent experiments. Statistical analysis was subjected to Student's t-test. *ns*, non-significant.

To gain insight on autophagy flux, we used the autophagy reporter strain *lgg-1p::gfp::lgg-1* crossed with *eri-1(lof)* worms, which are highly sensitive to simultaneous treatment with two different RNAi (Melendez et al., 2003). We showed that double RNAi of *pmt-2* and *ire-1* in *eri-1* background worms is efficient (Fig. 3.36A, B). In addition, we also showed that *eri-1;lgg-1p::gfp::lgg-1* worms treated with *ire-1* RNAi are incapable of activating the UPR during LBS (Fig. 3.36C). We detected an increased number of GFP::LGG-1 puncta in intestinal tissues of *pmt-2(RNAi)* animals, but not in *ire-1* and *pmt-2* double RNAi treated animals (Fig. 3.37). These puncta are indicative of autophagosomes as spermidine treatment increased the number of GFP::LGG-1 puncta (Jia et al., 2009). Next, we separated GFP::LGG-1 from its PE-conjugated form, GFP::LGG-1-PE, an autophagosomal marker (Kang et al., 2007). When entering the lysosome, GFP::LGG-1-PE is hydrolyzed, releasing stable and free GFP (Hosokawa et al., 2006). Significant increases in GFP::LGG-1-PE, as well as free GFP, were observed in *pmt-2(RNAi)* but not in *ire-1(RNAi);pmt-2(RNAi)* (Fig. 3.38). Together, these results indicate that autophagy is modulated by the IRE-1/XBP-1 axis upon UPR^{LBS}.

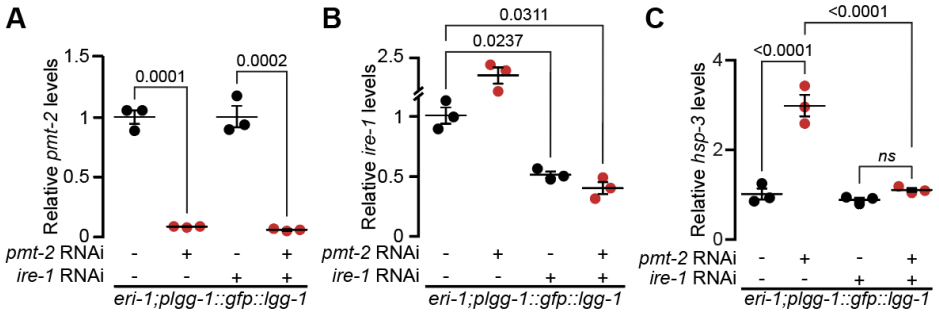

Figure 3:36: *pmt-2* RNAi efficiently depleted PC and induces UPR^{LBS} in *eri-1;lgg-1p::gfp::lgg-1* worms to the level similar to WT worms.

qPCR comparing expression of *pmt-2* (E), ire-1 (F), *hsp-3* (G) in *eri-1;lgg-1p::gfp::lgg-1* worms treated with *pmt-2*, *ire-1*, and *ire-1*:*pmt-2* RNAis. Data shown is the mean ± s.e.m. of at least three independent experiments. Statistical analysis was subjected to Student's t-test. *ns*, non-significant.

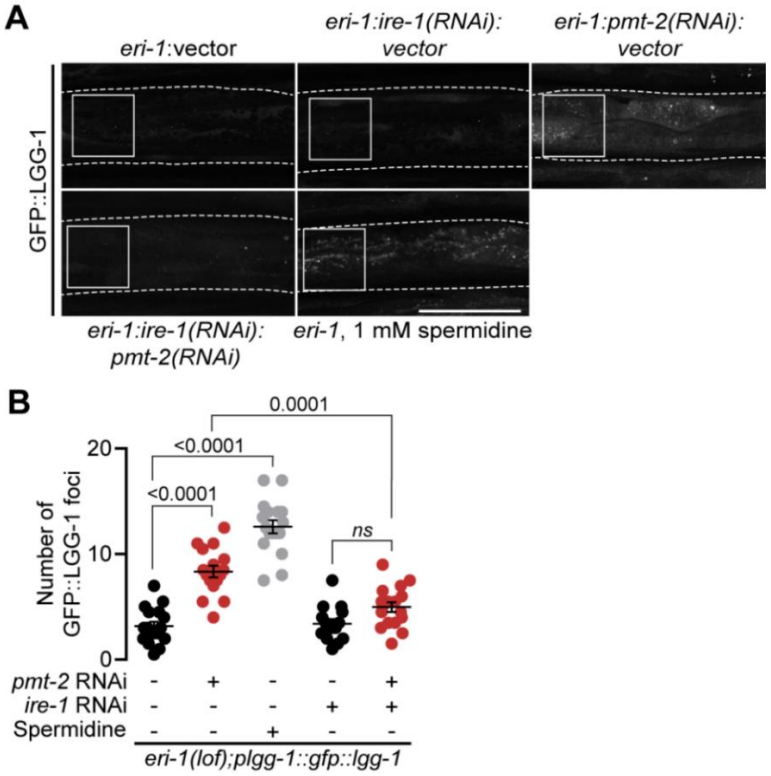

Figure 3:37: Autophagy activation during UPR^{LBS} is dependent on IRE-1.

Representative fluorescence images (A) and quantification (B) of GFP::LGG-1 puncta (I) in the anterior intestines of *eri-1;lgg-1p::gfp::lgg-1* worms treated for 48 h with *pmt-2* RNAi, *ire-1* RNAi, 1 mM spermidine or a combination of *ire-1* and *pmt-2* RNAis. Solid box depicts quantification area, dashed lines show the outline of worms. Scale bar, 50 µm. n=17, n=16, n=17, n=15, n=18, for *eri-1*:vector, *eri-1:pmt-2(RNAi)*, *eri-1* treated with 1 mM spermidine, *eri-1:ire-1(RNAi), eri-1:ire-1(RNAi)*:*pmt-2(RNAi)*, respectively. Data shown is the mean ± s.e.m. of at least three independent experiments. Statistical analysis was subjected to Student's t-test. *ns*, non-significant.

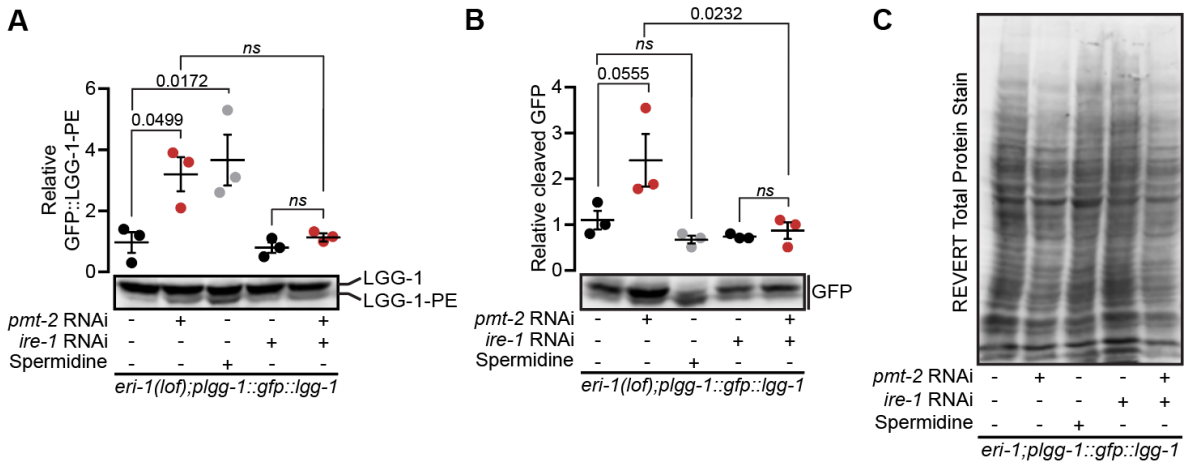

Figure 3:38: UPR^{LBS} animals present an increase in the autophagic flux that is dependent on IRE-1.

Separation of GFP::LGG-1-PE (A) and cleaved GFP (B) in *eri-1;lgg-1p::gfp::lgg-1* worm lysate. The lysates were prepared and analyzed by immunoblotting with anti-GFP antibodies and normalized to total protein loading control (C). Cleaved GFP represents autophagic flux where the GFP degradation takes place at the autolysosomes. As a measure of autophagic flux, ratios of GFP::LGG-1-PE to total protein and of cleaved GFP to total proteins were compared. Data shown is the mean ± s.e.m. of at least three independent experiments. Statistical analysis was subjected to one-way ANOVA followed by Tukey's multiple comparisons adjustment. *ns*, non-significant. Statistical analysis was subjected to Student's t-test.

3.8. Disruption in lipid metabolism-related gene *lpin-1* activates the UPR

We have shown that the saturation of cellular lipids is important in maintaining proper ER function as tipping the saturation/unsaturation ratio to either side of the scale is capable of altering the membrane lipid composition, causing LBS and thereby activating the UPR. Additionally, we demonstrated that PC depletion through *pmt-2* RNAi served as a good model in our understanding of the UPR^{LBS}. To systematically dissect currently unknown lipid-related factors and their relationship with the UPR, we decided to perform an RNAi screen. Our screening criteria involved identification of lipid metabolism-related candidate genes whose downregulation led to developmental defects in *ire-1(lof)* worm strain. To curate the RNAi sub-library, we curated 171 genes related to lipid and metabolism processes from literature, GO terms and KEGG pathways (Harris et al., 2004; Ho et al., 2020; Kanehisa and Goto, 2000). Age-synchronized L1 wild type or *ire-1(lof)* worms were subjected to four to five days of liquid-

based RNAi in 96-well plates. Phenotypes following RNAi treatment were scored and designated as 0 (little difference in growth and brood size), 1 (smaller brood size, sick), and 2 (sterile, very sick) compared to the empty vector negative control and *lbp-7* (lipid binding protein 7, human homolog of FABP5, fatty acid binding protein 5) where its silencing does not affect *ire-1(lof)* (Fig. 3.40). The RNAi screen was carried out twice and a gene candidate was classified as a hit if the sum of phenotype score from both screens is equal to or higher than 3 compared to the worms fed with empty vector and wild type worms treated with the same RNAi (Table A5, page 115-119). Based on our results, of the 171 RNAi gene candidates screened, inactivation of *dhs-18* and *lpin-1* reproducibly caused developmental defects in *ire-1(lof)* worms when compared to wild type worms (Fig 3.41).

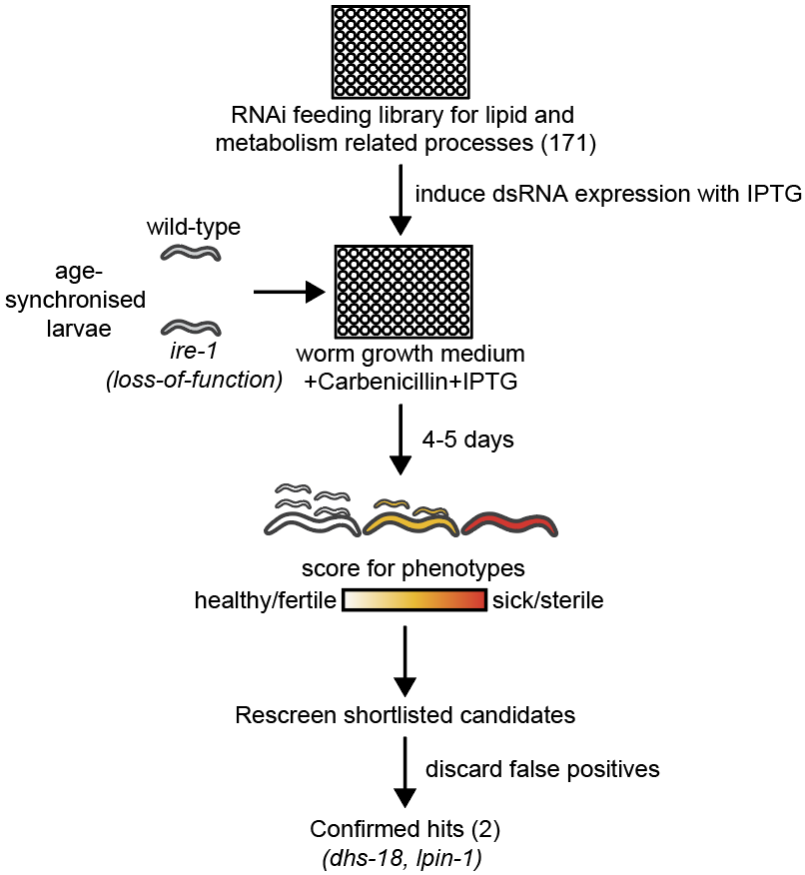

Figure 3:39: An RNAi enhancer screen designed to identify novel lipid or metabolism-related genes that exacerbate phenotypical defect caused by the absence of the UPR sensor IRE-1.

Wild type or *ire-1(lof)* worms were synchronized by hypochlorite treatment, and RNAi bacteria were cultured from the ORFeome RNAi library. Ten synchronized L1 animals were added to IPTG-induced RNAi culture resuspended in S-medium and were grown for 4-5 days until the WT worms in control wells reach adulthood and give rise to progenies. Worms were scored for growth defects, sterility, mobility, and embryonic lethality. The experiment was repeated twice with two technical replicates each.

Candidates were shortlisted when *ire-1(lof)* worms fed with the RNAi bacteria exhibit significant phenotypical difference when compared to wild-type worms fed with the same bacteria. Shortlisted candidates were then subjected to two independent RNAi feeding in liquid medium with two technical replicates each.

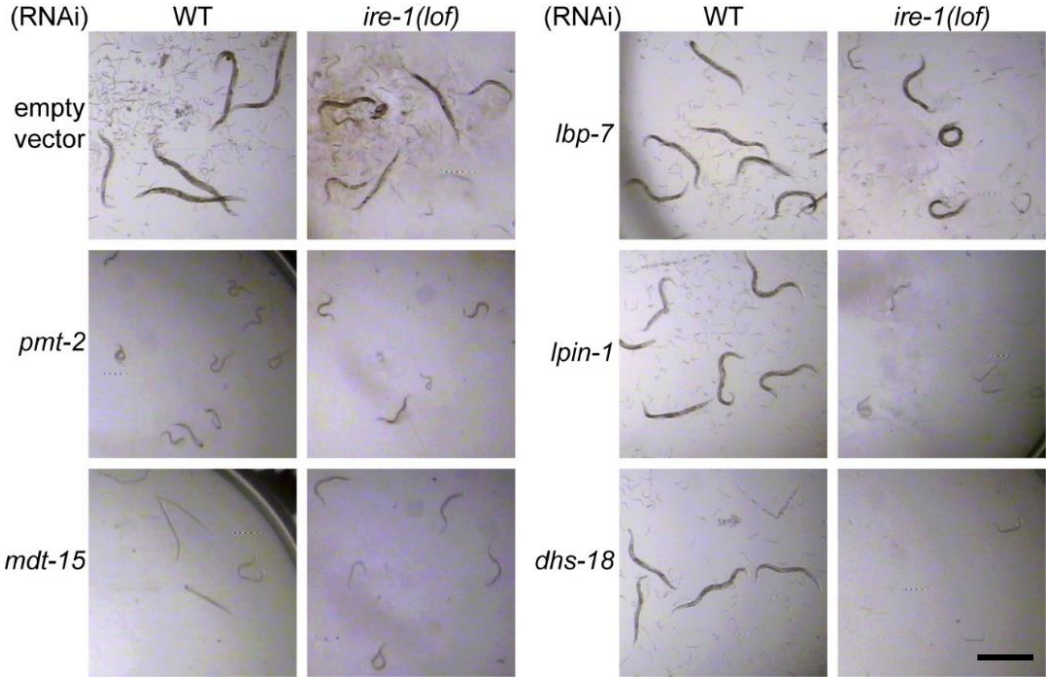

Figure 3:40: *lpin-1* and *dhs-18* RNAis exert enhancing effect in *ire-1(lof)* worms.

Representative micrographs show WT and *ire-1(lof)* worms were treated with empty vector and *lbp-7* as negative controls, *pmt-2* and *mdt-15* RNAis as positive control, and *lpin-1* and *dhs-18* RNAis for verification of confirmed hits from the RNAi screen. The worms were grown in liquid media in a 96-well plate for 5 days at 20°C. Images of the worms in 96-well plate were taken under a stereomicroscope at a total of 80X magnification. The experiment was performed twice with technical duplicates in each experiment. Refer to Table A5 (page 115-119) for phenotype scoring. Scale bar, 500 µm.

DHS-18 belongs to a short-chain dehydrogenase/reductases family of protein that resembles human hydroxysteroid dehydrogenase-like protein 2 (HSDL2) (Sun et al., 2018). It is highly expressed in the intestines and is predicted to be regulated by components of the insulin-signaling pathway such as *daf-2, daf-16,* and *glp-1* (Keshet et al., 2017). DHS-18 is localized in the peroxisomes, an organelle essential in synthesizing steroids and fatty acids. Loss of HSDL-2 in human is linked to ovarian cancer progression (Sun et al., 2018). LPIN-1 (mammalian homolog of Lipin protein) is a phosphatidic acid

phosphatase and a transcriptional regulator that regulates lipid metabolism in organisms ranging from yeast to mammals. Loss of Lipin in mice is known to cause lipodystrophy characterized by fatty liver and hypertriglyceridemia (Peterfy et al., 2001). The mammalian Lipin protein possesses two evolutionarily conserved regions known as the N-terminal (N-LIP) and C-terminal (C-LIP) domains. Additionally, lysine and arginine-rich nuclear-localization signal (NLS) can also be found in Lipin protein, indicating regulation of Lipin through phosphorylation event that allows Lipin to translocate into the nucleus. One study found that insulin was capable to promote phosphorylation of Lipin that resulted in its translocation to the nucleus (Harris et al., 2007). RNAi knockdown of *lpin-1* in *C. elegans* was shown to cause nuclear envelope breakdown and alterations in the ER membrane organization (Golden et al., 2009). C-terminal domain nuclear envelope-localized phosphatase-1 CTDNEP1 (CTD nuclear envelop phosphatase-1, CNEP-1 in worms) is an enzyme that positively regulates Lipin activity. CTDNEP1 silencing has been observed to cause ER patches formation in the nuclear envelope. As a result of *lpin-1* or *cnep-1* silencing, phospholipid flux is altered, where lack of Lipin favors phosphatidylinositol (PI) accumulation. This causes ER sheets formation and leads to the phenomenon of ER membrane disorganization (Bahmanyar et al., 2014).

To determine if *lpin-1* silencing similarly causes disorganization of the ER, we *utilized C. elegans* strain expressing the ER marker signal peptidase 12 (SP12) tagged with GFP (*vha-6p::gfp::sp12*). The ER morphology changes throughout embryo development (Poteryaev et al., 2005). To avoid confounding effect, we selectively images of worm embryos that are at two-cell stage. Consistent with their findings, *lpin-1* deficiency caused perturbation in the peripheral ER organization, resulting in the formation of ER clusters (Fig. 3.41) (Bahmanyar et al., 2014; Golden et al., 2009).

The C-LIP domain of Lipin contains a conserved phosphatase motif (DXDXT) that is required for phosphatidate phosphatase activity (Finck et al., 2006). In the cytosol, phosphorylation of Lipin by the mechanistic target of rapamycin (mTOR), a protein belonging to the phosphatidylinositol 3-kinase-related kinase family, inhibits its phosphatase activity by preventing the amino-terminal amphipathic helix from binding to ER membrane (Karanasios et al., 2010). On the contrary, dephosphorylation of Lipin by CTD nuclear envelope phosphatase 1 (CTDNEP1) activates Lipin, allowing it to translocate to the proximity of the ER membrane where phosphatidic acid (PA) is present at high concentration and convert PA to diacylglycerol (DAG). Regulation of PA levels by Lipin thus indirectly regulates

triacylglycerol (TAG) levels and production of lipid droplets (LDs). Upon *lpin-1* depletion, wild type and *ire-1(lof)* worms showed a marked decrease in neutral lipid accumulation, corroborating a finding where knockdown of *lpin-1* decreased lipid content (Fig. 3.42) (Jung et al., 2020).

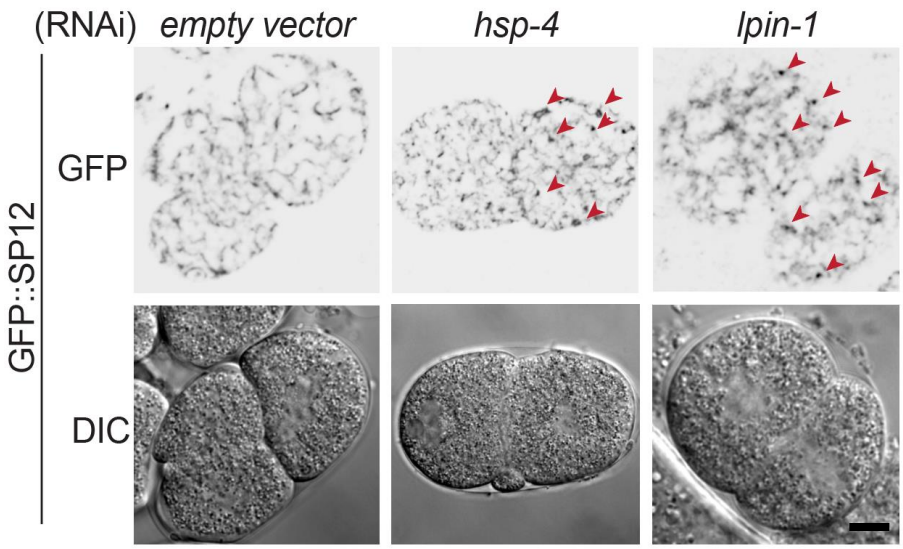

Figure 3:41: LPIN-1 silencing perturbs ER morphology.

Confocal microscopy and differential interference contrast (DIC) microscopy images of empty vector, *hsp-4(RNAi)* and *lpin-1(RNAi*) two-cell stage embryos expressing GFP::SP12. Age-synchronized L1 stage worms were treated with respective RNAi until day 1 adulthood. The gravid adult worms were dissected to release the embryos. The embryos were then mounted on a 2% agar pad and two-cell stage embryos were chosen for imaging using a 100X objective with a numerical aperture of 1.3. The red arrows point to ER clusters formation. Images shown are representative of two independent experiments. Scale bar, 10 µm.

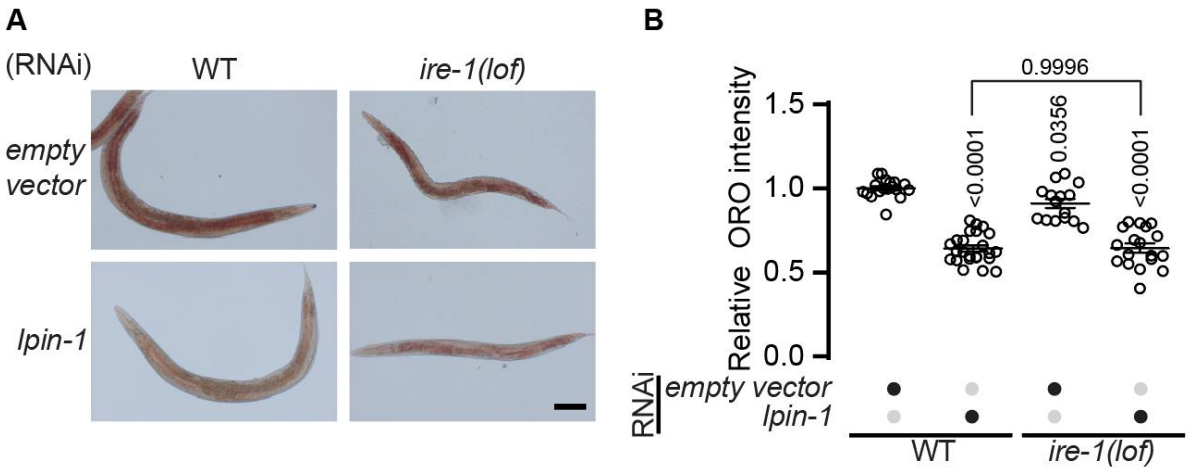

Figure 3:42: LPIN-1 depletion caused changes in fat accumulation.

Oil-Red-O staining of wild type and *ire-1(lof)* worms treated with empty vector and *lpin-1(RNAi)* for 72 h. Representative micrographs (A) and quantification (B) of fat content levels in the pharyngeal area of the worms as previously described (n = 15 – 24 worms from two independent experiments) (Yen et al., 2010). Scale bar, 100 µm. Data shown is the mean ± s.e.m. of two independent experiments. Two-tailed Student's t-test was carried out to evaluate statistical significance.

In *C. elegans*, RNAi of PC biosynthetic enzymes (*sams-1, pmt-1, cept-1,* and *pcyt-1)* or LPIN-1 silencing can both activate SBP-1 (the *C. elegans* ortholog of sterol regulatory element-binding protein 1, SREBP-1) to maintain lipid balance (Smulan et al., 2016). Similarly, our microarray data from the earlier study showed that PC depletion through *pmt-2* RNAi activated *lpin-1* in an IRE-1-dependent manner (Fig. 3.44) (Koh et al., 2018). In addition, an increase in *lpin-1* mRNA levels is independent of tunicamycin-induced proteotoxic stress (Figure 3.43). We hypothesized that silencing of *lpin-1* would affect lipid metabolism and the UPR may be induced to restore lipid homeostasis. To assess UPR activation from *lpin-1* RNAi, we performed qPCR and found that *lpin-1* depletion resulted in a mild increase in *hsp-4* mRNA levels, suggesting UPR activation that is dependent on IRE-1 (Fig. 3.45A). LPIN-1 is a known transcriptional regulator of fatty acid metabolism genes including *fat-5,* where the loss of *lpin-1* may increase SBP-1/SREBP-1 activity, thus increasing *fat-5* expression (Smulan et al., 2016). By performing qPCR, we observed an increase in *fat-5* mRNA levels resulting from *lpin-1* RNAi as observed in other studies, however, as this experiment has only been performed twice, more biological replicates are needed to affirm the claim (Fig. 3.45B) (Jung et al., 2020; Smulan et al., 2016). Together, these data suggest that *lpin-1* RNAi may perturb lipid metabolism and activate the UPR, which normally requires the compensatory function of IRE-1. However, the loss of *ire-1* impaired the compensatory response in *lpin-1* RNAi worms, leading to a severe phenotypical defect.

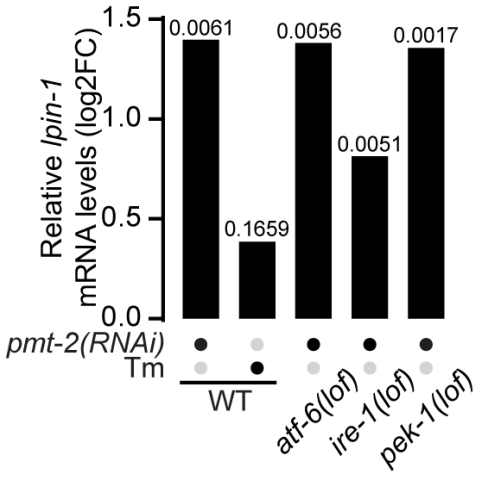

Figure 3:43: *lpin-1* mRNA expression increases from lipid bilayer stress and is partially dependent on IRE-1.

Log_2 fold-change of *lpin-1* mRNA in *pmt-2* RNAi treated wild type, *atf-6(lof)*, *ire-1(lof)* or *pek-1(lof)* worms were compared against mRNA expression levels of their respective empty vector treated control strain. *pmt-2* RNAi was carried out for 48 h. *lpin-1* expression data was extracted from microarray performed in (Koh et al., 2018). To induce proteotoxic stress, WT worms were treated with 25 µg/ml tunicamycin (Tm) for 4 h. Data shown here represents average mRNA expression of *lpin-1* from three independent experiments. Statistical analysis was subjected to One-way ANOVA. P-values above the bars represent changes in *lpin-1* mRNA levels relative to untreated wild type worms ($log_2FC = 0$).

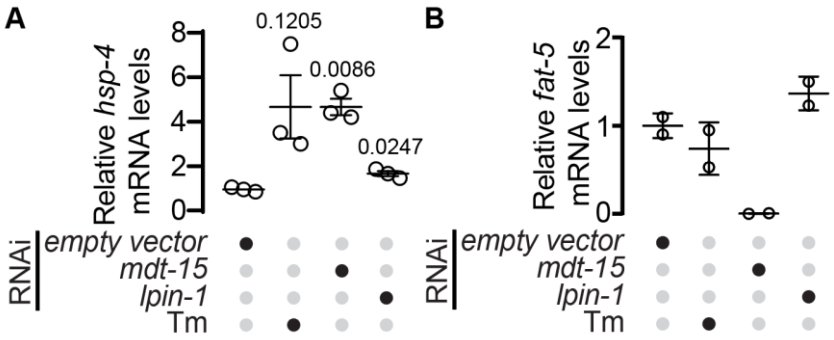

Figure 3:44: *lpin-1* knockdown activates the UPR.

qPCR results comparing the expression of the UPR marker gene *hsp-4* and LPIN-1 responsive gene *fat-5* in WT worms treated with *mdt-15* or *lpin-1* RNAi for 48 h in liquid culture. *mdt-15*(RNAi) was used to induce LBS and served as a positive control. To induce proteotoxic stress, WT worms were treated with 25 µg/ml tunicamycin (Tm) for 4 h. Data shown is the mean ± s.e.m. of three independent experiments for *hsp-4* mRNA levels evaluation and two independent experiments for *fat-5* mRNA levels evaluation. Two-tailed Student's t-test was used to evaluate statistical significance between the experimental conditions and empty vector for *hsp-4* mRNA levels evaluation.

Chapter 4: Discussion

Lipid dysregulation refers to excessive accumulation of lipids in tissues including the liver, pancreas, and adipose (Hotamisligil and Erbay, 2008; Rinella and Sanyal, 2015). Dysfunctional unfolded protein response (UPR) and apoptotic pathways resulting from this lipid dysregulation ultimately led to disease outcomes. To better understand the role of the UPR during lipid bilayer stress (LBS) and the consequence of a compromised UPR program, several studies have been conducted, focusing on their interconnection. As it is required for normal fatty acid synthesis as well as the regulation of very-low-density lipoprotein (VLDL) assembly and its secretion, *XBP1* ablation leads to hypolipidemia in mice due to an abnormal decrease in plasma levels of TAG and cholesterol (Lee et al., 2008; So et al., 2012; Wang et al., 2012). High dietary carbohydrate is sufficient to increase FAs and cholesterol synthesis through XBP1 (Lee et al., 2008). Consequently, XBP1 is required to channel excess carbohydrates into lipids as its absence leads to insulin resistance in obese mice (Ozcan et al., 2004). XBP1 is also required to modulate phospholipid synthesis to expand the ER membrane network during proteotoxic stress, a process that is proposed to accommodate the increased load of misfolded proteins (Sriburi et al., 2004). The UPR modulates lipid metabolism-related genes and the absence of its sole regulator in yeast, Ire1, confers auxotrophy of inositol, a building block of phospholipids (Cox et al., 1993). We have previously shown that Ire1 is essential for cell survival during LBS, thereby highlighting the important role of the UPR to overcome lipotoxicity in yeast (Thibault et al., 2012). The UPR sensor PERK also plays a role in pathogenesis from lipotoxicity. Lipotoxicity-induced CHOP (also known as DDIT3), the downstream target gene of PERK, promotes hepatic inflammation by activating the NK-κB pathway, thus promoting NASH and type 2 diabetes (T2D) (Cunha et al., 2008; Willy et al., 2015). The ablation of ATF6, the third UPR sensor, induces NASH owing to dysregulated lipid biosynthesis in mice upon tunicamycin treatment (Yamamoto et al., 2010). Thus, the three branches of the UPR are intimately linked to lipid homeostasis but their respective roles during LBS in comparison to proteotoxic stress remains elusive. Here, we took a systematic global approach to determine genes that are regulated by the UPR-specifically induced by LBS.

Activation of the UPR stemming from LBS is observed in metabolic diseases (Gregor et al., 2009; Pietilainen et al., 2011). Membrane lipid saturation as a cause of LBS is well studied and the mechanism governing IRE-1 sensing of LBS during increased membrane saturation is relatively well characterized (Cho et al., 2019; Halbleib et al., 2017; Volmer et al., 2013), In addition, our laboratory's findings showed

that membrane phospholipid ratio imbalance led to perturbation of ER membrane integrity that requires IRE-1 for achieving ER membrane homeostasis through UPR activation (Ho et al., 2020; Koh et al., 2018; Thibault et al., 2012).

To study the transmembrane function of IRE-1 in sensing LBS in worms, we adopted two methods where (1), we removed the luminal domain of *ire-1* to uncouple proteotoxic stress sensing function of IRE-1 to the LBS sensing transmembrane domain and (2) mutating selected amino acid residues of *ire-1* within the transmembrane region and the proximate amphipathic helix of *ire-1*. Approach (1) involved the expression of HA-IRE-1 construct that was prematurely degraded, leading us to Approach (2). In this approach, the amino acid substitution mutants did not render IRE-1 insensitive to LBS. Amino acid substitution of the IRE-1 TMD has been shown in yeast and mammalian cells. However, due to the sequence dissimilarity between different organisms, a more systematic approach is needed to screen for TMD important for LBS sensing.

In our study, we aimed to identify perturbation in lipid metabolism that can activate the UPR^{LBS} in *C. elegans*. Firstly, we showed that challenging the worms with cold stress activates the IRE-1 signaling pathway. Dynamic changes in the membrane lipid composition are essential to maintain structural integrity for the proper functioning of the cell (Spector and Yorek, 1985). During cold stress, low temperature causes saturated fatty acids with a higher melting point within the membrane to solidify and become phase separated from the membrane, thus causing loss of membrane fluidity and resulting in cytoplasmic leakage (Yu et al., 2015). To circumvent this detrimental event, remodeling of the cell membrane takes place by increasing the amount of unsaturated fatty acids in membrane lipids. Such increase in unsaturated fatty acids usually belongs to the class of polyunsaturated fatty acids (PUFAs) (Shaikh et al., 2015). Increased desaturation of membranes would prevent membrane stiffening and allow membrane proteins movement for their proper functioning. In wild type worms, cold stress-induced UPR activation through IRE-1 and drastically increased PUFA levels. This finding is correlated to enhanced survival of the worms during cold stress that is absent in *ire-1(lof)* worms, suggesting the importance of IRE-1 in orchestrating a UPR program that reshapes lipid metabolism for survival. UPR activation in cold stress as measured by *in vivo hsp-4* expression showed a gradual increase in UPR activation throughout cold exposure, hinting at sustained UPR activity, possibly through XBP-1.

Enhanced XBP-1 activation likely drives the expression of fatty acid desaturases responsible for increased PUFA synthesis such as *fat-1* and *fat-4* to increase survival (Imanikia et al., 2019).

Another condition causing a noticeable change in lipid composition was demonstrated in our analysis of worms fed with high glucose diet (HGD). We showed that high glucose diet increased saturated fatty acids (SFAs) content in worms, leading to UPR activation through ATF-6, IRE-1 and PEK-1. The excess production of SFAs is particularly pronounced in aged worms fed with high glucose diet (HGD5), likely due to diminished metabolic function due to aging. The accumulation of metabolically harmful SFAs can occur through the conversion of excess sugars to acetyl-CoA that serves as the two-carbon donor for palmitic acid (C16:0) synthesis, leading to decreased membrane fluidity (Fig. 3.12). In aged worms, downstream fatty acid synthesis from the acetyl-CoA precursor may be dampened due to reduced mitochondrial function, contributing to excess palmitic acid accumulation (Ma and Li, 2015). Our study thus links glucotoxicity with lipid metabolism, where HGD-induced membrane saturation likely resulted in UPR activation. Indeed, we observed a significant reduction of monounsaturated fatty acids (MUFAs) levels in HGD1 and HGD5-treated worms that is associated with a reduction in lifespan (Han et al., 2017; Lee et al., 2009). MUFAs contribute to lifespan extension by promoting membrane fluidity, reducing oxidative stress, and act as signaling molecules. In diabetic patients, studies have found that the membrane lipids are enriched with cholesterols and SFAs that promote membrane rigidity. Coupled with the reduction in MUFAs, the drastic changes in the lipid of HGD-treated worms likely reflect perturbed fat metabolism in worms that is pathologically relevant. The glucose transporter type 4 (GLUT4) is an insulin-regulated glucose transporter essential for maintaining glucose gradient. In HGD worms, ER stress induction was observed as a result of glucotoxicity (Fig. 3.11). One study found that GLUT4 (ortholog FGT-1 in *C. elegans*) mRNA and protein expression is reduced in both rat and human myotubules during glucotoxicity because of ATF6 activation. While the mechanism detailing negative regulation of GLUT4 by ATF6 remains to be studied, it can be established that glucose toxicity is intimately linked to perturbed lipid metabolism and ER stress activation.

In this study, while we found that cold stress and glucotoxicity altered the lipid composition and observed UPR activation in both conditions, the molecular mechanism linking the UPR and disrupted lipid composition remains unclear. To further our understanding of the UPR regulation during lipid dysregulation, we opted to perturb lipid metabolism via genetic means. To introduce LBS in *C. elegans*,

we opted to genetically attenuate *pmt-2*, which is required for PC biosynthesis (Fig. 1.3). A similar approach has been used by other groups to mimic the physiological conditions associated with NAFLD in *C. elegans* (Ding et al., 2015; Smulan et al., 2016; Yamamoto et al., 2010). Because both are required for PC biosynthesis, *pmt-2* and *sams-1* depletion led to enlarged lipid droplets in worms (Li et al., 2004). Generally, perturbing PC levels affects the abundance and size of lipid droplets, serving as a compensatory response to LBS that results in the channeling of excess neutral lipids, triacylglycerol, and sterol, into lipid droplets (LDs) (Guo et al., 2008; Li et al., 2011; Walker et al., 2011). Decreased hepatic PC in mice (Fu et al., 2011; Li et al., 2006; Ozcan et al., 2004; Walkey et al., 1998) and dietary deficiency of choline in humans are both associated with hepatic steatosis (Buchman et al., 1995; Gao et al., 2016). Initially, we subjected young adult worms to *pmt-2* RNAi for two days. However, no significant decrease in PC level was observed. This could be due to residual circulating PMT-2 enzymes in adult worms that could catalyze PC synthesis, thus rendering *pmt-2* RNAi ineffective to deplete PC in adult worms. In addition, adult worms are shown to have higher PC content relative to larval stage worms, which could explain milder PC reduction upon *pmt-2* RNAi treatment in adult worms (Gao et al., 2017). Contrastingly, radiolabeling experiments that tracked the fate of PC in *S. cerevisiae* showed PC turnover in a "close circuit" manner where PC can be degraded to glycerophosphocholine and subsequently get converted to PC through the CDP-choline pathway or stepwise acylation with lyso-PC as an intermediate (Anaokar et al., 2019; Boumann et al., 2003; Zaccheo et al., 2004).Thus, L1 stage worms treated with *pmt-2* RNAi were utilized as the UPR^{LBS} model. These latter conditions were sufficient to drastically induce LBS, lipid storage, and to strongly activate the UPR, all hallmarks of NAFLD. Using this approach, we interrogated the role of each UPR branch during LBS-induced ER stress.

We examined the individual effects of *atf-6, ire-1,* and *pek-1* deficiency *in vivo*. Interestingly, ER stress induced by unfolded protein accumulation and LBS were found to be distinct from each other (Hou et al., 2014; Lajoie et al., 2012). A global transcriptomic analysis of UPR mutants subjected to LBS in comparison to what was seen with proteotoxic-induced ER stress in WT animals allowed us to identify genes that are specifically regulated by UPR^{LBS} but not the UPR^{PT} (Figs. 3.24 – 3.28). To our knowledge, this is the first report identifying specific UPR-regulated genes induced by LBS but not proteotoxic stress. Our data show that many genes regulated by the UPR transducers are specific to LBS, while a smaller number of genes are commonly modulated under proteotoxic and LBS. As expected, LBS-

induced ER stress leads to altered gene regulation and protein modification processes through ATF-6, IRE-1, and PEK-1. IRE-1 is the most conserved UPR transducer from yeast to mammals and it regulates the largest number of genes among the three UPR transducers (Fig. 3.25).

Previous studies revealed LDs formation is associated with various cellular stress conditions. Mammalian cells experiencing ER stress from tunicamycin treatment are shown to have LDs accumulation (Lee et al., 2012). Our microarray data show that differential gene expression caused by UPR^{LBS} and UPR^{PT} are vastly different with some overlap. This suggests LDs accumulation from UPR^{LBS} could be regulated by a different mechanism. During proteotoxic stress, the presence of misfolded proteins is thought to be removed by LDs, hence reducing ER load (Ploegh, 2007). However, LBS elicits a different kind of stress response that could trigger LDs formation in another way. Our data showed that PC depletion did not cause accumulation of PC precursors, PE (Fig. 3.19). Instead, blocked PC synthesis leads to diacylglycerols (DAGs) accumulation, an intermediate product that is converted to TAGs and stored in LDs to reduce LBS (Kohlwein, 2010; Smulan et al., 2016). Interestingly, a recent study in *Drosophila* uncovered shunting of TAG storage to phospholipid synthesis via the Kennedy pathway through Xbp1 during infection, highlighting the dynamic regulation of lipid metabolism during various cellular stress conditions (Martinez et al., 2020).

Our autophagy screening revealed that autophagy is essential during LBS, suggesting that it has an important role in regulating lipid metabolism. The change in cellular lipid landscape is at least partially mediated by autophagy, through the IRE-1/XBP-1 axis (Fig. 4.1). Generally considered a cytoprotective response, autophagy can be modulated by ER stress. PERK has been reported to modulate autophagy by phosphorylating eIF2α resulting in a general translational inhibition (Avivar-Valderas et al., 2011; Fujita et al., 2007; Kouroku et al., 2007; Matsumoto et al., 2013). In parallel, PERK has also been reported to regulate autophagy through the transcription factor ATF4 (Carra et al., 2009; Dever, 2002; Talloczy et al., 2002). Likewise, IRE1 modulates autophagy, independently of XBP1, by activating the Jun N-terminal kinase (JNK) pathway (Ogata et al., 2006; Pattingre et al., 2009; Vidal et al., 2012; Wei et al., 2008a; Wei et al., 2008b; Younce and Kolattukudy, 2012). Autophagy has additionally been reported to be activated (Younce and Kolattukudy, 2012) or inhibited (Vidal et al., 2012) by the IRE1/XBP1 axis (Adolph et al., 2013; Hetz et al., 2009; Zhao et al., 2013).

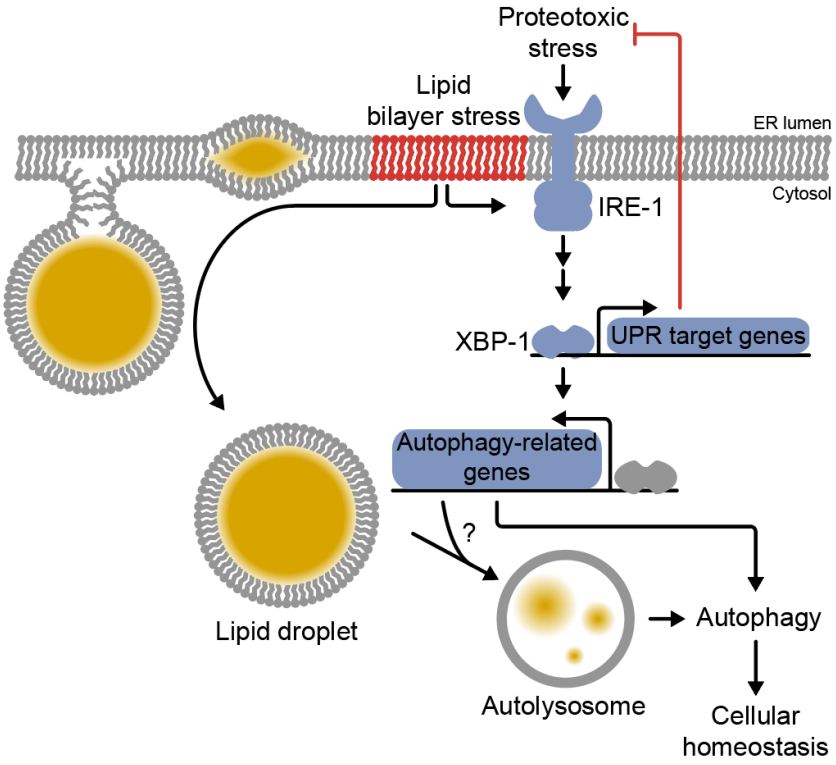

Figure 4:1: UPR^{LBS} regulates autophagy through the canonical IRE-1/XBP-1 UPR branch.

Proteotoxic-induced ER stress activates a subset of UPR target genes to restore ER homeostasis. In addition, LBS-induced ER stress partially induces autophagy through the IRE-1/XBP-1 axis. Intact of autophagy function during proteotoxic or LBS is essential in maintaining cellular homeostasis and contributes to organismal health span.

Muting the UPR during LBS revealed that the IRE-1/XBP-1 axis specifically modulates autophagy (Fig. 3.35). Our findings also demonstrate that a subset of autophagy genes is essential for organismal health during LBS (Fig. 3.31). Considering the important role of lipid homeostasis and how its impairment contributes to the pathology of metabolic diseases, our data revealed the important role of a functional UPR program to regulate autophagy and, consequently maintain cellular homeostasis. As increasing evidence suggests that reduced levels of autophagy contribute to a myriad of pathological outcomes (Mizushima et al., 2008; Singh et al., 2009), the autophagy process might be a useful target for therapeutic strategies in metabolic diseases. We have established that IRE-1 is highly responsive to LBS with the NAFLD model of *C. elegans* by genetic knockdown of the PC producing enzyme PMT-2. Our findings illuminated the need for a balanced phospholipid composition in the biological membrane where its dysregulation resulted in a strong homeostatic control through the UPR that activated

autophagy mechanism. We have shown that changes in membrane saturation and phospholipids composition perturb cellular homeostasis and activate the UPR. While a growing body of evidence have linked ER stress and UPR activation to lipid metabolism dysregulation, to our knowledge a systemic way of identifying lipid-related factors that requires an intact UPR function has not been well explored. Hence, we performed an RNAi screen and identified *dhs-18* and *lpin-1* as two candidates where their depletion caused detrimental phenotype in the absence of IRE-1, indicating the necessity of IRE-1-mediated UPR and intact DHS-18 or LPIN-1 activity for the healthspan of the worms. We chose to first focus our study on how LPIN-1 may regulate lipid metabolism in relation to the UPR due to its relevance to lipid dysregulation diseases, thus making it an enticing target for further studies (Reue, 2009).

From our RNAi screen, we showed that the UPR is essential when lipid metabolism is perturbed. Lipin mutation is known to cause the fatty liver dystrophy phenotype in mice and myoglobinuria, Majeed syndrome, and psoriasis in humans (Reue, 2009). We now uncover evidence that *lpin-1* expression is partially dependent on IRE-1 and *lpin-1* deficiency activates the UPR through IRE-1. Loss of LPIN-1 results in the diminished activity of phosphatidic acid phosphatase (PAP), possibly causing phosphatidic acid (PA) accumulation and tipping the balance of lipid landscape in worms, activating the UPR. PA is the precursor for phospholipid synthesis and is important for ER membrane expansion (Carman and Han, 2009). Its dephosphorylation by CTD nuclear envelope phosphatase 1, CNEP-1 (CTDNEP1 in humans), also leads to DAG synthesis necessary for TAG biosynthesis for lipid storage (Donkor et al., 2007; Han et al., 2006). Additionally, *lpin-1* depleted worms showed reduced lipid levels, likely caused by decreased TAG levels as a result of reduced PAP levels. Loss of *lpin-1* may also activate SBP-1/SREBP in a compensatory manner, thus altering lipid content and activate the UPR (Smulan et al., 2016). It will therefore be interesting to study the regulation of lipid metabolism in worms through understanding the relationship between *ire-1* and *lpin-1* as elucidating how the UPR is regulated during aberrant lipid metabolism will provide useful clues for therapeutic intervention.

We established an NAFLD model in worms through genetic manipulation of PC synthesis that exhibits signatures of NAFLD such as lipid droplets accumulation, UPR activation and alteration in lipid metabolism genes. Here, we uncovered parts of the mechanism that potentially explains the progression of NAFLD. A widely known working model for pathogenesis of NASH is the “two-hit” hypothesis described by Day and James (Day and James, 1998). The first “hit” describes fatty infiltration

of the liver because of fatty acid metabolism imbalance that is characteristic of NAFLD. The second "hit" describes involvement of sustained oxidative and metabolic stress as the liver tries to compensate for perturbed lipid metabolism, ultimately leading to hepatic inflammation and cell death (Day and James, 1998). Our work in worms shows that PC depletion through *pmt-2* RNAi causes TAG accumulation. While there were debates on accumulation of TAG being the initial cause of liver disease, recent literatures suggest that synthesis of TAG is an adaptive response to hepatic lipid overload, providing a buffer to redirect excess fatty acids to the relatively inert TAG and prevent formation of other toxic lipid species (Li et al., 2009; Listenberger et al., 2003; Schaffer, 2003). However, chronic lipid accumulation can directly promote insulin resistance commonly observed in patients with metabolic diseases and cause inflammation, leading to the second "hit" of the "two-hit" theory in NASH development (Kitade et al., 2017; Shulman, 2014).

In agreement with other findings, our model also showed responsiveness of IRE-1 as a homeostatic factor when PC is depleted (Ho et al., 2020; Thibault et al., 2012). We found that the activation of autophagy through IRE-1 as a possible protective response that could be dampened due to the sustained insult of LBS. In one study, severe downregulation of autophagy in the liver of obese mice is linked to insulin resistance (Yang et al., 2010). Accordingly, assessment of autophagic event through autophagic vesicles counting and immunohistochemistry against LC3 in human liver biopsies suggest that impaired autophagy promotes NAFLD and hepatic steatosis progression (Fukuo et al., 2014; Kashima et al., 2014). Studies shows NAFLD subjects are associated with significant baseline apolipoprotein B-100 (apoB 100) serum levels (Nass et al., 2017; Wang et al., 2017). Autophagy is found to regulate apoB 100, the protein synthesized in the liver and is the component of the lipoprotein very-low density lipoprotein (VLDL) (Ohsaki et al., 2006; Rutledge et al., 2010). Reduction of apoB through autophagy hence lead to a reduction in VLDL assembly and secretion. In addition, ER stress induction is also linked to apoB 100 degradation in an autophagy-dependent manner, further establishing the role of the UPR-autophagy-signaling cascade in regulating lipid metabolism (Qiu et al., 2006; Qiu et al., 2005; Qiu et al., 2011). Excess TAG in a cell, often seen accumulated in visceral adipose tissue of NAFLD patients, can be cleared by cytosolic lipolysis by adipose triglyceride lipase (ATGL) (Zechner et al., 2017). Alternatively, a subtype of macroautophagy, lipophagy, can also facilitate transport of LDs to lysosome for degradation (Singh et al., 2009). Dysfunction in excess lipids clearing through these pathways are associated with liver injury through apoptosis, inflammation, and fibrosis

(Liu et al., 2015). We have identified autophagy as a machinery essential to maintain homeostasis during LBS. However, substrate selectivity by autophagy during LBS remains to be uncovered. Our evidence of simultaneous lipid accumulation and autophagy activation suggests that lipophagy could be involved in resolving LBS, but further studies are required to elucidate this phenomenon.

One caveat of our study lies in the treatment length of *pmt-2* RNAi leading to PC depletion. Although we show complete PC depletion and high sensitivity of the UPR in response to LBS, it will be interesting to extend the PC depletion treatment through *C. elegans* aging and assess the difference in the UPR signaling as a function of chronicity of LBS. Additionally, despite the conservation of energy and lipid metabolism pathways between *C. elegans* and mammals, the lack of a distinctive hepatic organ should be taken into consideration when extrapolating any findings. Nonetheless, our study provides valuable addition to the expanding pool of knowledge surrounding NAFLD pathogenesis and the molecular mechanism underlying the disease.

Chapter 5: Future Work

Lipid bilayer stress (LBS) plays a significant role in the pathogenesis of metabolic diseases. The disease development often involves complex crosstalk and interactions between different aspects of metabolic pathways. The aim of this project is to help define the role of unfolded protein response (UPR) during lipid perturbation. Using *C. elegans* as a model to study UPR^{LBS}, we made several observations that can aid in directing future research in our field.

5.1. Involvement of lipophagy during UPR^{LBS}

Our present study uncovered the role of IRE-1/XBP-1 axis in regulating lipid homeostasis through autophagy. Elucidating the mechanism governing lipid turnover and its role in modulating ER homeostasis represents an important step forward for our research. Currently, we identified the involvement of autophagy through the IRE-1/XBP-1 axes during lipid perturbation. Two players of the autophagy machinery, *bec-1* and *lgg-1* were shown to be attenuated during lipid perturbation in the absence of IRE-1. Quantitative PCR was used to demonstrate the dependence of IRE-1 in activating autophagy during lipid perturbation on a transcriptional level. We also measured autophagy activity by immunoblot, showing autophagy flux through the formation of LGG-1-PE by immunoblotting and microscopy. Our study showed the accumulation of large lipid droplets from PC depletion. Contribution of lipophagy to the catabolism of neutral lipids is documented in cell types such as hepatocytes, adipocytes, as well as in *S. cerevisiae* and *C. elegans* (Lapierre et al., 2011; van Zutphen et al., 2014; Yang et al., 2010). Selectivity of lipophagy involves recognition of LD by LGG-1-PE positive membrane and delivery of LD cargo towards lysosomal degradation. RAB-7 is thought to be a requirement in this process. In addition, it was recently reported that RAB-10/EHBP-1/RME-1 (ras-related GTP-binding protein/EH domain binding protein/receptor mediated endocytosis) form a complex essential for lipophagy to take place. Furthermore, constitutive expression of *xbp-1* drove EHBP-1 expression that promoted lipid depletion and lifespan extension (Daniele et al., 2020). A study involving depletion or overexpression of the lipophagy complex would shed light into their participation, along with autophagy, in regulating lipid metabolism during chronic ER stress.

5.2. Involvement of ATF-6 and PEK-1 during UPR^{LBS}

Beyond this scope, a myriad of cellular processes exists that could be explored as a consequence of UPR^{LBS}. Our data show that the contribution of each UPR transducer during ER stress is distinct from each other. Indeed, UPR signal transduction is complex and remains an active field of research. For example, how two or more UPR transducers cooperate to alleviate ER stress from UPR^{LBS} is still not resolved as far as we are aware. Recently, Tam et al. demonstrated that mammalian ATF6 responds to proteotoxic stress and LBS by different mechanism. Mutation of Ile388 and Tyr392 residues within the ATF6 transmembrane domain rendered the worms insensitive to sense LBS (Tam et al., 2018). This piece of evidence, along with our microarray results suggest ATF-6 plays an equally important role in sensing LBS and initiating the UPR.

Our data suggest that immune response may be partly dependent on *pek-1* during UPR^{LBS} as the absence of *pek-1* seems to compromise immune function compared to worms lacking *atf-6* or *ire-1*. Indeed, defective lipid metabolism is linked to perturbed immune function via altered histone activity in *C. elegans* (Ding et al., 2015). To examine how *pek-1* attenuation affects immune response during UPR^{LBS}, we will assess the lifespan of *C. elegans* when challenged with the pathogenic bacteria *Pseudomonas aeruginosa*. Since PEK-1 is generally involved in translational inhibition, we will attempt to study how this aspect of UPR plays into immunity regulation in *C. elegans*. Therefore, by exploring PEK-1 targets that are dysregulated during UPR^{LBS}, we can shed light on cellular processes that are affected during a compromised immune function.

5.3. Other sources of LBS that activate the UPR

We showed that high glucose diet (HGD) in worms alters their lipid composition with the accumulation of toxic palmitic acid and reduction in monounsaturated fatty acids levels. HGD also induced UPR activation. To directly associate the UPR with detrimental lipid remodeling observed in HGD-fed worms, genetic regulation of lipid biosynthetic or catabolic pathways needs to be studied. mRNA levels of fatty acid desaturases related to SFAs and MUFAs such as *fat-3, fat-5,* and *fat-7* can be measured by qPCR. To test if their expression levels are dependent on the UPR pathways, UPR loss-of-function mutants can be used.

Our current RNAi screening revealed the need for IRE-1 in promoting the healthy development of the worms during perturbed lipid metabolism in *lpin-1*(RNAi) worms. Loss of both alleles of *lpin-1* is lethal in worms and rats lacking Lipin develops fatty liver characterized by the fatty liver dystrophy (fld) phenotype. However, loss of single copy of *lpin-1* in worms resulted in a superficially wild type worms. Therefore, it may seem that the dosage of LPIN-1 is essential for survival and *lpin-1* depletion through RNAi may more closely resemble worms with heterologous knockout of *lpin-1*. Hence, to complement the phenotype observed in our RNAi screen, *ire-1(lof)* worms can be crossed to partial *lpin-1* knockout worms. An exacerbated phenotype would corroborate our qPCR data where UPR activation through IRE-1 is required for the worm survival in the absence or low abundance of LPIN-1.

With this finding, our future goals include validating the shortlisted targets and perform assays to assess the need for IRE-1 to mediate a homeostatic response to LBS. To this end, we are in the process of creating UPR reporters that allows the visualization of UPR activation *in vivo*. It was reported that neuron-specific activation of *xbp-1* resulted in the depletion of lipids in the whole worms (Daniele et al., 2020). Furthermore, overexpression of *xbp-1* in the neurons also affected protein homeostasis in other tissues of the worms and promote lifespan extension (Taylor and Dillin, 2013). Therefore, to study tissue-specific activation of the UPR during LBS, we are also crossing worms expressing the active form of *xbp-1 (xbp-1s)* in three separate tissues: neurons, intestines, and muscles with the *ire-1(lof)* mutant. We hypothesized that during LBS homeostatic control is largely exerted by IRE-1. Restoration of its downstream transcription factor XBP-1 would achieve a similar outcome where the detrimental phenotypes seen in *ire-1(lof)* worms during LBS would be reversed. Furthermore, we may also pinpoint the mechanism of IRE-1 regulation by assessing the organ in which *xbp-1* is required to promote cellular homeostasis.

Chapter 6: Conclusion

The process of UPR activation during lipid perturbation is a research topic that is being actively pursued, but the consequence of UPR^{LBS} in comparison to UPR^{PT} has not been studied intensively as far as we know. By depleting PC synthesis, we recapitulated the process of ER stress activation seen in metabolic diseases. We found that autophagy regulated through the IRE-1/XBP-1 axis is essential in preserving homeostasis of the worms where the loss of the autophagy machinery during LBS resulted in reduced healthspan and hyperactivation of the UPR. In our study, changes in lipid desaturation through cold stress-induced the UPR^{LBS}. Conversely, high glucose diet-induced membrane lipid saturation coupled with a decrease in MUFA levels also induced the UPR^{LBS} and is physiologically important because of the impact of HGD on lifespan. However, downstream events resulting from changes in the lipid membrane saturation resulting from cold stress or HGD remain to be elucidated.

The physiological role of Lipin in regulating lipid metabolism is relatively known. Augmented Lipin activity is often associated with lipotoxicity, thus causing LBS and affect the lifespan of the worms. We report that PC depletion caused upregulation of *lpin-1* through IRE-1 could augment lipid metabolism to improve cellular homeostasis. Contrastingly, *lpin-1* deficiency through RNAi in *ire-1(lof)* background resulted in a severe phenotype, indicating the need for a functional UPR program regulated through IRE-1 during LBS. However, much research effort is needed to elucidate the link between the UPR and Lipin.

Currently, there is no unified view of how the UPR regulates homeostasis. Some studies pointed that during LBS, the proteostasis network takes over without remodeling of the lipids while other studies suggest that the UPR maintains lipid homeostasis, protein repair machinery, and chaperones to combat the existential ER stress. How does the cell balance between all the functional roles of the ER? Therefore, the exploration of the governing mechanisms between UPR and LBS is required and will aid in the development of more effective therapeutic approaches for metabolic disease.

References

1. Acosta-Alvear, D., Zhou, Y., Blais, A., Tsikitis, M., Lents, N.H., Arias, C., Lennon, C.J., Kluger, Y., and Dynlacht, B.D. (2007). XBP1 controls diverse cell type- and condition-specific transcriptional regulatory networks. Mol Cell *27*, 53-66.
2. Adams, C.J., Kopp, M.C., Larburu, N., Nowak, P.R., and Ali, M.M.U. (2019). Structure and Molecular Mechanism of ER Stress Signaling by the Unfolded Protein Response Signal Activator IRE1. Front Mol Biosci *6*, 11.
3. Adolph, T.E., Tomczak, M.F., Niederreiter, L., Ko, H.J., Bock, J., Martinez-Naves, E., Glickman, J.N., Tschurtschenthaler, M., Hartwig, J., Hosomi, S.*, et al.* (2013). Paneth cells as a site of origin for intestinal inflammation. Nature *503*, 272-276.
4. Anaokar, S., Kodali, R., Jonik, B., Renne, M.F., Brouwers, J., Lager, I., de Kroon, A., and Patton-Vogt, J. (2019). The glycerophosphocholine acyltransferase Gpc1 is part of a phosphatidylcholine (PC)-remodeling pathway that alters PC species in yeast. J Biol Chem *294*, 1189-1201.
5. Arunagiri, A., Haataja, L., Cunningham, C.N., Shrestha, N., Tsai, B., Qi, L., Liu, M., and Arvan, P. (2018). Misfolded proinsulin in the endoplasmic reticulum during development of beta cell failure in diabetes. Ann N Y Acad Sci *1418*, 5-19.
6. Avivar-Valderas, A., Salas, E., Bobrovnikova-Marjon, E., Diehl, J.A., Nagi, C., Debnath, J., and Aguirre-Ghiso, J.A. (2011). PERK integrates autophagy and oxidative stress responses to promote survival during extracellular matrix detachment. Mol Cell Biol *31*, 3616-3629.
7. Bahmanyar, S., Biggs, R., Schuh, A.L., Desai, A., Muller-Reichert, T., Audhya, A., Dixon, J.E., and Oegema, K. (2014). Spatial control of phospholipid flux restricts endoplasmic reticulum sheet formation to allow nuclear envelope breakdown. Genes Dev *28*, 121-126.
8. Bardou, P., Mariette, J., Escudie, F., Djemiel, C., and Klopp, C. (2014). jvenn: an interactive Venn diagram viewer. BMC Bioinformatics *15*, 293.
9. Bertolotti, A., Zhang, Y., Hendershot, L.M., Harding, H.P., and Ron, D. (2000). Dynamic interaction of BiP and ER stress transducers in the unfolded-protein response. Nat Cell Biol *2*, 326-332.
10. Bettaieb, A., Matsuo, K., Matsuo, I., Wang, S., Melhem, R., Koromilas, A.E., and Haj, F.G. (2012). Protein tyrosine phosphatase 1B deficiency potentiates PERK/eIF2alpha signaling in brown adipocytes. PLoS One *7*, e34412.
11. Boumann, H.A., Damen, M.J., Versluis, C., Heck, A.J., de Kruijff, B., and de Kroon, A.I. (2003). The two biosynthetic routes leading to phosphatidylcholine in yeast produce different sets of molecular species. Evidence for lipid remodeling. Biochemistry *42*, 3054-3059.
12. Braakman, I., and Bulleid, N.J. (2011). Protein folding and modification in the mammalian endoplasmic reticulum. Annu Rev Biochem *80*, 71-99.
13. Brendza, K.M., Haakenson, W., Cahoon, R.E., Hicks, L.M., Palavalli, L.H., Chiapelli, B.J., McLaird, M., McCarter, J.P., Williams, D.J., Hresko, M.C.*, et al.* (2007). Phosphoethanolamine N-methyltransferase (PMT-1) catalyses the first reaction of a new pathway for phosphocholine biosynthesis in Caenorhabditis elegans. Biochem J *404*, 439-448.
14. Brenner, S. (1974). The genetics of Caenorhabditis elegans. Genetics *77*, 71-94.
15. Buchman, A.L., Dubin, M.D., Moukarzel, A.A., Jenden, D.J., Roch, M., Rice, K.M., Gornbein, J., and Ament, M.E. (1995). Choline deficiency: a cause of hepatic steatosis during parenteral nutrition that can be reversed with intravenous choline supplementation. Hepatology *22*, 1399-1403.
16. Calfon, M., Zeng, H., Urano, F., Till, J.H., Hubbard, S.R., Harding, H.P., Clark, S.G., and Ron, D. (2002). IRE1 couples endoplasmic reticulum load to secretory capacity by processing the XBP-1 mRNA. Nature *415*, 92-96.
17. Cao, H., Gerhold, K., Mayers, J.R., Wiest, M.M., Watkins, S.M., and Hotamisligil, G.S. (2008). Identification of a lipokine, a lipid hormone linking adipose tissue to systemic metabolism. Cell *134*, 933-944.
18. Carman, G.M., and Han, G.S. (2009). Phosphatidic acid phosphatase, a key enzyme in the regulation of lipid synthesis. J Biol Chem *284*, 2593-2597.
19. Carra, S., Brunsting, J.F., Lambert, H., Landry, J., and Kampinga, H.H. (2009). HspB8 participates in protein quality control by a non-chaperone-like mechanism that requires eIF2{alpha} phosphorylation. J Biol Chem *284*, 5523-5532.
20. Casares, D., Escriba, P.V., and Rossello, C.A. (2019). Membrane Lipid Composition: Effect on Membrane and Organelle Structure, Function and Compartmentalization and Therapeutic Avenues. Int J Mol Sci *20*.
21. Chen, M., and Thelen, J.J. (2013). ACYL-LIPID DESATURASE2 is required for chilling and freezing tolerance in Arabidopsis. Plant Cell *25*, 1430-1444.

22. Chen, X., Zhang, F., Gong, Q., Cui, A., Zhuo, S., Hu, Z., Han, Y., Gao, J., Sun, Y., Liu, Z*., et al.* (2016). Hepatic ATF6 Increases Fatty Acid Oxidation to Attenuate Hepatic Steatosis in Mice Through Peroxisome Proliferator-Activated Receptor alpha. Diabetes *65*, 1904-1915.
23. Cho, H., Stanzione, F., Oak, A., Kim, G.H., Yerneni, S., Qi, L., Sum, A.K., and Chan, C. (2019). Intrinsic Structural Features of the Human IRE1alpha Transmembrane Domain Sense Membrane Lipid Saturation. Cell Rep *27*, 307-320 e305.
24. Cox, J.S., Chapman, R.E., and Walter, P. (1997). The unfolded protein response coordinates the production of endoplasmic reticulum protein and endoplasmic reticulum membrane. Mol Biol Cell *8*, 1805-1814.
25. Cox, J.S., Shamu, C.E., and Walter, P. (1993). Transcriptional induction of genes encoding endoplasmic reticulum resident proteins requires a transmembrane protein kinase. Cell *73*, 1197-1206.
26. Cox, J.S., and Walter, P. (1996). A novel mechanism for regulating activity of a transcription factor that controls the unfolded protein response. Cell *87*, 391-404.
27. Credle, J.J., Finer-Moore, J.S., Papa, F.R., Stroud, R.M., and Walter, P. (2005). On the mechanism of sensing unfolded protein in the endoplasmic reticulum. Proc Natl Acad Sci U S A *102*, 18773-18784.
28. Cunha, D.A., Hekerman, P., Ladriere, L., Bazarra-Castro, A., Ortis, F., Wakeham, M.C., Moore, F., Rasschaert, J., Cardozo, A.K., Bellomo, E*., et al.* (2008). Initiation and execution of lipotoxic ER stress in pancreatic beta-cells. J Cell Sci *121*, 2308-2318.
29. Dancy, B.C., Chen, S.W., Drechsler, R., Gafken, P.R., and Olsen, C.P. (2015). 13C- and 15N-Labeling Strategies Combined with Mass Spectrometry Comprehensively Quantify Phospholipid Dynamics in C. elegans. PLoS One *10*, e0141850.
30. Daniele, J.R., Higuchi-Sanabria, R., Durieux, J., Monshietehadi, S., Ramachandran, V., Tronnes, S.U., Kelet, N., Sanchez, M., Metcalf, M.G., Garcia, G*., et al.* (2020). UPR(ER) promotes lipophagy independent of chaperones to extend life span. Sci Adv *6*, eaaz1441.
31. Day, C.P., and James, O.F. (1998). Steatohepatitis: a tale of two "hits"? Gastroenterology *114*, 842-845.
32. Deng, X., Xiao, L., Lang, W., Gao, F., Ruvolo, P., and May, W.S., Jr. (2001). Novel role for JNK as a stress-activated Bcl2 kinase. J Biol Chem *276*, 23681-23688.
33. Dever, T.E. (2002). Gene-specific regulation by general translation factors. Cell *108*, 545-556.
34. Devkota, S., Jeong, H., Kim, Y., Ali, M., Roh, J.I., Hwang, D., and Lee, H.W. (2016). Functional characterization of EI24-induced autophagy in the degradation of RING-domain E3 ligases. Autophagy *12*, 2038-2053.
35. Ding, W., Smulan, L.J., Hou, N.S., Taubert, S., Watts, J.L., and Walker, A.K. (2015). s-Adenosylmethionine Levels Govern Innate Immunity through Distinct Methylation-Dependent Pathways. Cell Metab *22*, 633-645.
36. Donkor, J., Sariahmetoglu, M., Dewald, J., Brindley, D.N., and Reue, K. (2007). Three mammalian lipins act as phosphatidate phosphatases with distinct tissue expression patterns. J Biol Chem *282*, 3450-3457.
37. Donnelly, K.L., Smith, C.I., Schwarzenberg, S.J., Jessurun, J., Boldt, M.D., and Parks, E.J. (2005). Sources of fatty acids stored in liver and secreted via lipoproteins in patients with nonalcoholic fatty liver disease. J Clin Invest *115*, 1343-1351.
38. Dowd, S.R., Bier, M.E., and Patton-Vogt, J.L. (2001). Turnover of phosphatidylcholine in Saccharomyces cerevisiae. The role of the CDP-choline pathway. J Biol Chem *276*, 3756-3763.
39. Doycheva, I., Watt, K.D., and Alkhouri, N. (2017). Nonalcoholic fatty liver disease in adolescents and young adults: The next frontier in the epidemic. Hepatology *65*, 2100-2109.
40. Eden, E., Navon, R., Steinfeld, I., Lipson, D., and Yakhini, Z. (2009). GOrilla: a tool for discovery and visualization of enriched GO terms in ranked gene lists. BMC Bioinformatics *10*, 48.
41. Elahi, D., and Muller, D.C. (2000). Carbohydrate metabolism in the elderly. Eur J Clin Nutr *54 Suppl 3*, S112-120.
42. Ericson, M.C., Gafford, J.T., and Elbein, A.D. (1977). Tunicamycin inhibits GlcNAc-lipid formation in plants. J Biol Chem *252*, 7431-7433.
43. Fagone, P., and Jackowski, S. (2013). Phosphatidylcholine and the CDP-choline cycle. Biochim Biophys Acta *1831*, 523-532.
44. Finck, B.N., Gropler, M.C., Chen, Z., Leone, T.C., Croce, M.A., Harris, T.E., Lawrence, J.C., Jr., and Kelly, D.P. (2006). Lipin 1 is an inducible amplifier of the hepatic PGC-1alpha/PPARalpha regulatory pathway. Cell Metab *4*, 199-210.

45. Fu, S., Yang, L., Li, P., Hofmann, O., Dicker, L., Hide, W., Lin, X., Watkins, S.M., Ivanov, A.R., and Hotamisligil, G.S. (2011). Aberrant lipid metabolism disrupts calcium homeostasis causing liver endoplasmic reticulum stress in obesity. Nature *473*, 528-531.
46. Fujita, E., Kouroku, Y., Isoai, A., Kumagai, H., Misutani, A., Matsuda, C., Hayashi, Y.K., and Momoi, T. (2007). Two endoplasmic reticulum-associated degradation (ERAD) systems for the novel variant of the mutant dysferlin: ubiquitin/proteasome ERAD(I) and autophagy/lysosome ERAD(II). Hum Mol Genet *16*, 618-629.
47. Fukuo, Y., Yamashina, S., Sonoue, H., Arakawa, A., Nakadera, E., Aoyama, T., Uchiyama, A., Kon, K., Ikejima, K., and Watanabe, S. (2014). Abnormality of autophagic function and cathepsin expression in the liver from patients with non-alcoholic fatty liver disease. Hepatol Res *44*, 1026-1036.
48. Fun, X.H., and Thibault, G. (2020). Lipid bilayer stress and proteotoxic stress-induced unfolded protein response deploy divergent transcriptional and non-transcriptional programmes. Biochim Biophys Acta Mol Cell Biol Lipids *1865*, 158449.
49. Gao, A.W., Chatzispyrou, I.A., Kamble, R., Liu, Y.J., Herzog, K., Smith, R.L., van Lenthe, H., Vervaart, M.A.T., van Cruchten, A., Luyf, A.C.*, et al.* (2017). A sensitive mass spectrometry platform identifies metabolic changes of life history traits in C. elegans. Sci Rep *7*, 2408.
50. Gao, X., Wang, Y., Randell, E., Pedram, P., Yi, Y., Gulliver, W., and Sun, G. (2016). Higher Dietary Choline and Betaine Intakes Are Associated with Better Body Composition in the Adult Population of Newfoundland, Canada. PLoS One *11*, e0155403.
51. Glover-Cutter, K.M., Lin, S., and Blackwell, T.K. (2013). Integration of the unfolded protein and oxidative stress responses through SKN-1/Nrf. PLoS Genet *9*, e1003701.
52. Golden, A., Liu, J., and Cohen-Fix, O. (2009). Inactivation of the C. elegans lipin homolog leads to ER disorganization and to defects in the breakdown and reassembly of the nuclear envelope. J Cell Sci *122*, 1970-1978.
53. Gorjanacz, M., Klerkx, E.P., Galy, V., Santarella, R., Lopez-Iglesias, C., Askjaer, P., and Mattaj, I.W. (2007). Caenorhabditis elegans BAF-1 and its kinase VRK-1 participate directly in post-mitotic nuclear envelope assembly. EMBO J *26*, 132-143.
54. Gregor, M.F., Yang, L., Fabbrini, E., Mohammed, B.S., Eagon, J.C., Hotamisligil, G.S., and Klein, S. (2009). Endoplasmic reticulum stress is reduced in tissues of obese subjects after weight loss. Diabetes *58*, 693-700.
55. Guisbert, E., Czyz, D.M., Richter, K., McMullen, P.D., and Morimoto, R.I. (2013). Identification of a tissue-selective heat shock response regulatory network. PLoS Genet *9*, e1003466.
56. Guo, Y., Walther, T.C., Rao, M., Stuurman, N., Goshima, G., Terayama, K., Wong, J.S., Vale, R.D., Walter, P., and Farese, R.V. (2008). Functional genomic screen reveals genes involved in lipid-droplet formation and utilization. Nature *453*, 657-661.
57. Halbleib, K., Pesek, K., Covino, R., Hofbauer, H.F., Wunnicke, D., Hanelt, I., Hummer, G., and Ernst, R. (2017). Activation of the Unfolded Protein Response by Lipid Bilayer Stress. Mol Cell *67*, 673-684 e678.
58. Han, D., Lerner, A.G., Vande Walle, L., Upton, J.P., Xu, W., Hagen, A., Backes, B.J., Oakes, S.A., and Papa, F.R. (2009). IRE1alpha kinase activation modes control alternate endoribonuclease outputs to determine divergent cell fates. Cell *138*, 562-575.
59. Han, G.S., Wu, W.I., and Carman, G.M. (2006). The Saccharomyces cerevisiae Lipin homolog is a Mg2+-dependent phosphatidate phosphatase enzyme. J Biol Chem *281*, 9210-9218.
60. Han, J., and Kaufman, R.J. (2016). The role of ER stress in lipid metabolism and lipotoxicity. J Lipid Res *57*, 1329-1338.
61. Han, S., Schroeder, E.A., Silva-Garcia, C.G., Hebestreit, K., Mair, W.B., and Brunet, A. (2017). Mono-unsaturated fatty acids link H3K4me3 modifiers to C. elegans lifespan. Nature *544*, 185-190.
62. Harding, H.P., Zhang, Y., Zeng, H., Novoa, I., Lu, P.D., Calfon, M., Sadri, N., Yun, C., Popko, B., Paules, R.*, et al.* (2003). An integrated stress response regulates amino acid metabolism and resistance to oxidative stress. Mol Cell *11*, 619-633.
63. Harris, M.A., Clark, J., Ireland, A., Lomax, J., Ashburner, M., Foulger, R., Eilbeck, K., Lewis, S., Marshall, B., Mungall, C.*, et al.* (2004). The Gene Ontology (GO) database and informatics resource. Nucleic Acids Res *32*, D258-261.
64. Harris, T.E., Huffman, T.A., Chi, A., Shabanowitz, J., Hunt, D.F., Kumar, A., and Lawrence, J.C., Jr. (2007). Insulin controls subcellular localization and multisite phosphorylation of the phosphatidic acid phosphatase, lipin 1. J Biol Chem *282*, 277-286.
65. Haze, K., Yoshida, H., Yanagi, H., Yura, T., and Mori, K. (1999). Mammalian transcription factor ATF6 is synthesized as a transmembrane protein and activated by proteolysis in response to endoplasmic reticulum stress. Mol Biol Cell *10*, 3787-3799.

66. Hetz, C., Thielen, P., Matus, S., Nassif, M., Court, F., Kiffin, R., Martinez, G., Cuervo, A.M., Brown, R.H., and Glimcher, L.H. (2009). XBP-1 deficiency in the nervous system protects against amyotrophic lateral sclerosis by increasing autophagy. Genes Dev *23*, 2294-2306.
67. Hetz, C., Zhang, K., and Kaufman, R.J. (2020). Mechanisms, regulation and functions of the unfolded protein response. Nat Rev Mol Cell Biol *21*, 421-438.
68. Ho, N., Xu, C., and Thibault, G. (2018). From the unfolded protein response to metabolic diseases - lipids under the spotlight. J Cell Sci *131*.
69. Ho, N., Yap, W.S., Xu, J., Wu, H., Koh, J.H., Goh, W.W.B., George, B., Chong, S.C., Taubert, S., and Thibault, G. (2020). Stress sensor Ire1 deploys a divergent transcriptional program in response to lipid bilayer stress. J Cell Biol *219*.
70. Hollien, J., Lin, J.H., Li, H., Stevens, N., Walter, P., and Weissman, J.S. (2009). Regulated Ire1-dependent decay of messenger RNAs in mammalian cells. J Cell Biol *186*, 323-331.
71. Hollien, J., and Weissman, J.S. (2006). Decay of endoplasmic reticulum-localized mRNAs during the unfolded protein response. Science *313*, 104-107.
72. Horl, G., Wagner, A., Cole, L.K., Malli, R., Reicher, H., Kotzbeck, P., Kofeler, H., Hofler, G., Frank, S., Bogner-Strauss, J.G.*, et al.* (2011). Sequential synthesis and methylation of phosphatidylethanolamine promote lipid droplet biosynthesis and stability in tissue culture and in vivo. J Biol Chem *286*, 17338-17350.
73. Hosokawa, N., Hara, Y., and Mizushima, N. (2006). Generation of cell lines with tetracycline-regulated autophagy and a role for autophagy in controlling cell size. FEBS Lett *580*, 2623-2629.
74. Hotamisligil, G.S., and Erbay, E. (2008). Nutrient sensing and inflammation in metabolic diseases. Nat Rev Immunol *8*, 923-934.
75. Hou, N.S., Gutschmidt, A., Choi, D.Y., Pather, K., Shi, X., Watts, J.L., Hoppe, T., and Taubert, S. (2014). Activation of the endoplasmic reticulum unfolded protein response by lipid disequilibrium without disturbed proteostasis in vivo. Proc Natl Acad Sci U S A *111*, E2271-2280.
76. Huang, D.W., Sherman, B.T., Tan, Q., Collins, J.R., Alvord, W.G., Roayaei, J., Stephens, R., Baseler, M.W., Lane, H.C., and Lempicki, R.A. (2007a). The DAVID Gene Functional Classification Tool: a novel biological module-centric algorithm to functionally analyze large gene lists. Genome Biol *8*, R183.
77. Huang, D.W., Sherman, B.T., Tan, Q., Kir, J., Liu, D., Bryant, D., Guo, Y., Stephens, R., Baseler, M.W., Lane, H.C.*, et al.* (2007b). DAVID Bioinformatics Resources: expanded annotation database and novel algorithms to better extract biology from large gene lists. Nucleic Acids Res *35*, W169-175.
78. Imanikia, S., Sheng, M., Castro, C., Griffin, J.L., and Taylor, R.C. (2019). XBP-1 Remodels Lipid Metabolism to Extend Longevity. Cell Rep *28*, 581-589 e584.
79. Irshad, Z., Xue, M., Ashour, A., Larkin, J.R., Thornalley, P.J., and Rabbani, N. (2019). Activation of the unfolded protein response in high glucose treated endothelial cells is mediated by methylglyoxal. Sci Rep *9*, 7889.
80. Jia, K., Hart, A.C., and Levine, B. (2007). Autophagy genes protect against disease caused by polyglutamine expansion proteins in Caenorhabditis elegans. Autophagy *3*, 21-25.
81. Jia, K., Thomas, C., Akbar, M., Sun, Q., Adams-Huet, B., Gilpin, C., and Levine, B. (2009). Autophagy genes protect against Salmonella typhimurium infection and mediate insulin signaling-regulated pathogen resistance. Proc Natl Acad Sci U S A *106*, 14564-14569.
82. Jon Bremer, D.M.G. (1961). Methyl transfering enzyme system of microsomes in the biosynthesis of lecithin (phosphatidylcholine). Biochimica et Biophysica Acta *46*, 205-216.
83. Jones, D., Crowe, E., Stevens, T.A., and Candido, E.P. (2002). Functional and phylogenetic analysis of the ubiquitylation system in Caenorhabditis elegans: ubiquitin-conjugating enzymes, ubiquitin-activating enzymes, and ubiquitin-like proteins. Genome Biol *3*, RESEARCH0002.
84. Jonikas, M.C., Collins, S.R., Denic, V., Oh, E., Quan, E.M., Schmid, V., Weibezahn, J., Schwappach, B., Walter, P., Weissman, J.S.*, et al.* (2009). Comprehensive characterization of genes required for protein folding in the endoplasmic reticulum. Science *323*, 1693-1697.
85. Jung, Y., Kwon, S., Ham, S., Lee, D., Park, H.H., Yamaoka, Y., Jeong, D.E., Artan, M., Altintas, O., Park, S.*, et al.* (2020). Caenorhabditis elegans Lipin 1 moderates the lifespan-shortening effects of dietary glucose by maintaining omega-6 polyunsaturated fatty acids. Aging Cell *19*, e13150.
86. Kanehisa, M., and Goto, S. (2000). KEGG: kyoto encyclopedia of genes and genomes. Nucleic Acids Res *28*, 27-30.
87. Kang, C., You, Y.J., and Avery, L. (2007). Dual roles of autophagy in the survival of Caenorhabditis elegans during starvation. Genes Dev *21*, 2161-2171.
88. Kapulkin, W.J., Hiester, B.G., and Link, C.D. (2005). Compensatory regulation among ER chaperones in C. elegans. FEBS Lett *579*, 3063-3068.

89. Karabudak, T., Bor, M., Ozdemir, F., and Turkan, I. (2014). Glycine betaine protects tomato (Solanum lycopersicum) plants at low temperature by inducing fatty acid desaturase7 and lipoxygenase gene expression. Mol Biol Rep *41*, 1401-1410.
90. Karanasios, E., Han, G.S., Xu, Z., Carman, G.M., and Siniossoglou, S. (2010). A phosphorylation-regulated amphipathic helix controls the membrane translocation and function of the yeast phosphatidate phosphatase. Proc Natl Acad Sci U S A *107*, 17539-17544.
91. Karaskov, E., Scott, C., Zhang, L., Teodoro, T., Ravazzola, M., and Volchuk, A. (2006). Chronic palmitate but not oleate exposure induces endoplasmic reticulum stress, which may contribute to INS-1 pancreatic beta-cell apoptosis. Endocrinology *147*, 3398-3407.
92. Kashima, J., Shintani-Ishida, K., Nakajima, M., Maeda, H., Unuma, K., Uchiyama, Y., and Yoshida, K. (2014). Immunohistochemical study of the autophagy marker microtubule-associated protein 1 light chain 3 in normal and steatotic human livers. Hepatol Res *44*, 779-787.
93. Kaufman, R.J. (2002). Orchestrating the unfolded protein response in health and disease. J Clin Invest *110*, 1389-1398.
94. Kaur, J., and Debnath, J. (2015). Autophagy at the crossroads of catabolism and anabolism. Nat Rev Mol Cell Biol *16*, 461-472.
95. Keshet, A., Mertenskotter, A., Winter, S.A., Brinkmann, V., Dolling, R., and Paul, R.J. (2017). PMK-1 p38 MAPK promotes cadmium stress resistance, the expression of SKN-1/Nrf and DAF-16 target genes, and protein biosynthesis in Caenorhabditis elegans. Mol Genet Genomics *292*, 1341-1361.
96. Kim, I., Shu, C.W., Xu, W., Shiau, C.W., Grant, D., Vasile, S., Cosford, N.D., and Reed, J.C. (2009). Chemical biology investigation of cell death pathways activated by endoplasmic reticulum stress reveals cytoprotective modulators of ASK1. J Biol Chem *284*, 1593-1603.
97. Kim, M.H., Aydemir, T.B., Kim, J., and Cousins, R.J. (2017). Hepatic ZIP14-mediated zinc transport is required for adaptation to endoplasmic reticulum stress. Proc Natl Acad Sci U S A *114*, E5805-E5814.
98. Kimata, Y., Ishiwata-Kimata, Y., Ito, T., Hirata, A., Suzuki, T., Oikawa, D., Takeuchi, M., and Kohno, K. (2007). Two regulatory steps of ER-stress sensor Ire1 involving its cluster formation and interaction with unfolded proteins. J Cell Biol *179*, 75-86.
99. Kitade, H., Chen, G., Ni, Y., and Ota, T. (2017). Nonalcoholic Fatty Liver Disease and Insulin Resistance: New Insights and Potential New Treatments. Nutrients *9*.
100. Koh, J.H., Wang, L., Beaudoin-Chabot, C., and Thibault, G. (2018). Lipid bilayer stress-activated IRE-1 modulates autophagy during endoplasmic reticulum stress. J Cell Sci *131*.
101. Kohlwein, S.D. (2010). Triacylglycerol homeostasis: insights from yeast. J Biol Chem *285*, 15663-15667.
102. Kokame, K., Kato, H., and Miyata, T. (2001). Identification of ERSE-II, a new cis-acting element responsible for the ATF6-dependent mammalian unfolded protein response. J Biol Chem *276*, 9199-9205.
103. Kono, N., Amin-Wetzel, N., and Ron, D. (2017). Generic membrane-spanning features endow IRE1alpha with responsiveness to membrane aberrancy. Mol Biol Cell *28*, 2318-2332.
104. Korennykh, A.V., Egea, P.F., Korostelev, A.A., Finer-Moore, J., Zhang, C., Shokat, K.M., Stroud, R.M., and Walter, P. (2009). The unfolded protein response signals through high-order assembly of Ire1. Nature *457*, 687-693.
105. Kouroku, Y., Fujita, E., Tanida, I., Ueno, T., Isoai, A., Kumagai, H., Ogawa, S., Kaufman, R.J., Kominami, E., and Momoi, T. (2007). ER stress (PERK/eIF2alpha phosphorylation) mediates the polyglutamine-induced LC3 conversion, an essential step for autophagy formation. Cell Death Differ *14*, 230-239.
106. Kozutsumi, Y., Segal, M., Normington, K., Gething, M.J., and Sambrook, J. (1988). The presence of malfolded proteins in the endoplasmic reticulum signals the induction of glucose-regulated proteins. Nature *332*, 462-464.
107. Lagace, T.A., and Ridgway, N.D. (2013). The role of phospholipids in the biological activity and structure of the endoplasmic reticulum. Biochim Biophys Acta *1833*, 2499-2510.
108. Lajoie, P., Moir, R.D., Willis, I.M., and Snapp, E.L. (2012). Kar2p availability defines distinct forms of endoplasmic reticulum stress in living cells. Mol Biol Cell *23*, 955-964.
109. Lapierre, L.R., Gelino, S., Melendez, A., and Hansen, M. (2011). Autophagy and lipid metabolism coordinately modulate life span in germline-less C. elegans. Curr Biol *21*, 1507-1514.
110. Lee, A.H., Iwakoshi, N.N., and Glimcher, L.H. (2003). XBP-1 regulates a subset of endoplasmic reticulum resident chaperone genes in the unfolded protein response. Mol Cell Biol *23*, 7448-7459.
111. Lee, A.H., Scapa, E.F., Cohen, D.E., and Glimcher, L.H. (2008). Regulation of hepatic lipogenesis by the transcription factor XBP1. Science *320*, 1492-1496.

112. Lee, D., An, S.W.A., Jung, Y., Yamaoka, Y., Ryu, Y., Goh, G.Y.S., Beigi, A., Yang, J.S., Jung, G.Y., Ma, D.K.*, et al.* (2019). MDT-15/MED15 permits longevity at low temperature via enhancing lipidostasis and proteostasis. PLoS Biol *17*, e3000415.
113. Lee, D., Jeong, D.E., Son, H.G., Yamaoka, Y., Kim, H., Seo, K., Khan, A.A., Roh, T.Y., Moon, D.W., Lee, Y.*, et al.* (2015). SREBP and MDT-15 protect C. elegans from glucose-induced accelerated aging by preventing accumulation of saturated fat. Genes Dev *29*, 2490-2503.
114. Lee, J.S., Mendez, R., Heng, H.H., Yang, Z.Q., and Zhang, K. (2012). Pharmacological ER stress promotes hepatic lipogenesis and lipid droplet formation. Am J Transl Res *4*, 102-113.
115. Lee, S.J., Murphy, C.T., and Kenyon, C. (2009). Glucose shortens the life span of C. elegans by downregulating DAF-16/FOXO activity and aquaporin gene expression. Cell Metab *10*, 379-391.
116. Lehner, B., Tischler, J., and Fraser, A.G. (2006). RNAi screens in Caenorhabditis elegans in a 96-well liquid format and their application to the systematic identification of genetic interactions. Nat Protoc *1*, 1617-1620.
117. Levi-Ferber, M., Shalash, R., Thomas, A.L., Salzberg, Y., Shurgi, M., Ashkenazi, A., and Henis-Korenblit, S. (2020). Neuronal regulated Ire1-dependent mRNA decay controls germline differentiation in C. elegans. bioRxiv, 2020.2012.2029.424718.
118. Li, H., Korennykh, A.V., Behrman, S.L., and Walter, P. (2010). Mammalian endoplasmic reticulum stress sensor IRE1 signals by dynamic clustering. Proc Natl Acad Sci U S A *107*, 16113-16118.
119. Li, Y., Ge, M., Ciani, L., Kuriakose, G., Westover, E.J., Dura, M., Covey, D.F., Freed, J.H., Maxfield, F.R., Lytton, J.*, et al.* (2004). Enrichment of endoplasmic reticulum with cholesterol inhibits sarcoplasmic-endoplasmic reticulum calcium ATPase-2b activity in parallel with increased order of membrane lipids: implications for depletion of endoplasmic reticulum calcium stores and apoptosis in cholesterol-loaded macrophages. J Biol Chem *279*, 37030-37039.
120. Li, Y., Na, K., Lee, H.J., Lee, E.Y., and Paik, Y.K. (2011). Contribution of sams-1 and pmt-1 to lipid homoeostasis in adult Caenorhabditis elegans. J Biochem *149*, 529-538.
121. Li, Z., Agellon, L.B., Allen, T.M., Umeda, M., Jewell, L., Mason, A., and Vance, D.E. (2006). The ratio of phosphatidylcholine to phosphatidylethanolamine influences membrane integrity and steatohepatitis. Cell Metab *3*, 321-331.
122. Li, Z., Agellon, L.B., and Vance, D.E. (2005). Phosphatidylcholine homeostasis and liver failure. J Biol Chem *280*, 37798-37802.
123. Li, Z.Z., Berk, M., McIntyre, T.M., and Feldstein, A.E. (2009). Hepatic lipid partitioning and liver damage in nonalcoholic fatty liver disease: role of stearoyl-CoA desaturase. J Biol Chem *284*, 5637-5644.
124. Liang, X.H., Yu, J., Brown, K., and Levine, B. (2001). Beclin 1 contains a leucine-rich nuclear export signal that is required for its autophagy and tumor suppressor function. Cancer Res *61*, 3443-3449.
125. Ling, J., Reynolds, N., and Ibba, M. (2009). Aminoacyl-tRNA synthesis and translational quality control. Annu Rev Microbiol *63*, 61-78.
126. Listenberger, L.L., Han, X., Lewis, S.E., Cases, S., Farese, R.V., Jr., Ory, D.S., and Schaffer, J.E. (2003). Triglyceride accumulation protects against fatty acid-induced lipotoxicity. Proc Natl Acad Sci U S A *100*, 3077-3082.
127. Liu, X., Henkel, A.S., LeCuyer, B.E., Schipma, M.J., Anderson, K.A., and Green, R.M. (2015). Hepatocyte X-box binding protein 1 deficiency increases liver injury in mice fed a high-fat/sugar diet. Am J Physiol Gastrointest Liver Physiol *309*, G965-974.
128. Lochnit, G., and Geyer, R. (2003). Evidence for the presence of the Kennedy and Bremer-Greenberg pathways in Caenorhabditis elegans. Acta Biochim Pol *50*, 1239-1243.
129. Long, X., Spycher, C., Han, Z.S., Rose, A.M., Muller, F., and Avruch, J. (2002). TOR deficiency in C. elegans causes developmental arrest and intestinal atrophy by inhibition of mRNA translation. Curr Biol *12*, 1448-1461.
130. Ma, Y., and Li, J. (2015). Metabolic shifts during aging and pathology. Compr Physiol *5*, 667-686.
131. Martinez, B.A., Hoyle, R.G., Yeudall, S., Granade, M.E., Harris, T.E., Castle, J.D., Leitinger, N., and Bland, M.L. (2020). Innate immune signaling in Drosophila shifts anabolic lipid metabolism from triglyceride storage to phospholipid synthesis to support immune function. PLoS Genet *16*, e1009192.
132. Matsumoto, H., Miyazaki, S., Matsuyama, S., Takeda, M., Kawano, M., Nakagawa, H., Nishimura, K., and Matsuo, S. (2013). Selection of autophagy or apoptosis in cells exposed to ER-stress depends on ATF4 expression pattern with or without CHOP expression. Biol Open *2*, 1084-1090.

133. Melendez, A., Talloczy, Z., Seaman, M., Eskelinen, E.L., Hall, D.H., and Levine, B. (2003). Autophagy genes are essential for dauer development and life-span extension in C. elegans. Science *301*, 1387-1391.
134. Miquel, M., James, D., Jr., Dooner, H., and Browse, J. (1993). Arabidopsis requires polyunsaturated lipids for low-temperature survival. Proc Natl Acad Sci U S A *90*, 6208-6212.
135. Mizushima, N., Levine, B., Cuervo, A.M., and Klionsky, D.J. (2008). Autophagy fights disease through cellular self-digestion. Nature *451*, 1069-1075.
136. Moore, B.T., Jordan, J.M., and Baugh, L.R. (2013). WormSizer: high-throughput analysis of nematode size and shape. PLoS One *8*, e57142.
137. Moore, K., and Hollien, J. (2015). Ire1-mediated decay in mammalian cells relies on mRNA sequence, structure, and translational status. Mol Biol Cell *26*, 2873-2884.
138. Morein, S., Andersson, A., Rilfors, L., and Lindblom, G. (1996). Wild-type Escherichia coli cells regulate the membrane lipid composition in a "window" between gel and non-lamellar structures. J Biol Chem *271*, 6801-6809.
139. Mori, K., Ogawa, N., Kawahara, T., Yanagi, H., and Yura, T. (2000). mRNA splicing-mediated C-terminal replacement of transcription factor Hac1p is required for efficient activation of the unfolded protein response. Proc Natl Acad Sci U S A *97*, 4660-4665.
140. Mota, M., Banini, B.A., Cazanave, S.C., and Sanyal, A.J. (2016). Molecular mechanisms of lipotoxicity and glucotoxicity in nonalcoholic fatty liver disease. Metabolism *65*, 1049-1061.
141. Murray, P., Hayward, S.A., Govan, G.G., Gracey, A.Y., and Cossins, A.R. (2007). An explicit test of the phospholipid saturation hypothesis of acquired cold tolerance in Caenorhabditis elegans. Proc Natl Acad Sci U S A *104*, 5489-5494.
142. Nakatogawa, H., Ichimura, Y., and Ohsumi, Y. (2007). Atg8, a ubiquitin-like protein required for autophagosome formation, mediates membrane tethering and hemifusion. Cell *130*, 165-178.
143. Nass, K.J., van den Berg, E.H., Faber, K.N., Schreuder, T., Blokzijl, H., and Dullaart, R.P.F. (2017). High prevalence of apolipoprotein B dyslipoproteinemias in non-alcoholic fatty liver disease: The lifelines cohort study. Metabolism *72*, 37-46.
144. Ng, D.T., Spear, E.D., and Walter, P. (2000). The unfolded protein response regulates multiple aspects of secretory and membrane protein biogenesis and endoplasmic reticulum quality control. J Cell Biol *150*, 77-88.
145. Nikawa, J., and Yamashita, S. (1992). IRE1 encodes a putative protein kinase containing a membrane-spanning domain and is required for inositol phototrophy in Saccharomyces cerevisiae. Mol Microbiol *6*, 1441-1446.
146. Novoa, I., Zeng, H., Harding, H.P., and Ron, D. (2001). Feedback inhibition of the unfolded protein response by GADD34-mediated dephosphorylation of eIF2alpha. J Cell Biol *153*, 1011-1022.
147. Ogata, M., Hino, S., Saito, A., Morikawa, K., Kondo, S., Kanemoto, S., Murakami, T., Taniguchi, M., Tanii, I., Yoshinaga, K.*, et al.* (2006). Autophagy is activated for cell survival after endoplasmic reticulum stress. Mol Cell Biol *26*, 9220-9231.
148. Ogg, S., and Ruvkun, G. (1998). The C. elegans PTEN homolog, DAF-18, acts in the insulin receptor-like metabolic signaling pathway. Mol Cell *2*, 887-893.
149. Ohsaki, Y., Cheng, J., Fujita, A., Tokumoto, T., and Fujimoto, T. (2006). Cytoplasmic lipid droplets are sites of convergence of proteasomal and autophagic degradation of apolipoprotein B. Mol Biol Cell *17*, 2674-2683.
150. Okada, T., Haze, K., Nadanaka, S., Yoshida, H., Seidah, N.G., Hirano, Y., Sato, R., Negishi, M., and Mori, K. (2003). A serine protease inhibitor prevents endoplasmic reticulum stress-induced cleavage but not transport of the membrane-bound transcription factor ATF6. J Biol Chem *278*, 31024-31032.
151. Oursel, D., Loutelier-Bourhis, C., Orange, N., Chevalier, S., Norris, V., and Lange, C.M. (2007). Lipid composition of membranes of Escherichia coli by liquid chromatography/tandem mass spectrometry using negative electrospray ionization. Rapid Commun Mass Spectrom *21*, 1721-1728.
152. Oyadomari, S., Koizumi, A., Takeda, K., Gotoh, T., Akira, S., Araki, E., and Mori, M. (2002). Targeted disruption of the Chop gene delays endoplasmic reticulum stress-mediated diabetes. J Clin Invest *109*, 525-532.
153. Ozcan, U., Cao, Q., Yilmaz, E., Lee, A.H., Iwakoshi, N.N., Ozdelen, E., Tuncman, G., Gorgun, C., Glimcher, L.H., and Hotamisligil, G.S. (2004). Endoplasmic reticulum stress links obesity, insulin action, and type 2 diabetes. Science *306*, 457-461.
154. Palavalli, L.H., Brendza, K.M., Haakenson, W., Cahoon, R.E., McLaird, M., Hicks, L.M., McCarter, J.P., Williams, D.J., Hresko, M.C., and Jez, J.M. (2006). Defining the role of

phosphomethylethanolamine N-methyltransferase from Caenorhabditis elegans in phosphocholine biosynthesis by biochemical and kinetic analysis. Biochemistry *45*, 6056-6065.
155. Pattingre, S., Bauvy, C., Carpentier, S., Levade, T., Levine, B., and Codogno, P. (2009). Role of JNK1-dependent Bcl-2 phosphorylation in ceramide-induced macroautophagy. J Biol Chem *284*, 2719-2728.
156. Paz Gavilan, M., Vela, J., Castano, A., Ramos, B., del Rio, J.C., Vitorica, J., and Ruano, D. (2006). Cellular environment facilitates protein accumulation in aged rat hippocampus. Neurobiol Aging *27*, 973-982.
157. Peretti, D., Bastide, A., Radford, H., Verity, N., Molloy, C., Martin, M.G., Moreno, J.A., Steinert, J.R., Smith, T., Dinsdale, D.*, et al.* (2015). RBM3 mediates structural plasticity and protective effects of cooling in neurodegeneration. Nature *518*, 236-239.
158. Peterfy, M., Phan, J., Xu, P., and Reue, K. (2001). Lipodystrophy in the fld mouse results from mutation of a new gene encoding a nuclear protein, lipin. Nat Genet *27*, 121-124.
159. Pietilainen, K.H., Rog, T., Seppanen-Laakso, T., Virtue, S., Gopalacharyulu, P., Tang, J., Rodriguez-Cuenca, S., Maciejewski, A., Naukkarinen, J., Ruskeepaa, A.L.*, et al.* (2011). Association of lipidome remodeling in the adipocyte membrane with acquired obesity in humans. PLoS Biol *9*, e1000623.
160. Ploegh, H.L. (2007). A lipid-based model for the creation of an escape hatch from the endoplasmic reticulum. Nature *448*, 435-438.
161. Poteryaev, D., Squirrell, J.M., Campbell, J.M., White, J.G., and Spang, A. (2005). Involvement of the actin cytoskeleton and homotypic membrane fusion in ER dynamics in Caenorhabditis elegans. Mol Biol Cell *16*, 2139-2153.
162. Promlek, T., Ishiwata-Kimata, Y., Shido, M., Sakuramoto, M., Kohno, K., and Kimata, Y. (2011). Membrane aberrancy and unfolded proteins activate the endoplasmic reticulum stress sensor Ire1 in different ways. Mol Biol Cell *22*, 3520-3532.
163. Puri, P., Baillie, R.A., Wiest, M.M., Mirshahi, F., Choudhury, J., Cheung, O., Sargeant, C., Contos, M.J., and Sanyal, A.J. (2007). A lipidomic analysis of nonalcoholic fatty liver disease. Hepatology *46*, 1081-1090.
164. Qiu, W., Avramoglu, R.K., Rutledge, A.C., Tsai, J., and Adeli, K. (2006). Mechanisms of glucosamine-induced suppression of the hepatic assembly and secretion of apolipoprotein B-100-containing lipoproteins. J Lipid Res *47*, 1749-1761.
165. Qiu, W., Kohen-Avramoglu, R., Mhapsekar, S., Tsai, J., Austin, R.C., and Adeli, K. (2005). Glucosamine-induced endoplasmic reticulum stress promotes ApoB100 degradation: evidence for Grp78-mediated targeting to proteasomal degradation. Arterioscler Thromb Vasc Biol *25*, 571-577.
166. Qiu, W., Zhang, J., Dekker, M.J., Wang, H., Huang, J., Brumell, J.H., and Adeli, K. (2011). Hepatic autophagy mediates endoplasmic reticulum stress-induced degradation of misfolded apolipoprotein B. Hepatology *53*, 1515-1525.
167. Quinn, P.J. (1981). The fluidity of cell membranes and its regulation. Prog Biophys Mol Biol *38*, 1-104.
168. Ramirez-Zacarias, J.L., Castro-Munozledo, F., and Kuri-Harcuch, W. (1992). Quantitation of adipose conversion and triglycerides by staining intracytoplasmic lipids with Oil red O. Histochemistry *97*, 493-497.
169. Reue, K. (2009). The lipin family: mutations and metabolism. Curr Opin Lipidol *20*, 165-170.
170. Rinella, M.E., and Sanyal, A.J. (2015). NAFLD in 2014: Genetics, diagnostics and therapeutic advances in NAFLD. Nat Rev Gastroenterol Hepatol *12*, 65-66.
171. Rodriguez, D.A., Zamorano, S., Lisbona, F., Rojas-Rivera, D., Urra, H., Cubillos-Ruiz, J.R., Armisen, R., Henriquez, D.R., Cheng, E.H., Letek, M.*, et al.* (2012). BH3-only proteins are part of a regulatory network that control the sustained signalling of the unfolded protein response sensor IRE1alpha. EMBO J *31*, 2322-2335.
172. Ron, D., and Habener, J.F. (1992). CHOP, a novel developmentally regulated nuclear protein that dimerizes with transcription factors C/EBP and LAP and functions as a dominant-negative inhibitor of gene transcription. Genes Dev *6*, 439-453.
173. Ron, D., and Walter, P. (2007). Signal integration in the endoplasmic reticulum unfolded protein response. Nat Rev Mol Cell Biol *8*, 519-529.
174. Roy, B., and Lee, A.S. (1999). The mammalian endoplasmic reticulum stress response element consists of an evolutionarily conserved tripartite structure and interacts with a novel stress-inducible complex. Nucleic Acids Res *27*, 1437-1443.
175. Rubio, C., Pincus, D., Korennykh, A., Schuck, S., El-Samad, H., and Walter, P. (2011). Homeostatic adaptation to endoplasmic reticulum stress depends on Ire1 kinase activity. J Cell Biol *193*, 171-184.

176. Rutkowski, D.T., Arnold, S.M., Miller, C.N., Wu, J., Li, J., Gunnison, K.M., Mori, K., Sadighi Akha, A.A., Raden, D., and Kaufman, R.J. (2006). Adaptation to ER stress is mediated by differential stabilities of pro-survival and pro-apoptotic mRNAs and proteins. PLoS Biol *4*, e374.
177. Rutledge, A.C., Su, Q., and Adeli, K. (2010). Apolipoprotein B100 biogenesis: a complex array of intracellular mechanisms regulating folding, stability, and lipoprotein assembly. Biochem Cell Biol *88*, 251-267.
178. Rzechorzek, N.M., Connick, P., Patani, R., Selvaraj, B.T., and Chandran, S. (2015). Hypothermic Preconditioning of Human Cortical Neurons Requires Proteostatic Priming. EBioMedicine *2*, 528-535.
179. Safra, M., and Henis-Korenblit, S. (2014). A new tool in C. elegans reveals changes in secretory protein metabolism in ire-1-deficient animals. Worm *3*, e27733.
180. Saito, K., Fukuda, N., Matsumoto, T., Iribe, Y., Tsunemi, A., Kazama, T., Yoshida-Noro, C., and Hayashi, N. (2010). Moderate low temperature preserves the stemness of neural stem cells and suppresses apoptosis of the cells via activation of the cold-inducible RNA binding protein. Brain Res *1358*, 20-29.
181. Saldanha, A.J. (2004). Java Treeview--extensible visualization of microarray data. Bioinformatics *20*, 3246-3248.
182. Sasagawa, Y., Yamanaka, K., and Ogura, T. (2007). ER E3 ubiquitin ligase HRD-1 and its specific partner chaperone BiP play important roles in ERAD and developmental growth in Caenorhabditis elegans. Genes Cells *12*, 1063-1073.
183. Schaffer, J.E. (2003). Lipotoxicity: when tissues overeat. Curr Opin Lipidol *14*, 281-287.
184. Schneider, C.A., Rasband, W.S., and Eliceiri, K.W. (2012). NIH Image to ImageJ: 25 years of image analysis. Nat Methods *9*, 671-675.
185. Schroder, M., and Kaufman, R.J. (2005a). ER stress and the unfolded protein response. Mutat Res *569*, 29-63.
186. Schroder, M., and Kaufman, R.J. (2005b). The mammalian unfolded protein response. Annu Rev Biochem *74*, 739-789.
187. Shaikh, S.R., Kinnun, J.J., Leng, X., Williams, J.A., and Wassall, S.R. (2015). How polyunsaturated fatty acids modify molecular organization in membranes: insight from NMR studies of model systems. Biochim Biophys Acta *1848*, 211-219.
188. Shen, J., Chen, X., Hendershot, L., and Prywes, R. (2002). ER stress regulation of ATF6 localization by dissociation of BiP/GRP78 binding and unmasking of Golgi localization signals. Dev Cell *3*, 99-111.
189. Shen, X., Ellis, R.E., Lee, K., Liu, C.Y., Yang, K., Solomon, A., Yoshida, H., Morimoto, R., Kurnit, D.M., Mori, K.*, et al.* (2001). Complementary signaling pathways regulate the unfolded protein response and are required for C. elegans development. Cell *107*, 893-903.
190. Shen, X., Ellis, R.E., Sakaki, K., and Kaufman, R.J. (2005). Genetic interactions due to constitutive and inducible gene regulation mediated by the unfolded protein response in C. elegans. PLoS Genet *1*, e37.
191. Shen, X., Zhang, K., and Kaufman, R.J. (2004). The unfolded protein response--a stress signaling pathway of the endoplasmic reticulum. J Chem Neuroanat *28*, 79-92.
192. Shields, D.J., Lehner, R., Agellon, L.B., and Vance, D.E. (2003). Membrane topography of human phosphatidylethanolamine N-methyltransferase. J Biol Chem *278*, 2956-2962.
193. Shulman, G.I. (2014). Ectopic fat in insulin resistance, dyslipidemia, and cardiometabolic disease. N Engl J Med *371*, 1131-1141.
194. Shyu, P., Jr., Ng, B.S.H., Ho, N., Chaw, R., Seah, Y.L., Marvalim, C., and Thibault, G. (2019). Membrane phospholipid alteration causes chronic ER stress through early degradation of homeostatic ER-resident proteins. Sci Rep *9*, 8637.
195. Singh, R., Kaushik, S., Wang, Y., Xiang, Y., Novak, I., Komatsu, M., Tanaka, K., Cuervo, A.M., and Czaja, M.J. (2009). Autophagy regulates lipid metabolism. Nature *458*, 1131-1135.
196. Smulan, L.J., Ding, W., Freinkman, E., Gujja, S., Edwards, Y.J.K., and Walker, A.K. (2016). Cholesterol-Independent SREBP-1 Maturation Is Linked to ARF1 Inactivation. Cell Rep *16*, 9-18.
197. So, J.S., Hur, K.Y., Tarrio, M., Ruda, V., Frank-Kamenetsky, M., Fitzgerald, K., Koteliansky, V., Lichtman, A.H., Iwawaki, T., Glimcher, L.H.*, et al.* (2012). Silencing of lipid metabolism genes through IRE1alpha-mediated mRNA decay lowers plasma lipids in mice. Cell Metab *16*, 487-499.
198. Spector, A.A., and Yorek, M.A. (1985). Membrane lipid composition and cellular function. J Lipid Res *26*, 1015-1035.
199. Sriburi, R., Jackowski, S., Mori, K., and Brewer, J.W. (2004). XBP1: a link between the unfolded protein response, lipid biosynthesis, and biogenesis of the endoplasmic reticulum. J Cell Biol *167*, 35-41.

200. Stiernagle, T. (2006). Maintenance of C. elegans. WormBook, 1-11.
201. Stubbs, C.D. (1983). Membrane fluidity: structure and dynamics of membrane lipids. Essays Biochem *19*, 1-39.
202. Stubbs, C.D., and Smith, A.D. (1984). The modification of mammalian membrane polyunsaturated fatty acid composition in relation to membrane fluidity and function. Biochim Biophys Acta *779*, 89-137.
203. Sun, Q., Zhang, Y., Su, J., Li, T., and Jiang, Y. (2018). Role of Hydroxysteroid Dehydrogenase-Like 2 (HSDL2) in Human Ovarian Cancer. Med Sci Monit *24*, 3997-4008.
204. Supek, F., Bosnjak, M., Skunca, N., and Smuc, T. (2011). REVIGO summarizes and visualizes long lists of gene ontology terms. PLoS One *6*, e21800.
205. Svensk, E., Devkota, R., Stahlman, M., Ranji, P., Rauthan, M., Magnusson, F., Hammarsten, S., Johansson, M., Boren, J., and Pilon, M. (2016). Caenorhabditis elegans PAQR-2 and IGLR-2 Protect against Glucose Toxicity by Modulating Membrane Lipid Composition. PLoS Genet *12*, e1005982.
206. Szegezdi, E., Logue, S.E., Gorman, A.M., and Samali, A. (2006). Mediators of endoplasmic reticulum stress-induced apoptosis. EMBO Rep *7*, 880-885.
207. Takacs-Vellai, K., Vellai, T., Puoti, A., Passannante, M., Wicky, C., Streit, A., Kovacs, A.L., and Muller, F. (2005). Inactivation of the autophagy gene bec-1 triggers apoptotic cell death in C. elegans. Curr Biol *15*, 1513-1517.
208. Talloczy, Z., Jiang, W., Virgin, H.W.t., Leib, D.A., Scheuner, D., Kaufman, R.J., Eskelinen, E.L., and Levine, B. (2002). Regulation of starvation- and virus-induced autophagy by the eIF2alpha kinase signaling pathway. Proc Natl Acad Sci U S A *99*, 190-195.
209. Tam, A.B., Roberts, L.S., Chandra, V., Rivera, I.G., Nomura, D.K., Forbes, D.J., and Niwa, M. (2018). The UPR Activator ATF6 Responds to Proteotoxic and Lipotoxic Stress by Distinct Mechanisms. Dev Cell *46*, 327-343 e327.
210. Taylor, R.C., and Dillin, A. (2013). XBP-1 is a cell-nonautonomous regulator of stress resistance and longevity. Cell *153*, 1435-1447.
211. Thibault, G., Ismail, N., and Ng, D.T. (2011). The unfolded protein response supports cellular robustness as a broad-spectrum compensatory pathway. Proc Natl Acad Sci U S A *108*, 20597-20602.
212. Thibault, G., Shui, G., Kim, W., McAlister, G.C., Ismail, N., Gygi, S.P., Wenk, M.R., and Ng, D.T. (2012). The membrane stress response buffers lethal effects of lipid disequilibrium by reprogramming the protein homeostasis network. Mol Cell *48*, 16-27.
213. Tian, Y., Li, Z., Hu, W., Ren, H., Tian, E., Zhao, Y., Lu, Q., Huang, X., Yang, P., Li, X*., et al.* (2010). C. elegans screen identifies autophagy genes specific to multicellular organisms. Cell *141*, 1042-1055.
214. Timmons, L., and Fire, A. (1998). Specific interference by ingested dsRNA. Nature *395*, 854.
215. Tiniakos, D.G., Vos, M.B., and Brunt, E.M. (2010). Nonalcoholic fatty liver disease: pathology and pathogenesis. Annu Rev Pathol *5*, 145-171.
216. Travers, K.J., Patil, C.K., Wodicka, L., Lockhart, D.J., Weissman, J.S., and Walter, P. (2000). Functional and genomic analyses reveal an essential coordination between the unfolded protein response and ER-associated degradation. Cell *101*, 249-258.
217. UniProt, C. (2019). UniProt: a worldwide hub of protein knowledge. Nucleic Acids Res *47*, D506-D515.
218. Upton, J.P., Wang, L., Han, D., Wang, E.S., Huskey, N.E., Lim, L., Truitt, M., McManus, M.T., Ruggero, D., Goga, A*., et al.* (2012). IRE1alpha cleaves select microRNAs during ER stress to derepress translation of proapoptotic Caspase-2. Science *338*, 818-822.
219. Urano, F., Calfon, M., Yoneda, T., Yun, C., Kiraly, M., Clark, S.G., and Ron, D. (2002). A survival pathway for Caenorhabditis elegans with a blocked unfolded protein response. J Cell Biol *158*, 639-646.
220. van der Veen, J.N., Kennelly, J.P., Wan, S., Vance, J.E., Vance, D.E., and Jacobs, R.L. (2017). The critical role of phosphatidylcholine and phosphatidylethanolamine metabolism in health and disease. Biochim Biophys Acta Biomembr *1859*, 1558-1572.
221. van Meer, G., Voelker, D.R., and Feigenson, G.W. (2008). Membrane lipids: where they are and how they behave. Nat Rev Mol Cell Biol *9*, 112-124.
222. van Zutphen, T., Todde, V., de Boer, R., Kreim, M., Hofbauer, H.F., Wolinski, H., Veenhuis, M., van der Klei, I.J., and Kohlwein, S.D. (2014). Lipid droplet autophagy in the yeast Saccharomyces cerevisiae. Mol Biol Cell *25*, 290-301.
223. Vidal, R.L., Figueroa, A., Court, F.A., Thielen, P., Molina, C., Wirth, C., Caballero, B., Kiffin, R., Segura-Aguilar, J., Cuervo, A.M*., et al.* (2012). Targeting the UPR transcription factor XBP1

protects against Huntington's disease through the regulation of FoxO1 and autophagy. Hum Mol Genet *21*, 2245-2262.
224. Volmer, R., van der Ploeg, K., and Ron, D. (2013). Membrane lipid saturation activates endoplasmic reticulum unfolded protein response transducers through their transmembrane domains. Proc Natl Acad Sci U S A *110*, 4628-4633.
225. Walker, A.K., Jacobs, R.L., Watts, J.L., Rottiers, V., Jiang, K., Finnegan, D.M., Shioda, T., Hansen, M., Yang, F., Niebergall, L.J.*, et al.* (2011). A conserved SREBP-1/phosphatidylcholine feedback circuit regulates lipogenesis in metazoans. Cell *147*, 840-852.
226. Walkey, C.J., Yu, L., Agellon, L.B., and Vance, D.E. (1998). Biochemical and evolutionary significance of phospholipid methylation. J Biol Chem *273*, 27043-27046.
227. Walter, P., and Ron, D. (2011). The unfolded protein response: from stress pathway to homeostatic regulation. Science *334*, 1081-1086.
228. Wang, C., Saar, V., Leung, K.L., Chen, L., and Wong, G. (2018). Human amyloid beta peptide and tau co-expression impairs behavior and causes specific gene expression changes in Caenorhabditis elegans. Neurobiol Dis *109*, 88-101.
229. Wang, J., Song, M.Y., Bae, U.J., Lim, J.M., Kwon, K.S., and Park, B.H. (2015). n-3 Polyunsaturated fatty acids protect against pancreatic beta-cell damage due to ER stress and prevent diabetes development. Mol Nutr Food Res *59*, 1791-1802.
230. Wang, J., Zhu, W., Huang, S., Xu, L., Miao, M., Wu, C., Yu, C., Li, Y., and Xu, C. (2017). Serum apoB levels independently predict the development of non-alcoholic fatty liver disease: A 7-year prospective study. Liver Int *37*, 1202-1208.
231. Wang, S., Chen, Z., Lam, V., Han, J., Hassler, J., Finck, B.N., Davidson, N.O., and Kaufman, R.J. (2012). IRE1alpha-XBP1s induces PDI expression to increase MTP activity for hepatic VLDL assembly and lipid homeostasis. Cell Metab *16*, 473-486.
232. Wei, Y., Pattingre, S., Sinha, S., Bassik, M., and Levine, B. (2008a). JNK1-mediated phosphorylation of Bcl-2 regulates starvation-induced autophagy. Mol Cell *30*, 678-688.
233. Wei, Y., Sinha, S., and Levine, B. (2008b). Dual role of JNK1-mediated phosphorylation of Bcl-2 in autophagy and apoptosis regulation. Autophagy *4*, 949-951.
234. Wei, Y., Wang, D., Topczewski, F., and Pagliassotti, M.J. (2006). Saturated fatty acids induce endoplasmic reticulum stress and apoptosis independently of ceramide in liver cells. Am J Physiol Endocrinol Metab *291*, E275-281.
235. Willy, J.A., Young, S.K., Stevens, J.L., Masuoka, H.C., and Wek, R.C. (2015). CHOP links endoplasmic reticulum stress to NF-kappaB activation in the pathogenesis of nonalcoholic steatohepatitis. Mol Biol Cell *26*, 2190-2204.
236. Wong, V.W., Chan, W.K., Chitturi, S., Chawla, Y., Dan, Y.Y., Duseja, A., Fan, J., Goh, K.L., Hamaguchi, M., Hashimoto, E.*, et al.* (2018). Asia-Pacific Working Party on Non-alcoholic Fatty Liver Disease guidelines 2017-Part 1: Definition, risk factors and assessment. J Gastroenterol Hepatol *33*, 70-85.
237. Wu, H., Ng, B.S., and Thibault, G. (2014). Endoplasmic reticulum stress response in yeast and humans. Biosci Rep *34*.
238. Xu, S., Nam, S.M., Kim, J.H., Das, R., Choi, S.K., Nguyen, T.T., Quan, X., Choi, S.J., Chung, C.H., Lee, E.Y.*, et al.* (2015). Palmitate induces ER calcium depletion and apoptosis in mouse podocytes subsequent to mitochondrial oxidative stress. Cell Death Dis *6*, e1976.
239. Yamamoto, K., Takahara, K., Oyadomari, S., Okada, T., Sato, T., Harada, A., and Mori, K. (2010). Induction of liver steatosis and lipid droplet formation in ATF6alpha-knockout mice burdened with pharmacological endoplasmic reticulum stress. Mol Biol Cell *21*, 2975-2986.
240. Yamamoto, K., Yoshida, H., Kokame, K., Kaufman, R.J., and Mori, K. (2004). Differential contributions of ATF6 and XBP1 to the activation of endoplasmic reticulum stress-responsive cis-acting elements ERSE, UPRE and ERSE-II. J Biochem *136*, 343-350.
241. Yang, L., Li, P., Fu, S., Calay, E.S., and Hotamisligil, G.S. (2010). Defective hepatic autophagy in obesity promotes ER stress and causes insulin resistance. Cell Metab *11*, 467-478.
242. Ye, J., Rawson, R.B., Komuro, R., Chen, X., Dave, U.P., Prywes, R., Brown, M.S., and Goldstein, J.L. (2000). ER stress induces cleavage of membrane-bound ATF6 by the same proteases that process SREBPs. Mol Cell *6*, 1355-1364.
243. Ye, Q., Zou, B., Yeo, Y.H., Li, J., Huang, D.Q., Wu, Y., Yang, H., Liu, C., Kam, L.Y., Tan, X.X.E.*, et al.* (2020). Global prevalence, incidence, and outcomes of non-obese or lean non-alcoholic fatty liver disease: a systematic review and meta-analysis. Lancet Gastroenterol Hepatol *5*, 739-752.
244. Ye, R., Jung, D.Y., Jun, J.Y., Li, J., Luo, S., Ko, H.J., Kim, J.K., and Lee, A.S. (2010). Grp78 heterozygosity promotes adaptive unfolded protein response and attenuates diet-induced obesity and insulin resistance. Diabetes *59*, 6-16.

245. Yen, K., Le, T.T., Bansal, A., Narasimhan, S.D., Cheng, J.X., and Tissenbaum, H.A. (2010). A comparative study of fat storage quantitation in nematode Caenorhabditis elegans using label and label-free methods. PLoS One *5*.
246. Yoon, H.J., and Cha, B.S. (2014). Pathogenesis and therapeutic approaches for non-alcoholic fatty liver disease. World J Hepatol *6*, 800-811.
247. Yoshida, H., Haze, K., Yanagi, H., Yura, T., and Mori, K. (1998). Identification of the cis-acting endoplasmic reticulum stress response element responsible for transcriptional induction of mammalian glucose-regulated proteins. Involvement of basic leucine zipper transcription factors. J Biol Chem *273*, 33741-33749.
248. Yoshida, H., Matsui, T., Yamamoto, A., Okada, T., and Mori, K. (2001). XBP1 mRNA is induced by ATF6 and spliced by IRE1 in response to ER stress to produce a highly active transcription factor. Cell *107*, 881-891.
249. Younce, C., and Kolattukudy, P. (2012). MCP-1 induced protein promotes adipogenesis via oxidative stress, endoplasmic reticulum stress and autophagy. Cell Physiol Biochem *30*, 307-320.
250. Yu, X., Li, A., and Li, W. (2015). How membranes organize during seed germination: three patterns of dynamic lipid remodelling define chilling resistance and affect plastid biogenesis. Plant Cell Environ *38*, 1391-1403.
251. Zaccheo, O., Dinsdale, D., Meacock, P.A., and Glynn, P. (2004). Neuropathy target esterase and its yeast homologue degrade phosphatidylcholine to glycerophosphocholine in living cells. J Biol Chem *279*, 24024-24033.
252. Zechner, R., Madeo, F., and Kratky, D. (2017). Cytosolic lipolysis and lipophagy: two sides of the same coin. Nat Rev Mol Cell Biol *18*, 671-684.
253. Zhao, Y., Li, X., Cai, M.Y., Ma, K., Yang, J., Zhou, J., Fu, W., Wei, F.Z., Wang, L., Xie, D.*, et al.* (2013). XBP-1u suppresses autophagy by promoting the degradation of FoxO1 in cancer cells. Cell Res *23*, 491-507.

Appendix

Table A1: List of upregulated and downregulated genes in pmt-2(RNAi) and WT treated with tunicamycin compared to WT animals.

UPREGULATED GENES (Fold change > 1.5, ANOVA p-value < 0.05)
***pmt-2(RNAi)* (2110)**
aagr-4, aak-2, aakb-1, aakg-1, abf-2, abf-5, abf-6, abt-1, abt-2, abt-5, abts-3, abts-4, AC8.12, acbp-7, acdh-4, acdh-7, ace-3, acl-12, acl-13, acs-11, acs-18, acs-2, acs-20, acs-5, acs-6, adm-2, aex-3, aex-6, aip-1, ajm-1, aldo-2, alg-1, alh-5, alx-1, amx-2, ant-1.3, apl-1, apm-1, aqp-1, arl-13, arl-3, arrd-12, arrd-25, arrd-27, arrd-7, arrd-8, asd-2, asm-1, atf-6, atfs-1, atg-2, B0001.6, B0024.4, B0025.5, B0205.10, B0205.13, B0205.14, B0207.7, B0207.9, B0218.7, B0244.9, B0252.5, B0261.6, B0280.17, B0284.6, B0285.12, B0294.1, B0302.5, B0348.2, B0350.3, B0350.78, B0353.1, B0379.7, B0403.3, B0403.5, B0416.7, B0432.14, B0454.6, B0462.5, B0478.3, B0496.6, B0507.1, B0507.2, B0507.3, B0546.3, B0546.4, B0554.5, B0563.5, B0564.6, bam-2, basl-1, bath-25, bath-38, bath-46, bbs-5, bca-1, best-1, best-11, best-20, best-21, best-24, best-25, best-7, bicd-1, brp-1, btb-21, btb-9, btbd-10, C01A2.4, C01B10.44, C01B4.7, C01B4.8, C01C4.3, C01F6.2, C01G10.5, C01G5.4, C02B10.6, C02B4.8, C02B8.3, C02F4.4, C03B1.13, C03F11.2, C03G6.17, C03G6.5, C04A11.1, C04E6.5, C04F12.12, C04F12.7, C04G2.2, C04G2.5, C04G2.9, C05B5.12, C05B5.2, C05B5.8, C05C12.1, C05D11.5, C05D11.7, C05D12.7, C05E7.1, C05G5.2, C06A6.7, C06A8.6, C06B3.7, C06E4.8, C06E7.4, C06E8.6, C06G3.3, C07A12.12, C07A12.13, C07A12.2, C07A12.7, C07A9.12, C07B5.3, C07E3.3, C07G1.6, C08E8.3, C08E8.4, C08F11.10, C08F8.6, C08G5.7, C08G9.1, C09B9.4, C09B9.7, C09D4.1, C09D4.2, C09D4.3, C09F5.1, C09F9.8, C09G12.5, C09G9.5, C09H10.9, C09H5.7, C10A4.10, C10B5.3, C10C5.4, C10C5.7, C10G11.8, C10G11.9, C11E4.2, C13A10.2, C13B9.2, C13B9.3, C13C4.7, C14A4.12, C14A4.13, C14A4.8, C14B1.3, C14C10.1, C14C6.2, C14F11.11, C15C6.2, C15C7.5, C15C8.1, C15F1.5, C15H11.1, C15H11.12, C15H9.11, C16A11.7, C16B8.3, C16C8.18, C16D2.1, C16D9.4, C17G10.7, C17H11.6, C17H12.12, C17H12.8, C18A3.4, C18B12.10, C18B12.2, C18B12.4, C18B2.4, C18D11.1, C18E3.1, C18E9.8, C18G1.1, C18H2.5, C18H7.11, C18H9.5, C23G10.1, C23G10.11, C23G10.6, C23H3.11, C23H3.9, C23H4.8, C24A1.3, C24A11.1, C24A11.5, C24A8.6, C24H11.1, C24H11.2, C25D7.16, C25E10.12, C25E10.8, C25F9.11, C25F9.14, C25F9.5, C25H3.10, C26B2.2, C26B9.1, C26D10.4, C27A7.1, C27B7.6, C27D6.3, C27D8.1, C27D8.2, C27D8.3, C28C12.1, C28D4.4, C28G1.5, C29E4.14, C29F3.7, C29F5.3, C29H12.13, C30B5.7, C30E1.9, C30F12.1, C30F12.5, C30F2.4, C30G7.2, C30G7.3, C31B8.4, C31C9.6, C31H1.5, C31H5.7, C32C4.3, C32D5.1, C32D5.12, C32D5.4, C32D5.7, C32E12.4, C33A11.1, C33A11.2, C33A12.19, C33A12.4, C33C12.12, C33C12.7, C33D9.3, C33F10.11, C33G8.2, C33H5.13, C33H5.16, C34B4.3, C34C12.7, C34C6.3, C34D1.4, C34D10.1, C34D4.2, C34E11.7, C34F11.3, C34F11.5, C34F11.8, C34F6.7, C34H4.1, C34H4.2, C35A5.4, C35A5.6, C35B1.4, C35B8.4, C35C5.8, C35D10.8, C35E7.2, C36C5.12, C36F7.5, C36H8.1, C37C3.12, C37C3.7, C37H5.2, C37H5.3, C38C10.6, C38C3.3, C38C3.6, C38H2.3, C39D10.2, C39E9.7, C39F7.5, C40H1.7, C42D4.3, C42D8.1, C43C3.4, C43E11.5, C43F9.7, C44B11.4, C44B7.10, C44B9.2, C44C10.9, C44H9.4, C44H9.6, C45B11.2, C45B11.8, C45B11.9, C45E1.4, C45E5.4, C45G3.4, C45G9.9, C46E10.1, C46F11.6, C46G7.5, C47D2.1, C47E12.10, C47E12.12, C47E12.9, C47E8.1, C47E8.11, C48B4.12, C48B6.4, C48E7.6, C48E7.7, C49C3.9, C49C8.2, C49C8.5, C49F8.1, C49G7.12, C49G7.3, C49G7.6, C50B8.1, C50B8.4, C50C3.2, C50D2.6, C50E10.1, C50F4.2, C50F4.8, C51E3.9, C52A10.1, C52B11.5, C52E4.7, C52G5.9, C53A3.3, C53B7.2, C53C11.5, C53C9.2, C53D5.2, C54D1.8, C54D10.14, C54D10.16, C54D10.4, C54D2.1, C54D2.2, C54E4.5, C54F6.12, C54F6.15, C54F6.5, C55C2.4, C55C3.3, C56E10.5, C56G7.3, cab-1, cah-4, cah-6, camt-1, cas-1, casy-1, catp-1, catp-4, catp-7, ccch-1, cccp-1, ccg-1, cdd-1, cdka-1, cebp-1, ceeh-1, ceh-14, ceh-34, ceh-62, ceh-79, cept-1, cgt-1, chd-7, cho-1, ckk-1, ckr-2, clc-1, clec-123, clec-142, clec-145, clec-146, clec-147, clec-153, clec-17, clec-173, clec-184, clec-221, clec-265, clec-4, clec-62, clec-63, clec-65, clec-73, clh-1, clh-2, clp-4, clp-6, cls-1, cmd-1, cmk-1, cnp-3, cog-1, col-76, col-95, comt-3, cpb-2, cpg-7, cpn-4, cpna-1, cpna-4, cpna-5, cpz-2, crm-1, crtc-1, csp-2, cutl-15, cutl-23, cutl-24, cwp-4, cyn-17, cyp-13A5, cyp-33C7, cyp-36A1, cyp-42A1, cyp-43A1, cytb-5.1, cytb-5.2, D1022.9, D1037.5, D1044.1, D1046.15, D1053.3, D1054.5, D1065.3, D1081.12, D2005.6, D2007.2, D2030.12, D2063.4, daf-12, daf-16, daf-5, daf-7, daf-8, dat-1, dct-9, deg-1, deg-3, des-2, dgk-1, DH11.2, DH11.5, dhp-1, dhs-9, dlk-1, dmd-10, dmd-6, dmd-7, dmsr-8, dnj-14, dod-19, dod-20, dod-6, dop-5, dpf-6, dur-1, DY3.9, dyf-1, E01G6.2, E02A10.4, E02H9.2, E03H4.8, E04D5.4,

E04F6.4, ech-7, efk-1, egal-1, egl-21, egl-3, egl-44, egl-47, egl-9, egrh-1, elo-1, elo-2, elo-7, elo-8, elt-2, elt-3, emb-8, ent-3, enu-3, epg-5, epn-1, ets-4, exc-7, exp-2, F01D5.1, F01D5.5, F01D5.6, F01D5.7, F01D5.8, F02C9.4, F02E11.2, F02E8.9, F07A5.2, F07B7.12, F07C4.12, F07C6.3, F07F6.1, F07F6.10, F08A8.8, F08B12.1, F08B12.7, F08F3.9, F08G12.5, F09A5.2, F09A5.4, F09C3.2, F09C6.13, F09C8.2, F09E5.16, F09E8.8, F09G2.3, F10D2.10, F10D7.5, F10E9.12, F10G2.1, F10G7.5, F10G8.8, F11A5.9, F11G11.5, F12B6.2, F13A7.1, F13A7.11, F13B6.1, F13B6.3, F13B9.9, F13D11.4, F13D12.3, F13D12.9, F13E6.10, F13G11.2, F13H10.8, F13H6.1, F13H6.12, F13H6.24, F13H6.8, F13H8.1, F13H8.8, F14B6.2, F14B8.5, F14B8.6, F14D2.19, F14F11.2, F14F7.4, F14F9.3, F15A4.6, F15A8.6, F15B9.6, F15D4.4, F15D4.6, F16B12.4, F16H6.10, F17C11.11, F17C11.2, F17C11.6, F17C8.3, F17E9.5, F17H10.1, F17H10.2, F18E9.3, F19B2.5, F20A1.1, F20A1.10, F20A1.6, F20B10.3, F20B6.1, F20C5.4, F20D1.3, F20D6.1, F20D6.10, F20D6.8, F20G2.3, F20G2.5, F20G2.9, F21C10.3, F21C10.4, F21D12.3, F21D9.2, F21F3.2, F21F3.3, F21F3.6, F21F8.11, F21G4.1, F21H7.2, F21H7.5, F22A3.15, F22B5.4, F22B7.9, F22E12.1, F22E12.12, F22E5.13, F22H10.2, F23B12.4, F23C8.6, F23C8.8, F23D12.3, F23D12.7, F25A2.1, F25B3.4, F25B3.5, F25E5.4, F25E5.5, F25E5.8, F25H5.7, F26A1.3, F26A1.9, F26A10.1, F26A10.2, F26A3.4, F26A3.5, F26B1.5, F26B1.8, F26D2.10, F26F4.2, F26G1.2, F27B10.1, F27C1.1, F27C8.5, F27D9.2, F27E5.3, F28A10.4, F28F5.6, F29B9.12, F29G9.14, F30A10.11, F31E3.2, F31E8.5, F32A11.3, F32A5.4, F32B4.2, F32B5.7, F32B6.4, F32D8.7, F32H2.7, F32H5.3, F33D11.2, F33D11.8, F33H12.7, F34D10.9, F34H10.2, F35A5.9, F35B12.3, F35B12.9, F35B3.4, F35B3.7, F35C11.6, F35E12.10, F35E12.11, F35E12.8, F35E12.9, F35E2.9, F35G2.21, F35H10.3, F35H8.1, F35H8.4, F36A2.10, F36A2.3, F36A4.3, F36D3.16, F36D3.5, F36G3.3, F36H12.10, F36H12.14, F36H12.3, F36H12.5, F37A4.4, F37A4.5, F37A8.1, F37C4.5, F38A6.4, F38B2.2, F38B7.14, F38B7.2, F38G1.3, F38H4.4, F39B2.8, F39C12.4, F39E9.1, F40A3.1, F40B5.2, F40E10.6, F40E12.2, F40E3.5, F40F12.3, F40F12.9, F40F8.4, F40G12.10, F41B4.1, F41G3.10, F41G3.5, F41G4.8, F41H10.5, F42A9.7, F42G4.2, F42G8.8, F42H10.5, F42H10.6, F43C1.7, F43C9.2, F43C9.7, F43D9.1, F43D9.8, F44A2.3, F44A2.5, F44D12.8, F44E8.43, F44G3.7, F44G4.7, F45D3.3, F45E4.6, F45H7.12, F46A8.7, F46A9.1, F46C5.1, F46F11.7, F46F5.6, F46G10.2, F46H5.7, F47A4.5, F47B10.5, F47B3.2, F47B3.4, F47B3.5, F47B3.6, F47B7.2, F47B7.7, F47B8.3, F47B8.8, F47D12.7, F47E1.17, F47E1.5, F47G3.1, F47G3.4, F47G3.7, F47G6.3, F48C1.9, F48D6.4, F49C12.15, F49C12.6, F49E2.5, F49F1.6, F52E1.14, F52E10.4, F52E4.5, F52G3.1, F53A10.2, F53A9.2, F53B1.6, F53B2.5, F53C11.1, F53C3.13, F53C3.4, F53C3.5, F53C3.6, F53F1.6, F53F10.1, F53F10.2, F53F4.13, F53F8.4, F54B11.5, F54C9.11, F54C9.14, F54D1.6, F54D5.3, F54E2.1, F54F12.1, F54G2.1, F54H12.8, F54H5.3, F55A4.4, F55B12.10, F55C12.1, F55C12.15, F55C5.16, F55F8.7, F55G11.4, F56A11.6, F56C11.6, F56C4.4, F56C9.8, F56D5.2, F56D6.13, F56H11.2, F56H9.2, F57A8.6, F57A8.9, F57B10.18, F57B9.3, F58B4.3, F58B4.6, F58D2.2, F58D5.5, F58D5.7, F58E10.7, F58E6.5, F58F12.3, F58G1.9, F58H1.2, F58H1.7, F58H10.1, F59A1.15, F59A7.2, F59A7.5, F59B10.4, F59B10.6, F59B2.13, F59B8.5, F59C6.2, F59E10.3, F59E11.2, far-3, far-6, fard-1, fat-1, fat-2, fat-3, fat-4, fat-5, fat-6, fat-7, fbxa-115, fbxa-12, fbxa-125, fbxa-150, fbxa-162, fbxa-182, fbxa-199, fbxa-202, fbxa-21, fbxa-24, fbxa-37, fbxa-44, fbxa-74, fbxa-79, fbxa-90, fbxc-1, fbxc-2, fbxc-23, fbxc-54, fer-1, fhod-1, fipr-1, fipr-12, fipr-2, fis-1, fkh-6, flp-1, flp-11, flp-12, flp-13, flp-15, flp-16, flp-17, flp-18, flp-19, flp-2, flp-21, flp-22, flp-24, flp-25, flp-26, flp-27, flp-28, flp-3, flp-32, flp-33, flp-4, flp-5, flp-6, flp-7, flp-9, flr-2, fmo-4, fog-1, fog-3, fos-1, frm-10, frm-2, frm-7, frpr-6, fshr-1, ftt-2, gar-2, gbh-2, gei-1, gei-13, gei-3, ghi-1, gipc-1, glb-11, glb-15, glb-22, glb-24, glb-33, glc-2, glct-6, glna-1, glna-3, glrx-3, gmeb-1, gmeb-3, gnrr-5, gnrr-8, got-1.2, gpa-12, gpa-17, grh-1, grl-14, gska-3, gsp-3, gst-38, gst-9, gsto-3, gur-5, gyg-1, H04M03.12, H05L03.3, H06I04.5, H06I04.6, H08J11.2, H09F14.1, H10E21.1, H10E21.5, H12D21.5, H12I13.1, H14N18.4, H17B01.5, H24G06.1, H32K21.1, H35B03.1, H36N01.3, H36N01.5, H37A05.6, H38K22.6, H38K22.7, H40L08.1, H42K12.3, hacd-1, haly-1, hbl-1, hda-11, hda-4, hdl-1, hecw-1, his-71, hke-4.1, hlb-1, hlh-11, hlh-30, hpk-1, hpo-28, hpo-38, hpo-6, hsp-16.1, hsp-16.11, hsp-16.48, hsp-17, hsp-3, hsp-43, hsp-70, htas-1, ida-1, ifd-2, iff-2, ifp-1, igeg-1, igeg-2, ikb-1, ilys-4, ins-17, ins-20, ins-22, ins-24, ins-28, ins-30, ins-35, ins-37, ins-5, insc-1, inx-10, inx-4, inx-6, inx-7, irg-1, itx-1, jmjd-1.1, K01A12.4, K01A2.5, K01A6.8, K01H12.4, K02A2.5, K02B7.3, K02C4.5, K02E10.4, K02F2.5, K02F6.3, K03A1.4, K03C7.3, K03E5.2, K03H1.12, K03H1.16, K03H1.5, K04C2.7, K04H4.2, K04H4.5, K05F1.9, K06A1.2, K06A5.2, K06A5.3, K07A1.4, K07A1.5, K07A3.3, K07B1.8, K07C5.9, K07D4.9, K07E12.2, K07F5.20, K07H8.9, K08A2.2, K08B12.7, K08B5.1, K08C9.2, K08D8.12, K08D8.4, K08D8.6, K08D8.7, K08E4.3, K08F4.5, K08F8.1, K09B11.5, K09C6.9, K09D9.11, K09E4.4, K09F5.6, K09G1.2, K09H9.5, K09H9.8, K10B3.6, K10B4.3, K10C8.3, K10C9.7, K10D11.2, K10D11.5, K10D3.6, K10F12.8, K10G4.3, K10G9.2, K10H10.10, K11C4.1, K11D12.9, K11H12.3, K11H12.4, K11H12.8, K12C11.3, K12C11.5, kcnl-1, kcnl-3, kel-10, kel-8, kgb-1, kin-14, kin-20, kin-

24, kin-26, kin-29, kin-9, klc-2, klf-1, klf-3, kqt-2, kvs-5, lact-2, lact-4, lat-2, lbp-5, lbp-7, lea-1, lec-10, lec-11, lec-8, let-23, let-413, let-607, let-767, lgc-22, lgc-27, lgc-46, lim-6, lim-8, lin-1, lin-11, lin-14, lin-24, lin-33, lin-44, lin-66, lipl-5, lips-15, lit-1, lite-1, lmp-1, lntl-1, lpin-1, lpr-2, lpr-3, lpr-4, lron-2, lrp-1, lst-2, lys-2, lys-3, M01A8.2, M01B2.6, M01H9.4, M02B1.2, M02B1.4, M02E1.1, M02H5.8, M03A8.3, M03D4.3, M03E7.1, M04B2.6, M04C3.1, M04F3.4, M04G7.1, M04G7.2, M04G7.3, M05B5.2, M05B5.3, M05D6.3, M05D6.5, M117.1, M163.8, M176.4, M28.10, M28.4, M60.13, M60.2, M60.7, M60.9, M7.7, M70.1, M70.3, mab-21, mab-5, magu-2, mai-1, math-27, math-41, max-2, mbk-1, mbl-1, mboa-3, mboa-4, mca-1, mdl-1, mdt-15, mdt-28, mef-2, mev-1, mif-1, miz-1, mlk-1, mlt-11, mlt-8, mltn-1, mltn-9, mml-1, mnk-1, moc-2, mod-1, mod-5, mop-25.1, mps-3, mpst-4, mpz-3, mpz-4, mrp-2, msi-1, msp-64, myo-2, myo-5, nab-1, nac-1, nac-3, nas-31, nck-1, ncr-1, ncr-2, ncs-2, ncx-9, nekl-3, nep-11, nep-23, nep-26, nep-5, nep-6, nex-1, nex-2, nex-4, nhl-1, nhl-3, nhr-1, nhr-100, nhr-103, nhr-121, nhr-126, nhr-128, nhr-133, nhr-134, nhr-139, nhr-14, nhr-17, nhr-201, nhr-21, nhr-212, nhr-213, nhr-231, nhr-3, nhr-41, nhr-45, nhr-49, nhr-50, nhr-57, nhr-58, nhr-6, nhr-63, nhr-64, nhr-69, nhr-7, nhr-70, nhr-79, nhr-80, nhr-83, nhr-85, nhr-88, nhr-90, nhr-91, nhr-92, nhx-5, nipa-1, nipi-3, nlg-1, nlp-1, nlp-10, nlp-11, nlp-12, nlp-13, nlp-14, nlp-15, nlp-18, nlp-2, nlp-21, nlp-3, nlp-35, nlp-37, nlp-38, nlp-41, nlp-42, nlp-6, nlp-8, nlp-9, nmur-1, nmur-4, npax-2, npr-12, npr-23, npr-25, nspa-1, nspa-2, nspa-5, nspa-6, nspb-7, nspc-12, nspc-13, nspc-16, nspc-18, nspc-19, nspd-9, nsy-4, nucb-1, oac-14, oac-31, oac-46, obr-3, odr-10, oga-1, ogt-1, oig-3, oig-6, olrn-1, osm-11, osm-7, osm-8, pab-2, paf-2, pan-1, pck-2, pcp-4, PDB1.1, pde-6, pdf-1, pdfr-1, pef-1, pek-1, pept-2, pes-7, pgal-1, pghm-1, pgp-14, pgp-5, phat-6, phg-1, pho-4, pho-6, php-3, plc-2, plx-2, pme-4, pme-5, pmk-3, pmt-1, pnk-4, pod-2, pqm-1, pqn-13, pqn-18, pqn-25, pqn-31, pqn-35, pqn-44, pqn-48, pqn-53, pqn-73, pqn-89, pqn-92, pqn-94, prk-1, prl-1, prx-13, pry-1, psd-1, ptc-3, ptp-1, ptr-13, ptr-20, ptr-23, ptr-3, ptr-4, ptr-5, ptr-6, ptr-8, puf-9, pvf-1, pxl-1, pyp-1, R01B10.3, R01H10.4, R02D5.3, R02D5.7, R02F11.2, R03A10.5, R03D7.8, R03G5.6, R03H10.6, R04B5.11, R04D3.14, R04E5.9, R06C1.6, R06F6.7, R07E3.1, R07E3.7, R07E5.6, R07G3.12, R07G3.8, R07H5.9, R08B4.8, R08C7.12, R08C7.5, R08C7.8, R09A1.2, R09A1.5, R09A8.5, R09B5.11, R09D1.12, R09E10.1, R102.10, R102.5, R106.1, R106.5, R10D12.10, R10E4.7, R10E8.3, R10F2.6, R10H1.1, R11.2, R11A5.6, R11D1.3, R11F4.1, R12B2.12, R12B2.7, R12E2.13, R13A5.9, R13H4.13, R13H4.5, R13H7.2, R144.15, R148.7, R160.4, R166.6, rab-14, rab-6.2, ras-1, ras-2, rbf-1, rbg-1, rcn-1, rga-5, rgs-4, rhgf-2, rmd-4, rmd-6, rnh-1.1, rnt-1, rpl-25.1, rpl-37, rsd-3, saeg-1, sams-5, sbp-1, sbt-1, scd-1, scd-2, scl-22, scl-5, scrm-1, sdz-35, sea-2, secr-1, sek-1, sel-11, sem-4, ser-4, sfxn-1.2, sfxn-1.4, sgca-1, shn-1, sip-1, sipa-1, sir-2.3, skr-20, sli-1, sma-2, sma-4, sma-5, sma-9, smf-1, sms-3, snap-29, snb-1, snet-1, snf-11, snf-3, snf-5, snt-1, snt-4, snx-1, soc-2, somi-1, sox-3, sox-4, spc-1, spe-11, spe-15, spe-26, spe-4, spe-41, spe-8, spp-22, sptl-2, sqt-3, srj-14, srp-1, srp-6, srp-8, srr-4, srsx-3, srsx-34, srw-85, ssp-35, sss-2, sst-20, sta-1, sta-2, sue-1, sul-2, sulp-2, sulp-5, sup-12, svh-2, swt-6, sym-2, syx-2, T01B6.4, T01B7.8, T01C8.10, T01D3.6, T01E8.1, T01G1.2, T02B11.3, T02B11.4, T02B11.9, T02C12.5, T02D1.4, T02E1.6, T02G6.1, T03D8.6, T03F1.11, T03F6.6, T03G11.3, T04A11.1, T04A11.2, T04A6.3, T04B2.8, T04C12.3, T05A1.17, T05A1.5, T05A10.6, T05A7.6, T05A8.3, T05C1.1, T05C12.1, T05C12.15, T05D4.3, T05D4.5, T05E11.2, T05E7.4, T05F1.5, T06D8.1, T06E6.10, T07A9.9, T07C12.15, T07D1.2, T07F10.6, T08B1.4, T08B2.12, T08B6.4, T08B6.9, T08H10.3, T10B5.2, T10E9.4, T10E9.6, T10G3.1, T10H10.2, T11B7.2, T11B7.5, T11F8.4, T11F8.5, T12A7.2, T12B3.3, T12B3.9, T12G3.2, T14D7.1, T14G10.8, T14G11.1, T15B12.2, T15H9.4, T16A9.3, T16A9.5, T16A9.6, T16G12.7, T16H12.9, T17H7.7, T19A6.4, T19C4.5, T19C9.8, T19D12.4, T19D12.5, T19E7.25, T19E7.27, T20B12.11, T20B5.2, T20D4.11, T20D4.13, T20F5.4, T20F5.5, T21C12.3, T22B11.4, T22B3.2, T22B3.3, T22B7.3, T22C1.8, T22F3.11, T22F7.4, T22G5.1, T23B7.3, T23E1.6, T23F11.6, T23F2.2, T23F2.3, T23F2.4, T23F6.3, T23G11.7, T23G5.10, T24B8.4, T24B8.5, T24C4.4, T24F1.5, T25B2.2, T25B9.6, T25C12.5, T25C12.6, T25F10.3, T25G12.3, T26C12.1, T26C5.4, T26C5.5, T27A10.2, T27A10.6, T27A3.4, T27A3.5, T27C4.1, T27C5.8, T27E4.7, T27F6.8, T28A11.16, T28A11.19, T28A11.2, T28B11.1, T28B11.11, T28B11.22, T28B11.4, T28B4.4, T28B8.1, T28B8.6, T28C12.4, T28C6.8, T28F3.5, T28H10.2, T28H11.7, T28H11.8, tag-120, tag-191, tag-196, tag-209, tag-260, tag-299, tag-303, tag-304, tag-343, tag-344, tag-76, tat-2, tat-4, tax-6, tba-7, tbb-6, tbc-10, tbc-15, tbc-7, tbx-34, tep-1, tig-2, tir-1, tkr-1, tmbi-4, tmd-2, tni-4, toca-1, toe-4, tos-1, tpa-1, tps-1, tps-2, tre-3, trk-1, trpa-2, trpl-2, tsp-15, ttm-4, ttr-13, ttr-21, ttr-26, ttr-30, ttr-33, ttr-37, ttr-45, ttr-5, ttr-51, ttr-6, ttr-7, tts-2, tub-2, twk-1, twk-2, twk-33, ubc-1, ubc-16, ubc-23, ubc-3, ubxn-5, uggt-2, ugt-19, ugt-2, ugt-25, ugt-36, ugt-55, ugt-56, ulp-3, unc-108, unc-14, unc-23, unc-3, unc-43, unc-51, unc-53, unc-64, unc-75, unc-79, unc-82, unc-83, unc-94, unc-96, vab-19, vab-9, valv-1, vamp-8, VC5.2, vglu-2, vhp-1, vps-37, vps-4, W01B6.2, W01B6.4, W01B6.6, W01C8.5, W01C9.2, W01D2.3, W02B12.12, W02B12.13, W02D7.3, W02D9.10, W02H5.8, W03B1.5, W03B1.9, W03C9.1, W03C9.6, W03C9.8, W03D2.6, W03D8.1, W03D8.10, W03F11.4, W03G9.5, W04B5.3, W04D12.1,

W04E12.4, W05B5.1, W05E10.5, W05F2.4, W05F2.7, W05H12.1, W06D11.4, W06D4.2, W06F12.2, W06F12.3, W06H8.5, W06H8.6, W07A12.4, W07B8.4, W07G4.5, W07G4.8, W09D6.5, W09G12.7, W10D5.4, wht-8, wrt-2, wwp-1, xbp-1, xbx-5, Y102A11A.2, Y102A11A.9, Y105C5A.12, Y105C5A.15, Y105C5A.24, Y105C5B.11, Y105E8A.27, Y105E8A.36, Y106G6G.4, Y106G6H.13, Y111B2A.13, Y113G7C.1, Y116A8B.4, Y116A8C.23, Y116A8C.29, Y119C1B.6, Y12A6A.2, Y15E3A.4, Y17G7B.10, Y17G7B.17, Y18H1A.1, Y18H1A.10, Y18H1A.11, Y18H1A.15, Y1A5A.1, Y20F4.4, Y22D7AR.6, Y23B4A.2, Y23H5A.4, Y32G9A.5, Y34B4A.10, Y34F4.5, Y37A1A.2, Y37D8A.5, Y37D8A.6, Y37D8A.8, Y37E11AL.4, Y37E3.19, Y37F4.1, Y37F4.5, Y37H2A.14, Y38C1AA.6, Y38E10A.17, Y38F1A.1, Y38F1A.8, Y38H8A.4, Y39B6A.24, Y39B6A.25, Y39G10AR.16, Y41C4A.13, Y41D4A.7, Y41D4B.15, Y41D4B.17, Y42G9A.2, Y42H9AR.1, Y43C5A.4, Y43E12A.2, Y43E12A.6, Y43F4A.6, Y43F8A.1, Y43F8A.2, Y43F8B.12, Y43F8B.23, Y43F8B.24, Y43F8C.3, Y43F8C.5, Y43F8C.9, Y44A6D.3, Y44E3A.1, Y44E3A.4, Y45F10B.3, Y45F3A.4, Y45G5AM.3, Y45G5AM.6, Y46D2A.1, Y46D2A.2, Y46D2A.5, Y46G5A.22, Y46H3C.4, Y47D3A.13, Y47D9A.1, Y47G6A.13, Y47G6A.26, Y47G6A.5, Y48A6B.7, Y48B6A.5, Y48B6A.6, Y48C3A.5, Y48G1BM.9, Y48G1BR.1, Y48G1C.5, Y48G9A.9, Y49E10.10, Y49F6B.8, Y4C6B.3, Y4C6B.4, Y50D4B.1, Y50E8A.1, Y51A2B.5, Y51H4A.25, Y51H4A.935, Y52B11A.4, Y52D5A.2, Y53C10A.10, Y53C10A.5, Y53F4B.19, Y53F4B.51, Y53G8AM.8, Y53G8B.2, Y53H1B.2, Y53H1C.3, Y54E5A.2, Y54E5A.8, Y54F10AM.6, Y54F10BM.3, Y54G2A.11, Y54G2A.13, Y54G2A.15, Y54G2A.32, Y55B1AL.1, Y55B1BL.1, Y55B1BR.5, Y55F3AM.10, Y55F3BL.4, Y55F3BR.11, Y55F3BR.2, Y56A3A.6, Y57A10A.26, Y57A10B.1, Y57A10B.2, Y57E12B.10, Y57G11A.2, Y57G11C.1135, Y57G11C.23, Y57G11C.36, Y57G11C.5, Y57G11C.6, Y57G7A.6, Y58A7A.4, Y58A7A.5, Y58A7A.7, Y59C2A.1, Y59E9AL.6, Y60A3A.8, Y62F5A.10, Y64G10A.6, Y64G10A.7, Y65B4A.2, Y66A7A.7, Y66D12A.11, Y66D12A.24, Y67A10A.3, Y67A6A.1, Y67D8B.4, Y67D8B.5, Y69A2AR.14, Y69A2AR.23, Y69A2AR.32, Y69A2AR.9, Y69E1A.3, Y69H2.3, Y6E2A.10, Y6E2A.8, Y70G10A.3, Y71A12C.2, Y71F9B.13, Y71G12B.2, Y71G12B.25, Y71G12B.27, Y71G12B.32, Y71G12B.33, Y71G12B.37, Y71H2AM.13, Y71H2AM.14, Y71H2AM.25, Y73B6A.1, Y73B6BL.27, Y73B6BL.31, Y73B6BL.35, Y73B6BL.44, Y73F4A.2, Y73F8A.14, Y73F8A.35, Y75B8A.28, Y76A2B.5, Y76A2B.7, Y81G3A.1, Y82E9BR.23, Y8A9A.2, Y92H12A.2, Y94H6A.10, Y95B8A.4, Y97E10C.1, Y9C2UA.1, zag-1, ZC155.8, ZC168.2, ZC239.14, ZC239.6, ZC247.1, ZC328.2, ZC328.3, ZC412.13, ZC416.6, ZC443.4, ZC449.3, ZC455.1, ZC487.6, ZC513.3, ZC581.2, ZC581.3, ZC581.7, zer-1, zig-4, zig-5, zig-7, zip-1, zip-10, zip-5, ZK1010.5, ZK1010.8, ZK1037.6, ZK1053.2, ZK1055.6, ZK1055.7, ZK1073.1, ZK1086.5, ZK112.3, ZK1128.3, ZK121.2, ZK1225.4, ZK1290.13, ZK1290.14, ZK1307.2, ZK131.11, ZK154.6, ZK337.2, ZK353.4, ZK354.6, ZK354.7, ZK354.8, ZK355.2, ZK418.7, ZK470.2, ZK470.4, ZK484.1, ZK484.7, ZK546.4, ZK550.5, ZK593.2, ZK596.1, ZK616.61, ZK622.5, ZK632.10, ZK662.2, ZK669.3, ZK673.2, ZK675.7, ZK686.5, ZK688.10, ZK795.1, ZK795.2, ZK809.1, ZK822.1, ZK822.2, ZK822.8, ZK849.1, ZK856.18, ZK858.2, ZK892.5, ZK896.1, ZK896.4, ZK896.5, ZK909.3, ZK930.2, ZK930.7, ZK938.1, ZK945.6, ztf-12, ztf-14, ztf-16, ztf-2, ztf-22, ztf-7
Tunicamycin (766)
aat-3, aat-8, acs-22, acs-3, acs-7, aly-1, arr-1, arrd-1, arrd-2, atg-11, atg-16.2, atg-4.2, B0222.3, B0228.6, B0273.112, B0281.5, B0284.3, B0303.14, B0310.2, B0563.1, B0563.8, bath-10, bath-26, bath-9, BE10.3, bed-2, bre-1, btb-11, btb-6, btb-8, bus-18, C01A2.1, C01A2.5, C01B12.9, C01C10.2, C01F6.14, C01G6.3, C02C6.7, C03A3.1, C03C10.9, C03H5.9, C04C11.9, C04H4.2, C05B5.4, C05B5.5, C05C12.4, C05D12.5, C05D9.7, C05E11.3, C05G5.5, C06A6.11, C06E1.1, C06G3.6, C07D10.5, C08D8.1, C08F1.10, C08F1.11, C08F1.6, C08F11.3, C08G5.1, C11E4.8, C13C4.6, C14F11.28, C14F11.6, C14F5.9, C17E4.11, C17E4.2, C17E4.20, C17G10.11, C18D4.8, C24G6.10, C24H11.11, C24H12.1, C24H12.7, C25F6.22, C26B9.6, C27A7.8, C27B7.9, C28G1.4, C28G1.6, C29F7.2, C29F9.5, C32A9.5, C32B5.15, C32D5.8, C33E10.1, C33G3.4, C34E7.4, C35B8.3, C35E7.5, C35E7.6, C35E7.7, C36B1.6, C37A5.3, C38C6.7, C38C6.8, C38D9.8, C39B5.2, C39F7.8, C40A11.10, C40A11.2, C40A11.3, C40A11.6, C40H1.12, C41G11.1, C41G11.14, C41G7.13, C42D4.1, C43H6.4, C44E12.1, C45G7.4, C47D12.4, C47G2.14, C48B4.1, C48D1.1, C49F5.7, C52E2.2, C52E2.4, C52E2.5, C54D10.19, cav-1, ccch-5, cdc-25.2, cdh-4, cec-1, cec-8, ced-11, ced-8, ceeh-2, ceh-16, ceh-26, ceh-36, ceh-40, ceh-43, ceh-45, ceh-86, ces-1, ces-2, cfz-2, chd-3, cht-1, ckb-4, clec-121, clec-196, clec-218, clec-222, clec-266, clec-82, cnc-4, cnd-1, col-116, cpr-1, cpt-6, crb-1, ctbp-1, cutl-13, cutl-2, cutl-25, cutl-29, cutl-9, cwn-2, cyd-1, cyp-34A10, cyp-34A9, cyp-35B1, D1044.2, D1054.18, D1081.16, D1086.5, D2007.1, D2045.9, dct-13, ddr-2, dhs-2, dhs-31, die-1, dmd-5, dnj-27, dnj-7, dod-3, dpy-14, dpy-17, dsc-4, dsl-1, dsl-2, dsl-3, E02H9.6, eat-2, ech-9, EEED8.15, EEED8.2, EEED8.4, efl-3, efn-4, egl-1, elt-1, end-1, epg-2, ets-7, eya-1, F07B7.15, F07C3.11, F07H5.13, F08A7.1, F08C6.5, F08G2.7, F08G5.19, F09B9.5, F09F9.1, F10E7.1, F11E6.11, F12A10.1, F13C5.2, F13H8.11, F14B6.3, F14F8.8, F14H3.14,

F15B10.3, F15E6.3, F16B4.7, F16G10.11, F16G10.15, F17B5.1, F17E5.5, F17E9.2, F19F10.1, F21C10.11, F21D5.9, F21F8.2, F21H12.3, F22B8.7, F22D6.8, F23D12.4, F27C1.16, F27C1.2, F27E11.1, F28C6.1, F28D1.2, F31D5.6, F31E8.4, F31E9.6, F32B4.5, F32D8.13, F32H2.6, F33E2.5, F33H2.3, F34D6.1, F34H10.5, F35D2.3, F35E8.13, F35G2.3, F35G2.9, F36G9.15, F36G9.18, F36G9.7, F36H1.15, F36H5.13, F36H5.4, F36H5.8, F37B4.10, F37C12.10, F38B7.13, F39B2.7, F40E3.7, F40F8.13, F40G9.15, F40G9.6, F40G9.9, F42A10.12, F42C5.4, F43G6.5, F43G6.8, F43H9.4, F44F1.4, F44F1.6, F45D11.5, F45D3.15, F45E1.5, F46C8.3, F46E10.2, F47B10.9, F47C12.1, F47C8.8, F47E1.4, F48E3.6, F48F7.6, F48G7.2, F49H6.5, F52D4.1, F52E1.9, F52E10.2, F53A2.3, F53B3.5, F53F10.6, F53F8.7, F53G2.1, F54C8.7, F54D5.5, F55C12.6, F55C9.14, F55C9.5, F55G7.2, F55H2.8, F56A8.8, F56D5.5, F56F4.8, F57G9.3, F58F12.5, F58F9.7, F58H1.10, F58H1.11, F58H1.16, F58H1.5, F59C6.11, F59C6.16, fbxa-127, fbxa-128, fbxa-143, fbxa-154, fbxa-157, fbxa-29, fbxa-54, fbxa-6, fbxa-69, fbxa-92, fbxb-1, fbxb-103, fbxb-105, fbxb-106, fbxb-107, fbxb-108, fbxb-11, fbxb-112, fbxb-116, fbxb-119, fbxb-13, fbxb-15, fbxb-17, fbxb-18, fbxb-19, fbxb-20, fbxb-22, fbxb-24, fbxb-3, fbxb-35, fbxb-37, fbxb-38, fbxb-40, fbxb-41, fbxb-42, fbxb-43, fbxb-44, fbxb-45, fbxb-46, fbxb-47, fbxb-49, fbxb-51, fbxb-54, fbxb-59, fbxb-65, fbxb-66, fbxb-69, fbxb-75, fbxb-8, fbxb-82, fbxb-84, fbxb-88, fbxb-9, fbxb-90, fbxb-91, fbxb-92, fbxb-96, fbxc-12, fbxc-18, fbxc-21, fbxc-24, fbxc-25, fbxc-28, fbxc-29, fbxc-34, fbxc-36, fbxc-39, fbxc-51, fil-1, fipr-22, fipr-24, fipr-26, fkb-7, fkh-2, flh-2, flh-3, fmo-1, fox-1, frpr-11, gadr-2, gadr-3, gadr-4, gadr-5, gcl-1, ger-1, glb-16, glit-1, gst-20, H01M10.1, H08J11.12, H24K24.2, H29C22.1, H37A05.4, ham-1, hch-1, hid-1, hil-2, hil-7, his-13, his-19, his-20, his-22, his-24, his-28, his-37, his-39, his-4, his-47, his-5, his-50, his-51, his-55, his-57, his-59, his-6, his-61, his-64, his-8, hlh-1, hlh-14, hlh-3, hmg-1.2, hnd-1, hpo-15, hrg-3, hsp-12.6, hsp-4, igcm-4, igdb-3, ins-2, ins-23, ins-34, inx-2, inx-3, irx-1, jmjc-1, jmjd-3.1, jmjd-3.2, K02A11.4, K02B12.2, K02D10.4, K02E7.7, K03A11.1, K03C7.10, K03H4.6, K04B12.2, K04C1.3, K05C4.9, K06A4.11, K06A4.7, K06C4.23, K07A1.6, K07C11.4, K07E3.2, K08A8.17, K08B4.2, K08B5.2, K08F9.1, K08H10.15, K08H2.2, K09C4.12, K09C8.7, K09E9.1, K10D6.17, K10D6.18, K10D6.22, K10D6.24, K10G6.9, K10H10.14, K11H3.5, K12C11.6, K12G11.12, K12G11.8, K12H6.7, kal-1, kin-33, ksr-1, lam-3, lbp-1, lin-12, lin-32, lipl-2, lron-11, M03B6.4, M05B5.4, M116.1, M117.11, M117.6, M199.2, M79.2, mab-20, madf-10, math-37, mls-2, mltn-8, mtl-1, nac-2, nas-9, ncs-7, ndx-6, nep-1, ngn-1, nhr-152, nhr-163, nhr-2, nhr-67, nlr-1, nrde-3, old-1, pax-3, pes-10, pes-2.1, pqn-75, prx-6, R02C2.1, R02C2.6, R03G8.3, R03H10.1, R04A9.7, R05G6.10, R09D1.11, R09F10.3, R09H10.2, R107.2, R10E12.2, R10E9.3, R11.4, R11A5.3, R11G1.7, R12E2.2, R13A5.16, R148.5, ref-1, ref-2, rig-1, rig-3, rpr-1, scl-2, sdc-2, sdn-1, sdz-14, sdz-16, sdz-2, sdz-20, sdz-21, sdz-25, sdz-26, sdz-28, sdz-30, sdz-31, sdz-33, sdz-4, sdz-9, sem-2, sepa-1, set-10, sex-1, skr-10, skr-12, skr-13, skr-15, skr-7, skr-9, smf-3, spp-2, sptf-1, srj-9, stdh-1, str-103, swan-1, swt-7, T01G9.2, T02E9.21, T02G5.14, T02G6.5, T02H6.5, T03E6.13, T03E6.8, T04B8.2, T04C12.8, T04D1.2, T04D3.5, T04D3.8, T04G9.7, T05D4.2, T05E11.3, T05E11.9, T05E12.3, T05H10.4, T06D8.9, T08G5.1, T09B4.5, T10B10.13, T11B7.1, T14G8.3, T15B7.10, T16G12.4, T19H5.6, T22B2.1, T22B7.14, T22B7.4, T22C1.11, T22D1.17, T23C6.4, T23F11.1, T23F4.3, T24B8.3, T24C4.2, T25E12.6, T26C12.3, T26H5.4, T27A1.2, T27C5.10, T28A11.22, T28C6.3, tag-276, tag-52, tbx-11, tbx-2, tbx-38, tbx-43, tbx-8, tcl-2, thn-2, trim-9, ttm-2, ttr-50, ttr-52, ugt-31, ugt-54, unc-130, unc-39, utx-1, vab-15, vab-23, vang-1, vet-1, vet-2, vet-6, W01B11.6, W02C12.1, W02D7.11, W02D7.5, W02D7.8, W03F11.1, W03F9.4, W03G11.12, W04A8.5, W04G3.15, W07E11.6, W08A12.4, W09C2.7, W10G11.2, wee-1.1, Y105C5B.5, Y105E8A.38, Y106G6D.1, Y106G6H.9, Y108F1.5, Y110A2AL.10, Y110A7A.4, Y110A7A.7, Y113G7B.11, Y116A8C.1, Y116A8C.20, Y116F11A.1, Y11D7A.19, Y17G9A.4, Y17G9B.1, Y17G9B.2, Y18D10A.4, Y25C1A.6, Y32F6A.4, Y32G9A.10, Y34F4.3, Y38F1A.2, Y39B6A.81, Y39G10AL.1, Y41D4A.3, Y41D4B.26, Y43B11AL.1, Y43F11A.1, Y43F8B.17, Y44A6C.2, Y45F10C.2, Y45F10D.6, Y45G5AM.5, Y46G5A.7, Y46H3A.5, Y47D3B.1, Y48D7A.1, Y49A10A.2, Y49F6B.6, Y4C6B.2, Y51A2D.15, Y51H4A.1, Y51H4A.13, Y51H4A.5, Y52B11B.1, Y53F4B.17, Y53F4B.43, Y53G8AR.9, Y54E10A.27, Y54G2A.27, Y54G2A.52, Y55B1BR.6, Y57A10A.23, Y57A10C.1, Y57G11B.2, Y57G11C.1134, Y5H2B.3, Y62F5A.9, Y62H9A.3, Y65A5A.1, Y66D12A.13, Y68A4A.13, Y6E2A.4, Y6G8.2, Y71A12B.11, Y71A12B.2, Y71F9AL.6, Y71F9AL.7, Y73B6BL.36, Y73C8C.3, Y73F8A.1170, Y7A9D.1, Y82E9BL.3, Y82E9BR.1, Y82E9BR.17, ZC204.12, ZC239.21, ZC410.5, zeel-1, zip-7, zip-8, ZK1053.4, ZK1098.3, ZK131.14, ZK180.12, ZK218.5, ZK355.8, ZK430.5, ZK525.8, ZK550.6, ZK666.4, ZK688.11, ZK899.6, ztf-11, ztf-29, ztf-30, ztf-6

Common (492)

aakg-4, acl-14, acs-17, ain-1, akt-2, alr-1, aqp-2, arf-1.1, arrd-4, ast-1, atf-2, B0350.71, B0507.10, B0507.8, B0563.7, bath-47, C02F5.7, C05A9.10, C05A9.2, C05D9.9, C05E11.10, C06B3.6, C06B8.2, C06G3.5, C07E3.9, C08F11.13, C09F9.2, C10A4.13, C10C5.2, C11G10.1, C14B9.11,

C14B9.2, C14F11.2, C15B12.1, C16H3.3, C18A11.1, C18E9.9, C23H4.6, C25D7.5, C26E1.2, C28G1.2, C29F9.3, C29F9.4, C30F12.3, C30G4.4, C30G4.7, C31C9.2, C31H5.4, C32F10.4, C33D9.13, C34B7.1, C34C12.4, C34C6.7, C34D10.2, C34D10.4, C35C5.9, C36B7.8, C37E2.7, C38C3.4, C38H2.2, C39D10.11, C41G7.8, C44B7.6, C44C1.6, C44H4.10, C44H9.5, C49G7.10, C49H3.12, C50F4.1, C50F7.5, C51E3.10, C53B7.3, C54G10.4, cal-2, cdf-2, cdr-4, ceh-13, ceh-20, ceh-22, ceh-27, ceh-32, ceh-37, cex-1, cex-2, ckb-2, cki-1, clec-264, clec-66, clec-7, clec-83, coel-1, col-89, cpr-3, cpt-1, cpt-3, cpt-4, crt-1, ctl-1, ctl-2, ctl-3, cutl-16, cyp-14A5, cyp-32A1, cyp-32B1, cyp-33C8, cyp-34A4, cyp-37B1, D2021.4, D2030.2, dao-2, dcar-1, dct-1, dct-3, dgn-1, dhhc-1, dhs-18, dlg-1, dma-1, dod-22, dos-1, dpy-18, dpy-3, dve-1, ech-3, ech-8, egl-15, egl-27, egl-46, elt-7, ets-9, exc-9, F07C3.9, F07F6.8, F08B12.4, F08G2.4, F09E5.14, F09F7.5, F09F7.6, F09F7.7, F10D7.3, F12D9.12, F13C5.1, F13D11.3, F13E6.1, F13E6.4, F13E9.11, F13H10.6, F13H6.5, F14F9.4, F14H3.12, F16B4.2, F16C3.2, F17C11.4, F17E9.4, F18C5.10, F18G5.6, F18H3.4, F20C5.6, F21A10.2, F21A3.11, F21A9.2, F21C10.10, F22E5.6, F25B4.2, F25E2.3, F26D11.12, F26F12.19, F26F12.3, F27E5.9, F28H1.1, F28H7.6, F31E3.8, F31F7.1, F32D1.3, F34H10.3, F35B12.10, F36F2.2, F37A8.5, F37D6.4, F38A5.7, F38E9.1, F40F12.7, F41B4.3, F41C3.8, F42G2.2, F42G2.5, F43C11.7, F43G6.4, F43H9.5, F45D3.4, F45E10.2, F47B8.2, F47B8.4, F47D12.6, F48G7.10, F49H12.7, F52H3.5, F53A2.9, F53A9.1, F53A9.6, F53A9.7, F53A9.8, F53B2.8, F53E10.1, F54B8.4, F54F3.4, F56D2.5, F56D5.6, F56F3.7, F57A8.1, F59B10.5, faah-2, far-7, fbn-1, fbxa-208, fbxa-26, fbxa-48, fbxa-59, fbxa-60, fbxa-82, fbxa-98, fis-2, fkh-7, fkh-9, flp-10, fmo-2, fozi-1, gba-1, gem-4, glc-1, glt-5, gst-22, H19N07.3, H32K16.2, ham-2, hil-1, hil-3, hmg-11, icl-1, igcm-1, igcm-3, irg-2, ist-1, jmjd-3.3, K01A2.10, K01F9.2, K02A11.3, K02D7.1, K02G10.1, K03A11.5, K03E6.7, K03H1.10, K05B2.4, K06A9.2, K10C9.3, K10D3.4, K10D6.2, K10D6.4, K12C11.7, K12H6.6, kgb-2, klp-11, kpc-1, lact-5, ldb-1, let-4, lgg-1, lgg-2, lipl-3, ltd-1, M01A8.1, M01G12.9, M01H9.3, M03A1.8, M03D4.4, M04D5.3, M162.5, M163.1, M163.16, M60.4, M7.8, maa-1, mab-31, maea-1, mak-2, math-24, mboa-1, mec-8, mfb-1, mif-4, mig-10, mig-13, mnp-1, moe-3, nape-1, ncam-1, nfm-1, nhr-119, nhr-120, nhr-122, nhr-170, nhr-18, nhr-180, nhr-19, nhr-202, nhr-203, nhr-25, nhr-32, nhr-35, nhr-8, nlp-28, nlp-29, nlp-34, nnt-1, noah-1, noah-2, nob-1, npr-20, npr-28, pbo-4, peb-1, pes-4, pha-4, ptr-22, pxd-1, R02D5.1, R03H10.2, R03H10.7, R05H10.1, R09E10.13, R10E11.12, R10E8.8, R12B2.6, R160.10, rhi-1, rrf-2, sax-1, scrm-3, sfrp-1, shc-2, siah-1, sid-2, skr-19, skr-21, skr-3, skr-5, sma-1, snb-2, sod-4, sodh-1, sox-2, spp-15, spp-8, srg-34, srh-2, srp-7, srr-6, sto-1, sup-26, swan-2, swt-1, syd-9, sym-1, T01B10.5, T01D3.3, T02C5.1, T02E9.5, T03F1.6, T04A6.1, T04C12.11, T04C12.7, T04F8.7, T05F1.11, T07G12.5, T09B9.2, T09F5.12, T10C6.15, T10H9.8, T12A7.6, T12D8.5, T12G3.1, T13C5.6, T16G1.4, T18D3.7, T19C3.4, T19E7.6, T19H5.4, T20B3.1, T21F2.2, T21H8.9, T23B3.2, T23E7.6, T23F4.2, T24E12.5, T24F1.3, T25D10.4, T26H5.9, T28B11.17, T28F4.1, T28F4.4, T28F4.5, T28H10.3, tag-234, tag-243, tag-244, tag-253, tag-320, tbc-14, tli-1, tlp-1, tpra-1, tre-5, trx-3, tsp-1, tsp-17, tsp-2, tsp-3, tth-1, ttr-17, ttr-23, ttr-29, tts-1, twk-7, tyr-1, ubc-8, ugt-18, ugt-4, ugt-57, unc-120, unc-129, unc-5, unc-6, vab-2, vab-3, W01F3.2, W02A2.9, W03G11.4, W04A8.4, W05H9.1, W08A12.2, wht-1, wrt-10, Y105E8B.7, Y110A2AL.3, Y110A2AL.9, Y15E3A.5, Y17G7B.8, Y22D7AL.15, Y34F4.4, Y37D8A.16, Y39B6A.5, Y39G10AR.11, Y39H10A.6, Y41C4A.11, Y42G9A.1, Y43B11AR.3, Y43C5A.3, Y43F8B.9, Y44A6C.1, Y46E12BR.1, Y46G5A.20, Y47H10A.5, Y48G8AL.13, Y51A2D.13, Y51B9A.9, Y53F4B.45, Y54G2A.18, Y54G2A.36, Y55D5A.1, Y58A7A.3, Y65B4BL.1, Y69A2AL.2, Y69A2AR.7, Y73C8B.1, Y75B8A.6, Y77E11A.14, Y82E9BR.21, Y95B8A.6, Y97E10AR.1, ZC190.4, ZC239.22, ZC395.5, ZC443.3, zip-2, ZK1128.7, ZK6.8, ZK682.9, ZK836.3, ZK863.8, ZK899.1, ztf-13, ztf-19

DOWNREGULATED GENES (Fold change > 1.5, ANOVA p-value < 0.05)
***pmt-2(RNAi)* (1325)**
aagr-1, aagr-2, aars-1, aat-1, aat-7, abt-6, acd-2, acdh-1, acdh-13, acdh-3, acdh-9, acl-3, act-2, adm-4, agt-2, aho-3, alkb-8, aly-3, aman-2, amt-1, amx-3, aos-1, apc-10, apc-2, aph-2, app-1, aps-3, aqp-9, ard-1, asb-1, asg-1, asp-1, asp-2, aspm-1, atad-3, atl-1, atx-3, B0001.2, B0001.7, B0024.11, B0035.13, B0041.8, B0205.1, B0207.6, B0212.3, B0238.11, B0261.7, B0261.8, B0285.4, B0334.15, B0334.4, B0334.5, B0336.5, B0361.6, B0454.5, B0491.1, B0491.7, B0511.13, bath-19, best-19, bre-5, btf-1, bub-1, C01A2.3, C01B12.8, C01B12.9, C01B7.10, C01G10.10, C01H6.9, C03H5.3, C04C3.9, C04E6.11, C04F5.9, C04H5.1, C05C10.2, C05C10.3, C05C8.2, C05D11.9, C05D12.4, C06A5.1, C06A5.3, C06A5.6, C06A6.14, C06A8.2, C06E2.14, C06E4.1, C06H2.7, C07A9.2, C07C7.1, C07D8.6, C08A9.6, C08B11.9, C08F11.11, C08F11.12, C08F8.9, C08G5.9, C08H9.14, C09E7.8, C10A4.12, C10C6.12, C10E2.1, C10G11.17, C11D2.4, C13B9.5, C13F10.2, C13G5.2, C14B1.12, C14B1.2, C14B1.9, C14B9.10, C14C10.9, C14F11.31, C15F1.13,

C15H11.8, C16A11.5, C16A3.2, C16B8.9, C16C8.13, C16C8.16, C16C8.21, C16H3.6, C17A2.4, C17E7.12, C17G1.2, C17G10.1, C17G10.2, C18A3.3, C18D11.3, C18E9.4, C23G10.2, C23G10.7, C23H3.5, C24B5.4, C24B9.3, C24D10.5, C25A11.10, C25F9.17, C25H3.11, C25H3.3, C25H3.4, C26B2.7, C26E6.12, C26F1.3, C26G2.9, C27A7.6, C27B7.5, C28A5.2, C29A12.1, C29E4.12, C29E4.13, C29G2.1, C30F12.2, C31H2.4, C31H5.8, C32C4.11, C32D5.10, C32D5.6, C32E8.5, C34D1.9, C34D4.10, C34D4.13, C34E10.10, C35A5.8, C35B1.2, C35C5.14, C35D10.10, C35E7.3, C36B1.14, C37C3.1, C38D4.4, C39B5.6, C40H1.2, C41D11.9, C41G7.3, C42C1.12, C42C1.8, C42D8.15, C43E11.9, C44B7.12, C44B7.21, C45G9.5, C46A5.5, C46E10.8, C46G7.2, C47B2.2, C47E8.4, C47F8.1, C47F8.10, C47F8.9, C48B4.10, C48B4.11, C48B4.9, C48B6.2, C48G7.4, C49C3.6, C49F5.3, C49H3.3, C50B6.7, C50C3.1, C50E3.12, C50E3.13, C50F2.3, C50F2.4, C50F4.4, C51E3.12, C51E3.6, C52D10.1, C52E4.5, C53A5.16, C53B4.3, C53B7.10, C53D6.4, C53H9.3, C55B7.11, C56C10.10, C56E6.2, C56E6.9, calu-1, catp-6, CD4.10, cdc-7, cdd-2, cec-9, ced-9, ceh-10, ceh-49, ceh-7, ceh-74, ceh-99, cep-1, cey-3, chch-3, chhy-1, chin-1, chp-1, cids-1, clec-169, clec-190, clec-218, clec-46, clec-5, clec-52, clec-53, clec-8, clec-86, clec-97, cln-3.3, clu-1, cnc-8, cogc-2, col-108, col-123, col-135, col-158, col-171, col-43, coq-5, coq-8, cosa-1, cpf-1, cpi-1, cpsf-2, cri-3, crn-1, crn-6, csn-3, cuc-1, cux-7, cyb-2.1, cyb-2.2, cyn-1, cyn-15, cyn-16, cyp-14A2, cyp-31A2, cyp-31A3, cyp-33C2, cyp-44A1, D1007.4, D1025.10, D1046.2, D1054.14, D1081.7, D2030.1, D2030.3, D2030.4, D2030.8, dap-3, dars-2, dct-18, ddl-3, ddp-1, dhod-1, dhs-20, dis-3, DL2.1, dnc-6, dnj-11, dnj-2, dnj-21, dnj-22, dnj-3, dnj-8, dod-23, dod-24, dpf-7, dpm-1, duo-1, duo-3, E01A2.1, E01A2.2, E01G6.3, E02H1.2, E02H4.7, E02H9.1, E02H9.7, eat-3, eea-1, EEED8.13, eef-1B.2, egg-5, egl-6, ego-1, ehbp-1, eif-1.A, eif-3.C, eif-3.E, eif-3.H, ent-7, epi-1, erfa-3, eri-7, eri-9, etf-1, evl-14, evl-20, exo-3, exos-2, exos-3, exos-4.1, exos-4.2, F01E11.3, F01F1.11, F01F1.2, F02A9.4, F02E9.9, F02H6.2, F02H6.4, F07A11.9, F07G11.2, F08B6.1, F08D12.2, F09D5.3, F09E5.8, F09F7.4, F10B5.8, F10C2.5, F10C5.2, F10D11.2, F10E7.6, F10E9.11, F10E9.4, F10E9.5, F11A10.5, F11A3.2, F12A10.8, F12D9.5, F12E12.6, F13A2.4, F13D12.5, F13E9.1, F13H8.15, F14B4.3, F14D2.17, F14D2.8, F14D7.2, F14H3.3, F14H3.4, F14H8.10, F15A8.13, F15E11.1, F15E11.12, F15E11.13, F16A11.2, F16D3.4, F17A9.2, F17E5.2, F18A11.10, F19B10.10, F19B10.2, F19C6.5, F19C7.4, F19F10.9, F20A1.9, F21D5.1, F21D5.6, F21F3.4, F21F8.4, F21H12.1, F21H12.6, F21H12.8, F22A3.9, F22B3.4, F22B5.10, F22D3.5, F22E5.8, F22F1.8, F22G12.9, F23A7.4, F23A7.8, F23C11.2, F23F1.10, F25B3.6, F25B4.14, F25B4.4, F25D7.4, F25E2.2, F25G6.8, F25G6.9, F25H2.7, F25H8.2, F26F12.14, F26G1.11, F26H11.9, F27B3.5, F27B3.7, F27D4.4, F27D4.7, F27E5.1, F28B3.5, F28F5.17, F28F8.9, F28G4.2, F30A10.13, F30B5.4, F30F8.9, F30H5.8, F31B9.3, F31C3.14, F31C3.2, F31C3.4, F32A6.13, F32B6.3, F32H2.10, F33D11.10, F33D11.12, F33G12.3, F34D10.2, F34D10.3, F35E12.5, F35G12.11, F35H10.6, F36A2.9, F36D1.15, F36H5.12, F37A4.2, F37C12.3, F37C4.6, F39B1.4, F39G3.2, F39H11.1, F39H2.3, F40A3.6, F40F9.16, F40G9.2, F41C6.11, F41C6.4, F41E7.6, F41G4.11, F42A10.3, F42A10.5, F42A8.3, F42A9.6, F42D1.6, F42F12.4, F42G8.10, F43D2.10, F43G9.4, F43H9.3, F44B9.8, F44E2.7, F44E2.9, F44E5.14, F44E7.9, F44G4.3, F45D3.10, F46C5.10, F46C5.9, F46F11.10, F47G3.3, F48C1.13, F48C1.5, F48E8.2, F49C12.7, F49C5.13, F49E12.1, F49E2.1, F49E8.2, F52A8.5, F52B10.17, F52B11.1, F52B5.2, F52B5.3, F52B5.7, F52D10.9, F53B7.12, F53B7.3, F53E10.6, F53F4.16, F53F8.3, F54B3.1, F54C9.17, F54D11.3, F54D5.2, F54D7.9, F54E4.5, F54E7.8, F54F2.9, F54F7.6, F54H12.5, F55A11.4, F55B11.3, F55C12.2, F55F10.1, F55F8.3, F55F8.9, F55G1.20, F55G1.5, F55G1.9, F55G7.4, F56A12.5, F56A8.9, F56C9.6, F56D1.1, F56D1.2, F56F4.11, F56G4.4, F57B1.6, F57B10.14, F57B10.4, F57C2.5, F57C9.1, F58A4.9, F58B6.1, F58G11.11, F58H1.8, F59A6.12, F59A6.5, F59B2.9, F59D12.12, F59E12.9, fan-1, fars-1, fbxa-190, fbxa-200, fbxa-206, fbxa-210, fbxa-211, fbxa-215, fbxa-216, fbxb-67, fbxb-7, fbxc-37, fbxc-42, fbxc-45, fbxc-50, fib-1, fipr-13, flap-1, fog-2, gei-12, gei-14, gfl-1, glrx-21, glrx-22, gly-10, gnrr-3, gop-2, got-1.3, gpr-1, grsp-2, gss-1, gst-16, gst-37, gst-42, gstk-1, H02I12.5, H06H21.11, H06H21.8, H06I04.3, H11L12.1, H19M22.10, H22K11.2, H24K24.4, H25K10.2, H34C03.2, haf-6, har-2, hcp-3, hda-2, him-14, him-8, hpl-2, hpo-17, hpo-18, hpo-31, hpo-40, hpo-9, hpr-17, hpr-9, hrpf-1, hsd-2, hsp-60, hus-1, iars-2, icln-1, idi-1, ife-3, iff-1, imb-2, inx-14, JC8.5, K01D12.6, K01G12.3, K02B2.1, K02C4.3, K02E2.14, K02E2.15, K02E7.6, K03C7.5, K04C1.4, K04C1.5, K04G7.1, K05C4.7, K06B4.4, K06B9.4, K07A1.1, K07A1.10, K07A1.15, K07A1.17, K07C5.6, K07F5.12, K07F5.14, K07G5.6, K07H8.1, K07H8.10, K07H8.3, K08A2.1, K08C9.10, K08D10.14, K08F9.4, K08H10.9, K09A11.10, K09A9.8, K09C4.1, K09F6.5, K10C2.14, K10C8.5, K11B4.2, K11D12.13, K11E4.9, K11H3.4, K11H3.8, K12B6.11, K12D12.5, kat-1, kbp-3, klc-1, klo-2, klp-15, klp-19, knl-3, laf-1, lam-1, lbp-4, let-268, let-716, lgc-34, lipl-1, lips-5, lir-3, lmp-2, lpd-6, lpd-8, lsm-1, lsm-4, lsm-8, lys-4, M01E11.1, M01E11.2, M01E11.3, M02B7.2, M02D8.9, M03C11.8, M03E7.9, M04B2.4, M142.5, M153.2, M18.8, M199.9, M88.7, mat-2, math-17, math-45, math-49, math-8, mbd-2, mce-1, mdf-1, mdf-2, mdt-10, mdt-21, mdt-6, mdt-9, mec-15, mecr-1, mel-

28, mett-10, mig-22, mig-32, mnat-1, mppa-1, mpst-1, mrck-1, mrp-7, mrpl-12, mrpl-13, mrpl-16, mrpl-19, mrpl-20, mrpl-23, mrpl-24, mrpl-30, mrpl-32, mrpl-35, mrpl-39, mrpl-45, mrpl-46, mrpl-49, mrpl-50, mrpl-53, mrps-14, mrps-15, mrps-16, mrps-17, mrps-18C, mrps-2, mrps-21, mrps-22, mrps-23, mrps-25, mrps-30, mrps-31, mrps-33, mrps-34, mrps-35, mrps-7, mrt-2, msh-2, mspn-1, mtl-2, mtrr-1, mtss-1, mys-4, nars-2, ncbp-1, ncbp-2, ND3, nduf-2.2, ndx-4, nhr-12, nhr-250, nhr-68, nkb-1, nlp-36, nol-1, nol-5, npp-12, npp-15, npp-21, npp-23, nra-2, nrde-4, nspb-2, nspb-3, nspb-4, nuc-1, nud-1, nuo-4, nuo-6, ocrl-1, ooc-5, orc-4, pabp-2, par-4, pars-2, pas-5, pat-10, pcbd-1, pfd-2, pfd-4, pgl-3, pgp-2, phf-30, pho-11, plk-3, pole-2, polh-1, polk-1, pph-4.2, pph-5, ppp-1, pqbp-1.1, pqbp-1.2, pqn-68, pri-1, prp-31, prp-4, psr-1, pssy-2, pst-2, ptr-2, puf-4, qns-1, R02D3.7, R02F2.9, R03D7.11, R03G8.6, R04D3.2, R04D3.3, R04F11.5, R05D3.12, R05D7.4, R05D7.7, R05G9.3, R05H11.1, R07D5.8, R07E4.1, R07G3.7, R08D7.1, R09B3.3, R09F10.13, R09F10.8, R10D12.13, R10D12.19, R10H10.3, R10H10.6, R11.1, R119.1, R11A8.5, R12C12.6, R12C12.8, R13.8, R144.10, R144.11, R148.4, R166.2, R53.2, R53.6, R74.7, R74.8, rabs-5, rae-1, ran-4, rba-1, rbd-1, rbg-3, rde-1, rde-4, repo-1, rfc-4, rfp-1, rig-4, rme-2, rnf-113, rnf-121, rnf-5, rnh-2, rod-1, rpb-11, rpb-5, rpb-8, rpc-1, rpia-1, rpl-14, rpl-23, rpl-29, rpl-7A, rpn-5, rps-23, rrf-3, rsp-1, rsp-7, ruvb-2, scav-1, scav-6, sco-1, sdha-2, sdz-24, sdz-36, set-22, set-24, set-31, set-32, set-5, sin-3, skih-2, skr-17, skr-18, skr-8, slr-2, smg-4, smgl-1, smn-1, smu-2, sna-1, snr-1, snr-2, snr-3, snr-4, snr-7, spat-1, spds-1, spo-11, spp-16, spp-17, spp-3, spp-5, spr-1, sqv-2, sqv-4, sqv-8, srf-3, srg-38, srh-181, srh-268, sri-40, sri-69, sri-77, sru-25, srw-53, stl-1, str-240, str-92, sucg-1, suds-3, suf-1, sun-1, swd-2.2, swsn-3, syn-16, syp-3, syx-4, T01C3.2, T01C3.3, T01C8.3, T01G5.7, T02B5.1, T02B5.3, T02G5.11, T02G5.12, T02G5.3, T02G6.5, T04C12.24, T04C12.25, T04C12.28, T05A6.19, T05A8.6, T05F1.13, T05H10.1, T05H4.11, T06D4.1, T06G6.4, T07A9.8, T07D4.5, T07F10.3, T08A11.2, T08B2.5, T09A5.15, T09A5.17, T09A5.5, T09A5.7, T09B4.2, T09B4.9, T09B9.1, T10B11.7, T10B11.8, T10C6.19, T10E9.2, T11F8.2, T11F9.13, T12E12.1, T12F5.2, T12G3.6, T14B4.1, T14B4.11, T14B4.2, T14B4.3, T15B7.1, T15H9.2, T16G1.6, T16G1.7, T16G12.8, T16H12.1, T16H12.11, T18D3.5, T19B10.8, T19C4.19, T19H5.7, T20B12.1, T20H4.5, T21H3.6, T22B7.15, T22C1.15, T22C1.3, T22D1.5, T23B5.4, T23F2.5, T23F4.5, T23G11.11, T24A11.7, T24C2.8, T24C4.5, T24D8.15, T24E12.11, T24H7.4, T26A5.6, T26A8.4, T27A10.8, T27A3.11, T27A8.2, T27A8.5, T27E4.15, T27E9.2, T28A8.4, T28A8.5, T28B11.20, T28D9.11, T28D9.13, T28F4.7, taf-11.2, taf-7.2, tag-115, tag-124, tag-146, tag-170, tag-231, tag-261, tag-315, tag-322, tag-342, tag-345, tag-349, tag-72, tbck-1, thoc-2, tig-3, tin-10, tin-13, toe-1, tomm-22, tomm-40, tra-3, trap-4, trm-1, trpl-3, trr-1, tsfm-1, tsp-10, ttr-40, ttr-42, ttr-46, ttr-49, ttr-53, tut-2, ubc-9, ubh-4, ubl-5, ufd-1, ugt-1, ugt-17, ugt-28, ugt-44, ulp-5, unc-101, unc-45, unc-59, unc-68, unc-97, usp-14, usp-3, vars-2, VF13D12L.3, vha-18, vha-7, vig-1, vit-5, vps-26, vps-33.2, vps-51, vps-54, vrk-1, W02B12.1, W02D3.4, W02D7.4, W02F12.10, W02G9.9, W03C9.2, W03F8.3, W03G11.6, W03G9.8, W04A4.2, W04A4.5, W04A8.6, W06B3.6, W06D11.1, W06E11.1, W07G4.12, W09C5.7, W10C8.12, W10G11.2, W10G11.3, W10G11.4, wago-9, Y102A5C.2, Y102E9.5, Y104H12D.4, Y106G6A.7, Y106G6D.10, Y106G6D.7, Y110A2AL.13, Y111B2A.1, Y111B2A.19, Y116A8C.26, Y116A8C.27, Y116A8C.9, Y119D3B.13, Y119D3B.21, Y13C8A.1, Y14H12A.1, Y17G9B.9, Y18D10A.16, Y18H1A.7, Y19D10B.5, Y19D10B.7, Y22D7AR.10, Y23H5A.3, Y23H5B.5, Y24F12A.1, Y32B12A.3, Y37E11AL.3, Y37E11AM.3, Y37E11B.3, Y38A10A.7, Y38C1AA.14, Y38H6A.10, Y39A1A.14, Y39A1A.22, Y39A3B.1, Y39A3CL.3, Y39B6A.10, Y39B6A.13, Y39B6A.34, Y39B6A.41, Y39F10A.2, Y39G10AR.21, Y39G10AR.32, Y40A1A.3, Y41E3.459, Y43D4A.3, Y43D4A.4, Y43F4B.10, Y43F4B.7, Y43F8C.7, Y44F5A.1, Y45F10C.2, Y45F10C.4, Y45G12C.11, Y46E12A.5, Y46G5A.28, Y47D3B.12, Y47D3B.22, Y47D3B.4, Y47D7A.16, Y47G6A.25, Y47H9A.4, Y47H9C.8, Y48A6B.3, Y48B6A.13, Y48E1B.2, Y48G10A.1, Y48G1C.7, Y49A3A.1, Y49E10.4, Y49F6B.2, Y49F6C.8, Y4C6A.3, Y50D7A.9, Y51A2D.25, Y51H4A.6, Y51H7C.15, Y52B11A.2, Y53C10A.6, Y53C12A.11, Y53C12A.3, Y53C12A.6, Y53C12B.1, Y53F4B.42, Y53G8AL.2, Y53G8AR.6, Y53G8AR.8, Y54E10A.10, Y54E10A.21, Y54E10A.26, Y54E10BR.1, Y54E10BR.2, Y54G2A.10, Y54G2A.12, Y54G2A.67, Y54G9A.8, Y55D9A.2, Y55F3AM.13, Y56A3A.16, Y57A10A.2, Y57G11B.5, Y57G11C.1140, Y59A8A.3, Y59A8B.12, Y61A9LA.11, Y62E10A.14, Y62E10A.2, Y62E10A.20, Y62E10A.6, Y62H9A.2, Y62H9A.4, Y63D3A.4, Y63D3A.7, Y66A7AL.7, Y66D12A.10, Y66D12A.19, Y66D12A.9, Y66H1A.4, Y69A2AR.3, Y70C5B.2, Y71F9AL.12, Y71F9AL.19, Y71F9B.6, Y71G12B.13, Y71H2AM.11, Y71H2AM.5, Y73B3A.21, Y73B6BL.14, Y73E7A.2, Y73E7A.6, Y73F8A.1172, Y75B8A.16, Y75B8A.7, Y75D11A.1, Y77E11A.6, Y82E9BR.19, Y82E9BR.2, Y82E9BR.5, Y92H12BR.7, Y94H6A.12, Y95D11A.1, Y97E10AL.3, Y97E10AR.3, ZC155.4, ZC196.4, ZC204.14, ZC262.9, ZC266.1, ZC317.7, ZC395.10, ZC410.3, ZC434.7, ZC449.8, ZC477.3, ZC53.1, zhit-3, zhp-3, zif-1, zim-3, ZK1058.5, ZK1067.2, ZK1067.3, ZK1098.4, ZK1127.5, ZK1127.6, ZK1128.1, ZK1236.1, ZK1236.5, ZK1248.11, ZK1248.13, ZK1290.19, ZK1320.7, ZK177.4, ZK265.13,

ZK265.6, ZK328.4, ZK370.8, ZK377.7, ZK381.35, ZK381.41, ZK402.2, ZK418.5, ZK418.8, ZK484.10, ZK546.5, ZK550.3, ZK616.1, ZK616.3, ZK617.22, ZK632.11, ZK632.16, ZK637.19, ZK686.1, ZK686.2, ZK688.9, ZK792.5, ZK809.10, ZK809.5, ZK856.10, ZK858.7, zyg-1
Tunicamycin (1052)
aat-6, abt-4, abt-5, abts-3, AC3.5, acbp-1, acd-1, acdh-8, acl-1, aco-1, acp-1, acp-7, acr-18, acs-1, acs-15, acs-5, acs-6, act-5, acy-3, adt-2, ahcy-1, aldo-1, alh-6, alp-1, aman-3, amx-2, anc-1, apy-1, aqp-1, aqp-4, aqp-7, aqp-8, arl-3, arrd-10, arrd-14, art-1, asb-2, asg-2, asns-1, asns-2, atf-5, atgp-2, B0025.5, B0034.1, B0207.9, B0218.7, B0222.5, B0228.1, B0244.10, B0252.1, B0261.6, B0273.1, B0280.17, B0286.3, B0395.3, B0403.3, B0454.6, B0457.6, B0496.6, B0511.11, bath-25, bcmo-2, best-17, best-22, bli-1, bli-6, C01B10.3, C01G10.1, C01H6.4, C02G6.1, C03F11.4, C03H5.5, C03H5.6, C04E12.4, C04E6.7, C04F12.7, C04G2.5, C04G2.8, C04G2.9, C05C10.8, C05C9.7, C05E7.2, C05G5.1, C06A8.3, C06E1.3, C06H5.6, C07B5.8, C07G1.6, C08B6.17, C08F11.1, C08F8.6, C08H9.2, C09B9.4, C09E8.1, C09G1.4, C10A4.4, C10C5.3, C10G8.8, C11E4.1, C11E4.2, C11H1.9, C12D12.1, C12D8.24, C13C4.5, C14A6.6, C14B1.7, C14B4.2, C14C6.5, C14F11.4, C14H10.1, C15C7.4, C15C7.5, C15F1.1, C15H11.1, C16A11.7, C16B8.2, C16D6.1, C16D9.5, C17C3.1, C17C3.15, C17D12.15, C17D12.3, C17F3.1, C17H12.3, C17H12.4, C18B2.3, C18D11.1, C18E9.8, C23H3.2, C23H4.10, C24A3.2, C24G6.2, C25D7.1, C26B9.5, C26G2.2, C27B7.6, C27D6.3, C28D4.4, C28D4.5, C28H8.11, C29F3.7, C29G2.6, C30F12.9, C30G7.3, C31B8.8, C31H1.5, C32E8.9, C32H11.4, C33D12.2, C33F10.1, C33F10.12, C33G8.2, C33G8.4, C34D4.3, C34F11.5, C34H4.2, C35A5.4, C35B1.5, C36A4.11, C36F7.5, C36H8.1, C38C3.3, C38D4.1, C39B10.7, C39B5.5, C39E9.8, C39H7.1, C41A3.5, C43C3.9, C43G2.3, C44F1.1, C45B11.8, C45B11.9, C45B2.2, C45E1.4, C45E5.4, C45G9.12, C46C11.2, C46E10.1, C46F2.1, C46G7.108, C47A4.2, C47A4.5, C47E12.10, C48E7.7, C49A9.3, C49A9.4, C49A9.9, C49C8.5, C49F8.3, C50B8.6, C50D2.3, C51E3.9, C52B11.5, C52B11.6, C52E4.7, C52G5.2, C53C9.2, C54E4.2, C54G6.7, C55A6.12, C55B7.3, cah-1, cah-3, cah-4, cah-5, catp-5, cav-2, cbs-1, cdd-1, ceh-14, ceh-18, cept-1, cka-2, clc-3, clec-173, clec-184, clec-186, clec-187, clec-198, clec-205, clec-265, clec-41, clec-51, clh-1, col-110, col-117, col-118, col-119, col-122, col-125, col-126, col-13, col-133, col-140, col-142, col-144, col-147, col-149, col-150, col-154, col-155, col-159, col-160, col-167, col-168, col-38, col-39, col-7, col-81, col-88, col-92, col-94, col-96, comt-3, cor-1, cpn-4, cpt-5, ctg-2, cup-4, cut-4, cyc-2.2, cyp-33C3, cyp-36A1, cysl-2, cytb-5.1, D1005.1, D1007.15, D1007.3, D1081.12, D1086.17, D2062.6, D2092.1, D2096.6, daf-12, daf-28, daf-36, daf-7, dapk-1, ddo-2, deb-1, decr-1.2, del-6, dig-1, dim-1, dmd-10, dnj-24, dod-17, dod-19, dop-2, dpf-6, dpy-13, dpy-6, dyc-1, dylt-2, E01H11.6, E04D5.5, E04F6.6, ech-7, egl-19, elo-2, elp-1, F01D5.5, F01G10.5, F01G10.9, F02D8.5, F02E9.3, F07A5.2, F07G6.10, F08H9.2, F09B12.3, F09C3.2, F09G2.3, F10D11.6, F10D7.1, F11A5.9, F11C7.2, F11E6.3, F11F1.1, F11G11.4, F13B6.2, F13C5.5, F13D2.1, F13H6.1, F14B8.4, F14D7.6, F14H12.3, F15A4.6, F15A8.4, F15E6.6, F16H6.7, F17A9.5, F17C11.1, F17C11.12, F17E9.5, F19B2.5, F19H8.2, F20A1.10, F20D6.6, F20G2.6, F21A3.3, F21C10.7, F21F8.11, F21H7.2, F21H7.5, F22D6.15, F22F7.1, F22H10.2, F23B12.4, F23F12.13, F26B1.8, F26E4.3, F26F4.2, F27C1.1, F27E5.3, F31D4.8, F31E8.5, F32A5.2, F32A7.5, F32B5.1, F32B5.6, F32B6.4, F32D8.11, F32D8.12, F32H2.7, F33C8.4, F33D4.12, F34D10.4, F34D10.6, F35A5.1, F35E12.10, F35E12.8, F35F10.13, F35F10.6, F35G2.12, F35H10.10, F35H10.14, F35H10.3, F35H8.4, F36A2.12, F36A2.3, F36A4.5, F36G3.2, F36H1.3, F36H12.9, F36H5.14, F37A4.5, F37B12.1, F37H8.3, F38B2.2, F40A3.2, F40F4.6, F40F8.4, F40F9.3, F41C3.2, F41D9.2, F41E6.12, F41G4.4, F42A9.7, F42H10.5, F43C1.5, F43D2.6, F44E5.5, F45D3.2, F45E1.4, F46C3.6, F46F5.6, F46G11.2, F47B3.2, F48C5.2, F48G7.5, F49C12.15, F49E12.9, F49E2.5, F49H12.5, F52F12.17, F53B3.6, F53B6.4, F53B6.7, F53C11.1, F53F1.4, F54C1.1, F54C1.8, F54D1.1, F54E2.1, F54E2.4, F54H5.3, F55A11.11, F55A12.16, F55B11.1, F55D12.1, F55D12.2, F55G11.8, F55H12.3, F55H12.4, F56B3.6, F56C3.9, F56D6.13, F56F4.3, F57B1.5, F57B10.18, F57F4.1, F58A6.9, F58D2.2, F58E6.5, F58F12.3, F59A1.10, F59D6.2, fah-1, far-5, fat-6, fat-7, fbl-1, fbp-1, fbxb-76, fbxc-1, fbxc-2, fig-1, fipr-10, fipr-2, fipr-21, fkb-3, flp-1, fmo-3, fpn-1.1, fut-4, gas-1, gcy-15, gei-3, gipc-1, gipc-2, glb-24, glc-2, glna-2, glt-1, gly-8, gon-1, got-1.2, gpd-2, grd-1, grd-14, grd-5, grl-4, grl-8, grsp-1, gsa-1, gspd-1, gst-27, gst-36, gst-39, gst-6, gyg-1, H02F09.3, H03A11.2, H05L03.3, H05L14.1, H06A10.1, H10D18.5, H10E21.5, H11E01.3, H12D21.5, H14N18.4, H18N23.2, H20J04.1, H28G03.1, H32K16.1, H38K22.6, H43E16.1, hacd-1, haf-4, haf-9, him-4, his-41, hpd-1, hpo-28, hpo-6, hsp-16.1, hsp-16.11, hsp-16.2, hsp-16.48, hsp-17, hsp-43, hsp-70, htas-1, idh-1, idhb-1, ifa-1, ifb-1, ifd-2, ifp-1, immt-1, ins-33, ins-37, ins-6, inx-12, inx-17, K01A11.1, K01H12.4, K02E11.3, K03B8.6, K03B8.8, K04G2.4, K04G2.9, K05F1.10, K05F1.12, K05F1.9, K06A5.2, K06A5.3, K06A9.1, K07C11.8, K08A2.2, K08B5.6, K08D12.6, K08D8.3, K08D8.4, K08D8.5, K08D8.6, K08E4.7, K08H2.10, K09B11.20, K09C6.7, K09C6.9, K09G1.1, K10C2.1, K10C9.7, K10D3.6, K10G9.2, K11C4.2, K11D9.3,

K11G12.5, K11G9.5, K11H12.11, K11H12.7, K12C11.1, ketn-1, kin-1, kin-15, kin-2, kri-1, kvs-5, lact-8, lbp-6, lec-3, let-2, let-756, let-767, let-805, lgc-26, lgc-32, lim-9, lin-10, lin-29, lips-10, lron-3, M02D8.2, M03F8.6, M04C9.3, M199.8, M28.9, M70.3, M88.4, mab-3, madf-5, math-26, math-3, mbl-1, mca-2, mdl-1, mec-12, mec-17, mef-2, mig-6, mlp-1, mpst-5, mpst-6, mpst-7, mpz-1, mpz-2, mrp-1, msd-1, msd-3, msd-4, msp-10, msp-113, msp-142, msp-33, msp-38, msp-40, msp-50, msp-55, msp-63, msp-74, msp-76, msp-78, msp-79, mth-1, mth-2, mua-3, mua-6, mup-2, mup-4, mxl-3, myo-1, myo-2, myo-3, nac-1, nac-3, nas-11, nas-36, nas-4, nas-7, ncx-1, ncx-2, ncx-8, nep-22, nhr-114, nhr-17, nhr-31, nhr-33, nhr-5, nhr-6, nhr-76, nhx-1, nkb-2, nkb-3, nlp-24, npa-1, npr-5, nspa-1, nspa-2, nspd-10, nspd-5, nspd-7, nspd-9, oac-20, oac-59, oat-1, oig-2, osm-1, osm-10, otpl-3, pat-12, pat-2, pck-1, pcp-4, pde-1, pept-1, pes-22, pes-9, pfn-3, pgp-1, pgp-14, pgp-9, phat-4, pho-1, pho-8, phy-2, pkc-2, pkg-2, pod-2, poml-3, ppw-2, pqn-22, pqn-37, pqn-72, pqn-74, ptb-1, ptps-1, ptr-12, ptr-14, ptr-24, pxn-1, pyk-2, qdpr-1, R03E1.2, R06C1.4, R07B1.8, R07E3.1, R07E3.4, R07E5.4, R07H5.8, R08D7.8, R08E3.1, R08E3.2, R09E10.1, R09E10.2, R09E10.6, R102.10, R102.4, R10D12.1, R10E4.7, R10E9.2, R11D1.3, R11F4.1, R11F4.3, R12A1.3, R13A5.10, R13A5.9, R57.1, R90.12, ram-2, rap-3, rgs-2, rhr-1, rhy-1, rmd-3, rmd-4, rmd-6, rol-1, rol-3, scl-22, scl-3, sdha-1, set-18, sfxn-5, shl-1, sir-2.3, snf-3, snf-5, sod-3, spe-11, spe-41, spon-1, sptl-2, sptl-3, sra-27, srg-20, srr-9, srt-18, srv-1, ssp-16, ssp-35, ssq-2, ssq-3, ssq-4, sss-1, sss-2, sur-5, T01B11.2, T01C1.4, T01C8.10, T01D1.3, T01D1.4, T01H8.6, T02B11.3, T02G5.7, T02G6.1, T04A11.1, T04B8.5, T04F3.1, T04F8.8, T05A1.16, T05A8.10, T05C12.1, T05F1.5, T06D8.1, T06E4.12, T07A5.1, T07C12.9, T07E3.4, T07F12.4, T08B2.12, T08H10.4, T10E9.3, T10E9.4, T10H10.2, T11B7.2, T11F9.12, T11G6.4, T12A2.1, T12B3.2, T12D8.9, T14A8.2, T16A9.5, T16A9.6, T16G1.13, T17H7.1, T19C3.3, T19D2.1, T19D7.4, T19H12.3, T20D3.2, T20D4.3, T20D4.4, T20D4.5, T21B6.3, T21G5.1, T21G5.2, T21G5.4, T21G5.6, T22B3.2, T22B3.3, T22C1.14, T23B12.11, T23B3.5, T23E7.2, T23G11.1, T25B9.9, T25G12.6, T27A3.4, T27D12.1, T27E7.1, T28A11.6, T28C12.10, T28C12.4, T28F3.4, T28H10.2, T28H11.7, tag-147, tag-209, tag-290, tag-83, tba-9, tbc-7, tkt-1, tni-1, tnt-4, toh-1, tps-2, trap-1, tre-2, tsp-11, tsp-8, ttll-15, ttm-4, ttr-1, ttr-12, ttr-14, ttr-18, ttr-31, ttr-33, ttr-36, ttr-38, ttr-44, twk-13, tyr-2, ubxn-5, ugt-16, ugt-21, ugt-40, ugt-49, ugt-6, ugt-60, unc-1, unc-22, unc-23, unc-49, unc-52, unc-54, unc-58, unc-89, unc-9, unc-95, upb-1, vab-10, vap-1, vglu-3, vha-10, vha-11, vha-12, vha-13, vha-14, vha-15, vha-16, vha-19, vha-3, vha-4, vha-5, vha-8, VM106R.1, W01B6.2, W01F3.1, W02B12.12, W02F12.2, W03C9.8, W03D8.10, W03D8.8, W03G9.3, W04B5.3, W05F2.4, W06A11.1, W06A11.4, W10D5.4, W10G11.17, wht-8, xbx-5, Y102A11A.3, Y105C5B.18, Y105C5B.25, Y105E8A.27, Y106G6D.3, Y106G6G.1, Y106G6G.2, Y106G6G.4, Y106G6H.1, Y106G6H.13, Y113G7C.1, Y12A6A.1, Y18D10A.8, Y24D9A.11, Y26E6A.3, Y34B4A.4, Y34B4A.5, Y34B4A.6, Y37A1A.4, Y37A1B.5, Y37D8A.12, Y37D8A.8, Y38C1AA.7, Y38E10A.17, Y38F1A.1, Y39B6A.30, Y39D8A.1, Y39G10AR.16, Y40C5A.1, Y40D12A.2, Y41C4A.13, Y41C4A.18, Y41D4B.17, Y43C5B.3, Y43F8A.2, Y43F8B.1, Y45G12C.1, Y46G5A.29, Y47G6A.15, Y47G6A.19, Y47G6A.3, Y48C3A.3, Y49E10.29, Y49G5A.1, Y50D4B.3, Y50D4B.4, Y51A2D.14, Y51A2D.21, Y53C10A.5, Y53F4B.12, Y53F4B.19, Y53F4B.23, Y53G8B.1, Y54E10A.17, Y54F10AM.8, Y54G2A.13, Y54G2A.3, Y56A3A.6, Y57G11A.2, Y57G11A.4, Y57G11C.15, Y57G11C.23, Y58A7A.1, Y59E9AL.4, Y59E9AL.6, Y59E9AR.1, Y59E9AR.10, Y59H11AM.1, Y59H11AR.4, Y62E10A.13, Y69A2AR.22, Y69E1A.1, Y69E1A.2, Y69E1A.3, Y71F9B.1, Y71F9B.13, Y71H10B.1, Y72A10A.1, Y73B6A.3, Y73C8B.3, Y73E7A.3, Y73F8A.20, Y7A5A.1, Y82E9BL.18, Y87G2A.19, Y94H6A.10, ZC101.1, ZC21.3, ZC412.10, ZC416.6, ZC434.9, ZC449.5, ZC581.9, zip-10, zip-3, zip-9, ZK1010.5, ZK105.1, ZK1058.9, ZK121.2, ZK1248.4, ZK1248.5, ZK265.3, ZK287.9, ZK354.6, ZK354.7, ZK470.2, ZK470.4, ZK484.5, ZK546.3, ZK593.11, ZK6.11, ZK617.7, ZK669.2, ZK688.10, ZK742.4, ZK822.4, ZK84.1, ZK856.18, ZK856.6, ZK858.8, ZK938.1, ZK945.7, ZK973.12, ZK973.13, zyx-1
common (420)
aat-4, acdh-2, acox-1, acp-6, acr-16, alh-10, alh-12, alh-9, aman-1, amt-4, aqp-11, arrd-9, asm-2, asm-3, B0244.7, B0410.3, bas-1, C01B10.47, C01B9.1, C02C2.4, C04E12.2, C05C9.3, C05D12.3, C05D2.8, C08B6.11, C09B8.4, C11E4.7, C12D5.9, C15C8.3, C15H9.7, C15H9.9, C16A3.10, C18A11.12, C18A11.3, C18E9.5, C23H4.3, C23H5.8, C27H5.4, C30A5.11, C30G12.2, C31H5.6, C35A11.4, C35A5.3, C35C5.10, C41A3.1, C42D4.2, C43H6.1, C44B7.11, C44B7.7, C44C1.5, C45B2.1, C45E5.1, C49A9.2, C49A9.5, C49C3.22, C49C3.4, C50A2.3, C52D10.3, C55A6.4, C55F2.1, cat-4, cbl-1, cdr-6, ckc-1, clec-1, clec-10, clec-160, clec-165, clec-166, clec-170, clec-172, clec-204, clec-209, clec-227, clec-56, clec-57, clec-80, cln-3.1, cof-2, col-101, col-103, col-106, col-124, col-129, col-139, col-143, col-179, col-184, col-19, col-20, col-37, col-8, col-80, col-93, col-98, cpg-9, cpr-5, cth-2, cya-2, cyp-13A2, cyp-14A1, cyp-25A1, cyp-25A2, cyp-29A3, cyp-35C1, D1054.8, D1086.3, D2024.2, D2092.4, dct-16, dct-17, dhs-21, dhs-25, dhs-26, dhs-3, dhs-7, dpyd-1, E01G4.3, ech-5, ech-6, efn-3, EGAP4.1, elo-5, elo-6, elo-9, emo-1, F01D5.3, F01F1.14,

F07A11.5, F08A8.2, F08A8.3, F08A8.4, F08F3.4, F08G5.6, F09A5.1, F09C8.1, F10A3.4, F11D5.7, F13D12.6, F13H6.3, F13H8.3, F15E11.15, F17C8.9, F18E2.1, F18E3.11, F18E3.12, F18E3.13, F19C6.4, F20D1.9, F20G2.2, F21C10.9, F22H10.6, F23D12.11, F23F12.3, F26C11.1, F28A12.4, F28B4.3, F28H7.3, F29B9.14, F29C4.2, F31D5.2, F32A5.3, F32B6.2, F32H5.1, F36D1.23, F38B6.4, F40H3.2, F41E6.15, F42A10.6, F42A10.7, F42A10.9, F42A8.1, F42D1.12, F42G10.1, F44B9.2, F45D11.1, F45D11.14, F46F2.3, F49C12.14, F49F1.1, F52H2.6, F54B11.11, F54D5.12, F54H12.4, F55E10.6, F55F3.2, F55G11.2, F56A4.13, F56A4.3, F56A4.4, F56C9.7, F57F4.4, F57F5.1, F58B4.5, F58F9.4, F58G6.3, F58G6.7, F58G6.9, F59A1.18, F59D6.3, F59D8.3, fbxa-72, folt-2, fpn-1.2, gba-4, gcsh-1, gfi-1, glb-1, glh-1, grd-10, grd-13, grd-3, grsp-4, gst-10, gst-13, gst-26, gst-28, gst-30, gst-4, gta-1, H11E01.2, H16O14.77, H21P03.4, H25K10.1, H41C03.3, haao-1, hmit-1.2, hrg-4, ifc-1, ilys-5, K03H6.2, K08C7.1, K09A9.6, K09C4.5, K09F6.6, K10B2.2, K10C2.12, K10C2.3, K10C2.8, K11G9.3, K12H4.7, klp-3, lact-1, lgc-45, lips-14, LLC1.2, lon-1, lron-8, M02D8.1, M02D8.5, M03B6.2, mec-5, mel-32, msra-1, nas-20, ncx-6, ncx-7, ndg-4, nep-17, nhr-244, nhr-43, nhr-74, nhx-2, nid-1, nkat-3, nlp-26, nrf-6, pcp-1, pcp-2, pcp-3, pho-13, pho-7, pmp-1, pmp-5, pmt-2, poml-2, prmt-6, R02D3.1, R03G8.4, R07B7.10, R07B7.5, R07E4.3, R07E5.13, R08F11.1, R09H10.5, R11A8.1, R12C12.1, R12C12.9, R160.3, R17.3, R193.2, sams-1, scav-4, sdz-6, sesn-1, set-33, sfxn-2, smd-1, spl-1, spp-23, spp-4, sra-14, srbc-10, srh-60, srh-70, suca-1, swt-3, T01C8.2, T01G5.8, T02D1.8, T04A8.5, T05B11.4, T05C3.6, T05E12.6, T05E7.1, T07A9.14, T08A9.4, T08B1.1, T08H10.1, T09B4.8, T10G3.3, T12B5.15, T13F3.6, T14B4.5, T16G12.1, T16G12.3, T19H12.14, T22B7.7, T24A6.20, T25B9.1, T25C12.3, T28D6.3, tag-10, tag-173, tba-4, trap-2, tsn-1, ttr-35, twk-16, twk-22, twk-26, twk-42, ucr-2.2, ugt-12, ugt-13, ugt-22, ugt-26, ugt-30, ugt-41, ugt-46, ugt-47, ugt-48, ugt-53, ugt-62, ugt-63, ugt-64, ugt-65, ugt-8, ugt-9, vha-6, vit-1, vit-4, W02G9.4, W02H3.1, W06A7.2, W06A7.4, W06A7.7, W07A12.8, W07B8.1, W10C8.5, wago-2, Y105C5B.15, Y105E8B.5, Y111B2A.2, Y116F11A.6, Y11D7A.3, Y16B4A.2, Y22D7AL.11, Y38F1A.6, Y39B6A.1, Y39E4A.3, Y39F10A.1, Y40H7A.10, Y43C5A.7, Y43F4B.5, Y43F8C.13, Y47G6A.33, Y48E1B.8, Y49A3A.6, Y49E10.18, Y51A2D.18, Y52E8A.4, Y53G8AR.7, Y54G2A.45, Y54G9A.4, Y57A10A.1, Y69H2.14, Y69H2.9, Y73B6BL.275, Y73B6BL.288, Y73F4A.1, ZC116.3, ZC250.4, ZC374.2, ZC376.2, ZC412.4, ZK1193.2, ZK1193.3, ZK1193.4, ZK1290.5, ZK185.3, ZK228.3, ZK228.4, ZK455.5, ZK512.7, ZK6.6, ZK669.4, ZK742.3, ZK856.5, ztf-26

Table A2: List of upregulated genes in the four-way Venn diagram.

ATF-6 (181)
abf-6, abt-1, acl-13, B0207.9, B0218.7, B0261.6, B0302.5, C01B10.44, C04F12.12, C04F12.7, C04G2.9, C05B5.8, C09D4.1, C09F9.8, C10G11.8, C13C4.7, C14F11.11, C16A11.7, C18B12.10, C23G10.1, C24A11.1, C25D7.16, C26B2.2, C27A7.1, C27D8.1, C28C12.1, C28D4.4, C33F10.11, C37C3.12, C39F7.5, C43E11.5, C44H9.6, C45B11.2, C45B11.9, C48E7.6, C51E3.9, C52E4.7, ceeh-1, ckk-1, clec-153, clec-173, clec-73, clh-1, cpn-4, cpz-2, crm-1, cwp-4, D1037.5, D2007.2, D2063.4, F07B7.12, F08B12.7, F09G2.3, F10G8.8, F13A7.1, F14D2.19, F17C8.3, F20D6.1, F20D6.10, F20G2.3, F22B7.9, F25H5.7, F26B1.5, F26B1.8, F27C1.1, F36H12.3, F38A6.4, F40E12.2, F41G3.5, F43C9.2, F46F11.7, F46H5.7, F47D12.7, F47G3.7, F53F10.1, F54C9.11, F56A11.6, F58H1.2, fis-1, flp-33, glc-2, glna-3, gpa-12, gsp-3, hecw-1, hpo-28, hsp-16.48, iff-2, ins-28, K06A1.2, K07A1.4, K07A1.5, K07A3.3, K07F5.20, K08C9.2, K11C4.1, kin-24, lat-2, lbp-7, M02B1.4, M03A8.3, M28.10, M28.4, mab-5, mpst-4, nep-23, nhr-139, nspa-6, nspb-7, nspc-13, odr-10, pme-4, pqn-48, R03D7.8, R03H10.6, R09E10.1, R10D12.10, R10E4.7, R148.7, ras-2, rmd-6, rnh-1.1, snf-11, snf-5, spe-11, spe-15, spe-26, ssp-35, sul-2, T01B7.8, T01D3.6, T02B11.9, T03D8.6, T03F1.11, T04B2.8, T05A7.6, T05D4.3, T07C12.15, T10G3.1, T15B12.2, T16A9.5, T23F2.2, T25C12.5, tps-2, ttr-7, uggt-2, W04D12.1, W06D11.4, wht-8, Y105C5A.24, Y106G6H.13, Y111B2A.13, Y116A8B.4, Y119C1B.6, Y34B4A.10, Y38E10A.17, Y38F1A.1, Y39G10AR.16, Y43C5A.4, Y43F4A.6, Y45F10B.3, Y47G6A.26, Y48G1C.5, Y4C6B.4, Y51H4A.935, Y53C10A.10, Y53F4B.19, Y54F10AM.6, Y55B1BR.5, Y57G11C.6, Y59C2A.1, Y59E9AL.6, Y67D8B.5, Y6E2A.8, Y71H2AM.14, Y73B6BL.44, Y76A2B.5, ZC581.2, ZK484.7, ZK795.2, ZK809.1
IRE-1 (417)
B0001.6, B0024.4, B0205.13, B0348.2, B0350.78, B0403.3, B0546.4, B0554.5, C01A2.4, C05D11.5, C05D11.7, C06B3.7, C06E4.8, C06G3.3, C10A4.10, C10B5.3, C10C5.4, C13B9.2, C13B9.3, C15C7.5, C16D9.4, C17H11.6, C18B12.2, C18B12.4, C18G1.1, C18H7.11, C23H3.11, C25F9.11, C25F9.14, C25F9.5, C26B9.1, C26D10.4, C28G1.5, C29H12.13, C30F12.1, C31H5.7, C32D5.7, C33A11.2, C33H5.13, C34D10.1, C34F11.3, C34F6.7, C34H4.1, C34H4.2, C35B8.4, C35E7.2, C37H5.2, C37H5.3, C42D8.1, C43C3.4, C45E5.4, C46F11.6, C47D2.1, C49G7.6, C50B8.4, C52A10.1, C52B11.5, C52G5.9, C53B7.2, C53C11.5, CELE_AC8.12, CELE_B0462.5, CELE_C03G6.17, CELE_C08E8.4, CELE_C14C6.2, CELE_C23G10.11, CELE_C27D8.3, CELE_C34B4.3, CELE_C38C3.6, CELE_C44H9.4, CELE_C49C3.9, CELE_C50F4.8, CELE_C54F6.12, CELE_C54F6.15, CELE_C54F6.5, CELE_D1054.5, CELE_F01D5.7, CELE_F13A7.11, CELE_F16H6.10, CELE_F17C11.11, CELE_F19B2.5, CELE_F20G2.5, CELE_F22E5.13, CELE_F23C8.6, CELE_F33H12.7, CELE_F35E12.8, CELE_F39E9.1, CELE_F40F12.9, CELE_F46A8.7, CELE_F49F1.6, CELE_F53C11.1, CELE_F53C3.13, CELE_F59A7.2, CELE_F59E11.2, CELE_K08B12.7, CELE_K08D8.4, CELE_K08D8.7, CELE_K10F12.8, CELE_K10G4.3, CELE_M03D4.3, CELE_R102.5, CELE_T28A11.2, CELE_W01B6.4, CELE_Y105C5B.11, CELE_Y105E8A.36, CELE_Y37H2A.14, CELE_Y39B6A.24, CELE_Y41D4B.15, CELE_Y41D4B.17, CELE_Y47G6A.5, CELE_Y51A2B.5, CELE_Y53C10A.5, CELE_Y53F4B.51, CELE_Y60A3A.8, CELE_Y69A2AR.23, CELE_Y69A2AR.32, CELE_Y71A12C.2, CELE_ZC239.14, CELE_ZC239.6, CELE_ZK1073.1, CELE_ZK673.2, CELE_ZK795.1, CELE_ZK896.1, CELE_ZK896.5, DH11.5, E01G6.2, E04D5.4, F08F3.9, F08G12.5, F09A5.2, F09A5.4, F09C8.2, F10D7.5, F11G11.5, F13H10.8, F15B9.6, F15D4.6, F17H10.2, F20D6.8, F21C10.4, F21F3.6, F22A3.15, F22H10.2, F25B3.5, F26A10.1, F32H5.3, F37C4.5, F40B5.2, F40E10.6, F41B4.1, F46A9.1, F47B7.2, F47B8.8, F47G3.1, F47G3.4, F52G3.1, F53F10.2, F54B11.5, F54E2.1, F55C12.15, F57B10.18, F57B9.3, F58B4.6, H14N18.4, H40L08.1, K01A6.8, K08E4.3, K09F5.6, K10B4.3, K10D3.6, K11D12.9, K11H12.4, K11H12.8, M02B1.2, M04C3.1, M60.2, R03A10.5, R03G5.6, R07G3.12, R07H5.9, R08C7.12, R09B5.11, R12B2.12, T01B6.4, T05A1.17, T05E7.4, T07D1.2, T14G11.1, T15H9.4, T19A6.4, T19D12.4, T19E7.27, T23F11.6, T23F2.3, T23F2.4, T23G11.7, T24C4.4, T25C12.6, T28B11.1, T28B11.4, T28C12.4, VC5.2, W03D2.6, W05F2.7, W06F12.2, Y102A11A.2, Y102A11A.9, Y17G7B.10, Y17G7B.17, Y32G9A.5, Y37D8A.5, Y42H9AR.1, Y44E3A.4, Y45G5AM.3, Y46D2A.5, Y47D9A.1, Y48G9A.9, Y4C6B.3, Y53G8AM.8, Y55F3AM.10, Y55F3BR.2, Y57E12B.10, Y58A7A.5, Y58A7A.7, Y71G12B.2, Y71G12B.32, Y71G12B.37, Y71H2AM.13, Y94H6A.10, ZC328.2, ZC412.13, ZC416.6, ZC449.3, ZC487.6, ZC581.3, ZK1055.6, ZK1055.7, ZK121.2, ZK355.2, ZK418.7, ZK484.1, ZK632.10, ZK669.3, ZK822.1, aak-2, acbp-7, acdh-7, adm-2, alx-1, arrd-12, arrd-7, arrd-8, atf-6, bath-25, bicd-1, cah-4, cah-6, cas-1, cccp-1, ceh-34, cgt-1, chd-7, clc-1, clec-145, clec-146, clec-265, clec-65, cls-1, comt-3, cpb-2, cutl-24, cyp-36A1, daf-16, daf-5, daf-8, dgk-1, dhp-1, dmd-7, dnj-14, dod-20, egl-44, egl-9, egrh-1, elt-2, epn-1, fbxa-115, fbxa-12, fbxa-125, fbxa-150, fbxa-199,

fbxa-37, fbxa-79, fipr-2, flp-28, flr-2, frm-10, frm-2, frm-7, ftt-2, glct-6, glrx-3, gmeb-1, gpa-17, grl-14, gsto-3, hbl-1, hda-4, his-71, hpo-38, hsp-17, hsp-3, hsp-43, igeg-2, kcnl-1, kcnl-3, kgb-1, klc-2, kqt-2, lact-4, lec-10, lec-11, let-23, let-607, lin-24, lin-66, lmp-1, lst-2, mab-21, magu-2, max-2, mbk-1, mca-1, mdt-15, mdt-28, miz-1, mlk-1, mml-1, moc-2, mod-5, mop-25.1, msi-1, nab-1, nhr-201, nhr-212, nhr-231, nhr-49, nhr-50, nhr-57, nhr-64, nhr-69, nhx-5, nipa-1, nlp-10, nmur-4, npr-23, npr-25, nspd-9, obr-3, pab-2, phat-6, php-3, pme-5, pmk-3, prl-1, pry-1, ptr-20, rab-14, rab-6.2, rbg-1, rnt-1, rsd-3, sbp-1, scrm-1, sdz-35, secr-1, sek-1, sel-11, sir-2.3, sli-1, sma-9, sms-3, sox-4, spc-1, sptl-2, srp-6, srp-8, svh-2, swt-6, tag-120, tag-303, tat-4, tba-7, tbc-15, tbc-7, toca-1, toe-4, trk-1, trpl-2, ttr-5, ttr-51, tub-2, twk-33, ubc-1, ubc-23, unc-108, unc-3, unc-64, unc-75, unc-83, vamp-8, vglu-2, zer-1, zig-5, zip-10, zip-5, ztf-12, ztf-22
PEK-1 (25)
C35D10.8, C49G7.12, clec-142, E02H9.2, F26D2.10, F40F8.4, F54D5.3, fat-1, got-1.2, hacd-1, K03A1.4, K04C2.7, K09G1.2, nhr-126, nspc-18, R10F2.6, T04A11.2, T12B3.3, tag-209, W03B1.9, Y62F5A.10, Y95B8A.4, ZC328.3, ZK593.2, ZK675.7
ATF-6 & IRE-1 (183)
ace-3, aex-6, aip-1, asm-1, B0205.14, B0546.3, B0563.5, bath-38, bca-1, btbd-10, C03F11.2, C03G6.5, C08E8.3, C17G10.7, C24A1.3, C24A11.5, C25E10.12, C29E4.14, C30B5.7, C32D5.1, C33C12.7, C35A5.6, C38C10.6, C43F9.7, C49C8.2, C49C8.5, C49F8.1, C56G7.3, cdka-1, cho-1, clec-63, clp-6, cmd-1, cytb-5.2, D1046.15, D2030.12, dmsr-8, dod-19, efk-1, emb-8, enu-3, epg-5, exp-2, F01D5.1, F09E5.16, F13H6.12, F13H6.8, F13H8.1, F14B8.6, F15D4.4, F21F8.11, F21G4.1, F23D12.3, F28F5.6, F35B3.7, F35C11.6, F35G2.21, F36G3.3, F38B7.14, F39B2.8, F41H10.5, F43C9.7, F43D9.8, F44E8.43, F45D3.3, F47B8.3, F47G6.3, F53B1.6, F54G2.1, F55C5.16, F55G11.4, F56C4.4, far-6, fbxa-182, flp-26, fog-1, H06I04.6, H09F14.1, H36N01.3, hda-11, ins-20, insc-1, inx-10, K03H1.16, K07C5.9, K07H8.9, K08D8.6, K10C8.3, K11H12.3, let-413, lgc-46, lim-6, lin-44, lntl-1, M01B2.6, M02E1.1, M04F3.4, M04G7.3, M163.8, mai-1, mev-1, mod-1, nck-1, ncs-2, nhl-3, nhr-100, nhr-121, nhr-134, nhr-70, nmur-1, nspc-19, nucb-1, pde-6, pnk-4, pqn-53, prx-13, psd-1, ptr-13, ptr-6, pxl-1, R01H10.4, R106.5, R11A5.6, R12B2.7, R12E2.13, R13A5.9, R13H4.13, R13H7.2, ras-1, rga-5, scl-5, sip-1, smf-1, snap-29, snb-1, snx-1, srsx-3, T01C8.10, T10E9.6, T19D12.5, T19E7.25, T22F7.4, T27C5.8, T28A11.19, T28H10.2, tag-299, tmbi-4, trpa-2, ttr-45, twk-1, ubc-16, ubc-3, ugt-19, ugt-55, unc-79, unc-94, vps-37, vps-4, W01B6.6, W03C9.6, W03D8.1, Y37A1A.2, Y37D8A.6, Y41D4A.7, Y43F8B.12, Y47G6A.13, Y48C3A.5, Y51H4A.25, Y54E5A.2, Y55F3BR.11, Y57A10B.2, Y66D12A.11, Y66D12A.24, Y73B6BL.27, Y76A2B.7, ZK1010.8, ZK1086.5, ZK470.4, ZK550.5, ZK822.2, ZK945.6
IRE-1 & PEK-1 (61)
arl-13, atfs-1, bath-46, C05G5.2, C07A12.12, C07B5.3, C15F1.5, C33G8.2, C56E10.5, clec-147, clec-17, clec-184, col-76, col-95, cpna-4, E03H4.8, E04F6.4, elo-2, F07C4.12, F07C6.3, F09C6.13, F10D2.10, F10G7.5, F12B6.2, F14B6.2, F42H10.6, F44G4.7, F55B12.10, fbxa-74, fbxc-1, fbxc-2, fipr-12, gur-5, H04M03.12, inx-7, irg-1, K08D8.12, K12C11.3, M05D6.3, nhr-128, nhr-90, nhr-92, pqn-73, rhgf-2, sulp-5, T05A10.6, T06E6.10, T12B3.9, T19C9.8, T24B8.5, W02H5.8, W04E12.4, W07G4.8, wwp-1, Y34F4.5, Y38C1AA.6, Y55F3BL.4, Y82E9BR.23, zag-1, ZK622.5, ZK822.8
ATF-6 & PEK-1 (43)
B0252.5, btb-21, C04E6.5, C09D4.2, C09G9.5, C18H2.5, C23G10.6, C40H1.7, C47E12.9, C50F4.2, C53A3.3, C54D10.16, C55C2.4, DH11.2, dhs-9, dop-5, F21H7.5, F22B5.4, F25B3.4, F36A2.10, F36A4.3, F53F4.13, F56D6.13, F58G1.9, F59A1.15, gar-2, gst-38, hsp-70, htas-1, ins-35, K09H9.5, msp-64, R07E3.1, R09A1.2, srsx-34, T04A11.1, T04A6.3, T20B12.11, twk-2, Y43F8B.24, Y73F8A.14, Y73F8A.35, ZK354.8
ATF-6 & IRE-1 & PEK-1 (159)
aldo-2, alh-5, arrd-27, B0350.3, bbs-5, best-21, btb-9, C01B4.8, C03B1.13, C05B5.12, C05C12.1, C07A12.13, C09G12.5, C09H5.7, C15H11.12, C17H12.8, C23H4.8, C29F3.7, C30F2.4, C33A12.4, C33H5.16, C37C3.7, C48B4.12, C50B8.1, C54D1.8, cdd-1, csp-2, D1044.1, D1053.3, D2005.6, deg-1, DY3.9, dyf-1, elo-1, F10G2.1, F13B9.9, F13E6.10, F13H8.8, F16B12.4, F20A1.6, F20B10.3, F20G2.9, F21D9.2, F21F3.2, F23D12.7, F25A2.1, F30A10.11, F33D11.2, F35A5.9, F35E12.10, F35H8.1, F40E3.5, F43C1.7, F49C12.6, F52E1.14, F53C3.4, F54H5.3, F55A4.4, F59A7.5, F59B2.13, F59E10.3, fbxa-21, fbxa-44, fbxa-90, fbxc-23, fbxc-54, frpr-6, glb-15, glb-22, gnrr-5, gst-9, H10E21.1, H32K21.1, H35B03.1, hke-4.1, ins-22, inx-4, K02B7.3, K03C7.3, K07E12.2, K09D9.11, K12C11.5, kin-9, lbp-5, lys-2, M01H9.4, M04G7.2, M05D6.5, M117.1, M60.9, M7.7, math-41, nas-31, nhr-133, nhr-213, nhr-79, nhr-83, nspc-12, nspc-16, oga-1, ogt-1, pef-1, pgp-5, R08B4.8, R09D1.12, R106.1, R10E8.3, R11D1.3, rpl-37, sgca-1, skr-20, sma-2, snt-1, srp-1, srw-85, T02B11.3, T02C12.5, T02D1.4, T03G11.3, T05C12.15, T07F10.6, T11B7.5, T20D4.13, T22G5.1, T23G5.10, T27A10.2, T28F3.5, tag-304, tbc-10, tig-2, tkr-1, ttr-13, ttr-21, ttr-6, ugt-56,

ulp-3, W01C9.2, W02B12.13, W03G9.5, W05E10.5, W06F12.3, Y116A8C.29, Y18H1A.1, Y18H1A.10, Y20F4.4, Y37E11AL.4, Y37F4.5, Y42G9A.2, Y43F8B.23, Y44E3A.1, Y46D2A.1, Y46H3C.4, Y48A6B.7, Y53H1C.3, Y64G10A.7, Y69H2.3, Y71H2AM.25, Y73B6A.1, ZK1037.6,

Table A3: Predominant GO terms for each cluster.

WT UP		
Category	***P* value**	**Genes**
GO:0006470~protein dephosphorylation	8.84E-15	R10F2.6, F38H4.4, ZK484.7, W03F11.4, T22C1.8, F47B3.2, ZK809.1, Y57G11C.6, W01B6.6, Y62F5A.10, M05D6.3, C09H5.7, OGT-1, Y113G7C.1, C02B10.6, PTP-1, F26A3.4, C34D4.2, F26B1.5, C27B7.6, IDA-1, T16G12.7, C48B6.4, R08C7.8, M04G7.2, C33H5.16, GSP-3, PEF-1, VHP-1, Y54F10BM.3, C43E11.5, F40G12.10, OGA-1, C23G10.1, ZK354.8, F54F12.1, F20B6.1, Y48G1C.5, F42G8.8, ZK938.1, H06I04.5, F47B3.6, Y48G9A.9, F55F8.7, F25B3.4, TAX-6, T27A3.5, F25H5.7, Y18H1A.1, C24H11.2, C24H11.1, F36H12.10
GO:0045087~innate immune response	9.38E-12	F01D5.5, PYP-1, TIR-1, LYS-2, C29F3.7, F01D5.1, T24C4.4, IRG-1, F35E12.9, TRK-1, K08D8.4, F22H10.2, FOS-1, SOX-4, DAF-16, CLEC-62, FAT-6, CLC-1, K09B11.5, LEC-11, PDB1.1, PQM-1, FAT-2, GST-38, KIN-14, ELT-2, ZC581.7, C08E8.4, C34F11.5, KIN-24, R12E2.13, VALV-1, C17H12.8, ZIP-10, C34H4.1, MEV-1, Y47G6A.5, NHR-57, ZK1055.7, C33H5.13, Y69E1A.3, Y52D5A.2, C42D8.1, SEK-1, CLD-9, T19D12.4, FBXA-150, KLF-3, M60.2, F16H6.10, C49C8.5, F35E12.10, F20C5.4, DOD-19, T27C5.8, AQP-1, C49C3.9, F40A3.1, F20G2.5, F53C11.1, F13A7.11, T24B8.5, SPE-8, APM-1, VAB-9, FSHR-1
GO:0019915~lipid storage	0.0159	M70.3, C18H9.5, DUR-1, M70.1, MOD-5, ZK909.3, MOD-1, C30F12.1, R10D12.10, H09F14.1, T05C12.1, NHR-79, C14A4.12, DAF-16, F54H5.3, SBP-1, TBA-7, F45E4.6, NHR-70, FAT-7, C09G12.5, C17G10.7, DAF-12, FAT-6, PMT-1, F15A8.6, RGA-5, LIPL-5, F49C12.15, F57B9.3, OGT-1, NHR-64, HLH-30, EPN-1, UNC-96, GST-9, NLP-11, F13B6.1, AAK-2, LBP-5, SPTL-2, LPIN-1, F13D12.9, ELO-2, ELO-1, LIN-1, B0207.9, T27E4.7, PTR-3, DOD-20, TKR-1, NHR-91, R160.4, H05L03.3, ACS-5, ABHD-5.1, C04G2.2, C04G2.5, PES-7, ACL-12, OGA-1, ACS-2, WWP-1, KLF-3, Y67A6A.1, NHR-49, NHR-45, C15C7.5, F42H10.6, F47B8.3, NHR-41, NHR-88, T10E9.6, TAX-6, K02E10.4, MDT-15, MARC-5, Y37D8A.8
GO:0000166~nucleotide binding	0.0483	CKK-1, CATP-1, KGB-1, C01C4.3, CPB-2, PAB-2, MRP-2, RAB-6.2, C14A4.13, W06F12.3, C27D8.1, ABT-5, F07F6.1, MCA-1, ABT-2, F31E3.2, F57B9.3, KIN-14, ZC581.7, FOG-1, TPA-1, ZC581.2, KIN-20, KIN-24, MLK-1, T19D12.5, B0207.7, Y47G6A.5, MNK-1, Y69E1A.3, C26D10.4, Y52B11A.4, DLK-1, Y17G7B.10, MSI-1, SCD-2, SEK-1, MBK-1, R11F4.1, RAS-1, RAS-2, SVH-2, NEKL-3, VPS-4, UNC-82, NIPI-3, HSP-70, UNC-75, EFK-1, PFK-1.2, WHT-8, SPE-8, T05A7.6, LET-23, SYM-2, PMK-3, C05C12.1, HSP-3, Y73B6A.1, SPE-15, TBA-7, W02B12.12, SMA-5, TAG-344, TBB-6, HPK-1, F20D6.8, ARL-3, K09B11.5, SUP-12, LIT-1, EXC-7, SAMS-5, Y105C5A.24, AAK-2, C34F11.5, CMK-1, Y38H8A.4,

		K07A3.3, T28F3.5, PGP-14, UBC-1, RPL-25.1, PRK-1, KIN-29, MAX-2, UBC-3, KIN-26, UNC-51, GPA-17, PEK-1, C10G11.8, GPA-12, C08F8.6, TAT-4, PGP-5, TAT-2, Y52D5A.2, T15B12.2, DGK-1, UNC-43, ZK354.6, ARL-13, F09A5.2, C09D4.3, MYO-2, MYO-5, CATP-7, CATP-4, POD-2, ZK673.2, C50B8.1

WT DOWN		
Category	***P* value**	**Genes**
GO:0006898~receptor-mediated endocytosis	3.35E-24	SCO-1, SNR-7, LSM-4, T24C4.5, F10E9.4, LET-268, ICLN-1, CRN-1, B0238.11, TIN-44, TOMM-22, SKR-18, RTFO-1, C32E8.5, SWSN-3, C17G10.2, Y53C12B.1, NOL-5, C23H3.5, IARS-2, EIF-1.A, KNL-3, ERFA-3, C18A3.3, COX-11, C48B4.9, C48B6.2, CPF-1, Y44F5A.1, Y62E10A.2, MRPL-23, MRPL-24, APC-2, Y48A6B.3, TRR-1, LPD-6, ATAD-3, HPO-31, GPR-1, SMGL-1, C26F1.3, C43E11.9, MRPS-18C, DNJ-8, T14B4.2, T14B4.3, F25H8.2, NKB-1, EIF-3.E, GOP-2, EIF-3.H, Y53G8AL.2, Y73B3A.21, Y49F6B.2, RSP-7, KLP-19, Y71H2AM.5, ZK686.2, F10E7.6, PABP-2, RPB-8, F10E9.5, SNR-1, K04G7.1, SNR-4, SNR-2, AARS-1, RPB-11, C05D11.9, K08F9.4, INST-1, C50F4.4, EVL-14, T09A5.5, F11A3.2, TSFM-1, B0361.6, RUVB-2, MRPS-21, MRPS-22, NDUF-2.2, PARS-2, MRPS-23, W06E11.1, MRPL-50, C18E9.4, RME-2, OXA-1, ACDH-13, EPI-1, SFTB-1, MIG-22, UNC-97, Y75B8A.7, COL-108, FARS-1, RAE-1, DNJ-22, DNJ-21, RPC-25, TRD-1, NUO-6, D2030.3, CHP-1, D1046.2, MRPS-2, K07F5.14, KBP-3, ZK265.6, ACT-2, PAT-10, EXOS-3, F55F10.1, PPP-1, IMB-2, UNC-45, R08D7.1, RFT-1, C06A5.3, REPO-1, RABS-5, PRP-38, C07A9.2, Y66H1A.4, H06I04.3, MRPS-16, SYX-4, Y54E10BR.2, NCBP-2, NCBP-1, ZK858.7
GO:0006413~translational initiation	0.0031	LAF-1, EIF-3.H, EIF-1.A, IFF-1, ZK1098.4, IFE-3, C25H3.4, PPP-1, EIF-3.C, EIF-3.E

ATF-6 UP		
Category	***P* value**	**Genes**
GO:0006470~protein dephosphorylation	4.14E-05	C23G10.1, Y57G11C.6, C43E11.5, Y48G1C.5, F25H5.7, GSP-3, ZK484.7, F26B1.5, ZK809.1
GO:0018105~peptidyl-serine phosphorylation	3.58E-04	T15B12.2, C27D8.1, F41G3.5, K11C4.1, T05A7.6, R10D12.10, ZC581.2
GO:0055085~transmembrane transport	0.0323	C09D4.1, PITR-5, WHT-8, SNF-11, ABT-1, Y4C6B.4, CLH-1, SNF-5
GO:0004725~protein tyrosine phosphatase activity	0.0018	Y57G11C.6, C43E11.5, Y48G1C.5, F25H5.7, ZK484.7, ZK809.1

ATF-6 DOWN

Category	*P* value	Genes
GO:0006898~receptor-mediated endocytosis	1.71E-06	RME-2, LSM-4, RABS-5, PABP-2, COL-108, F10E9.5, NCBP-1, CPF-1, Y62E10A.2, C32E8.5, IMB-2, F25H8.2, K08F9.4
GO:0000003~reproduction	1.85E-04	RME-2, F01F1.11, PRI-1, ZK632.11, PABP-2, HDA-2, UNC-59, F10E9.5, F32H2.10, F35G12.11, NCBP-1, CPF-1, C32E8.5, T02G5.11, F25H8.2, IMB-2, MSH-2, K08F9.4
GO:0006397~mRNA processing	0.0223	LSM-4, NCBP-1, CPF-1
GO:0000387~spliceosomal snRNP assembly	0.0410	F10E9.5, LSM-4

IRE-1 UP		
Category	***P* value**	**Genes**
GO:0003700~transcription factor activity, sequence-specific DNA binding	0.0026	DAF-8, NHR-69, LET-607, NHR-49, RNT-1, NHR-231, ATF-6, ELT-2, NHR-201, NHR-64, EGL-44, NHR-57, NHR-50, ZIP-5, NHR-212, MML-1, DAF-16, SBP-1, DMD-7, HBL-1
GO:0000166~nucleotide binding	0.0452	LET-23, UBC-1, MAX-2, PMK-3, GPA-17, KGB-1, Y47G6A.5, HSP-3, CPB-2, PAB-2, C26D10.4, TAT-4, RAB-6.2, Y17G7B.10, MCA-1, DGK-1, TBA-7, MSI-1, SEK-1, MBK-1, F20D6.8, F09A5.2, F57B9.3, SVH-2, AAK-2, UNC-75, ZK673.2, MLK-1
GO:0045087~innate immune response	2.62E-11	T24C4.4, Y47G6A.5, NHR-57, ZK1055.7, TRK-1, C33H5.13, K08D8.4, F22H10.2, SOX-4, DAF-16, C42D8.1, SEK-1, CLD-9, CLC-1, FBXA-150, T19D12.4, M60.2, F16H6.10, LEC-11, C49C3.9, ELT-2, F20G2.5, F53C11.1, F13A7.11, C08E8.4, ZIP-10, C34H4.1
GO:0016310~phosphorylation	1.91E-04	LET-23, MAX-2, PMK-3, F09A5.2, KGB-1, Y47G6A.5, SVH-2, ZK795.1, TRK-1, C26D10.4, AAK-2, Y17G7B.10, DGK-1, SEK-1, TOE-4, MBK-1, ZK673.2, MLK-1
GO:0000122~negative regulation of transcription from RNA polymerase II promoter	0.0010	DAF-8, NHR-69, DAF-16, DAF-5, SMA-9, HDA-4, F57B9.3, HBL-1
GO:0040014~regulation of multicellular organism growth	0.0015	LET-607, UNC-64, SBP-1, MDT-15, OBR-3
GO:0007179~transforming growth factor beta receptor signaling pathway	0.0018	DAF-8, DAF-5, SMA-9, OBR-3
GO:0010468~regulation of gene expression	0.0150	SEL-11, SBP-1, F57B9.3, MDT-15
GO:0090390~phagosome acidification involved in apoptotic cell clearance	0.0358	UNC-108, RAB-14, LMP-1
GO:0019217~regulation of fatty acid metabolic process	0.0358	NHR-49, MDT-15
GO:0016567~protein ubiquitination	0.0387	UBC-1, SLI-1, ZER-1, SEL-11, Y53C10A.5, C17H11.6
GO:0006914~autophagy	0.0010	T23G11.7, UNC-64, VAMP-8, LMP-1

IRE-1 DOWN		
Category	***P* value**	**Genes**
GO:0006412~translation	1.93E-07	MRPL-16, MRPL-19, NARS-2, F11A3.2, TSFM-1, MRPS-7, MRPS-21, PARS-2, EEF-1B.2, MRPS-23, PPP-1, EIF-3.C, MRPL-32, EIF-3.E, MRPL-12, EIF-1.A, RPS-23, R07B7.10, F20D1.9, SAMS-1, MRPS-16, MRPS-15, ZK1236.1, F55G1.5, FARS-1, MRPL-20, MRPS-30, MRPL-23, MRPL-24, AARS-1
GO:0008152~metabolic process	1.16E-05	PMP-1, GST-28, AFMD-1, TBA-4, ABT-6, C50B6.7, UGT-64, UGT-65, T02B5.3, ABHD-11.2, MCCC-1, PINN-1, ACDH-13, C26E6.12, AMAN-1, W02B12.1, AGT-2, F13H6.3, ACL-3, UGT-53, ALH-9, NRF-6, UGT-9, ASM-2, AAGR-2, F08A8.4, ALKB-8, ACDH-3, C05C10.2, UGT-28, C05C10.3, CHHY-1, F26C11.1, ECH-5, UGT-22, UGT-41, H41C03.3, ECH-6, UGT-26, UGT-46, ACDH-9, UGT-48, ILYS-5, UGT-47, T09B4.8, ALH-12, AAGR-1, T05C3.6, KLP-15, F08F3.4, UGT-17, F21C10.9, C16A3.10, SUCG-1, PGP-2, GST-13, DBT-1, F55F3.2, MPST-1, APP-1, UGT-30, B0491.7, UGT-12, CATP-6, ACOX-3, ACOX-2, MRPL-46, CBL-1, TAG-173
GO:0006508~proteolysis	7.26E-05	Y16B4A.2, F19C7.4, DPT-1, USP-3, PAS-5, T16G12.1, TRPP-12, F41C6.4, NAS-20, ASP-14, ASP-8, PCP-1, ASP-1, ASP-2, MPPA-1, PCP-2, K02C4.3, CPR-8, K12H4.7, USP-14, Y40H7A.10, R03G8.4, R03G8.6, C01G10.10, TPP-2, C44B7.11, UBH-4, APP-1, F13D12.6, F57F5.1, F32A5.3
GO:0006635~fatty acid beta-oxidation	3.29E-04	ECH-5, ECH-6, F09F7.4, F08A8.4, ACOX-3, ACOX-2
GO:0033539~fatty acid beta-oxidation using acyl-CoA dehydrogenase	0.0018	F08A8.4, ACDH-9, ACOX-3, ACOX-2, ACDH-13, ACDH-3
GO:0055088~lipid homeostasis	0.0037	F08A8.4, ACDH-9, ACOX-3, ACOX-2, ACDH-13, ACDH-3
GO:0006631~fatty acid metabolic process	0.0084	ELO-5, ECH-6, DBT-1, F08A8.4, ACOX-3, ACOX-2, MECR-1
GO:0051603~proteolysis involved in cellular protein catabolic process	0.0223	Y16B4A.2, Y40H7A.10, F13D12.6, PAS-5, F57F5.1, F32A5.3, CPR-8

PEK-1 UP		
Category	***P* value**	**Genes**
GO:0006470~protein dephosphorylation	0.00724	R10F2.6, F25B3.4, Y62F5A.10, ZK354.8, M05D6.3
GO:0009058~biosynthetic process	0.01100	GOT-1.2, T04A11.1, T04A11.2
GO:0035335~peptidyl-tyrosine dephosphorylation	0.01298	R10F2.6, Y62F5A.10, ZK354.8, M05D6.3
GO:0006631~fatty acid metabolic process	0.01831	FAT-1, ELO-2, HACD-1
GO:0004725~protein tyrosine phosphatase activity	0.02698	R10F2.6, Y62F5A.10, ZK354.8, M05D6.3

PEK-1 DOWN		
Category	***P* value**	**Genes**
GO:0045087~innate immune response	0.0170	DCT-17, UGT-44, K08D10.14

Table A4: Phenotype scoring from RNAi screen of autophagy genes.

RNAi candidates		WT						
		phenotype ranking**				total ranking	Positive clone?	Gene description
		vector		*pmt-2(RNAi)*				
Transcript	**Gene**	**a**	**b**	**a**	**b**			
-	vector	0	0	0	0	0	NO	RNAi vector control (pL4440).
M03A8.2	*atg-2*	0	0	0	0	0	NO	Required for both autophagosome formation and regulation of lipid droplet morphology and dispersion.
M7.5	*atg-7*	0	0	1	2	3	YES	E1-like activating enzyme involved in the 2 ubiquitin-like systems required for cytoplasm to vacuole transport (Cvt) and autophagy.
D2007.5	*atg-13*	0	0	2	1	3	YES	Autophagy factor required for autophagosome formation and mitophagy.
K06A1.5	*atg-16.2*	0	0	0	2	2	NO	Interacts with ATG12-ATG5 to mediate the conjugation of phosphatidylethanolamine (PE) to LC3 (MAP1LC3A, MAP1LC3B or MAP1LC3C).
T19E7.3	*bec-1*	0	0	2	2	4	YES	Acts as core subunit of the PI3K complex that mediates formation of phosphatidylinositol 3-phosphate.
C47E8.5	*daf-21*	0	0	0	0	0	NO	Molecular chaperone that promotes the maturation, structural maintenance and proper regulation of specific target proteins involved in cell cycle.
F37C12.2	*epg-4*	0	0	0	1	1	NO	Involved in autophagy. Thought to act in autophagasome and omegasome formation.
Y39A1A.1	*epg-6*	0	0	0	0	0	NO	Encodes a WD40 repeat-containing protein that is related to the mammalian WIPI3/4 family of proteins (WD40 repeat protein interacting with phosphoinositides).
Y105E8B.8	*ero-1**	2	2	2	2	0	NO	Encodes an endoplasmic reticulum oxidoreductase that affects ER-stress response and affects reactive oxygen species levels.
W02C12.3	*hlh-30*	0	0	0	0	0	NO	Transcription factor TFEB orthologie that specifically recognizes and binds E-box sequences.
W02D3.7	*lbp-5*	0	0	0	2	2	NO	Fatty acid-binding protein homolog 5.
T22G5.2	*lbp-7*	0	0	0	0	0	NO	Fatty acid-binding protein homolog 7.

C32D5.9	*lgg-1*	0	0	0	0	0	NO	Ubiquitin-like modifier involved in autophagy. Through HOPS complex subunit vps-39, tethers lysosomes with autophagosomes to form autolysosomes.
ZK593.6	*lgg-2*	0	0	2	0	2	NO	Ubiquitin-like modifier involved in autophagy. Through HOPS complex subunit vps-39, tethers lysosomes with autophagosomes to form autolysosomes
B0336.8	*lgg-3*	0	0	0	0	0	NO	Ubiquitin-like protein ATG12. Modifier protein required for a protein conjugation system essential for autophagy.
K04A8.5	*lipl-4*	0	0	0	0	0	NO	Triglyceride lipase.
C03B1.12	*lmp-1*	0	0	0	0	0	NO	Lysosomal associated membrane glycoprotein. Required for the fusion of autophagosomes with lysosomes during autophagy.
C05D9.2	*lmp-2*	0	0	0	2	2	NO	Lysosomal associated membrane glycoprotein. Required for the fusion of autophagosomes with lysosomes during autophagy.
F38A6.1	*pha-4*	0	0	2	0	2	NO	Encodes a FoxA transcription factor; during embryonic development. PHA-4 plays a key role in regulation of diet-restriction-induced longevity in adult animals.
F54D11.1	*pmt-2**	2	2	2	2	0	NO	Phosphatidylethanolamine N-methyltransferase. Catalyzes PMME to phosphatidyldimethylethanolamine (PDME), and PDME to phosphatidylcholine (PC).
K09A9.2	*rab-14*	0	0	0	0	0	NO	Ras-related protein Rab-14. Involved in membrane trafficking between the Golgi complex and endosomes.
T24F1.1	*raga-1*	0	0	0	1	1	NO	RAs-related GTP-binding protein A.
F20D1.6	*rbg-1*	0	0	0	2	2	NO	Rab3 GTPase-activating protein catalytic subunit. Rab3 proteins are involved in regulated exocytosis of neurotransmitters and hormones.
Y47D3A.16	*rsks-1*	0	0	1	2	3	YES	Serine/threonine-protein kinase which regulates mRNA translation. Negatively regulates lifespan and resistance to starvation, oxidative stress, protein aggregation.
M01E5.6	*sepa-1*	0	0	2	1	3	YES	Adapter protein that connects P-granules in somatic cells with the autophagic machinery.
F48C1.7	*spe-11*	0	0	1	0	1	NO	Spermatocyte protein spe-11.
Y40C5A.1	*sqst-2*	0	0	0	0	0	NO	Autophagy receptor required for selective macroautophagy (aggrephagy). Functions as a bridge between polyubiquitinated cargo and autophagosomes.
R06B10.5	*tbc-10*	0	0	0	0	0	NO	The small GTPase RHEB is a direct activator of the protein kinase activity of mTORC1.
F46F11.9	*trpp-8*	0	0	2	1	3	YES	Specific subunit of the TRAPP III complex that acts as an autophagy-specific guanine nucleotide exchange factor (GEF) for YPT1.

Y60A3A.1	*unc-51*	0	0	1	0	1	NO	Promotes P-granule degradation in somatic cells through autophagy by modulating atg-13.
F53F10.4	*unc-108*	0	0	0	0	0	NO	Encodes a small GTPase homologous to the Rab GTPases that function in endocytosis, membrane fusion, and vesicular trafficking events.
B0513.9	*vamp-8*	0	0	0	0	0	NO	SNARE involved in autophagy through the direct control of autophagosome membrane fusion with the lysososome membrane.
ZK930.1	*vps-15*	0	0	2	0	2	NO	Serine/threonine-protein kinase required for cytoplasm to vacuole transport (Cvt) and autophagy as a part of the autophagy-specific VPS34 PI3-kinase complex I.
CD4.4	*vps-37*	0	0	0	0	0	NO	Component of the ESCRT-I complex, a regulator of vesicular trafficking process. Required for the sorting of endocytic ubiquitinated cargos into multivesicular bodies.
C26H9A.2	*wdfy-3*	0	0	2	1	3	YES	Required for selective macroautophagy, acts as an adapter protein by linking specific proteins destined for degradation to the core autophagic machinery members.
C52B11.5	*C52B11.5*	0	0	0	0	0	NO	Ortholog of human RAB20. Plays a role in apical endocytosis/recycling. Plays a role in the maturation and acidification of phagosomes.
C56E6.2	*C56E6.2*	0	0	0	0	0	NO	Predicted to have GTP binding activity and GTPase activity, based on protein domain information.
T01H3.2	*T01H3.2*	0	0	0	2	2	NO	Encodes a large (980-residue) uncharacterized protein, with multiple dysferlin and beta-propeller domains.
T23G11.7	*T23G11.7*	0	0	2	0	2	NO	Protein that is involved in regulation of different cellular pathways implicated in membrane trafficking including maturation of autophagosomes.
T28F4.5	*T28F4.5*	0	0	0	0	0	NO	Negative regulator of autophagy. Involved in mediating interferon-gamma-induced cell death.

*positive controls of known RNAi with severe phenotypes

**0, little difference in growth and brood size; 1, smaller brood size, sick; 2, sterile, very sick; all compared to control

Table A5: Phenotype scoring from RNAi screen of lipid and metabolism-related genes.

RNAi candidates		phenotype ranking**				average ranking (WT)	average ranking (*ire-1*)	Positive clone?
		WT		*ire-1(ok766)*				
Transcript	**Gene**	**a**	**b**	**a**	**b**			
-	vector	0	0	0	0	0	0	NO
F54D11.1	*pmt-2**	2	2	2	2	4	4	YES
R12B2.5	*mdt-15*	0	1	1	2	1	3	NO
D2063.1	*D2063.1*	0	0	2	1	0	4	NO
F40F4.3	*lbp-1*	0	0	2	2	0	4	NO
ZK742.5	*lbp-4*	0	0	0	0	0	0	NO
EEED8.2	*EEED8.2*	0	0	2	0	0	3	NO
F56H11.4	*elo-1*	0	0	0	0	0	0	NO
F01G4.2	*ard-1*	0	0	2	1	0	3	NO
B0272.3	*B0272.3*	0	0	1	0	0	1	NO
C25A1.5	*C25A1.5*	0	1	1	0	1	1	NO
D1054.1	*D1054.1*	0	0	1	0	0	1	NO
K11D2.2	*asah-1*	0	0	2	0	0	2	NO
F08C6.2	*pcyt-1*	0	0	1	0	0	1	NO
K12G11.3	*sodh-1*	0	0	1	0	0	1	NO
W02A2.1	*fat-2*	0	0	0	0	0	0	NO
F47G4.3	*gpdh-1*	0	0	1	1	0	2	NO
T02G5.7	*T02G5.7*	2	1	1	1	3	2	NO
R06F6.9	*ech-4*	0	0	0	1	0	1	NO
M03A8.1	*dhs-28*	0	0	0	0	0	0	NO
T27F6.6	*T27F6.6*	0	0	0	0	0	0	NO
T22G5.5	*sptl-3*	0	0	1	0	0	1	NO
Y45F3A.3	*acdh-11*	0	0	1	0	0	1	NO
T20B3.1	*T20B3.1*	0	0	0	0	0	0	NO
F59G1.1	*cgt-3*	0	0	0	0	0	0	NO
F13D12.4	*alh-8*	0	0	0	0	0	0	NO
R07H5.2	*cpt-2*	1	1	1	1	2	2	NO
T22H6.2	*alh-13*	0	0	0	2	0	2	NO
Y75B12B.6	*plc-2*	0	0	0	0	0	0	NO
Y66H1B.4	*spl-1*	0	0	2	0	0	2	NO
Y48B6A.7	*ace-4*	0	0	1	1	0	2	NO
EEED8.3	*EEED8.3*	2	1	1	1	3	2	NO
C01G8.3	*dhs-1*	0	0	0	1	0	1	NO
H02I12.8	*cyp-31A2*	0	0	1	1	0	2	NO
F27C8.6	*trcs-1*	0	0	0	0	0	0	NO
R148.6	*heh-1*	2	1	1	1	3	2	NO
K04G2.5	*ath-1*	0	0	2	0	0	2	NO
W06D12.3	*fat-5*	0	0	2	0	0	2	NO

F46E10.1	*acs-1*	1	1	2	0	2	2	NO
F54D8.3	*alh-1*	0	0	0	0	0	0	NO
K06A5.6	*acdh-3*	0	0	1	0	0	1	NO
K12H4.5	*K12H4.5*	0	0	0	1	0	1	NO
K10F12.3	*pll-1*	0	0	0	0	0	0	NO
F54C8.1	*F54C8.1*	0	0	1	1	0	2	NO
F10F2.3	*lips-3*	0	0	1	0	0	1	NO
Y56A3A.19	*Y56A3A.19*	0	0	0	0	0	0	NO
T05G5.6	*ech-6*	0	0	0	1	0	1	NO
Y49E10.16	*Y49E10.16*	0	0	2	2	0	4	NO
W09B12.1	*ace-1*	0	0	0	0	0	0	NO
B0395.3	*B0395.3*	0	0	0	0	0	0	NO
F26E4.12	*F26E4.12*	0	0	2	1	0	3	NO
K11H3.1	*gpdh-2*	0	0	1	2	0	3	NO
C36A4.9	*acs-19*	0	0	0	0	0	0	NO
C05C10.3	*C05C10*	0	0	0	0	0	0	NO
C02D5.1	*acdh-6*	0	0	1	0	0	1	NO
F54G8.2	*dgk-3*	0	0	0	1	0	1	NO
E04F6.5	*acdh-12*	0	0	0	0	0	0	NO
C48B4.1	*C48B4.1*	0	0	0	0	0	0	NO
B0361.5	*psd-1*	0	0	2	2	0	4	NO
C56G2.6	*let-767*	0	0	2	1	0	3	NO
F37C12.7	*acs-4*	0	0	2	0	0	2	NO
F01F1.6	*alh-9*	0	0	0	0	0	0	NO
F42G9.6	*F42G9.6*	0	0	0	1	0	1	NO
ZK370.4	*ZK370.4*	0	0	0	0	0	0	NO
W02D3.7	*lbp-5*	0	0	0	0	0	0	NO
ZK1053.5	*scrm-2*	0	0	0	1	0	1	NO
C49C8.4	*cyp-33E1*	0	0	1	2	0	3	NO
W02D3.5	*lbp-6*	0	0	1	0	0	1	NO
T22H2.5	*scrm-1*	0	0	1	0	0	1	NO
T05F1.10	*dhs-4*	0	0	0	1	0	1	NO
Y6B3B.10	*lagr-1*	0	0	1	1	0	2	NO
C37A2.3	*acdh-5*	0	0	2	0	0	2	NO
T10B11.2	*T10B11.2*	0	0	0	2	0	2	NO
F11E6.1	*F11E6.1*	0	0	2	0	0	2	NO
C07E3.9	*C07E3.9*	0	0	1	0	0	1	NO
R07G3.2	*lips-17*	0	0	0	0	0	0	NO
F49E12.9	*F49E12.9*	0	0	1	1	0	2	NO
H41C03.2	*H41C03.2*	0	0	0	1	0	1	NO
E04F6.7	*dhs-7*	0	0	2	2	0	4	NO
K05F1.3	*acdh-8*	0	0	0	1	0	1	NO
R07C3.4	*acs-15*	0	0	0	0	0	0	NO
C33C12.8	*C33C12.8*	0	0	0	0	0	0	NO

F58G1.5	*lips-9*	0	0	1	0	0	1	NO
T24H7.5	*tat-4*	0	0	1	1	0	2	NO
C09E8.2	*lips-7*	0	0	1	1	0	2	NO
W09H1.5	*mecr-1*	0	0	0	1	0	1	NO
T02G5.8	*kat-1*	0	0	2	0	0	2	NO
F28A10.6	*acdh-9*	0	0	1	0	0	1	NO
C01G6.7	*acs-7*	0	0	0	0	0	0	NO
ZK1127.2	*acs-6*	0	0	0	0	0	0	NO
C33C12.3	*C33C12.3*	0	0	0	0	0	0	NO
C04G6.3	*pld-1*	0	0	2	0	0	2	NO
W09B6.1	*pod-2*	0	0	0	0	0	0	NO
T25G3.4	*T25G3.4*	0	0	0	1	0	1	NO
M110.7	*M110.7*	0	0	1	1	0	2	NO
T04B2.6	*dhs-31*	0	0	0	0	0	0	NO
F56H11.3	*elo-7*	0	0	2	0	0	2	NO
K08D10.7	*scrm-8*	0	0	2	1	0	3	NO
F33D4.4	*F33D4.4*	0	0	1	2	0	3	NO
F01G10.3	*ech-9*	0	0	0	0	0	0	NO
F01G10.2	*ech-8*	0	0	2	2	0	4	YES
F42A9.5	*cyp-33E2*	0	0	2	2	0	4	YES
Y7A9A.1	*Y7A9A.1*	0	0	0	1	0	1	NO
K08F4.9	*dhs-12*	0	0	0	0	0	0	NO
ZK809.2	*acl-13*	0	0	2	2	0	4	YES
F38H4.8	*ech-2*	0	0	0	0	0	0	NO
F41H10.8	*elo-6*	0	0	0	0	0	0	NO
R09E10.3	*acs-18*	0	0	0	2	0	2	NO
R05G6.8	*plc-4*	0	0	0	0	0	0	NO
ZC416.6	*ZC416.6*	0	0	0	0	0	0	NO
W03G1.7	*asm-3*	0	0	0	2	0	2	NO
F28D1.9	*acs-20*	0	0	0	0	0	0	NO
H06H21.10	*tat-2*	0	0	2	2	0	4	YES
F58F9.7	*F58F9.7*	0	0	0	0	0	0	NO
F36H1.6	*alh-3*	0	0	2	2	0	2	YES
Y54E5A.1	*ttm-5*	0	0	0	2	0	2	NO
ZC416.8	*cha-1*	0	0	0	0	0	0	NO
T22G5.2	*lbp-7*	0	0	2	2	0	4	YES
F44C4.5	*ppt-1*	0	0	0	0	0	0	NO
F43H9.1	*ech-3*	0	0	0	0	0	0	NO
C50H11.1	*acs-21*	0	0	0	1	0	1	NO
R08H2.1	*dhs-23*	0	0	0	0	0	0	NO
F11A5.12	*stdh-2*	0	0	0	0	0	0	NO
C06B3.4	*stdh-1*	0	0	0	2	0	2	NO
K12B6.3	*lips-4*	0	0	0	0	0	0	NO
F10D2.9	*fat-7*	0	0	0	0	0	0	NO

C03G6.15	*cyp-35A2*	0	0	0	0	0	0	NO
F08F3.2	*acl-6*	0	0	0	0	0	0	NO
F43H9.2	*sptl-2*	0	0	0	0	0	0	NO
T03D8.6	*T03D8.6*	0	0	0	0	0	0	NO
C45B11.3	*dhs-18*	0	0	2	2	0	4	YES
K07B1.5	*acl-14*	0	0	2	0	0	2	NO
T11F9.11	*dhs-19*	0	0	0	0	0	0	NO
K07C6.5	*cyp-35A5*	0	0	0	1	0	1	NO
F28F8.2	*acs-2*	0	0	0	0	0	0	NO
F25B4.6	*hmgs-1*	0	0	0	0	0	0	NO
F55B12.5	*nrf-5*	0	0	1	1	0	2	NO
F09F3.9	*cpt-5*	0	0	0	0	0	0	NO
F25C8.4	*acs-12*	0	0	0	1	0	1	NO
W07A8.2	*W07A8.2*	0	0	0	0	0	0	NO
F02C9.3	*tat-6*	0	0	0	0	0	0	NO
F59F4.4	*acl-1*	0	0	0	0	0	0	NO
T27A10.3	*ckc-1*	0	0	0	0	0	0	NO
F45E6.4	*lips-1*	0	0	0	0	0	0	NO
F53B3.2	*F53B3.2*	0	0	0	0	0	0	NO
C11E4.1	*C11E4.1*	0	0	0	0	0	0	NO
F40F4.2	*lbp-2*	0	0	0	0	0	0	NO
T08G2.3	*acdh-10*	0	0	0	0	0	0	NO
C05C9.1	*C05C9.1*	0	0	0	0	0	0	NO
T25G12.5	*acdh-7*	0	0	0	0	0	0	NO
C54D1.4	*alh-10*	0	0	1	1	0	2	NO
C54G7.2	*mboa-3*	1	0	0	0	1	0	NO
T03G6.3	*T03G6.3*	0	0	0	1	0	1	NO
C46F4.2	*acs-17*	0	0	0	0	0	0	NO
C52B9.9	*acs-8*	0	0	0	0	0	0	NO
F59F4.1	*F59F4.1*	0	0	0	0	0	0	NO
D1009.1	*acs-22*	0	0	0	0	0	0	NO
C03H5.4	*C03H5.4*	0	0	0	0	0	0	NO
H21P03.3	*sms-1*	0	0	0	0	0	0	NO
C06B3.5	*stdh-3*	0	0	0	2	0	2	NO
H37A05.1	*lpin-1*	0	0	2	2	0	4	YES
T05H4.1	*acl-8*	1	2	1	2	3	3	NO
ZK40.1	*acl-9*	0	0	0	2	0	2	NO
C49G7.8	*cyp-35A4*	0	0	0	0	0	0	NO
C46C11.1	*hosl-1*	0	0	0	0	0	0	NO
C52B9.1	*cka-2*	0	0	0	2	0	2	NO
F02E8.6	*ncr-1*	0	0	0	0	0	0	NO
R03G5.5	*R03G5.5*	0	0	1	0	0	1	NO
F11A6.2	*scrm-4*	0	0	0	0	0	0	NO
K10H10.3	*dhs-8*	0	0	0	1	0	1	NO
T02G5.4	*T02G5.4*	0	0	0	0	0	0	NO

R11F4.1	*R11F4.1*	0	0	0	0	0	0	NO
F55C5.2	*F55C5.2*	0	0	0	1	0	1	NO
F40F4.4	*lbp-3*	0	0	0	0	0	0	NO

*positive controls of known RNAi with severe phenotypes

**0, little difference in growth and brood size; 1, smaller brood size, sick; 2, sterile, very sick; all compared to control